ENG.20041111.0001

OCRWM	DESIGN CALCULATION OR ANALYSIS COVER SHEET	1. QA:QA
		2. Page 1 of 222

3. System	4. Document Identifier
Subsurface	800-K0C-SS00-00200-000-00A

5. Title

Lithophysal Rock Mass Mechanical Properties of the Repository Host Horizon

6. Group

Design & Engineering/Design Engineering/Mining/Geotechnical

7. Document Status Designation

☒ Preliminary   ☐ Final   ☐ Cancelled

8. Notes/Comments

None

Appendices	Total Number of Pages
A. Simulation of Lithophysal Porosity Spatial Variation	18
B. Computer Files Supporting Calculation	4
C. Derivation of Data Reduction Formulae	4

RECORD OF REVISIONS

9. No.	10. Reason For Revision	11. Total # of Pgs.	12. Last Pg. #	13. Originator (Print/Sign/Date)	14. Checker (Print/Sign/Date)	15. QER (Print/Sign/Date)	16. Approved/Accepted (Print/Sign)	17. Date
00A	Initial Issue	222	222	Douglas B. Rigby *Douglas B. Rigby* 11/10/04	David Tang *David Tang* 11/10/04	William Dockery *William Dockery* 10 NOV 2004	Fei Duan *Fei Duan*	11/10/04

DISCLAIMER

This report was prepared as an account of work sponsored by an agency of the United States Government. Neither the United States Government nor any agency thereof, nor any of their employees, nor any of their contractors, subcontractors or their employees, makes any warranty, express or implied, or assumes any legal liability or responsibility for the accuracy, completeness, or any third party's use or the results of such use of any information, apparatus, product, or process disclosed, or represents that its use would not infringe privately owned rights. Reference herein to any specific commercial product, process, or service by trade name, trademark, manufacturer, or otherwise, does not necessarily constitute or imply its endorsement, recommendation, or favoring by the United States Government or any agency thereof or its contractors or subcontractors. The views and opinions of authors expressed herein do not necessarily state or reflect those of the United States Government or any agency thereof.

CONTENTS

Page

FIGURES

Page

TABLES

<div align="right">Page</div>

ACRONYMS AND ABBREVIATIONS

Acronyms

AP	administrative procedure (DOE)
BSC	Bechtel SAIC Company, LLC
CD-ROM	compact disk-read-only-memory
DIRS	Document Input Reference System
DOE	U.S. Department of Energy
DTN	data tracking number
DVD-ROM	digital versatile disc-read-only-memory
ECRB	Enhanced Characterization of the Repository Block (drift)
ESF	Exploratory Studies Facility
GFM2000	Geologic Framework Model, version 2000
GSI	geological strength index
ICN	Interim Change Notice
KTI	Key Technical Issue
NRC	U.S. Nuclear Regulatory Commission
OCRWM	Office of Civilian Radioactive Waste Management
PC	personal computer (specifically IBM compatible)
PFC	Particle Flow Code
QA	quality assurance
TDMS	Technical Data Management System
TIC	Technical Information Center
UCS	uniaxial (or unconfined) compressive strength
UDEC	Universal Distinct Element Code
YMP	Yucca Mountain Project

Abbreviations

A   cross-section area

b   average block size

C   Celsius
cm   centimeter

E   Young's modulus

F   force

I   moment of inertia
in   inch

ft   foot

G   shear modulus

k   stiffness
K   bulk modulus
km   kilometer

m   meter
M   bending moment
mi   mile
mm   millimeter

R   particle radius

Tpt   Topopah Spring Tuff
Tptpll   Topopah Spring Tuff crystal poor lower lithophysal
Tptpln   Topopah Spring Tuff crystal poor lower nonlithophysal
Tptpmn   Topopah Spring Tuff crystal poor middle nonlithophysal
Tptpul   Topopah Spring Tuff crystal poor upper lithophysal

U   displacement

θ rotational angle
ν Poisson's ratio
σ normal or tensile stress
τ shear stress

1. PURPOSE

The purpose of this calculation is to develop estimates of key mechanical properties for the lithophysal rock masses of the Topopah Spring Tuff (Tpt) within the repository host horizon, including their uncertainties and spatial variability. The mechanical properties to be characterized include an elastic parameter, Young's modulus, and a strength parameter, uniaxial compressive strength. Since lithophysal porosity is used as a surrogate property to develop the distributions of the mechanical properties, an estimate of the distribution of lithophysal porosity is also developed. The resulting characterizations of rock parameters are important for supporting the subsurface design, developing the preclosure safety analysis, and assessing the postclosure performance of the repository (e.g., drift degradation and modeling of rockfall impacts on engineered barrier system components).

1.1 BACKGROUND

1.1.1 Laboratory Characterization of Mechanical Rock Properties

Laboratory testing of Yucca Mountain rock samples to determine the mechanical behavior of the rock has occurred intermittently over several decades (Section 6.3). Small-cores (25 mm, 1-in diameter) from boreholes were tested in the late 1970s to early 1980s, outcrop samples were tested in the mid-1980s, and larger-size borehole cores (50 mm, 2-in diameter) were tested from the mid-1980s to the mid 1990s. Three studies of these historical laboratory testing efforts determined that several rock mechanical properties were related to specimen porosity (Price 1983 [DIRS 102941][*], Price and Bauer 1985 [DIRS 106590], and Price et al. 1994 [DIRS 161290]). For characterizing the repository rock, the historical laboratory-testing program focused primarily on the middle nonlithophysal zone within the Topopah Spring Tuff. Until recently, only one set of 10 laboratory tests was available to characterize the mechanical behavior of larger rock samples (267 mm, 10.5-in diameter) containing lithophysae (Price et al. 1985 [DIRS 106602] and DTN: SNSAND84086000.000 [DIRS 160011]). The main distinguishing characteristic among the lithophysal and nonlithophysal units is the percentage of large-scale (centimeters to meters size) voids within the rock.

Before 2001 mechanical properties of Topopah Spring Tuff were estimated for assumed homogeneous thermal-mechanical rock units that combined vitric, lithophysal, and nonlithophysal rocks. Rock mass properties were developed for these thermal-mechanical units using the traditional empirical approaches. Subsequently, it was recognized that (1) most of the repository will reside in lithophysal rock, (2) the mechanical rock behavior of lithophysal rock is significantly different from that of nonlithophysal rock, and (3) the traditional methods of empirical classification of rock mass may not be applicable to lithophysal rock. As a result, a new approach was presented by Board that divided the study of repository rock into lithophysal and nonlithophysal rocks (Board 2003 [DIRS 165036], Sections 5.2.3 and 6) and involved new mechanical testing to better characterize lithophysal rock in the laboratory (Section 6.3.2) and

---

[*] In this report, a unique six-digit numerical identifier (the Document Input Reference System [DIRS] number) is placed in the text following the reference callout (e.g., BSC 2003 [DIRS 123456]), the purpose of which is to assist the reader in locating a specific reference in the DIRS database. Within the reference list (Section 7), multiple sources by the same author and date (e.g., BSC 2003) are sorted alphabetically by title.

field (Section 6.7). This calculation summarizes what has been gathered and learned about lithophysal rock, and provides the technical basis for accounting for the effects of lithophysae on lithophysal rock properties.

1.1.2 Yucca Mountain Geology and the Repository Footprint

The Topopah Spring Tuff underlying Yucca Mountain (Figure 1-1) is part of a large-volume (greater than 1,000 km^3) pyroclastic flow deposit that was deposited 12.8 million years ago (Sawyer et al. 1994 [DIRS 100075], p. 1305). A number of formative processes including deposition, welding (material compaction), and crystallization occurred early in the Topopah Spring Tuff history producing a rock formation that has been divided by geologic criteria into lithostratigraphic members, zones, subzones, and intervals that are stratiform (laterally continuous) on a repository scale, but locally may vary (Figure 1-2; Buesch et al. 1996 [DIRS 100106]); also Section 5.1). Thick pyroclastic flow deposits, like the Topopah Spring Tuff, exhibit the complete range in zones of welding (non welded, partially welded, moderately welded, and densely welded) and the crystallization and cooling processes, which is conducive to the development of the zones, subzones, and intervals that have been identified.

The repository host horizon is the body of rock in which the repository is proposed to be excavated, and it spans four lithostratigraphic zones (the lower part of the Tptpul, Tptpmn, Tptpll, and Tptpln) as part of the Topopah Spring Tuff formation (Figures 1-1 to 1-3 and BSC 2003 [DIRS 165572])[*]. Lithophysal rocks (Tptpul and Tptpll; Figure 1-3) comprise approximately 85 percent of the emplacement area for the repository (*Subsurface Geotechnical Parameters Report* (BSC 2003 [DIRS 166660], Section 5.4, p. 5-20). Approximately 81 percent of the planned emplacement drifts will be excavated within the Topopah Spring lower lithophysal zone (Tptpll) and about 4 percent within the Topopah Spring upper lithophysal zone (Tptpul). These estimates do not include the lithophysal-bearing subzone that is frequently observed as part of the Topopah Spring middle nonlithophysal zone (Tptpmn, Buesch and Spengler 1998 [DIRS 101433]).

A key element of the approach to estimate ranges of rock properties is using knowledge of the geologic processes, features, and classifications of volcanic rock zones and subzones. In particular, rock bulk properties (such as bulk density, total porosity, and lithophysal porosity) and the rock mechanical properties of Young's modulus and uniaxial compressive strength have been correlated at different scales, and with characterized lithostratigraphic features (such as volume fraction of lithophysae). Accordingly, lithostratigraphic thickness, geometry, and internal heterogeneity and relations between lithostratigraphic features and mechanical behavior are important for estimating and predicting mechanical properties (including their uncertainties and spatial variation) in poorly sampled areas of the repository host rock, which constitutes most of the rock volume intersected by the repository footprint (Figure 1-4). The repository footprint covers an area defined by a length of approximately 5 km (3 mi) and a width of about 2.5 km (1.5 mi) which is about 12.5 km^2 or 4.5 mi^2 (BSC 2004 [DIRS 164519, Figure 1]).

---

[*] The word "tuff" is a term of formal stratigraphic nomenclature but also carries the connotation of a mappable pyroclastic flow cooling unit that was emplaced in an instant of geologic time (Byers et al. 1976 [DIRS 104639], p. 2).
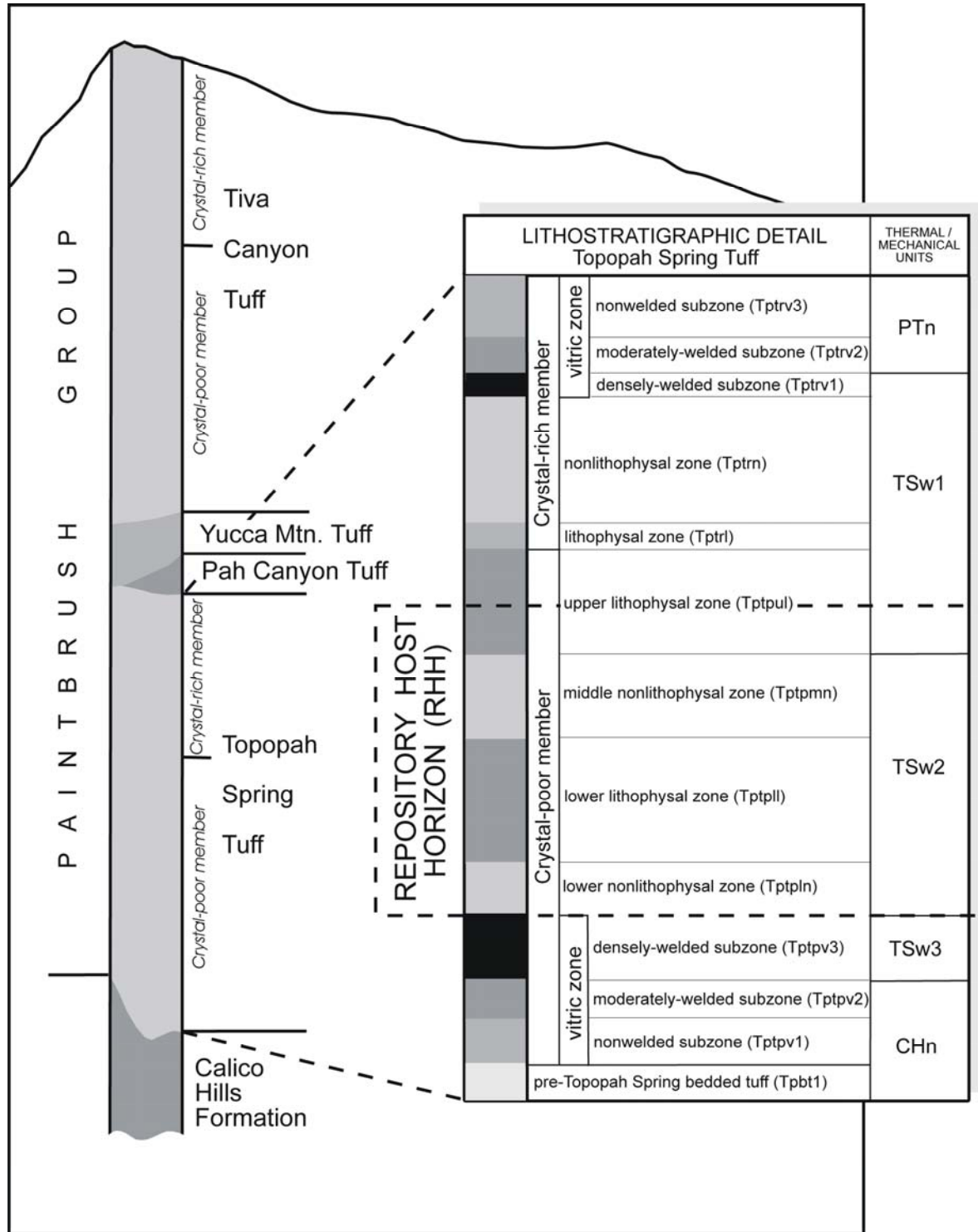
Source: Modified from BSC 2003 [DIRS 166660], Section 5.3.1, Figure 5-1.

NOTE: The detailed lithostratigraphic and thermal-mechanical nomenclature are shown for the Topopah Spring Tuff, including lithostratigraphic positions of the Repository Host Horizon, the ESF main drift, and the repository

Figure 1-1. General Stratigraphic Column for Yucca Mountain, Nevada
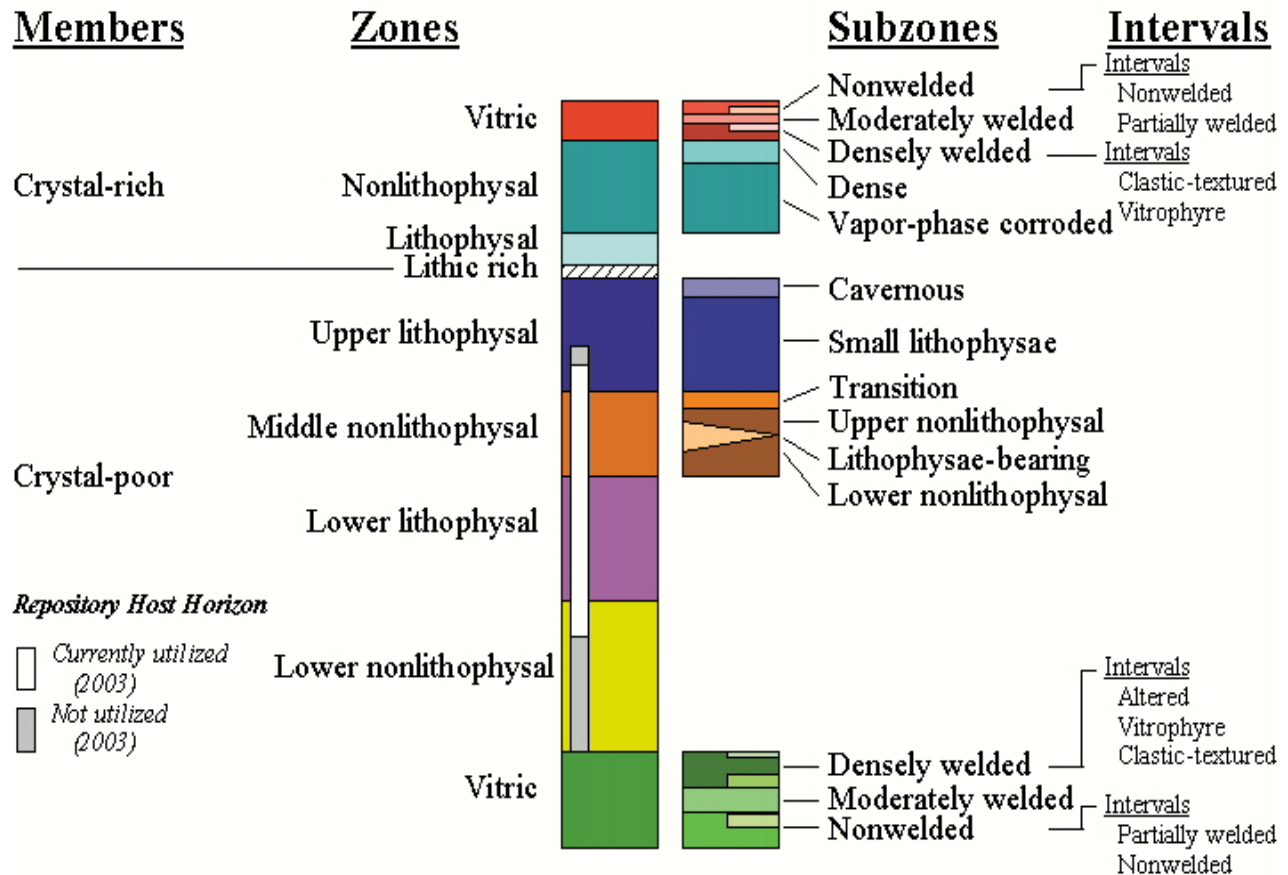
Source: Information used to create this figure is derived from geological data in Buesch et al. 1996 [DIRS 100106] and *Underground Layout Configuration* (BSC 2003 [DIRS 165572]).

NOTE: More than 90 percent of the thickness of the Topopah Spring Tuff at Yucca Mountain compacted sufficiently to be classified as densely welded tuff (Buesch et al. 1999 [DIRS 165483]) with progressively less welded (moderately to partially welded and nonwelded) rocks near the top and bottom of the formation. During welding, the redistribution of the interstitial vapor initially flowed through the compacting matrix, was later focused along fractures, and locally this redistribution resulted in development of lithophysal cavities, rims, and spots in the rock matrix, and streaks, veinlets, stringers, and partings along fractures (Buesch and Spengler 1998 [DIRS 101433], p. 21). The "(2003)" notation in the figure refers to the design details provided in BSC 2003 [DIRS 165572].

Figure 1-2. Lithostratigraphic Units (Members, Zones, Subzones, and Intervals) of the Topopah Spring Tuff at Yucca Mountain
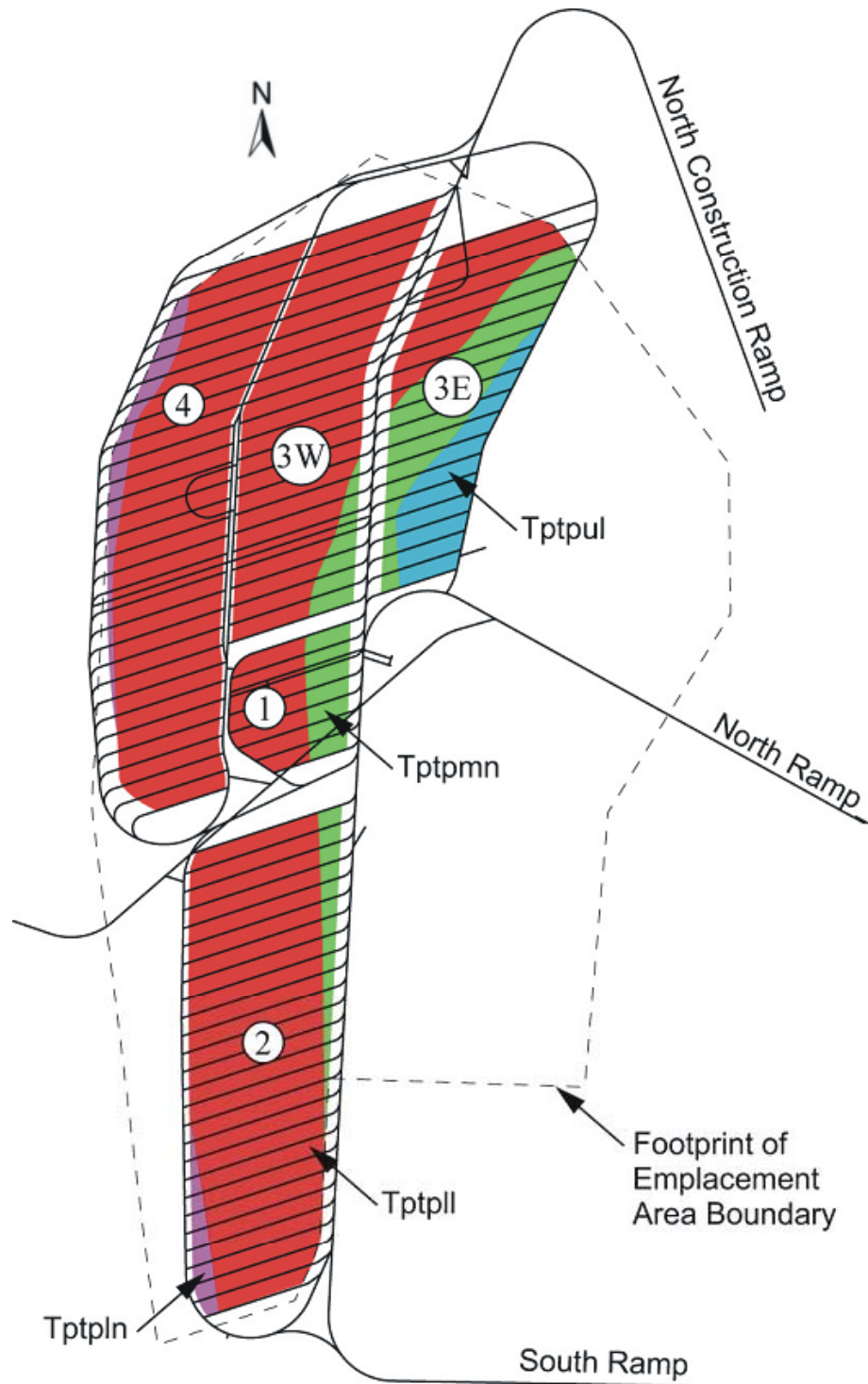
Source: Modified from BSC 2004 [DIRS 168370, Figure 3]

NOTE: Footprint of emplacement area boundary is shown as a dashed line. This footprint represents the currently characterized area in which emplacement drifts can be located. Circled numbers are Construction Panel Numbers.

Figure 1-3. Plan View of Repository Layout Showing An Overlay of the Lithostratigraphic Rock Zones
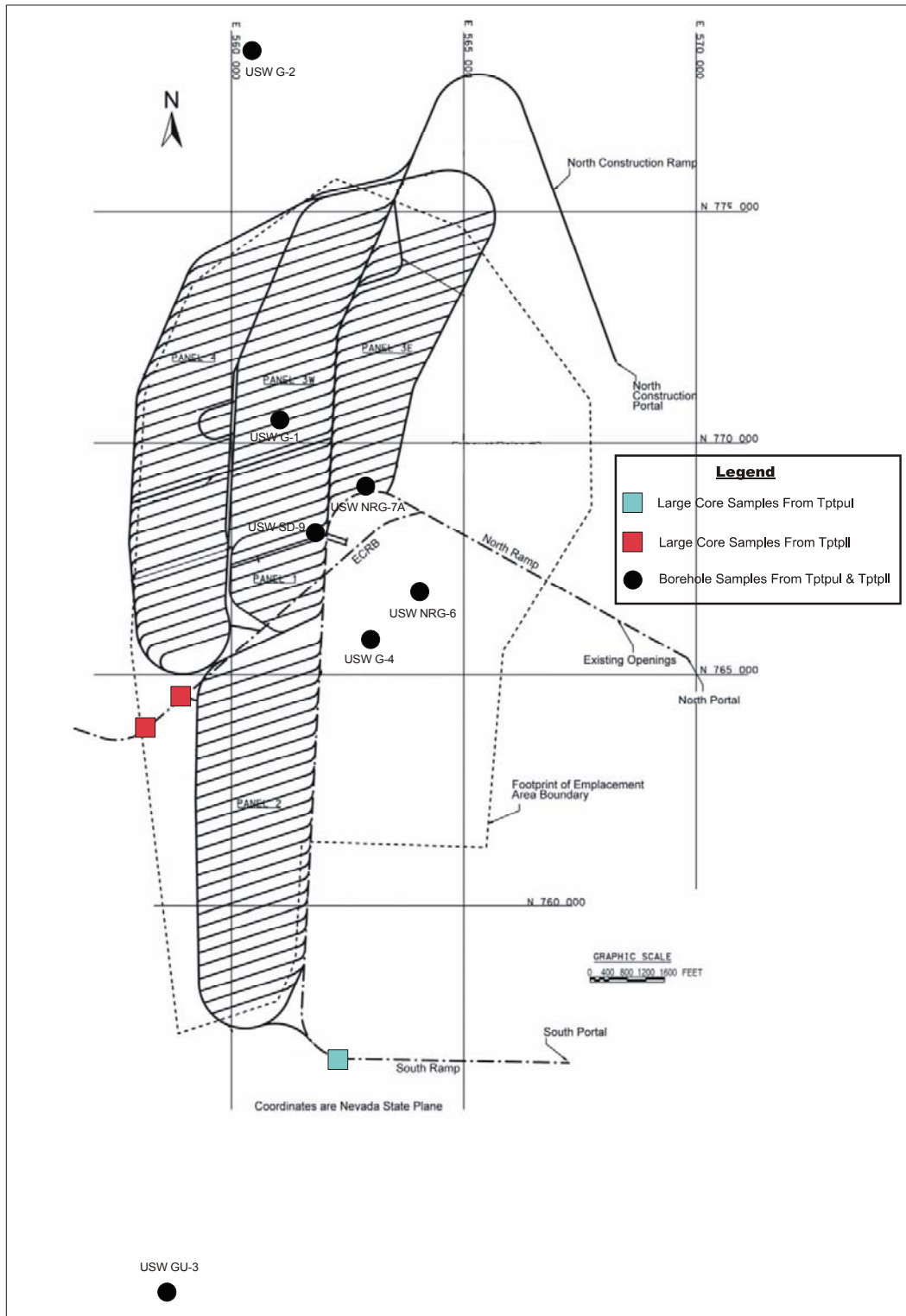
Source: Modified from BSC 2004 [DIRS 164519, Figure 1]. Borehole location coordinates added from Bores3Q [DTN: MO0103COV01031.000]. ESF and ECRB Cross-Drift Stationing from Figures 3 and 4 of BSC 2003 [DIRS 165572]. Specimen boreholes and stationing taken from DTNs in Table 4-2. Compare with borehole locations in Figure II-4 of BSC 2003 [DIRS 165572] and historical borehole locations (BSC 2003 [DIRS 166660], Attachment IV, Figures IV-1 and IV-9).

Figure 1-4. Sampling Locations of Mechanically Tested Lithophysal Rock Specimens

The primary lithostratigraphic features in the crystallized rocks include the matrix-groundmass, lithophysal cavities, rims on lithophysae, and spots (BSC 2003 [DIRS 166660], Sections 5.3.3 and 8.2.3, Table 8-3). The matrix consists of a crystallized ignimbrite mix of fine-grained groundmass, shards, pumice, and lithic clasts (typical matrix porosity is approximately 10 percent). Lithophysae are hollow cavities (100 percent porosity, typically a few centimeters to a few decimeters in diameter, but can be more than 1 m in diameter) observed in the matrix rock, which are typically surrounded by a porous rim. Spots, which occur separately from lithophysae, and lithophysae rim material, have a similar weak crystalline structure having a measured porosity that averages approximately 30 percent. Abundances and variability of these features within lithophysal rock are discussed later in Section 6.2. The lithophysal porosity is selected as the surrogate property for modeling both its uncertainty and spatial variability and that of the dependent mechanical properties in the mechanical material model of lithophysal rock behavior. Lithophysal porosity is defined as the fractional volume of large-scale (centimeters-meters) void space per unit volume of rock.

1.2   METHODOLOGY

1.2.1   General Approach

Applying traditional empirical techniques of estimating rock mass properties to lithophysal rock is considered not to be suitable at this time because the behavior of lithophysal rock mass is strongly porosity- and size-dependent and has limited dependence on fracture characterization. Also the current empirical approaches and classification techniques are of limited value for rock having an abundance of lithophysal cavities and highly porous crystallized materials due to the lack of case histories in such rock (Board 2003 [DIRS 165036], pp. 2-3 and 5-9). Rather, the approach (Figure 1-5) adopted in this calculation relies on indirectly estimating the ranges of mechanical properties using correlations between porosity and mechanical behavior linked to field measured variations of rock porosity.

This calculation provides a detailed summary of the laboratory test results for small- and large-diameter cores of rock that include porosity measurements. These mechanical testing results are used to relate specimen strength and modulus to porosity, which is the primary factor controlling variability of mechanical properties in lithophysal rock (Section 6.3). An initial set of base-case strength and modulus values (termed lithophysal rock mass "categories") are developed from laboratory and field testing results with upper and lower strength bounds that span the entire range of lithophysal porosity conditions measured in the host rock.

To supplement the laboratory data base and improve understanding of the mechanical response of lithophysal rock, two discontinuum numerical models, Particle Flow Code (PFC) and Universal Distinct Element Code (UDEC), are first calibrated to reproduce the observed mechanical response of laboratory specimens tested by uniaxial loading, and then used to conduct numerical biaxial experiments on simulated lithophysal rock specimens. In particular, the PFC and UDEC models are used to study the effect that lithophysal geometry (void porosity, size, shape and distribution) has on the variability of rock strength and elastic mechanical properties. These results of the numerical investigation are used to update the estimated upper and lower rock mass property bounds for the respective lithophysal rock mass categories that

were established based on the laboratory and field-testing of rock. The validation activities required for building more confidence in the predicted results are also described.
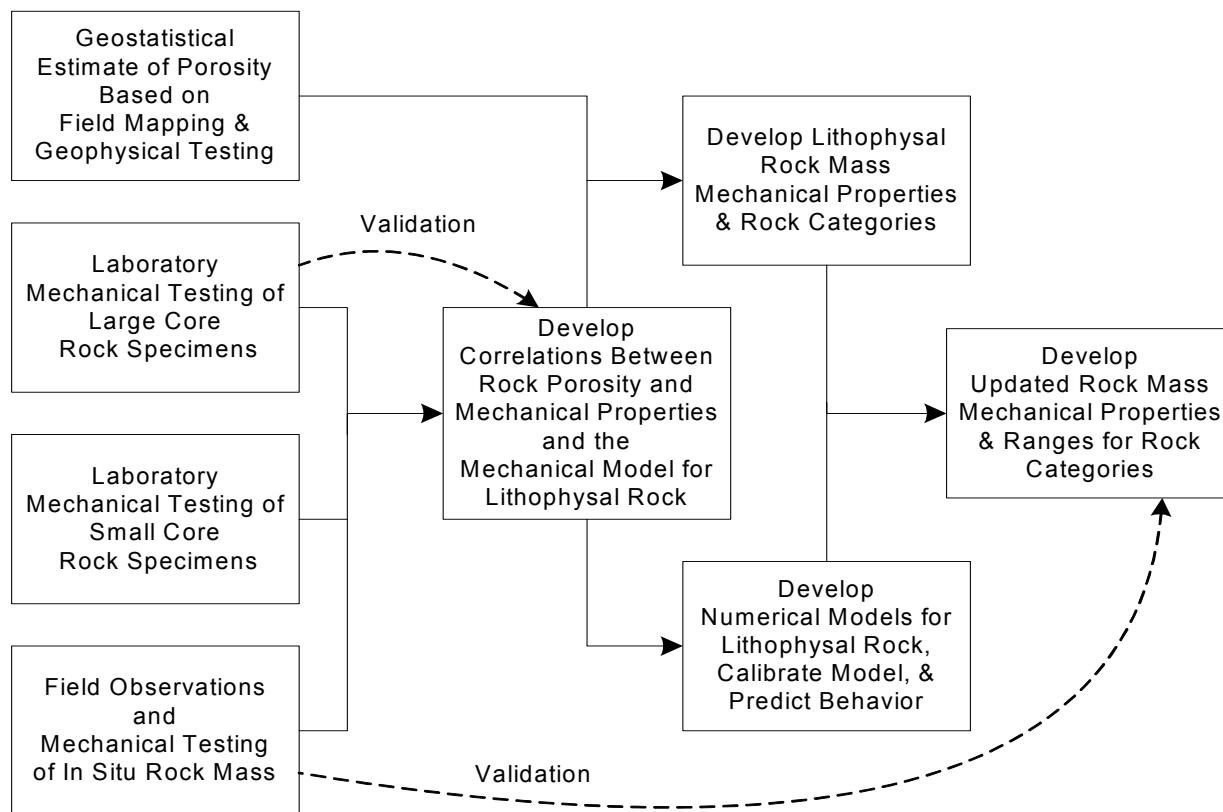
Figure 1-5. Strategy for Developing Rock Mass Mechanical Properties and Rock Classification Categories for Lithophysal Rock

1.2.2 Method of Addressing Uncertainty and Variation

In recent years, there has been an increased emphasis on treating "uncertainty" and "variability" of data and models separately in probabilistic risk assessments. Variability refers to diversity or heterogeneity among members of a population. Uncertainty arises due to a lack of knowledge regarding the true value of a quantity or regarding a true distribution for variability. Uncertainty has a precision component (random error or statistical variation) and an accuracy component (systematic error or bias). Ideally, the uncertainties and spatial and/or temporal variability of model input parameters are quantified, the uncertainties related to how well conceptual models of physical behavior match with physical reality are quantified, and, if computational modeling is employed, the further uncertainties arising in the numerical implementation of conceptual models are quantified. Subsequently, the identified uncertainties and variabilities are propagated through the risk assessment model(s) in two separate dimensions in order to quantify variability and uncertainty in the model outputs. The separation of uncertainty and variability is desirable because, in many instances, each has different decision-making and policy implications.

The risk modeling of lithophysal rock mass properties is not one of those instances. The approach of this calculation is to estimate the combined uncertainty and spatial variation of the rock parameters identified and the modeling based on these parameter inputs. There are several reasons for adopting the combined approach:

- Unlike human-engineered materials, the repository rock is uniquely heterogeneous and variable in its properties, and the rock cannot be duplicated for further study. This is typical of geologic materials and, because there is no practical way to rigorously probe and recover sufficiently sized samples from the large volume of repository rock for mechanical testing, a strong geostatistical basis to directly define mechanical property variability does not exist. However the underlying geology does indicate significant vertical variation in rock properties, particularly porosity, and an effort is made to model this variability by using stratiform models (lithostratigraphic zones) of the rock as well as more detailed vertical variations within some zones, where they can be identified (Sections 5.1 and 6.2).

- The geologic heterogeneity present in Yucca Mountain repository rock, especially for lithophysal rock, means that even a nearby sample of rock can have vastly different properties (Section 6.3). As a consequence, any effort to determine the imprecision of rock measurements (random error or statistical variation) is compromised by the spatial variation of rock properties.

- The accuracy component of uncertainty (systematic errors, bias, model uncertainty) is large in this calculation relative to precision uncertainty. As is often the case in geomechanical measurements and modeling, it is the subjective determinations of inaccuracy of methods and approach that generally dominate both uncertainty and spatial variation. In geology and geomechanics, professional judgment is implicit in the process of determining uncertainties and variability and is used in this calculation.

- Finally, the *measurement* uncertainty of rock properties (involving both imprecision and inaccuracy) can be determined to some degree, but they are only marginally significant compared to the spatial variation. Again, because a rock sample is a tested population of one, the imprecision or statistical variation in the determination cannot be rigorously determined in the traditional sense. However, the uncertainty of particular measurement instruments used (e.g., load cells, displacement transducers, weighing machines) can be determined with precision, and the theory underlying less precise measurements (e.g., estimates of lithophysal porosity) can be examined to estimate measurement uncertainty. The combined instrument uncertainty involved in determining laboratory strength and Young's moduli is on the order of ±3 percent (Section 6.3). The measurement uncertainty associated with the one-dimensional determinations (based on point counting) of lithophysal rock porosity of laboratory samples is estimated at approximately 20 percent (Section 6.3), while the range of porosity values is close to 100 percent of the mean value. The measurement uncertainty associated with the determinations of lithophysal rock porosity of Tptpll field rock is typically about ±5 percent for angular and panel map data and upwards of ±10 percent for tape traverse data (Section 6.2), while the field range of lithophysal porosity is more than 200 percent larger than the mean.

As is mentioned above, the large-diameter core laboratory data set is necessarily limited due to the inherent variability of rock porosity and practical difficulty of sampling and testing specimens with sufficient volume to properly characterize the lithophysal rock. Limited sample statistics is used with professional judgment to quantify ranges of uncertainty for lithophysal porosity in Section 6.4. These ranges of lithophysal rock porosity are correlated with a relationship between uniaxial compressive strength and Young's modulus to develop a number of rock mass categories, which represent the general condition of rock mass from weak to strong. The relative occurrence of each rock mass category is determined using statistical estimates of expected lithophysal porosity across the repository rock together with the assigned lithophysal porosity ranges for each rock category.

To summarize, the combined uncertainty and spatial variation of the rock mass parameters is accounted for by first establishing an uncertainty range over which mechanical parameters are expected to vary as a function of lithophysal porosity and each other. Second, the spatial variation of repository lithophysal porosity is estimated and used to establish five rock mass categories ranging from weak rock of high porosity to strong rock of low porosity. Each rock mass category is defined by a specific range of uncertain mechanical property values. The user of this data must determine the suitable use of the rock category property data for their purposes.

1.3   SCOPE OF CALCULATION

The scope of the work for this calculation includes:

- Defining the purpose, context, and surrogate porosity approach for developing mechanical rock mass properties for lithophysal rock (Sections 1 and 6.1),

- Discussing the plausible conceptual models of lithophysal rock behavior (Section 6.1.2),

- Describing the field characterization of lithophysal rock and developing a geostatistical approach for estimating the uncertainty and spatial variability of lithophysal porosity over the scale of the repository footprint (Section 6.2),

- Describing the mechanical properties of lithophysal rock based on laboratory testing and developing a mechanical model of lithophysal rock (Section 6.3),

- Developing a mechanical property bounding analysis based on actual rock testing and proposing rock mass categories for lithophysal rock (Section 6.4),

- Describing the adopted computational models for predicting lithophysal rock behavior (Section 6.5),

- Describing the prediction of mechanical properties of lithophysal rock based on numerical modeling (Section 6.5),

- Updating the estimate of rock mass mechanical parameters for lithophysal rock including setting bounds for the parameters (Section 6.6),

- Summarizing the limitations and uncertainty analysis of the lithophysal rock property characterization (Section 6.6), and

- Addressing the confirmation and validation of the lithophysal rock parameter estimates and modeling (Section 6.7).

1.4   LIMITATIONS

The rock mass mechanical property estimates developed in this calculation represent reasonable parameter values, especially considering the uncertainties assigned to these estimates. However, the developed properties are based on several assumptions that are discussed in Section 5 and include the following:

- The lithophysal rock in the repository area is assumed similar in geologic structure and laterally continuous. As a corollary to this, the lithophysal porosity characterization (obtained from underground surface mapping) is assumed to statistically reflect the actual spatial variation, both horizontally and vertically, of Tptpll lithophysal porosity across the repository footprint.

- The quantified lithophysae abundance data obtained by underground mapping of the Tptpll unit is assumed to be statistically undifferentiated from the distribution of lithophysal porosity of the Tptpul unit.

- Lithophysal rock is conceptualized as being a composition of a two-component conceptual model consisting of solid matrix and air-filled lithophysal voids (lithophysae).

- The estimated range of mechanical rock properties of lithophysal rock at the 1 m and larger scale can be suitably estimated from the available large-core (approximately 0.3 m diameter) specimen laboratory testing results.

- The simulation model developed to represent the spatial variability of lithophysal porosity (Appendix A) can be applied to other uncertain model parameters (e.g., elastic Young's modulus, E, and uniaxial compressive strength, UCS).

These assumptions represent the primary limitations of this calculation. These estimates of mechanical rock parameters are not applicable to nonlithophysal rock mass, except for lithophysal subzones. The reported mechanical parameters and rock behavior described assume no effects of geochemical alterations to the rock that might significantly alter geomechanical rock mass properties.

The calculations contained in this document were developed by Design & Engineering, Geotechnical Discipline and are intended solely for the use of the Design & Engineering, Geotechnical Discipline in its work regarding the design and analysis of subsurface excavations and rock behavior. Yucca Mountain Project personnel from the Design & Engineering, Geotechnical Discipline should be consulted before use of the calculations for purposes other

than those stated herein or use by individuals other than authorized personnel in the Design & Engineering, Geotechnical Discipline.

2. QUALITY ASSURANCE

This document has been prepared with a QA:QA status and technical tasks supporting this report are subject to the requirements of the *Quality Assurance Requirements and Description* (DOE 2004 [DIRS 171539]). The lithophysal rock descriptions and parameters developed and presented in this calculation may be used as inputs in a number of analysis and modeling activities that support performance assessment, and to design ground support systems in emplacement drifts and other underground openings. As a result, this calculation activity addresses in part characteristics of the Subsurface Facility (p. A-3), the Emplacement Drift Excavated Opening component of the Emplacement Drift System (p. A-5), the Natural Barrier component of the Upper Natural Barrier System (p. A-8), and possibly other systems and subsystems that are classified as "Safety Category (SC)" in the *Q-List* (BSC 2004 [DIRS 168361], Appendix A) in accordance with procedure AP-2.22Q, *Classification Analyses and Maintenance of the Q-List.* The "SC" classification requires compliance with the *Quality Assurance Requirements and Description* requirements.

This report and its supporting technical analyses and calculations have been prepared in accordance with the Office of Civilian Radioactive Waste Management (OCRWM)-approved quality assurance (QA) program. The report was developed in accordance with procedures AP-3.12Q, *Design Calculations and Analyses* Rev 002 ICN 002*, AP-3.15Q, *Managing Technical Product Inputs* Rev 004 ICN 004, LP-SI.11Q-BSC, *Software Management* Rev 000, and reviewed following AP-2.14Q, *Document Review* Rev 003.

Electronic data used in the preparation of this activity were obtained from the Yucca Mountain Site Characterization Project (YMP) Technical Data Management System (TDMS), as appropriate, in accordance with AP-SV.1Q, *Control of the Electronic Management of Information* Rev 001 ICN 001. AP-SV.1Q was also used to ensure the accuracy and completeness of the information generated by this report by: (1) controlling access to the information stored on personal computers with password protection, and (2) employing authorized process controls to ensure error-free data transfers. These process controls included verification of data by examining file check sums, file size and date, and/or making a thorough visual check of file contents or printouts. The personal computer files used in preparation of this report were stored on a network drive that is backed up daily per YMP standards. During the checking process, the accuracy and completeness of the data retrieved from the TDMS, developed during report activities, and reported in this document were verified, as applicable.

Upon completion of this work, files (including the information residing in DTNs created while preparing this report) were transferred to DVD-ROM/CD-ROM, appropriately labeled, and verified by using the above process controls. The DVD-ROMs/CD-ROMs were then transmitted to Document Control for transfer to the Records Processing Center, according to AP-17.1Q, *Records Management* Rev 003 ICN 002, which is the primary source for OCRWM records.

3. USE OF COMPUTER SOFTWARE

3.1   QUALIFIED COMPUTER SOFTWARE

Controlled and baselined software used in the development of this lithophysal rock mass calculation is identified in Table 3-1, including the software tracking number, version, operating environment, and range of use. Table 3-1 also includes a discussion of why the software was selected and describes any limitations on outputs from the software. Software documented in this section is appropriate for the applications used in this calculation, and is consistent with its intended use. Each software item was obtained from Software Configuration Management in accordance with LP-SI.11Q-BSC. All software was used only within the range of its validation as specified in the software qualification documentation, in accordance with LP-SI.11Q-BSC. All files associated with software used in this analysis have been attached to this report as noted in Appendix B on CD-ROM.

Table 3-1. List of Qualified Software Supporting the Lithophysal Rock Mass Calculation

Software Title/Version	Software Tracking Number	Operating Environment (Platform/Operating System)	Brief Description of Software (Range of Use/Selection/Limitations)
UDEC V3.1 (BSC 2002 [DIRS 161949])	10173-3.1-00	PC/Windows 2000	UDEC was used to characterize and model the mechanical behavior of lithophysal rock (Sections 6.5 and 6.7). Input to the program, for calibration purposes, consisted of laboratory test results of large-diameter cores of lithophysal rock described in Section 6.3.2.2. UDEC was selected for its capability of modeling fracturing and block slip in a plane strain condition. The software was used within its range of validation (BSC 2002 [DIRS 172041]). There are no known limitations on outputs.
EarthVision V.5.1 (Dynamic Graphics 2000 [DIRS 167994])	10174-5.1-00	SGI/IRIX 6.5	EarthVision was used to extract strike and dip of the top of the Tptpll in the ECRB Cross-Drift (used in Appendix A, Section A.5). Input to the program consists of the Geological Framework Model (GFM2000, DTN: MO0012MWDGFM02.002). EarthVision was selected for its capability of extracting specific data from GFM2000 and presenting the data in a common graphical format. EarthVision was not used to perform data manipulation in this report. The software was used within its range of validation (CRWMS M&O 2000 [DIRS 153526]). There are no known limitations on outputs.

Table 3-1. List of Qualified Software Supporting the Lithophysal Rock Mass Calculation (Continued)

Software Title/Version	Software Tracking Number	Operating Environment (Platform/Operating System)	Brief Description of Software (Range of Use/Selection/Limitations)
PFC2D V2.0 (BSC 2002 [DIRS 161950])	10828-2.0-00	PC/Windows 2000	PFC2D was used to characterize and model the behavior of lithophysal rock (Section 6.5). Input to the program, for calibration purposes, consisted of laboratory test results of large-diameter cores of lithophysal rock described in Section 6.3.2.2. PFC2D was selected for its capability of modeling behaviors of a rock material by combining behaviors of individual grain particles to simulate complicated non linear deformation of a rock material. The software was used within its range of validation (DOE 2004 [DIRS 171619]). There are no known limitations on outputs from PFC2D.
PFC2D V2.0 (BSC 2004 [DIRS 169930])	10828-2.0-01	PC/Windows 2000	This version of PFC2D was used to run impact analyses to confirm the initial PFC2D results (using software tracking number 10828-2.0-00). The initial PFC2D software qualification did not specifically identify the library of support functions (known as Fish functions) that are used within the code. This new version (software tracking number 10828-2.0-01) specifically qualifies FishTank 041b, which is the library of Fish functions included within the code. The impact assessments in *Drift Degradation Analysis* (BSC 2004 [DIRS 166107], Appendix Q, Section Q3) confirm that the results are identical using either the initial or new version of PFC2D.
PFC3D V2.0 (BSC 2002 [DIRS 160612])	10830-2.0-00	PC/Windows 2000	PFC3D was used to characterize and model the behavior of lithophysal rock (Section 6.5). Input to the program, for calibration purposes, consisted of laboratory test results of large-diameter cores of lithophysal rock described in Section 6.3.2.2. PFC3D was selected for its capability of modeling behaviors of a rock material by combining behaviors of individual grain particles to simulate complicated non linear deformation of a rock material. The software was used within its range of validation (DOE 2004 [DIRS 171620]). There are no known limitations on outputs from PFC3D.
PFC3D V2.0 (BSC 2004 [DIRS 169931])	10830-2.0-01	PC/Windows 2000	This version of PFC3D was used to run impact analyses to confirm the initial PFC3D results (using software tracking number 10830-2.0-00). The initial PFC3D software qualification did not specifically identify the library of support functions (known as Fish functions) that are used within the code. This new version (software tracking number 10830-2.0-01) specifically qualifies FishTank 041b, which is the library of Fish functions included within the code. The impact assessments in *Drift Degradation Analysis* (BSC 2004 [DIRS 166107], Appendix Q, Section Q3) confirm that the results are identical using either the initial or new version of PFC3D.

3.2   EXEMPT SOFTWARE

In addition to the above listed items, the standard functions of commercial off-the-shelf software, including Microsoft Excel 2000 SP-3, JMP Version 5.1 (statistical analysis software), and CorelDRAW Version 8.369, were used in this calculation. These software items were used to perform support calculation activities and visual representation as described in Section 6, and associated Appendices. Appendix B provides a listing of all calculation files (Table B-1), including the location in this report where specific details of the calculation can be found.

Software products such as operating systems, utilities, compilers and their associated libraries, spreadsheets, desktop database managers, graphical representations of data, computer aided design systems, and acquired software that is embedded in the test and measurement equipment and the standard functions of commercial off-the-shelf software products are exempt software products in accordance with LP-SI.11Q-BSC, *Software Management*, Section 2.1. Accordingly, Microsoft Excel 2000 SP-3, JMP Version 5.1, and CorelDRAW Version 8.369 are exempted software applications. All software in this category was performed on personal computers with a Pentium microprocessor and Microsoft Windows 2000 operating system. All supporting files are archived on CD-ROMs and submitted to the records processing center as part of the records package for this calculation.

MS Excel 2000 was used to determine parameter summary statistics, to plot data, and to determine linear and exponential fits to data. Standard functions of Excel were used in Section 6.

JMP was used to determine 95 percent confidence intervals around the linear fit of Young's modulus to lithophysal porosity for large core test results (Section 6.4.1).

CorelDRAW was used to edit, crop, and prepare a number of photographs and figures for insertion into MS Word 2000 for this calclucation in Section 6.

- Appendix A and the files listed in Appendix B document the use of standard functions of commercial off-the-shelf software in sufficient detail to allow independent repetition of the software in accordance with AP-3.12Q, *Design Calculations and Analyses*.

4. INPUTS

This section describes the direct inputs and criteria used for this calculation. The sources of these inputs, where they are used within this calculation, and the rationale for their selection are also discussed.

4.1 DIRECT INPUT

4.1.1 Field Measurements of Lithophysal Rock Features and Porosity

A detailed study of the lithostratigraphic features in the Topopah Spring lower lithophysal zone (Tptpll) exposed in ECRB Cross-Drift is provided in DTN: GS021008314224.002 and is described in the *Subsurface Geotechnical Parameters Report* (BSC 2003 [DIRS 166660], Section 8.8.4 and Attachment VII). The data package documents the distributions of size, shape, and abundance of lithophysal cavities, rims, spots, and lithic clasts. The methods used to document the distribution of lithostratigraphic features in this DTN include: full peripheral maps, detailed line surveys, small-scale fracture surveys, tape traverses, angular traverses, panel maps, and a large-lithophysae inventory. The percents of lengths and areas of features on the tunnel wall are typically referred to as "abundance." The basic data used is found in Microsoft Excel file, *Drift Deg AMR AF T-A-P Fit_V1_DBR.xls*, which can be found on the attached CD-ROM (Table B-1, Appendix B). The file has been modified from the original version (BSC 2003 [DIRS 166660], Attachment VIII, file *Drift Deg AMR AF T-A-P Fit.xls*) by replacing old estimates with new measured component porosity values (Section 4.1.2) and statistical summaries of the data. Since the large-lithophysal inventory data from the Tptpll is now complete (DTN: GS040608314224.001), this data has also been added to *Drift Deg AMR AF T-A-P Fit_V1_DBR.xls*. These data are used as direct inputs in Sections 6.2, 6.4, and Appendix A of this calculation. These geologic data are suitable for use in this calculation because they represent the available geologic information on the feature characteristics observed in the lithophysal units of the Topopah Spring Tuff.

4.1.2 Component Porosity of Tptpul and Tptpll Samples

Forty-seven core samples from the ESF and ECRB Cross-Drift boreholes were divided into their component parts (matrix-groundmass, rims, and spots, which resulted in 91 material specimens) and the porosity of each material specimen was determined (DTN: GS030483351030.001). As part of the *Subsurface Geotechnical Parameters Report* (BSC 2003 [DIRS 166660], Section 8.2.3), the data from this DTN was assigned appropriate lithostratigraphic units and statistically summarized. The following porosity values in Table 4-1 taken from the combined statistics for both Tptpul and Tptpll samples (BSC 2003 [DIRS 166660], Table 8-3) are used indirectly in Section 4.1.2 and as direct inputs in Section 6.2. These laboratory data are suitable for use in this calculation because they represent the available geologic information on the component porosities measured in the lithophysal units of the Topopah Spring Tuff. Other porosity determinations in the record do not distinguish between matrix groundmass and rim or spot material.

Table 4-1. Component Porosity Values for Lithophysal Rock

Component	Sample Count	Mean Porosity (cm^3/ cm^3)
90 to 100% Matrix Groundmass	39	0.103
90 to 100% Rims and Spots	35	0.300

Source: BSC 2003 [DIRS 166660], Section 8.2.3.1, Table 8-3

4.1.3   Laboratory Mechanical Test Data

A primary source document that compiles the mechanical testing data (Young's modulus and compressive strength are used in this calculation) on Topopah Spring Tuff is the *Subsurface Geotechnical Parameters Report* (BSC 2003 [DIRS 166660]). The specific data sources used that have porosity measurements associated with the tested rock specimens are listed in Table 4-2. These data are used as direct inputs in Sections 6.3 and 6.4 of this calculation. The results of laboratory testing used in this calculation to determine the mechanical properties of lithophysal rock are suitable for use because they represent the available mechanical test information from tests on specimens with porosity estimates and other large core specimens of lithophysal rock within the Topopah Spring Tuff. The results from large diameter samples better reflect the behavior of the in situ rock since they can include more representative lithophysae than smaller samples. Many of the companion porosity determinations are not yet qualified, but are used here since there are no known technical problems with the porosity values of record.

Table 4-2. DTNs of Tested Rock Specimens Having Porosity Data

Yucca Mountain Mechanical Tests on Rock Specimens with Porosity Data		
Source of Rock	**Size Specimen (Diameter)**	**DTNs**
Borehole cores	25 mm (1-in)	SNL02030193001.019, SNSAND83164600.000, SNSAND84110100.000, and SNSAND85070300.000
Borehole cores	50 mm (2-in) and 57 mm (2.2-in)	SNL02030193001.001, SNL02030193001.002, SNL02030193001.004, SNL02030193001.012, SNL02030193001.014, SNL02030193001.016, SNL02030193001.018, SNL02030193001.019, SNL02030193001.020, SNSAND80145300.000, SNSAND83164600.000, and SNSAND85070300.000
Busted Butte cores	50 mm (2-in)	SNL02040687003.001
Busted Butte cores	267 mm (10.5-in)	SNSAND84086000.000
ESF and ECRB Cross-Drift	290 mm (11.5-in)	SN0208L0207502.001, SN0211L0207502.002, SN0305L0207502.005, and SN0305L0207502.006
Yucca Mountain Mechanical Tests on Large-Size Rock Specimens without Porosity Data		
Busted Butte	various sizes	SN0306L0207502.008
ESF and ECRB Cross-Drift	146 mm (5.75-in)	SN0302L0207502.003 and SN0305L0207502.004

Source: BSC 2003 [DIRS 166660], Section 8.4. In addition to the above DTNs the DTN of qualified compressive strength values is MO0311RCKPRPCS.003 and DTN of qualified Young's Modulus values is MO0402DQRIRPPR.003.

4.1.4   In Situ Mechanical Field Testing

The mechanical in situ field tests conducted in lithophysal rock consisted of three slot tests, which are discussed in the *Subsurface Geotechnical Parameters Report* (BSC 2003 [DIRS 166660], Section 8.7.4.3). Source DTNs for each slot test are given in Table 4-3. These data are used as validation input data in Section 6.73 of this calculation. These field data are suitable for use in this calculation because they represent the available geologic information on the mechanical field behavior measured in the lithophysal units of the Topopah Spring Tuff.

Table 4-3. Source DTN Data for the In Situ Slot Tests

Slot Test #	Data Type	DTNs
1	Slot Test Results:	SN0207F4102102.001, SN0208F4102102.002
	Feature Abundances:	SN0301F4102102.007, SN0301F4102102.008
2	Slot Test Results:	SN0212F4102102.003, SN0212F4102102.004
	Feature Abundances:	SN0302F4102102.009, SN0302F4102102.010
3	Slot Test Results:	SN0301F4102102.005, SN0301F4102102.006
	Feature Abundances:	SN0303F4102102.011, SN0303F4102102.012

Source: BSC 2003 [DIRS 166660], Section 8.7.4.3

4.1.5   Strike, Dip, and Gradient of the Tptpll Along the ECRB Cross-Drift

The orientation of the top of the Tptpll (Tptpmn – Tptpll contact) at Station 14+44 is given by Mongano et al. 1999 [DIRS 149850], Table 1, p. 12, to be "270/07." Standard geological convention indicates that the strike (angle from north of a horizontal line in the inclined plane) of the Tptpll is 270 degrees and the dip (angle from horizontal measured in a vertical plane that is 90 degrees to the strike of the inclined plane) is 7 degrees. These data are used as direct inputs in Section A.5 of Appendix A. This strike and dip data is uncertain since there is not a distinct physical Tptpmn – Tptpll contact that can be measured, rather, the contact is transitional based on abundance of lithophysae and other lithostratigraphic features.

The gradient of the ECRB Cross-Drift is 1.5 percent (0.86°) from 07+73 to 16+02 and is 0.9 percent (0.52°) from 16+02 to 24+67 (Mongano et al. 1999 [DIRS 149850], pp. 3 and 6). These field estimates are suitable for use in this calculation because they represent the best available geometry information on the data of interest. The data is used as a direct input in Section A.5 of Appendix A.

4.1.6   PFC and UDEC Numerical Modeling of Lithophysal Rock

To complement the results of laboratory testing, numerical modeling of the mechanical behavior of lithophysal rock from the Topopah Spring Tuff (BSC 2003 [DIRS 166660], Sections 9.1, 9.2, and Attachments V, VI, and VIII) are used in Sections 6.5 and 6.6 to further characterize lithophysal rock mechanical behavior and to validate the proposed lithophysal rock categories and uncertainty bounds. For simulations of compression tests (1.0 m diameter) using the software code PFC2D, lithophysae were represented as circular (90 mm diameter circles), triangular, and star-shaped voids and as realistically dimensioned voids based on mapping observations in the ECRB Cross-Drift. For simulations of compression tests (1.0 m diameter) using the software code UDEC, lithophysae were represented as 90 mm diameter circles.

Specific data used from each compression test simulation are Young's modulus and peak compressive strength. For the simulations that used the software code PFC2D, these data are taken from the files *shapestudy.xls* and *shapestudy_bf2-bf4.xls* (BSC 2003 [DIRS 166660], Attachment VIII, CD#2 "PFC_runs\ShapeStudy\shapestudy.xls" and "PFC_runs\ShapeStudy\shapestudy_bf2-bf4.xls"). For the simulations that used the software code UDEC, these data are taken from the file *Summary2_newest.xls* (BSC 2003 [DIRS 166660], Attachment VIII, CD#20 "UDEC_CD1\Summary2_newest.xls"). These numerical results are suitable for use in this calculation because they represent the best available, simulated, mechanical behavior of lithophysal rock at the laboratory scale.

The UDEC numerical modeling of drift-scale mechanical behavior of lithophysal rock used in Section 6.7 are the result of modeling activities described in the *Drift Degradation Analysis* (BSC 2004 [DIRS 166107], Section 7.6, Appendices E and S). They are appropriate inputs because they model the strains developed in such rock as the rock is stressed to failure. They complement the results from laboratory testing by modeling larger samples (containing larger lithophysae) than can be physically tested, allowing a larger number of tests to be run at smaller relative cost, and making possible full control and monitoring of the testing process. These numerical results are suitable for use in this calculation because they represent the best available, simulated, mechanical behavior of lithophysal rock at the drift-scale.

4.2 REQUIREMENTS AND CRITERIA

The Yucca Mountain *Projects Requirements Document* (Canori and Leitner 2003 [DIRS 166275]) identifies the high-level requirements pertaining to the Yucca Mountain Project. This calculation was prepared to comply with licensing criteria provided in subparts of the U.S. Nuclear Regulatory Commission's rules governing the *Disposal of High-Level Radioactive Wastes in a Geologic Repository at Yucca Mountain, Nevada* (10 CFR Part 63 [DIRS 156605]). The *Yucca Mountain Review Plan, Final Report* (NUREG-1804, NRC 2003 [DIRS 163274]) lists the review methods and acceptance criteria that will be used by the U.S. Nuclear Regulatory Commission to determine whether the above technical requirements have been met. The pertinent requirements and NUREG-1804 acceptance criteria for this calculation are summarized in Table 4-4.

Table 4-4. Project Requirements for this Calculation

Requirement Number	Information Category	10 CFR 63 Reference	NUREG-1804 Reference
PRD-002/P-019	Completeness and Accuracy of Information	63.10	N/A
PRD-002/T-004	Content of Application	63.21	Section 1.5.3 Acceptance Criteria 1 and 2
PRD-002/T-011	Purpose and Nature of Findings	63.101	Section 2.2.1
PRD-002/T-012	Performance Objectives for the Geologic Repository Operations Area Through Permanent Closure	63.111	Section 2.1.1.7.3.3 Part II Acceptance Criterion 5
PRD-002/T-013	Requirements for Preclosure Safety Analysis	63.112	Section 2.1.1.1.3 Acceptance Criteria 5 and 8
PRD-002/T-015	Requirements for Performance Assessment	63.114	Section 2.2.1.3.1.3 Acceptance Criteria 1 to 3 Section 2.2.1.3.2.3 Acceptance Criteria 1 to 3 Section 2.2.1.3.3.3 Acceptance Criteria 1 to 3
PRD-002/T-018	Confirmation of Geotechnical and Design Parameters	63.132	Section 2.4.3 Acceptance Criteria 1 and 2

4.2.1 PRD-002/P-019: Completeness and Accuracy of Information

Relevant NRC requirements for site characterization content of the license application from Section 10 of 10 CFR Part 63 are:

(a) Information provided to the Commission by an applicant for a license or by a licensee, or information required by statute, or required by the Commission's regulations, orders, or license conditions to be maintained by the applicant or the licensee must be complete and accurate in all material respects.

The inputs, assumptions, calculated estimates of geotechnical parameters, stated limitations, and references presented in this calculation are deemed to be complete and accurate.

4.2.2   PRD-002/T-004: Content of Application

Relevant NRC requirements for site characterization content of the license application from Section 21 of 10 CFR Part 63 are:

(a) An application consists of general information and a Safety Analysis Report…

(b) The general information must include… (5) A description of work conducted to characterize the Yucca Mountain site.

(c) The Safety Analysis Report must include: (1) A description of the Yucca Mountain site, with appropriate attention to those features, events, and processes of the site that might affect design of the geologic repository operations area and performance of the geologic repository…. The information referred to in this paragraph must include… (ii) Information regarding the geology, hydrology, and geochemistry of the site, including geomechanical properties and conditions of the host rock…

Relevant NRC acceptance criteria from NRC 2003 [DIRS 163274], Section 1.5.3 are:

• Acceptance Criterion 1: The "General Information" Section of the License Application Contains an Adequate Description of Site Characterization Activities.

  (1) An adequate overview is provided of the site characterization activities related to geology; hydrology; geochemistry; geotechnical properties and conditions of the host rock…

• Acceptance Criterion 2: The "General Information" Section of the License Application Contains an Adequate Description of Site Characterization Results.

   (1) A sufficient understanding is provided of current features and processes present in the Yucca Mountain region…

Relevant NRC review methods for assessing compliance with the above criteria from NRC 2003 [DIRS 163274], Section 1.5.2 are:

• Review Method 2: Summary of Site Characterization Results.

  Confirm that the results of site characterization activities have been described…. An acceptable summary description should include areas such as:

  (1) An overview of geology, consistent with other site characterization summaries, that includes… (b) A description of the principal rock units… in the subsurface, and their stratigraphic relationships… (d) A description of geotechnical properties of stratigraphic units involved in the operation and safety of the proposed repository…

  (4) An overview of geotechnical properties and conditions consistent with other site characterization summaries, that includes… (b) A discussion of the results of site investigations necessary to characterize the engineering properties of the rock types present at the site, with particular emphasis on the host rock and its immediate environs necessary for the underground excavation of the geologic repository; and (c) A discussion and description of other site characterization work conducted to define the relevant

geotechnical properties and anticipated response/performance of both surface and subsurface facilities.

This calculation addresses these stipulated requirements and criteria by providing a summary of site characterization information useful for understanding and modeling the mechanical behavior of repository lithophysal rock mass. This report describes important geological features and their abundance in the Tptpul and Tptpll lithostratigraphic zones, summarizes the results of laboratory testing of lithophysal rock, and develops geotechnical properties for lithophysal rock mass suitable for modeling inputs. It thus provides information needed for a complete description of the site. This work is consistent with other site characterization data.

4.2.3 PRD-002/T-011: Purpose and Nature of Findings

Relevant NRC requirements for site characterization content of the license application from Section 101 of 10 CFR Part 63 are:

> (a) (2)…Proof that the geologic repository will conform with the objectives for postclosure performance is not to be had in the ordinary sense of the word because of the uncertainties inherent in the understanding of the evolution of the geologic setting, biosphere, and engineered barrier system…. The performance assessments and analyses should focus upon the full range of defensible and reasonable parameter distributions rather than only upon extreme physical situations and parameter values.

Relevant NRC instructions from NRC 2003 [DIRS 163274], Section 2.2.1 are:

> • The staff will review parameter ranges and distributions to evaluate whether they are technically defensible, whether they appropriately represent uncertainty, and the potential for risk dilution. …the U.S. Department of Energy may use conservative assumptions to simplify its approaches and data collection needs. However, a technical basis that supports the selection of models and parameter ranges or distributions must be provided.

This calculation describes the technical basis and justification of the mechanical rock mass parameters estimated for lithophysal rock. Since these parameters depend upon lithophysal porosity, this approach is simplified to create lithophysal rock mass categories linked to suitable ranges of lithophysal porosity. For each lithophysal rock mass category there corresponds an estimated uniform distribution of Young's modulus and trapezoidal (upper to lower bound) distribution of uniaxial compressive strength. These distributions are used in developing the subsurface design, developing the preclosure safety analysis, and assessing the postclosure performance of the repository.

4.2.4 PRD-002/T-012: Performance Objectives for the Geologic Repository Operations Area Through Permanent Closure

As described in Section 2 this calculation is relevant to a number of systems and subsystems classified as "Safety Category (SC)." The relevant NRC requirements for design to meet preclosure performance objectives from Section 111 of 10 CFR Part 63 are:

(c) *Preclosure safety analysis*. A preclosure safety analysis of the geologic repository operations area that meets the requirements specified at Section 63.112 must be performed….

The relevant NRC acceptance criterion from NRC 2003 [DIRS 163274], Section 2.1.1.7.3.3 for II. *Designs and Design Analyses for Structures, Systems… That are Safety Related for Subsurface Facility* is:

- Acceptance Criterion 5: Design Analyses Use Appropriate Models and Site-Specific Properties of the Host Rock, and Consider Spatial and Temporal Variation and Uncertainties is Such Properties.

  (4) For continuum rock-mass modeling, the values for rock-mass elastic parameters (Young's modulus and Poisson's ratio) and strength parameters (friction angle and cohesion) are consistent with properly interpreted site-specific data. If the parameter values are obtained through empirical correlations with a rock quality index, the empirical equations used are appropriate for the site and are applied correctly, and the values of the index are consistent with site-specific data. If intact-rock-scale values are used, the bases for application of the values to the rock-mass scale are adequate;

  (6) For discontinuum modeling, the selection of stiffness and strength parameters for rock blocks between any fractures that are explicitly represented in the model are appropriate, and accounts for fractures that are not explicitly represented;

  (9) Uncertainties in rock-mass and fracture-mechanical properties are adequately estimated, and considered in both continuum and discontinuum modeling;

The relevant NRC review method for design in addition to the above criterion from NRC 2003 [DIRS 163274], Section 2.1.1.7.2.2 "Design Methodologies" is:

- Review Method 1: Geologic Repository Operations Area Design Methodologies.

  …Verify that uncertainties associated with the proposed methodologies have been adequately addressed. If the design methodologies depend on site-specific test data, confirm that such data are available. Also, verify that any analytical or numerical modeles used to support the design methodologies have been verified, calibrated, and validated. Verify that any assumptions or limitations relating to the proposed methodologies are identified, and that their implications for the design have been adequately analyzed and documented.

This calculation develops estimates of lithophysal rock mass mechanical properties and is based on site-specific rock properties. The technical bases for the inputs, the assumptions, parameter uncertainties and variations, supporting numerical modeling, calculated parameter estimates, validation of parameter distributions, and associated limitations for use of the parameters have been provided in this calculation.

4.2.5 PRD-002/T-013: Requirements for Preclosure Safety Analysis

As described in Section 2 this calculation is relevant to a number of systems and subsystems classified as "Safety Category (SC)." Accordingly, the relevant NRC requirements for preclosure safety analysis from Section 112 of 10 CFR Part 63 are:

(a) A general description of the structures, systems… and process activities at the geologic repository operations area…

(c) Data pertaining to the Yucca Mountain site… used to identify naturally occurring and human-induced hazards at the geologic repository operations area.

Relevant NRC acceptance criteria relative to the input data supporting the design and safety analysis of the repository from NRC 2003 [DIRS 163274], Section 2.1.1.1.3 are:

- Acceptance Criterion 5: The License Application Contains Descriptions of the Site Geology and Seismology Adequate to Permit Evaluation of the Preclosure Satety Analysis and the Geologic Repository Operations Area Design.

    (1) The license application provides sufficient data on the geology of the site to support the preclosure safety analysis and geologic repository operations area design, including the stratigraphy and lithology for the entire surface and subsurface construction area;

    (2) Site characterization data adequately include rock mechanics properties based on *in situ* and laboratory test results for the rock formations where major construction activities will take place. Collection and processing of these data are based on accepted industry techniques;

    (3) Rock mechanics testing data adequately support the license application analyses of the stability of subsurface materials.

- Acceptance Criterion 8: The License Application Contains Site-Sufficient Geochemical Information to Support Evaluation of the Preclosure Satety Analysis and the Geologic Repository Operations Area Design.

    (3) Potential geochemical alterations to the rock fractures and the rock matrix, through heating or other processes that might significantly alter geomechanical rock mass properties, are adequately characterized.

Relevant NRC review methods for assessing compliance with the above criteria from NRC 2003 [DIRS 163274], Section 2.1.1.1.2 are:

- Review Method 5: Descriptions of Site Geology and Seismology.

    Verify that the U.S. Department of Energy has provided sufficient data on the geology of the site to support the preclosure safety analysis and geologic repository operations area design…. Confirm that site characterization data include geomechanical properties and conditions of host rock, based on *in situ* and laboratory test results for the rock formations, where major construction activities will take place. Collection and processing of these data should be based on accepted industry techniques and standards. Verify that rock mechanics testing data support the license application analyses of the

stability of subsurface materials. Note that evaluation of the sufficiency of data and appropriateness of design parameters will be conducted using the appropriate subsection of Section 2.1.1.7… of the Yucca Mountain Review Plan.

- Review Method 8: Site Geochemical Information

    Evaluate the description of the geochemical information at Yucca Mountain that is relevant to the preclosure safety analysis and geologic repository operations area design, to confirm that it is adequate, including items such as:

    (3) Any geochemical alterations to the rock fractures and rock matrix through heating or other processes that might significantly alter geomechanical rock mass properties.

This calculation provides estimates of lithophysal rock mass properties for repository rocks (Tptpul and Tptpll) based on site-specific data and numerical modeling that can be utilized to design ground support and for modeling rockfall during the preclosure period. Proper use of these mechanical parameters requires a description of the representative in situ lithophysal porosity for the repository rock, which is provided in this calculation, along with a suggested method of spatially modeling the lithophysal porosity. The assumptions employed in developing the rock mass parameter characterizations are provided, along with the resulting uncertainties and spatial variability associated with these parameters, and guidelines for appropriate use of the parameter information. The potential geochemical alterations that may affect the rock matrix are discussed, and it is concluded that no geochemical alterations will significantly alter the lithophysal geomechanical rock mass properties during preclosure.

4.2.6 PRD-002/T-015: Requirements for Performance Assessment

Relevant NRC requirements for performance assessment from Section 114 of 10 CFR Part 63 are:

Any performance assessment used to demonstrate compliance with Sec. 63.113 must: (a) Include data related to the geology, hydrology, and geochemistry... of the Yucca Mountain site… used to define parameters and conceptual models used in the assessment. (b) Account for uncertainties and variabilities in parameter values and provide for the technical basis for parameter ranges, probability distributions, or bounding values used in the performance assessment. (c) Consider alternative conceptual models of features and processes that are consistent with available data and current scientific understanding…

Relevant NRC acceptance criteria relative to the input data supporting the degradation of engineered barriers (Section 2.2.1.3.1.3) are discussed below. Similar requirements are found in the mechanical disruption of engineered barriers (Section 2.2.1.3.2.3), the quantity and chemistry of water contacting engineered barriers and waste forms (Section 2.2.1.3.3.3), and possibly other sections from NRC 2003 [DIRS 163274].

- Acceptance Criterion 1: System Description and Model Integration are Adequate

    (2) Assessment abstraction of the degradation of engineered barriers uses assumptions, technical bases, data, and models that are appropriate and consistent with other related

U.S. Department of Energy abstractions…. The descriptions and technical bases provide transparent and traceable support for the abstraction of the degradation of engineered barriers.

- Acceptance Criterion 2: Data Are Sufficient for Model Justification

  (1) Parameters used to evaluate the degradation of engineered barriers in the license application are adequately justified…. The U.S. Department of Energy describes how the data were used, interpreted, and appropriately synthesized into the parameters;

  (2) Sufficient data have been collected on the characteristics of the engineered components, design features, and the natural system to establish initial and boundary conditions for abstraction of degradation of engineered barriers.

- Acceptance Criterion 3: Data Uncertainty is Characterized and Propagated Through the Model Abstraction.

  (1) Models use parameter values, assumed ranges, probability distributions, and/or bounding assumptions that are technically defensible, reasonably account for uncertainties and variabilities, and do not result in an under-representation of the risk estimate;

  (3) For the selection of parameters used in conceptual and process-level models of engineered barrier degradation that can be expected under repository conditions, assumed range of values and probability distributions are not likely to underestimate the actual degradation and failure of engineered barriers as a result of corrosion;

  (5) Where sufficient data do not exist, the definition of parameter values and conceptual models, used by the U.S. Department of Energy, is based on appropriate use of other sources, such as expert elicitation…. If other approaches are used, the U.S. Department of Energy adequately justifies their use.

The relevant NRC review methods for assessing compliance with the above criteria from NRC 2003 [DIRS 163274], Sections 2.2.1.3.1.2, 2.2.1.3.2.2, and 2.2.1.3.3.2 are:

- Review Method 1: Model Integration

  …Examine assumptions, technical bases, data, and models used by the U.S. Department of Energy in the total system performance assessment abstraction of degradation process models for consistency with other related U.S. Department of Energy abstractions. Evaluate whether the descriptions and technical bases provide transparent and traceable support for the abstraction of the degradation of the engineered barriers….

- Review Method 2: Data and Model Justification

  Evaluate the sufficiency of the experimental and site characterization data used to support parameters used in conceptual models, process-level models, and alternative conceptual models, considered in the total system performance assessment abstraction of degradation of engineered barriers….

Verify whether sufficient data have been collected to adequately model degradation processes, as well as characteristics of the geochemistry, hydrology, design features, and thermal effects, to establish initial and boundary conditions for the total system performance assessment abstraction of degradation of engineered barriers. For example, mechanical property data should cover the range of anticipated temperatures and microstructural conditions….

Evaluate and confirm that data used to support the U.S. Department of Energy total system performance assessment abstraction of degradation of engineered barriers are based on appropriate techniques, and are adequate for the accompanying sensitivity/uncertainty analyses. Evaluate the need for additional data, based on the sensitivity analyses….

- Review Method 3: Data Uncertainty

Evaluate the technical bases for parameter values, assumed ranges, probability distributions, and bounding values used in conceptual models, process models, and alternative conceptual models considered in the total system performance assessment abstraction of degradation of engineered barriers. The reviewer should verify that the technical bases support the treatment of uncertainty and variability of these parameters in the performance assessment….

Confirm that the U.S. Department of Energy has used parameters, in the abstraction of degradation of engineered barriers, that are based on laboratory experiments, field measurements, natural analog or industrial analog research… conducted under conditions relevant to the range of environmental conditions in the emplacement drifts located in the unsaturated zone at Yucca Mountain….

Verify that the U.S. Department of Energy appropriately established possible statistical correlations between parameters. Verify that an adequate technical basis or bounding argument is provided for neglected correlations

This calculation provides estimates of lithophysal rock mass properties for repository rocks (Tptpul and Tptpll) based on site-specific data and numerical modeling that can be utilized for modeling rockfall during the postclosure period. Proper use of these mechanical parameters requires a description of the representative in situ lithophysal porosity for the repository rock, which is provided in this calculation, along with a suggested method of spatially modeling the lithophysal porosity. The assumptions employed in developing the rock mass parameter characterizations are provided, along with the resulting uncertainties and spatial variability associated with these parameters, and guidelines for appropriate use of the parameter information. The potential geochemical alterations that may affect the rock matrix are discussed, and it is concluded that no geochemical alterations will significantly alter the geomechanical lithophysal rock mass properties during postclosure.

4.2.7 PRD-002/T-018: Confirmation of Geotechnical and Design Parameters

Section 131 of 10 CFR Part 63 lays out the general requirements of the performance confirmation program, which begins during site characterization and provides the baseline information of parameters that need to be monitored and analyzed. Relevant NRC requirements for the geotechnical and design parameters of the license application from Section 132 of 10 CFR Part 63 are:

(a) During repository construction and operation, a continuing program of surveillance, measurement, testing, and geologic mapping must be conducted to ensure that geotechnical and design parameters are confirmed…

(b) Subsurface conditions must be monitored and evaluated against design assumptions.

(c) Specific geotechnical and design parameters to be measured or observed, including any interactions between natural and engineering systems and components, must be identified in the performance confirmation plan.

Relevant NRC acceptance criteria from NRC 2003 [DIRS 163274], Section 2.4.3 are:

- Acceptance Criterion 1: The Performance Confirmation Program Meets the General Requirements Established for Such a Program.

    (1) The objectives of the performance confirmation program are consistent with the general requirements in that the program will provide data to indicate whether: (i) actual subsurface conditions encountered and changes in those conditions during construction and waste emplacement operations are within the limits assumed in the licensing review; and (ii) natural and engineered systems and components that are designed or assumed to operate as barriers after permanent closure are functioning as intended and expected. The performance confirmation plan provides sufficient technical information and plans for *in situ* monitoring, laboratory and field testing, and *in situ* experiments to carry out the objectives in that: (a) It identifies the natural and engineered systems and components that are designed or assumed to operate as barriers… (c) It identifies specific geotechnical and design parameters, pertaining to natural systems and components that are assumed to operate as barriers after permanent closure including natural processes and any interactions between natural and engineered systems and components…

    (3) The U.S. Department of Energy will implement the performance confirmation program in a manner consistent with the general requirements in that: (b) It provides baseline information and analysis of that information on those parameters and natural processes pertaining to pertaining to natural systems and components that are assumed to operate as barriers after permanent closure that may be changed by site characterization, construction, and operations.

- Acceptance Criterion 2: The Performance Confirmation Program to Confirm Geotechnical and Design Parameters Meets the Requirements Established for Such a Program.

(1) The performance confirmation plan establishes… (a) Geotechnical and design parameters the U.S. Department of Energy will monitor and analyze are selected using a performance-based method that focuses on those parameters that could affect health and safety.… (c) The baseline of selected geotechnical and design parameters was determined using analytical or statistical methods appropriate for the particular parameter; (d) The baseline of selected geotechnical and design parameters considered all data available at the time of the submittal.

Relevant NRC review methods for assessing compliance with the above criteria from NRC 2003 [DIRS 163274], Section 2.4.2 are very similar in content to the stated acceptance criteria.

Since the mechanical parameters estimated in this calculation are inputs to subsurface design, preclosure safety analysis, and postclosure performance assessment, these geotechnical parameters are candidates for performance confirmation. In this regard it is important to confirm the assumptions of Section 5 on which the parameter estimates depend by continuing to characterize repository rock lithophysal porosity, validate the two-component conceptual material model, continue large-scale in situ mechanical testing in lithophysal rock, and continue to develop and validate the model estimating spatial variability of lithophysal porosity across the repository. Furthermore, the relationship between porosity and mechanically tested specimens needs to be confirmed by: continued laboratory testing of large-diameter core samples, full qualification of the companion specimen porosity data, and continued numerical modeling of lithophysal rock to address the limitations stated in Section 6.5.

4.3   CODES, STANDARDS, AND REGULATIONS

There are no specific codes or standards that have been identified as being applicable to this calculation. The regulation applicable to the development of this calculcation is 10 CFR Part 63 [DIRS 156605].

5. ASSUMPTIONS

Assumptions are used in this calculation, in the absence of direct confirming data or evidence, to develop estimates of lithophysal rock mass properties. These assumptions are described in this section.

5.1 OBSERVED CHARACTERIZATION FROM THE ECRB CROSS-DRIFT REPRESENTS THE VARIATION OF LITHOPHYSAL POROSITY EXPECTED IN THE REPOSITORY HOST LITHOPHYSAL ROCK

Assumption: The lithophysal rock in the repository area is both similar in geologic structure (Figure 6.1-3) and laterally continuous, having formed under similar depositional, pressure, and temperature conditions. More specifically, the lithophysae data that was developed from the ECRB Cross-Drift measurements of the Tptpll lithostratigraphic unit provides an adequately representative and statistically reliable sampling of the horizontal and vertical spatial variation of lithophysal porosity across lithophysal rock in the repository host-horizon Tptpll unit.

Used: This assumption is used in Section 6.2, Characterization of the Lithophysal Host Rock Porosity, and Appendix A, Simulation of Lithophysal Porosity Spatial Variation, a calculation estimating the vertical and horizontal variations in lithophysal porosity across parts of the repository area. The range of porosity is subsequently used in Sections 6.4 and 6.6, where the ranges of rock mass categories for lithophysal rock are developed.

Basis: The Topopah Spring Tuff was created by the cooling and welding of a regionally extensive and large volume (about 1200 km^3) of pyroclastic flow deposits that derived from a massive caldera eruption located north of the repository site, which occurred approximately 12.8 million years ago (BSC 2004 [DIRS 169734], pp. 3-8, 2-11, 2-12, 3-18, 3-19, 3-29; Sawyer et al. 1994 [DIRS 100075], pp. 1305-1306; Sawyer et al. 1995 [DIRS 104580], p. 18; Schuraytz et al. 1989 [DIRS 107248], p. 5927, and an older study by Byers et al. 1976 [DIRS 104639], pp. 21-25, 66). Such huge eruptions in the geological record are characteristic of large caldera systems that can generate extensive (to distances of tens of kilometers), large-volume (from tens to a few thousand cubic kilometers of ejecta) pyroclastic flow sheets in one individual eruption (Sparks et al. 1997 [DIRS 144352], pp. 34 and 145). For comparison, the largest historic eruption occurred in 1815 at Tambora volcano in Indonesia when 50 km^3 of magma was ejected (Sparks et al. 1997 [DIRS 144352], p. 34, less than 5 percent of the ejecta volume estimated for the Topopah Spring Tuff).

To formulate a reasonable argument that the host rock for the repository is structurally and laterally homogenous, four conditions involving the newly deposited ignimbrite material need to be shown to be reasonably true: (1) the Topopah Spring pyroclastic flow deposit(s) in the repository area consisted of a relatively homogeneous material, (2) the pyroclastic flow material accumulated roughly in a horizontal layer across the repository area, (3) the top and bottom boundary temperature conditions were similar across the repository area, and (4) the same fundamental set of physical governing laws applied to the material during cooling, welding, and development of rock features.

Condition 1. The source caldera for the Topopah Spring Tuff lies within the southwestern Nevada volcanic field and is assumed to be in the general vicinity of the Timber Mountain caldera complex, but its exact location is buried and remains uncertain (Sawyer et al. 1994 [DIRS 100075], pp. 1304-1308) and Sawyer et al. 1995 [DIRS 104580], p. 18). The center and southern boundary of the Timber Mountain Caldera Complex are approximately 25 km and 10 km north of the repository footprint center, respectively (determined from BSC 2004 [DIRS 169734], Figures 2-4, 2-9, and 3-20). Given the distance from the volcanic source and a repository footprint length (north-south direction) of approximately 5 km (3 miles) (BSC 2003 [DIRS 165572], Table 7 and Figure 10), it is likely that the pyroclastic flow material deposited over the repository area was relatively homogeneous in composition (BSC 2004 [DIRS 169734], pp. 2-12 and 2-13). Assuming that the source magma itself is essentially a homogenous viscous fluid, the fluid mechanics of pyroclastic flows involve fluidization and mixing of the ejecta, which would have contributed to a homogeneous flow deposit (Sparks et al. 1997 [DIRS 144352], pp. 142-144).

However, Lipman et al. 1966 [DIRS 100773]; Byers et al. 1976 [DIRS 104639]; Schuraytz et al. 1989 [DIRS 107248] have concluded that the source magma body that produced the Topopah Spring pyroclastic flow sheet was composed of two magmas of different geochemistry, separated by an abrupt boundary. The resulting pyroclastic flow sheet was also compositionally zoned: a cooler and less dense phenocryst-poor high-silica rhyolite flow material transitions gradually into an overlying hotter and more dense phenocryst-rich quartz latite. In terms of the mechanical behavior of the tuff, both the rhyolite and latite compositions cooled and developed strong and stiff matrix groundmass as compared to rock with significant rim, spot, or lithophysae content. Further, the repository host lithostratigraphic units of interest in this calculation all lie within the crystal-poor rhyolite rock (Buesch et al. 1996 [DIRS 100106], p. 10). As a result, the pyroclastic flow sheet can still be considered homogeneous for the purposes of this analysis.

Condition 2. In volcanic units, thickness tends to be systematically distributed over large areas as a function of factors including magma type, eruptive process, wind speed and direction, preexisting topography, and erosion (BSC 2004 [DIRS 170029], Section 6.4, p. 6-16). The following geologic concepts pertaining to the thickness of the Topopah Spring Tuff and its lithostratigraphic zones are deemed suitable (BSC 2004 [DIRS 170029], Section 6.4.1, p. 6-19): (a) volcanogenic rocks generally thin away from their sources; (b) the major volcanic deposits at Yucca Mountain generally filled in preexisting topography, so that the top of a formation may have been originally more planar than the base; (c) the top of a formation may have eroded after deposition; (d) the lower vitric zones of the Topopah Spring Tuff blanketed preexisting topography and began the process of filling in topographic lows; and (e) the Topopah Spring Tuff lithophysal and nonlithophysal rocks were produced by multiple processes and, although approximating a stratiform geometry, these lithostratigraphic zones may have irregular thickness distributions.

Even though the Topopah Spring Tuff is considered to be a single cooling unit derived from a single continuous eruption of one magma chamber, other conditions could have affected deposit thickness (Lipman et al. 1966 [DIRS 100773] and Schuraytz et al. 1989 [DIRS 107248], pp. 5927-28, 5939, Buesch and Spengler (1998 [DIRS 101433], p. 21). For instance, a short eruption hiatus could have led to multiple flow events, an abrupt increase or decrease in magma discharge rate, or a change in the composition of the erupted magma could all affect the lateral

variation of the pyroclastic flow deposit thickness. Lipman et al. 1966 ([DIRS 100773], p. F7) concluded that a compound cooling unit is indicated by the repetition of porous zones (containing abundant vapor-phase material and lithophysae) and contiguous densely-welded (nonporous) zones. Although multiple flow deposits over a short time frame could contribute to some zonal variations in the tuff, these lateral variations would not undermine the assumption of this section that the resulting tuff is structurally similar and laterally continuous. In particular, for the area of Yucca Mountain, Lipman et al. 1966 ([DIRS 100773], pp. F14, F16, and F26) recognizes two voluminous early rhyolitic flow units that may correlate with the creation of the laterally continuous Tptpul and Tptpll lithophysal units identified by Buesch et al. 1996 ([DIRS 100106], p. 20). Or both lithophysal units may have developed from one pyroclastic flow event, in which compaction (welding) of the vitric deposit led to the transfer of vapor and the creation of lithophysae above and below the area of maximum initial compaction, near the stratigraphic center of the deposit forming the middle nonlithophysal zone (Buesch and Spengler 1998 [DIRS 101433], p. 21).

Condition 3. Before the eruption the ground temperature would have been similar across the repository area. After deposition of the Topopah Spring Tuff source material, atmospheric conditions affecting the top of the deposit would have been similar over the succeeding time. The mechanisms of eruption (explosive or effusive) and transport (pyroclastic flow or fallout, or lava flow) influence the geometry and type of resulting deposit, and this determines the initial temperature of the deposit that ultimately governs whether (1) the rock can weld, (2) the deposit is composed of volcanic glass or is crystallized to a high-temperature mineral assemblage, or (3) fractures and other features can develop (Buesch and Spengler 1999 [DIRS 107236], p. 44). The bulk of the pyroclastic flow material that formed the repository units was the cooler rhyolite material and estimated temperatures for this vitric rock ranged from about 700°C to 800°C (Schuraytz et al. 1989 [DIRS 107248], pp. 5933-5934).

Condition 4. The scientific principles of causality and admissibility dictate that the same physical laws of nature governing the processes of welding (material consolidation under pressure), crystallization, formation of lithophysae, vapor movement, and fracturing were active throughout the entire pyroclastic deposit during creation of the Topopah Spring Tuff. Buesch and Spengler (1998 [DIRS 101433], pp. 20-21) describe some of these processes and the development of lithostratigraphic features in lithophysal and nonlithophysal zones and subzones (Figure 1-2).

Consideration of these conditions reveals that spatial variation of ignimbrite material properties, boundary conditions, and loading forces occurs primarily in the vertical direction. There is no reason to suspect significant spatial variation of any of these conditions laterally, or accordingly, in the final resulting rock formation. This analysis is valid for the Topopah Spring Tuff formation generally in the repository footprint only, and not for localized areas of rock with dimensions of about a decimeter and smaller, which can approach the scale of individual rock features such as fractures or large lithophysae.

Confirming the Assumption: Across the approximately 5 mile repository footprint length, the Topopah Spring Tuff is estimated to have a relatively uniform thickness (DIRS 170029], Figure 6-9; and BSC 2004 [DIRS 169734], Figures 3-9 and 3-10) ranging from about 370 m (1210 feet) at its northern point to approximately 310 m (1010 feet) to the south (BSC 2004 [DIRS 170029],

Section 6.5.1.4, Figure 6-15). Estimates of the thickness of the repository host horizon across the repository footprint range from 220 m (730 ft) in the north to 195 m (640 ft) to the south, with a further 30 m (100 ft) reduction locally at the southern tip of the footprint (BSC 2004 [DIRS 170029], Section 6.5.1.4, Figure 6-18).

The stratiform geometry of the lithostratigraphic zones in the Topopah Spring Tuff occur throughout the repository area (Buesch et al. 1996 [DIRS 100106], pp. 8-10 and 19-21; Buesch et al. 1996 [DIRS 101202], pp. 1-5, 22, 26-27, 39, and 56-57; Buesch and Spengler 1999 [DIRS 107236], p. 31; and BSC 2004 [DIRS 169734], Figures 3-9 and 3-10, pp. F3-11 and F3-12). Not only are Topopah Spring Tuff lithostratigraphic units mappable and laterally continuous, but so are many of the lithostratigraphic subzones (Figure 1-2) such as the subzones of the Tptpmn (Buesch et al. 1996 [DIRS 100106], p. 21; Buesch and Spengler 1998 [DIRS 101433]), although some subzones might not occur across the entire repository area (Buesch and Spengler 1998 [DIRS 101433], pp. 16 and 22). Variations in the orientation of lithostratigraphic contacts (Mongano et al. 1999 [DIRS 149850], Table 1) and the abundance (or percent) of lithostratigraphic features in the lower lithophysal zone, including lithophysal cavity porosity (BSC 2003 [DIRS 166660], Attachment VII), are consistent with the ECRB Cross-Drift transecting a dipping lithostratigraphic section (Appendix A, Section A.5).

The variation of lithophysal porosity in Sections 6.1 and 6.2 is based substantially on the "fitted" cavity data from Figure VII-15, Attachment VII of the *Subsurface Geotechnical Parameters Report* (BSC 2003 [DIRS 166660]). The 5 m averaged large-lithophysae inventory (brown curve of Figure 6.1-2a) has recently been included as part of the lithophysal and total porosity curves (Figure 6.1-2b). The variation of lithophysal porosity in Sections 6.1 and 6.2 together with the frequency of lithophysal porosity associated with the five rock mass categories (Figure 6.4-8) are believed to be representative of the repository Tptpll rock.

A number of historical boreholes have been drilled around the boundaries of repository footprint that extend down to the repository host horizon. An updated analysis of the geophysical and caliper data will be helpful to test this assumption of the lateral homogeneity of lithophysal porosity. Also, short of new excavations into the repository area, mapping of the historical or new boreholes may provide the best information to confirm the validity of this assumption.

5.2 THE CURRENT TPTPLL CHARACTERIZATION FROM THE ECRB CROSS-DRIFT ADEQUATELY REPRESENTS THE DISTRIBUTION AND VARIATION OF LITHOPHYSAL POROSITY EXPECTED FOR THE TPTPUL LITHOSTRATIGRAPHIC UNIT

Assumption: For determining a suitable range of lithophysal rock mechanical properties, the quantified lithophysae abundance data obtained by mapping the Tptpll unit is assumed to be statistically similar to the distribution and spatial variation of lithophysal porosity of the Tptpul unit.

Used: This assumption is used in Section 6.2, Characterization of the Lithophysal Host Rock Porosity, and Appendix A, Simulation of Lithophysal Porosity Spatial Variation. The range of porosity is subsequently used in Sections 6.4 and 6.6, where the ranges of rock mass categories for lithophysal rock are developed.

Basis: Approximately 4 percent of the emplacement drifts are planned to be located within the Tptpul lithostratigraphic unit (81 percent in the Tptpll, BSC 2003 [DIRS 166660], Section 5.4), but a detailed study of lithostratigraphic features for the Tptpul is not yet available. It is assumed that the ECRB Cross-Drift Tptpul characterization of lithophysae will not vary significantly from the current Tptpll characterization.

A description of the abundance of lithophysal cavities in the Tptpul and Tptpll zones is given in Mongano et al. (1999 [DIRS 149850]). The central and lower parts of the Tptpul are part of the repository host horizon (Figure 1-1), and lithophysae were reported to comprise 25 to 40 percent of the rock, but as much as 60 percent locally (Mongano et al. 1999 [DIRS 149850], p. 17). The Tptpll was estimated by Mongano et al. to be composed of from 5 to 30 percent lithophysae (Mongano et al. 1999 [DIRS 149850], pp. 25 and 29). Figure 13 of the Mongano et al. report (1999 [DIRS 149850], p. 77), clearly shows an average greater percentage of lithophysae in the Tptpul versus the Tptpll. The unqualified Mongano et al. data indicate that assumption 5.2 may not be valid, but since only a small portion of the Tptpul is in the repository, it may not be significant.

Confirming the Assumption: A detailed study of the lithostratigraphic features to characterize the Tptpul zone will be out shortly. These characterization results can be directly compared to the Tptpll study results. Future characterizations of lithophysal rock involving geophysical techniques and mapping of both boreholes and new underground openings will help confirm the current Tptpul and Tptpll variations of porosity.

5.3   LITHOPHYSAL ROCK IS DESCRIBED BY A TWO-COMPONENT CONCEPTUAL MATERIAL MODEL

Assumption: Lithophysal rock is conceptualized as being a composition of (1) solid matrix and (2) air-filled lithophysal voids (lithophysae). In terms of the mechanical behavior of the rock matrix, the explicit presence of preexisting fractures and spot or rim features in the lithophysal rock are ignored. An unknown number of small fractures or amount of spot or rim material may be present in some laboratory samples, which may be influencing the reported laboratory mechanical behavior, but this is ignored in the analysis. In terms of physical properties, the rock porosities of interest for this calculation are the: matrix porosity (combining the matrix groundmass and rim or spot porosities), the lithophysal porosity, and the total porosity.

Used: This assumption is used throughout this calculation, both for laboratory analysis of data and numerical modeling of lithophysal rock.

Basis: Due to the limited physical characterization of rock samples and for simplicity and ease of numerical modeling, a two-component material model is adopted (solid matrix and voids) for preliminary characterization of lithophysal rock mass behavior. Accordingly, lithophysal rock mechanical behavior, ignoring fractures, is based primarily on the geometry of matrix rock with lithophysal voids. However, it is well known that besides the matrix groundmass and cavities, lithophysal rock at the drift scale and smaller may also composed of significant amounts of spot or rim material and some fractures. A description of the abundance of spots and rims ("vapor-phase features") in the Tptpul and Tptpll zones is given in Mongano et al. (1999 [DIRS 149850]). The central and lower parts of the Tptpul are part of the repository host horizon

(Figure 1-1), and vapor-phase features were reported to comprise 10 to 40 percent of the rock (Mongano et al. 1999 [DIRS 149850], p. 17). The amount of vapor-phase features in the Tptpll was estimated by Mongano et al. to be between 3 and 12 percent, and locally 15 to 40 percent of the rock (Mongano et al. 1999 [DIRS 149850], p. 25). Buesch measured slightly smaller abundances of rims and spots (than Mongano et al.) in the Tptpll (Figure 6.1-1).

The *rock-matrix* material-model component includes both matrix groundmass and rim or spot materials. The matrix groundmass consists of solid minerals and their associated intergranular pore space. Typically, matrix groundmass porosity in the Tptpul and Tptpll zones has been measured to be about 10 percent (BSC 2003 [DIRS 166660], Section 8.2.3, Table 8-3). The porosity of rim or spot (also termed vapor-phase altered) material in the Tptpul and Tptpll zones has been measured to be significantly larger, about 30 percent (BSC 2003 [DIRS 166660], Section 8.2.3, Table 8-3). The mechanical properties of rim and spot material have not yet been determined in the laboratory or field, however, informal reports from field and laboratory workers indicate that rim or spot material tends to fall apart easily, and doesn't appear to have significant strength.

Although the material model ignores preexisting rock fractures, rims, and spots; small fractures and rim or spot material may be present in tested rock specimens, and so their effects on mechanical behavior may be included as part of laboratory characterization. To the extent that these effects are represented in the laboratory mechanical characterization, they will also be represented in the numerical modeling since model calibration was based on laboratory testing. On the other hand, many small and large-diameter cores could not be recovered intact, due to the sampling procedures used and presumably due to the presence of fractures, lithophysae, and spot or rim material. As a result, core samples of rock with significant-size fractures, lithophysae, and/or spots and rims (relative to the coring diameter) would likely result in broken cores, and bias the resulting intact laboratory samples for these effects. The extent to which the population of laboratory samples may be representative or biased against the effects of spot or rim material and fractures is not currently known. If the underrepresentation of spots and rims is significant in the determination of matrix porosity and the mechanical intact rock behavior, then the distributions (and uncertainty) of elastic modulus and uniaxial compressive strength of intact rock would likely be overestimated. Since the lithophysal rock mass mechanical behavior is based on the laboratory testing of intact rock and numerical modeling calibrated to the same intact rock testing, then it is potentially affected by any bias in the laboratory data. However, because of spatial heterogeneity considerations (one does not observe meter-size spot or rim material) at the drift scale and smaller, the bias or uncertainty of underrepresenting fractures, rims, or spots in the mechanical characterization of intact rock is not considered to be large or significant.

With more focused effort, the magnitude of the influence of these features on the mechanical behavior of lithophysal rock could be quantified in terms of uncertainty. For instance, if the presence of spots and rims was shown to weaken matrix rock significantly more than the current characterization, then (1) the uncertainty in the current properties could be increased, (2) rock mass mechanical behavior could be based on total (with the specific inclusion of field observed abundances of spot or rim material) rather than on lithophysal porosity, or the material model could be changed to either (3) model spots and rims as lithophysae instead of matrix (conservative), or (4) model them as a separate third component of the rock material model.

Confirming the Assumption: It may be difficult to rigorously confirm that the use of the two-component model with the current range in mechanical properties is adequate for modeling the mechanical behavior of repository lithophysal rock without further effort that is beyond the scope of this calculation. Observations of the conditions in the underground tunnels and modeling predictions (Section 6.7) tend to confirm the current model and associated range of mechanical properties for the rock volume excavated under base-case loading conditions (no thermal loads, no earthquake loading, and continual gravity loading on the scale of years). For instance, in areas of large abundances of spot material, the lithophysal rock is observed to be stable. To better quantify the uncertainties involved and better confirm this assumption, additional laboratory and/or field-testing of spot or rim material to determine its mechanical properties would be very helpful. In addition, to explicitly account for spot or rim material and/or fractures as part of the development of lithophysal rock mass properties, a more detailed analysis and additional numerical modeling may need to be performed.

5.4 LABORATORY LITHOPHYSAL ROCK MASS MECHANICAL BEHAVIOR DOES NOT NEED TO BE SCALED BEYOND THE AVAILABLE LARGE-CORE TESTING RESULTS

Assumption: The estimated range of mechanical rock properties of lithophysal rock at the 1 m and larger scale can be suitably estimated from the available large-core (approximately 0.3 m or 12-in diameter) specimen laboratory testing results. This assumes that the dominant mechanical failure mechanism in a lithophysal rock mass is the creation and/or reactivation of matrix-groundmass fractures that weaken the intact blocks of tuff (as observed in laboratory testing and numerical modeling), and not slip along preexisting fracture planes that form the boundaries of strong intact blocks of tuff (analogous to the dominant failure method expected for a nonlithophysal rock mass).

Used: This assumption is used in Sections 6.4 and 6.6, where the ranges of rock mass categories for lithophysal rock are developed.

Basis: Laboratory results (Section 6.3) indicate that there is a scaling effect of mechanical properties at the laboratory scale (ranging from diameters of 25 to 290 mm). However, due to the limited number of mechanical tests, uncertain specimen porosities, the presence of fractures and other imperfections (lithophysae and spots), and testing over a range of environmental conditions (moisture content and rock temperature), there is a large amount of scatter in the laboratory results. It is assumed that this scatter can capture the property scaling effect present in rock mass up to dimensions of about 5-10 m. The numerically simulated laboratory testing of meter-size specimens (Section 6.5.5) are generally within the property bounds estimated for large-core testing.

Confirming the Assumption: Since laboratory and numerical modeling of mechanical behavior is based on the distribution of lithophysal porosity, this part of the assumption can be confirmed by validating that the laboratory and drift-scale mechanical behavior are related to the lithophysal porosity in exactly the same way. It is difficult to rigorously confirm this assumption since laboratory testing of drift-scale or even meter-scale lithophysal rock specimens is impractical. It was hoped that the field-testing conducted of in situ meter-sized blocks of lithophysal rock (slot-tests) could provide substantial confirmation, but these tests involved a number of complexities

and reliable results are not yet available. Of the slot tests carried out, slip along some preexisting fracture planes was inferred, but this occurred only near unconfined rock boundaries.

Topopah Spring Tuff fracture analysis indicates that lithophysal rock has been competent for millions of years and if sufficient stresses were to develop causing new fracturing in lithophysal rock, then there is no reason to suspect a fracture mechanism different from one of short trace-length fracturing within the matrix-groundmass, with termination at lithophysae if encountered. A systematic investigation of fractures observed in boreholes and along the ECRB Cross-Drift supports the conclusion that most fractures observed in the underground exposures of lithophysal rock of the Topopah Spring Tuff were formed as a result of cooling and welding processes that were complete approximately 12.8 million years ago (BSC 2004 [DIRS 170137], Section 6.3). Analysis of twenty photographs of tunnel walls containing lithophysae from the Topopah Spring lithophysal rock infers a mechanism of localized in situ fracturing of the matrix-groundmass during cooling and welding of the rock mass (BSC 2004 [DIRS 170137], Section 6.3). Most observed fractures have short trace lengths (less than 30 cm long), are steeply dipping, developed in the matrix-groundmass, and terminate in the matrix-groundmass or at lithophysae (BSC 2004 [DIRS 170137], Section A1.1.3). Of the 1444 lithophysae inspected during geological mapping, only 7 are transected (or intersected) by fractures greater than 1 m in trace length, and only 5 are transected by shears (BSC 2004 [DIRS 170137], Section 6.3), indicating that most fractures terminate if they encounter a rock void. Direct observation of lithophysal rock in the underground reveals that the lithophysal rock mass is still competent and a distinct relationship between fracturing in lithophysal and nonlithophysal rock (Section 6.1). However, future rock loading conditions (e.g., due to increased temperature) may develop stresses high enough to locally fail lithophysal rock in the same manner as described in Section 6.3.2.2 (i.e., by micro-fracturing of the matrix-groundmass that coalesce into inter-lithophysal macro-fractures where the stresses are sufficiently high). Numerical simulations of compressive tests on lithophysal rock to failure appear to confirm this mechanism since with increasing shear strain increments, microfractures integrate to form observable inter-lithophysal fractures (Section 6.5.9). One of the strongest arguments that properties determined from the large-core samples are good representation of mechanical behavior of the lithophysal rock mass is agreement between model predictions based on large-core properties and underground observation of behavior of ESF and ECRB Cross-Drift.

5.5 THE SPATIAL VARIABILITY MODEL DEVELOPED FOR LITHOPHYSAL POROSITY IS APPLICABLE TO OTHER MECHANICAL PARAMETERS

Assumption: The simulation model developed to represent the spatial variability of lithophysal porosity (Appendix A) can be applied to other uncertain model parameters (e.g., elastic Young's modulus, E, and uniaxial compressive strength, UCS). In other words, the spatial variation of lithophysal porosity, defined by field mapping techniques, can be used to indirectly determine the spatial variation of rock mass mechanical parameters, based on correlations between specimen lithophysal porosity and the mechanical parameters determined from these tested rock specimens.

Used: This assumption is used throughout Section 6.

Basis: The assumption of using rock lithophysal porosity as a surrogate for modeling the spatial variability of other variables is described in Section 6.1.1. The spatial variability of the elastic Young's modulus and uniaxial compressive strength cannot be developed directly because only a small number of mechanical laboratory tests have been carried out on rock specimens containing lithophysal voids.

Confirming the Assumption: The repository horizon layers are similar in mineralogical composition (BSC 2003 [DIRS 164670], Table 6.2) and differ primarily in terms of matrix groundmass and lithophysal porosity percentages. Because the mineralogical abundance and chemical composition for these units are similar, the mechanical behavior of the matrix groundmass material in all units should be similar.

As demonstrated in Section 6.3, sample porosity is the primary factor controlling the mechanical behavior in compression testing. The significance of this key controlling factor is confirmed by the validation provided by the numerical modeling of mechanical lithophysal rock behavior discussed in Sections 6.5 and 6.7. In the future, the lithophysal porosity variability can be further characterized in boreholes, the ESF and ECRB Cross-Drift, and in new excavated underground openings by direct mapping and indirectly by geophysical methods (Section 6.2). Additional laboratory tests and field-testing of in situ meter-sized blocks of lithophysal rock (slot-tests) could provide further confirmation of the correlations between porosity and mechanical parameters. Once the relations between porosity and mechanical properties are well established (Section 6.3), porosity can be more confidently used as an indicator for variability of other mechanical properties. Direct confirmation of the spatial variability of rock mechanical properties is impractical to carry out and is not needed.

6. ANALYSIS

The approach taken to estimate the uncertainty and spatial variation of lithophysal rock mass mechanical properties is described in Section 1.2.1 and Figure 1-5. This section provides the documentation and details for the steps outlined in this approach. Section 6.1 discusses the the nature of the problem, the use of lithophysal porosity as a surrogate property, and the plausible conceptual models of lithophysal rock. Section 6.2 summarizes the characterization of field lithophysal rock porosity. Section 6.3 provides a summary and analysis of the lithophysal rock mechanical behavior and properties based on laboratory testing. Section 6.4 develops the mechanical property bounding analysis and rock mass categories. Section 6.5 describes the simulated numerical compression tests of lithophysal rock and analyzes the resulting behavior. Section 6.6 evaluates the mechanical property bounding analyses based on the numerical modeling. Section 6.7 discusses means of confirming the lithophysal rock mechanical property estimates and numerical modeling.

6.1 DISCUSSION OF THE LITHOPHYSAL ROCK PROBLEM AND SURROGATE POROSITY APPROACH

The Yucca Mountain exploratory excavations for the repository extend down into the Topopah Spring formation, to a volcanic welded tuff that has been subdivided into four zones based on their observed geologic features and structure. These four repository zones are the upper lithophysal unit (Tptpul), the middle nonlithophysal unit (Tptpmn), the lower lithophysal unit (Tptpll), and the lower nonlithophysal unit (Tptpln). The nonlithophysal units (Tptpmn and Tptpln) are fine-grained, low porosity (i.e., approximately 10-13 percent, BSC 2004 [DIRS 169854], Figure 6-7), strong volcanic rocks that contain abundant but relatively nonpersistent cooling fractures, and limited numbers of lithophysae, rims, and spots. The lithophysal units (Tptpul and Tptpll) are composed of the same densely welded, fine-grained matrix material but have significant porosity contributed by lithophysae (i.e., open voids that result from gas localization during the cooling process) and by rims and spots formed from the crystallization of vitric rock in the presence of vapor (Buesch and Spengler 1998 [DIRS 101433], pp. 20-21; see also Figure 6.1-3). Figure 6.1-1 shows the measured abundance of various mapped lithophysal rock features along the ECRB Cross-Drift and Figure 6.1-2 provides the corresponding calculated feature porosities (Section 6.2). Formerly only the "fitted" lithophysal cavity data was available, but recently the 5 m averaged inventory of large-lithophysae was completed and is now used to provide an improved estimate of lithophysal porosity. The lithophysae, which vary in size from the millimeter to meter scale, range from about 3 to 35 percent of the volume of the Tptpll zone, and average approximately 15 percent (Figure 6.1-2b). Rim and spot material has a porosity averaging 30 percent (Table 4-1) and consist of approximately 4 percent of the volume of the Tptpll, ranging from about 0 to 10 percent (Figure 6.1-2b). The lithophysal porosity of the Tptpul zone generally ranges from 25 to 40 percent (Mongano et al. 1999 [DIRS 149850], p. 17).
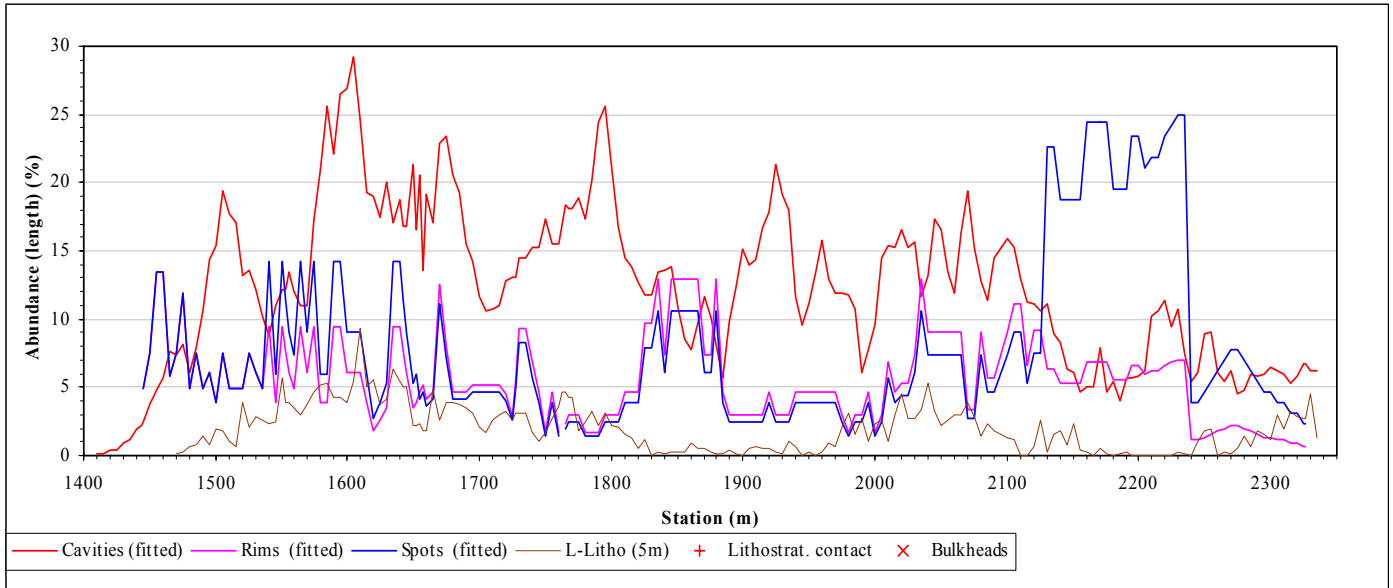
a. Abundance curves of "fitted" lithophysal cavities, rims, spots, and the 5 m averaged large-lithophysal inventory along the ECRB Cross-Drift. "Fitted" data refers to the process of combining panel map, tape, and angular traverse abundance data to obtain the best overall estimates of component abundance.
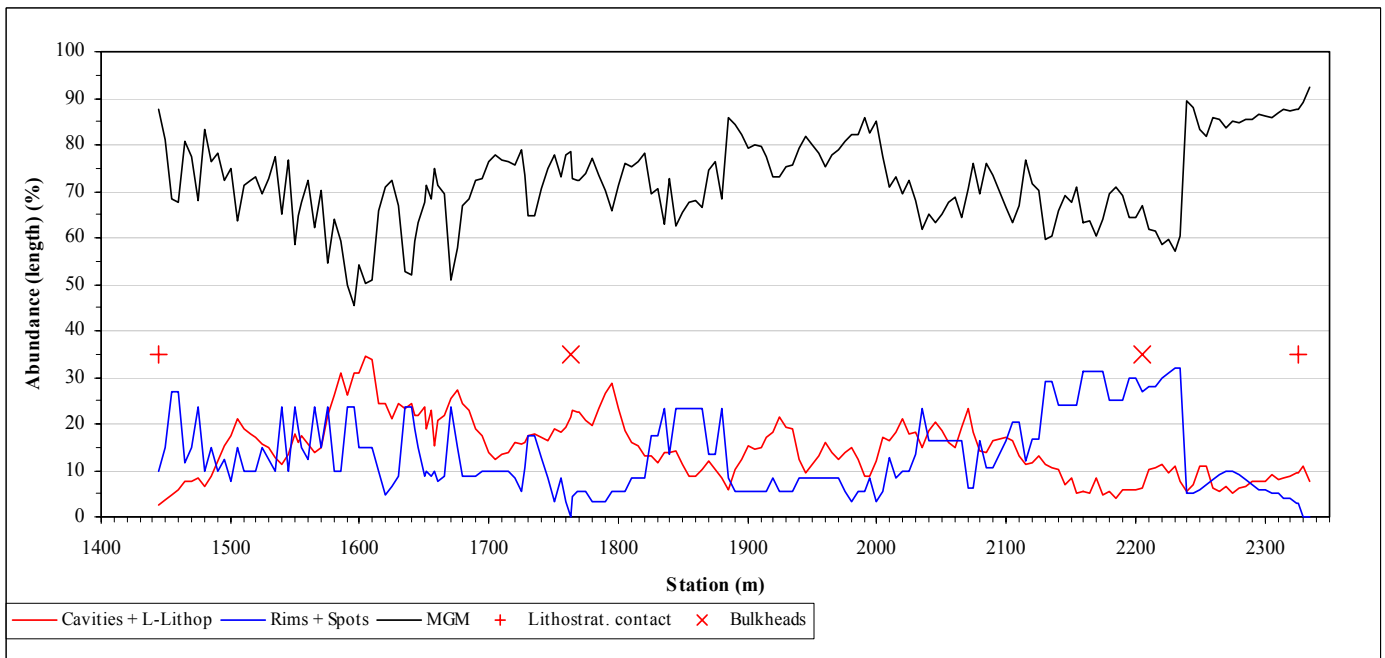
b. Abundance curves for a three-component rock material model (matrix groundmass, "fitted" lithophysal cavities plus the 5 m large-lithophysal inventory, and rims plus spots) along the ECRB Cross-Drift. The combination of "fitted" lithophysal cavities and the large-lithophysal inventory is considered to represent the best estimate of lithophysal cavity abundance.

Source: Appendix B, Microsoft Excel file "Drift Deg AMR AF T-A-P Fit_V1_DBR.xls," Worksheet "Length - Fit and Stats"

Figure 6.1-1. Abundance Curves of Lithophysal Rock Cavities, Rims, Spots, and Matrix-Groundmass in the Tptpll Exposed along the ECRB Cross-Drift
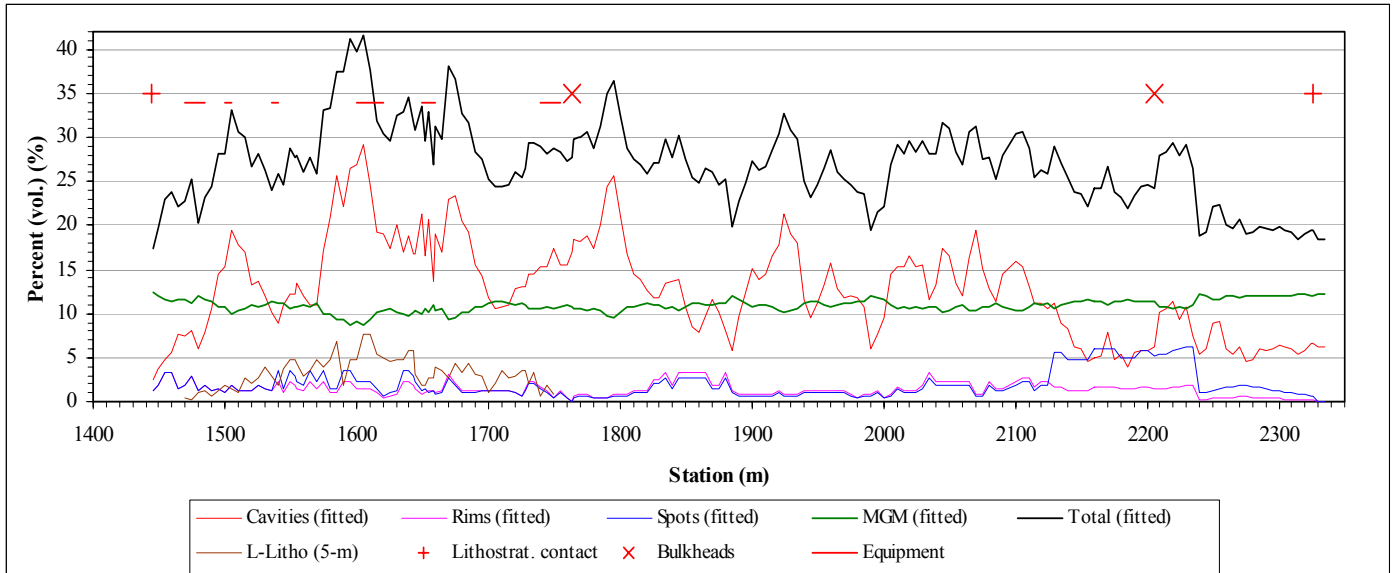
a. Calculated porosity along the ECRB Cross-Drift displayed as total porosity, five porosity components, and a plot of the 5 m averaged large-lithophysae inventory. The total porosity and "fitted" cavity porosity curves do not include the 5 m large-lithophysal inventory.
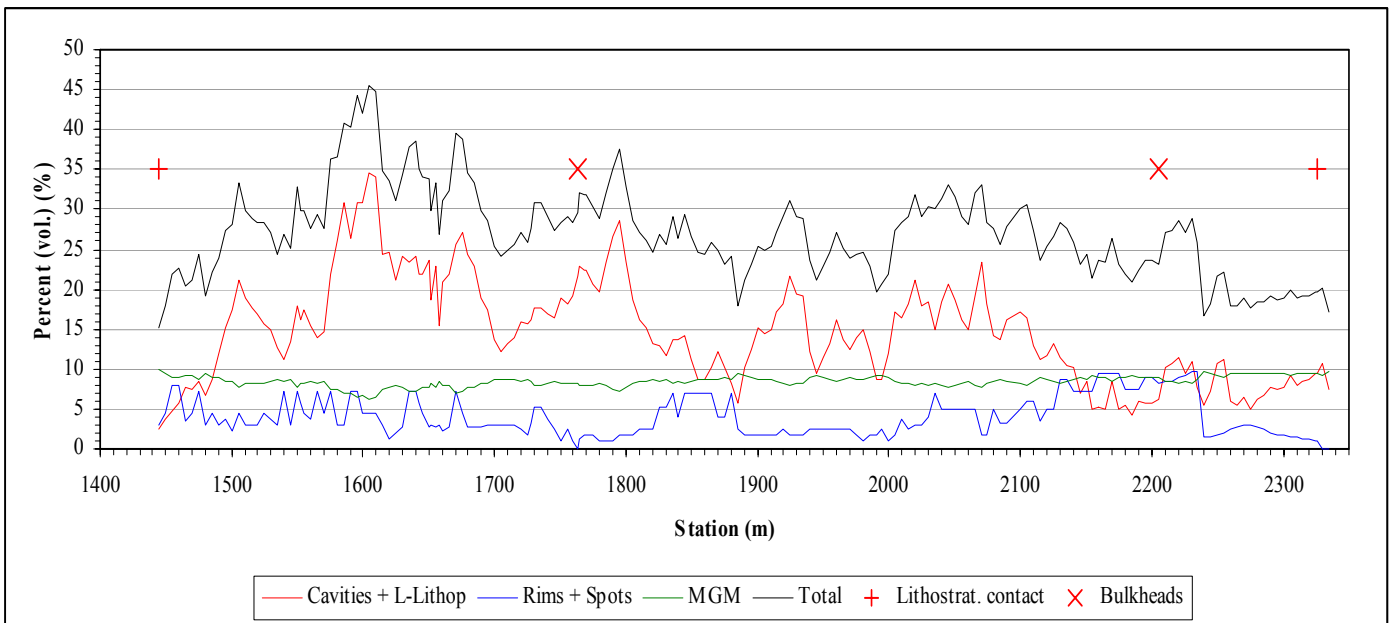
b. Calculated porosity along the ECRB Cross-Drift displayed as total porosity and in three components ("fitted" lithophysal cavities and 5 m large-lithophysae Inventory are combined, and rims and spots are combined)

Source: Appendix B, Microsoft Excel file "Drift Deg AMR AF T-A-P Fit_V1_DBR.xls," Worksheet "Volume Percent - Stats"

Figure 6.1-2. Calculated Porosity of Lithophysal Cavities, Rims, Spots, Matrix-Groundmass, and the Total Porosity in the Tptpll Exposed along the ECRB Cross-Drift

Compared to nonlithophysal rock lithophysal rock contains far fewer fractures, and they typically have shorter trace lengths (Mongano et al. 1999 [DIRS 149850], pp. 12-43, 65-79 and also discussed in BSC 2003 [DIRS 166660], Section 5.3.3). Figure 6.1-3 shows a schematic of the Topopah Spring Tuff illustrating the general occurrence of fracturing and lithophysae in the various lithostratigraphic zones of the formation. As shown in Figure 6.1-4, detailed line mapping in the ECRB Cross-Drift (Mongano et al. (1999 [DIRS 149850], p. 76 and Figure 13) has demonstrated an inverse relationship between fracture density and lithophysal porosity in repository rocks. The density of fractures with trace length greater than 1 m is significantly larger in the Tptpmn and Tptpln (20-35 fractures/10 m), as compared to five fractures/10 m or less in the Tptpul and Tptpll. Additionally, whereas the Tptpul tends to have some small-scale fractures in the matrix-groundmass between lithophysae, and a few that intersect lithophysae (Figure 6.1-5a), the Tptpll has abundant small-scale fractures. Figure 6.1-5b, from the upper portion of the Tptpll, shows the intensive fracturing of the matrix-groundmass between lithophysae. The fractures, which exist throughout the Tptpll, have a primary vertical orientation, and have lateral spacing of a few centimeters.

The mechanical behavior of lithophysal rock is significantly different from nonlithophysal rock in that intact lithophysal rock is mechanically weaker and the rock mass fails by aggregating compression failure of the intact rock blocks, whereas sliding failure of the fracture interfaces between intact nonlithophysal rock blocks controls nonlithophysal rock mass failure. Accordingly, for the design and performance assessment of mechanical models of lithophysal rock mass, it is important to account for the rock porosity, and especially the presence of lithophysae. The fundamental problem is that there is no reasonable way to directly determine the needed site-specific mechanical rock-mass properties. The standard approach used for most rock is based on the recognition that, in general, nonlithophysal rocks are composed of strong, intact blocks that are separated by fracture planes. These fracture surfaces provide the primary weaknesses in the system and control the failure mode and resulting rock block dimensions. Empirical classification systems (e.g., Barton's Q index and Bieniawski's rock mass rating (RMR)) are then widely used in mining and rock engineering for estimating rock mass mechanical properties of jointed rock masses. However, the databases upon which the conventional classification methods are based do not include lithophysal rock masses, and so existing classification approaches are not considered suitable for estimating the rock mass mechanical properties of lithophysal rock mass. This is especially true in that the mechanism of failure assumed to dominate in lithophysal rock involves the rock breaking into smaller block sizes controlled by fracturing between lithophysal voids, rather than slip along preexising fracture planes.

Vitric / **Crystal-rich Member**
- Nonwelded (Tptrv3)
- Moderately Welded (Tptrv2)
- Densely Welded (Tptrv1)
- Nonlithophysal Zone (Tptrn)

Crystalline / **Crystal-poor Member**

Upper Lithophysal Zone (Tptpul): Small-scale interlithophysal fracturing, with occasional throughgoing fractures traversing the unit: most lithophysae vary from 1 to 30 cm, becoming larger near base, generally oval or spherical in shape

Middle Nonlithophysal (Tptpll): Several well-developed fracture sets, most developed during cooling, distinctive vapor-phase partings: less that 5% lithophysae

Lower Lithophysal Zone (Tptpll): Abundant inter-lithophysal fracturing, sparse throughgoing fract-ures; lithophysae vary from 1 cm to 1.8 m, smooth and spherical to irregular and jagged in shape

Lower Nonlithophysal Zone (Tptpln): Some well-developed fracture sets, generally less continu-ous than those in the Tptpmn

Vitric
- Densely Welded (Tptpv3)
- Moderately Welded (Tptpv2)
- Nonwelded (Tptpv1)

Repository Horizon

Diagrammatic Cross Section of the Topopah Spring Tuff Illustrating Relative Discontinuity Densities and Orientations: This figure indicates how fractures, faults, and lithophysae are typically distributed through the ignimbrite.

Legend

Densely welded, crystalline rocks; white dashed lines indicate vapor-phase partings; white circles and ellipses indicate lithophysae; black lines indicate fractures.

Densely welded, vitric rock; black lines indicate fractures.

Nonwelded to moderately welded, vitric rocks; black lines with "F" designation indicate faults.

00387DC_327.ai
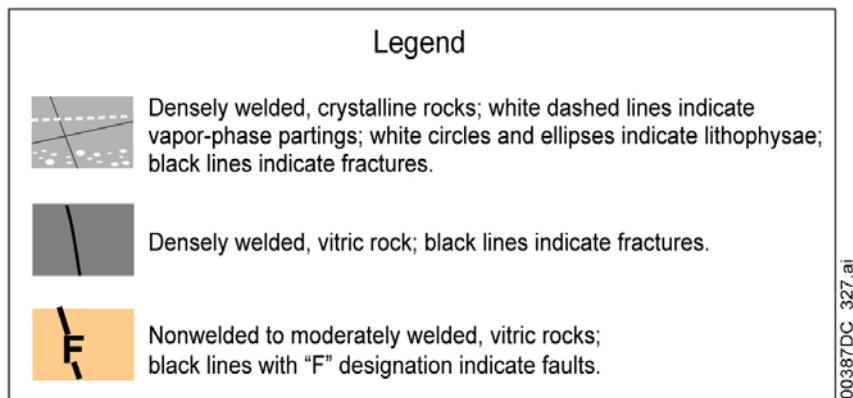
NOTE: Information shown in figure is derived from Buesch et al. 1996 [DIRS 100106], Appendix 2; Mongano et al. 1999 [DIRS 149850], pp. 12 to 43, 65-79.

Source: BSC 2004 [DIRS 166107], Figure 6-4

Figure 6.1-3. Schematic Illustration of the Structure of the Topopah Spring Tuff
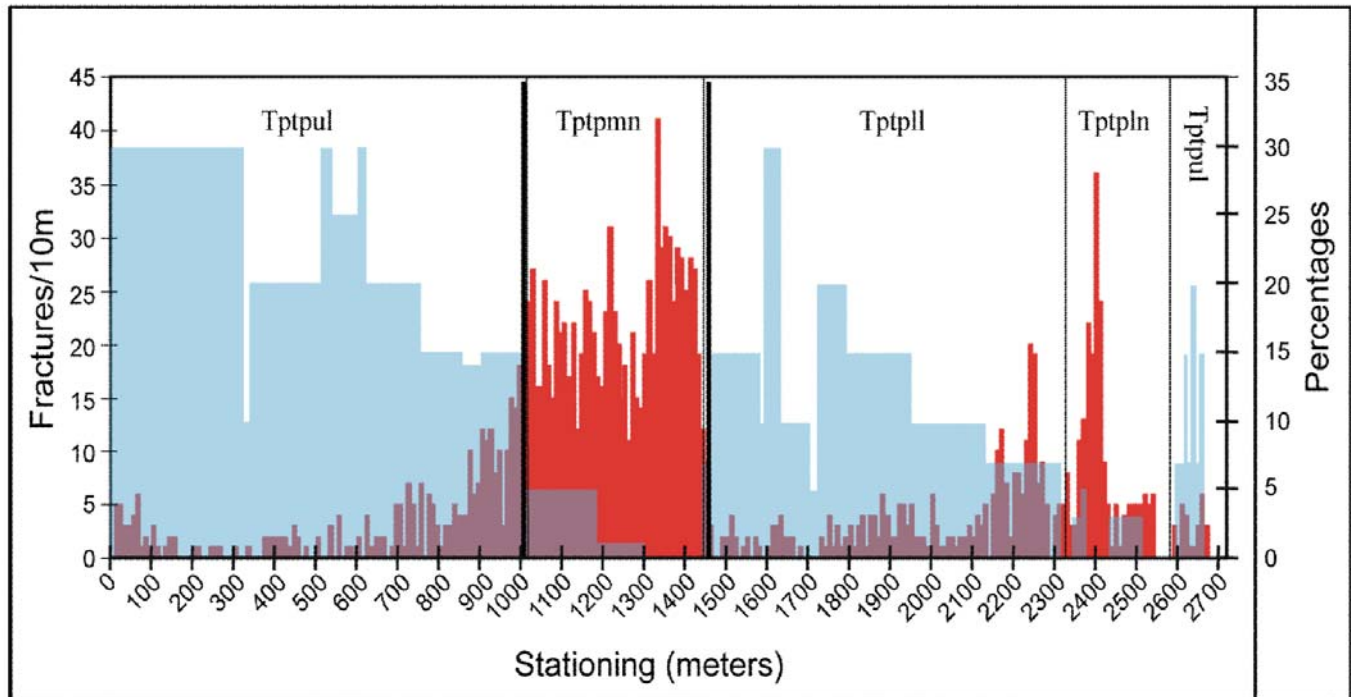
Fracture frequency/ Lithophysal %

Source: Mongano et al. 1999 [DIRS 149850], Figure 13, p. 77

Figure 6.1-4. Fractures and Lithophysal Abundance in the ECRB Cross-Drift from Stations 0+00 to 27+00

The approach adopted to handle this problem (described further in Section 6.1.1) is based on a geostatistical description of lithophysal porosity, which is used as a surrogate property to develop the desired rock mass mechanical properties. This approach involves estimating lithophysal rock-mass properties based on incorporating site-specific laboratory and field testing, in particular the correlation between rock mechanical properties and specimen lithophysal porosity, supplemented by numerical modeling of lithophysal rock. As a result, tests of large-diameter core (up to 0.3 m diameter) and in situ compression tests (slot tests up to 1.1 m across) have been conducted and analyzed on lithophysal rock in the Tptpul and Tptpll units. Additionally, the Tptpll portion of the ECRB Cross-Drift has been systematically measured by a number of different methods to identify lithophysal rock characteristics (abundance, shape, and size variability), and work is underway to similarly measure and study portions of the Tptpul unit in the ECRB Cross-Drift as well. The measured abundance of lithophysae was used to produce a simulation of the spatial variation of lithophysal porosity in the repository area (Appendix A). Lastly, two- and three-dimensional numerical modeling of larger-scale samples (1 m scale) with realistic lithophysal voids have been carried out using the PFC and UDEC discontinuum programs. These numerical simulations have been utilized to further develop the stress-strain response of lithophysal rocks and to confirm rock parameter ranges necessary to extrapolate the possible behavior and material properties of lithophysal bulk rock.
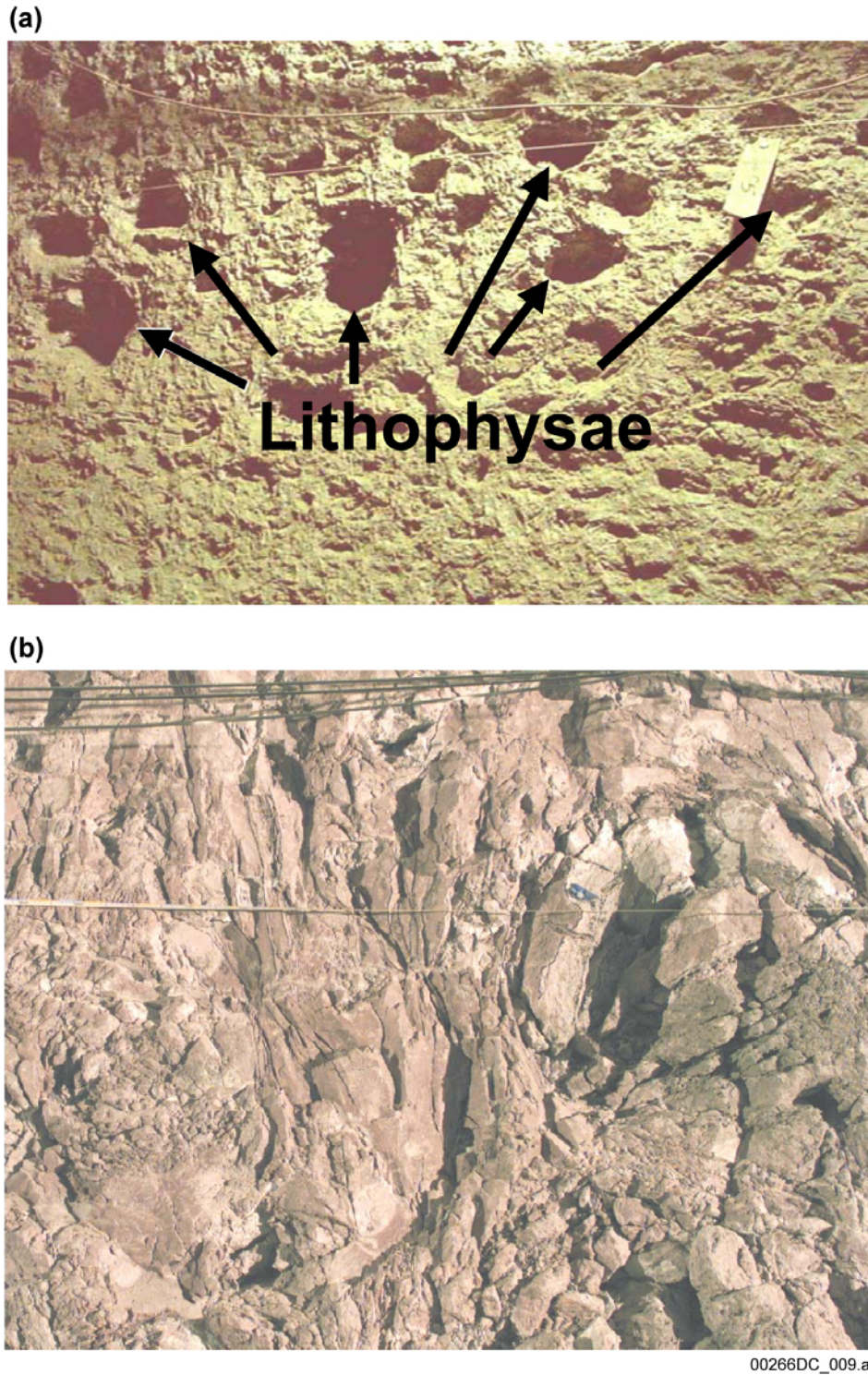
Source: BSC 2004 [DIRS 166107], Figure 6-10

NOTE: The Tptpul (a) is characterized by a relatively few fractures in the matrix-groundmass between lithophysae whereas the Tptpll (b) has abundant, natural, short-length fractures in the matrix-groundmass, some of which intersect or connect lithophysae.

Figure 6.1-5. Comparison of Lithophysae and Fracturing in the Tptpul and Tptpll

6.1.1 Modeling of Spatial Variability of Rock Mass Mechanical Properties Using Porosity as a Surrogate

A geostatistical approach assumes that collected data has an underlying spatial structure, dependence between observations in space. Based on this spatial structure, geostatistics provides: (1) a systematic approach for expanding (by interpolation, extrapolation, or simulation) a limited number of isolated data measurements in space, and (2) a means to quantify the associated prediction uncertainty. The key feature of a geostatistical model is the adopted conceptual model that describes the underlying spatial structure of the property of interest. The spatial model is based on a spatial data analysis of three-dimensional coordinates and their spatial variation with the rock parameter of interest. The main assumption of a statistical approach is that the analyzed phenomenon is considered to be a random function. Often, the developed geostatistical properties are represented by stationary random functions within an idealized geologic stratum. A geostatistical random function is a set of spatially dependent, distributed random variables and stationarity infers that the probabilistic mechanism describing the relation of random variables is independent of spatial location. Note that the rock property itself is not considered to be a random variable, rather, the variability of the original geologic spatial process is random (since the actual geologic process is unknowable), which is reflected by the correlation structure of the distribution of spatial measurements.

The philosophy and general approach of using porosity as part of a geostatistical method to characterize spatial heterogeneity and uncertainty of other rock parameters is discussed in the *Rock Properties Model Analysis Model Report* (BSC 2002 [DIRS 159530]). Key parts of this report that summarize the approach are given below (BSC 2002 [DIRS 159530], Sections 5.1 and 6.3).

Modeling Approach. A fundamental principle involved in the numerical representation of real-world physical processes is that the relevant material properties of the modeled domain must be known at all positions within that domain. However, in contrast to this requirement for an "exhaustive" spatial description, the process of describing or characterizing a site invariably consists of collecting observations of properties or state variables at a limited number of locations, the exact positions of which are frequently determined by less-than-optimal external factors. This is particularly true for the three-dimensional characterization of a geologic site, such as Yucca Mountain. A geologic descriptive characterization is incomplete due the limits of access (particularly to the subsurface) and the availability of resources. Therefore, the exhaustive description of a geologic site for purposes of numerical modeling requires the *prior assumption* of some type of conceptual model for the site, which is then implemented to assign the necessary properties and other variables at every relevant point in space (BSC 2002 [DIRS 159530], Section 6.3.1).

A more realistic conceptual model of rock than the isotropic, homogeneous model is one that makes use of the known vertical and lateral heterogeneity within geologic layers. Knowledge of property values at one location imposes limits on the values of those properties *likely to exist* at "nearby" locations. Therefore, an alternative conceptual model of "filling-in" a geologic framework with values randomly assigned from some inferred univariate distribution without regard for other nearby values (spatial correlation) is an unnecessary oversimplification (and

potentially an unwarranted distortion) of the real world (BSC 2002 [DIRS 159530], Section 6.3.1.1).

Heterogeneity versus Uncertainty. In contrast to heterogeneity, which is an objective feature of the real world, uncertainty is a knowledge-based concept. Distinguishing properly between uncertainty (as a state of imperfect information resulting from less-than-complete observation and scientific judgment) and spatial heterogeneity (as a state of being, unaffected by the availability or lack of information) becomes critically important in the application of predictive engineering methods to the geologic environment. Incomplete information must be accounted for in predictive modeling, as must the effects of material properties that are different in different locations. A key attribute, therefore, of the rock properties modeling activities, has been the description and quantification of the effects of geologic uncertainty on the physical description of the Yucca Mountain site (BSC 2002 [DIRS 159530], Section 6.3.1.2).

Porosity-as-a-Surrogate. The rock property model approach involves the use of "porosity-as-a-surrogate" for modeling the spatial variability of other, "secondary" material properties that are typically of greater interest in performance modeling than porosity itself, but which are almost universally undersampled at Yucca Mountain. This concept of using the more abundant porosity data as a surrogate for other properties is not a new YMP approach. Characterization of the rock mass hydraulic conductivity already incorporates the "porosity as a surrogate" approach (BSC 2002 [DIRS 159530], Section 5.1).

Using porosity as a surrogate for mechanical rock parameters is supported by consideration of the physics involved in the site-specific rock types being modeled. For example, for a given rock type, increasing the volume of pore space must decrease the bulk density of the rock mass. The part of the rock that "isn't there" is available to hold fluids, but it contributes nothing to the total mass contained within a unit volume: the definition of bulk density. Again for a given rock type, the conduction of heat energy through the material is directly related to the density (or, inversely to the pore space) of the material. All else being equal, a higher porosity–lower density tuff will conduct heat less readily, leading to a lower thermal conductivity value. Note here that it is the total amount of void space in a rock that affects thermal conductivity, not simply the amount of pore space that is conducting water within the unsaturated rock. This fact has important implications to modeling of whole-rock thermal conductivity in the presence of large-diameter (up to 1 meter) lithophysal cavities (BSC 2002 [DIRS 159530], Section 5.1).

The concept of porosity as a surrogate is based on empirically observed correlations of porosity with undersampled secondary properties. A consequence of undersampling is that the spatial variability of the undersampled variable cannot be described confidently on a stand-alone basis. It is important to understand that modeling the spatial distribution of several material properties without considering the inter-variable correlations can lead to highly unrealistic input to physical-process modeling codes, which in turn can lead to highly unreasonable estimates of performance parameters. Simply sampling randomly from separate (univariate) probability density functions may easily produce such un-physical combinations as a low porosity–high thermal conductivity–high hydraulic conductivity tuff. The severity of neglecting cross-variable correlations in modeling spatially variable domains increases as physical-process modeling attempts to capture multiple coupled processes (BSC 2002 [DIRS 159530], Section 5.1).

6.1.2 Conceptual Models Proposed to Describe Material Model of Lithophysal Rock

The following ways of modeling the material model of lithophysal rock for mechanical loading have been proposed:

1. Two-component model. The two components are solid rock and voids, with behavior assumed to be that of common rock having no lithophysal voids.

2. Three-component model. Solid rock, voids, and spot or rim material, with behavior assumed to be that of common rock having no lithophysal voids or rim or spot material.

3. Either of the above two models with the addition of preexisting fractures in the rock at some scale.

Only the first conceptual model is adopted as part of this calculation as discussed in Assumption 5.3. For this calculation, lithophysal porosity is defined as the fractional volume of lithophysal voids per unit volume of rock.

6.2 CHARACTERIZATION OF THE LITHOPHYSAL HOST ROCK POROSITY

6.2.1 Tptpll Lithophysal Variability of the Rock Mass

Using the adopted conceptual model for lithophysal rock, the Tptpll rock mass is characterized in this calculation by lithophysal porosity that varies with position in the rock mass. A detailed study of the lithophysal features in the Tptpll from geologic data collected in the ESF and ECRB Cross-Drift (DTNs: GS021008314224.002 and GS040608314224.001) is described in the *Subsurface Geotechnical Parameters Report* (BSC 2003 [DIRS 166660], Attachment VII). The abundance of lithophysal features is measured using a variety of one and two-dimensional mapping techniques. The variation in abundance of lithophysal cavities and other features along the ECRB Cross-Drift is shown in Figure 6.1-1, which also represents a description of the vertical variation of lithophysae from the top to the bottom of the Tptpll unit, adopting the assumption of Section 5.1. BSC 2003 [DIRS 166660], Attachment VII, Section VII.6.7 discusses several reasons why the tape traverse method is least accurate of the measuring methods; accordingly, the data has been corrected or adjusted. Figure 6.2-1 shows histograms of the acquired and corrected tape traverse data based on 5 m measurements and averaging over 15 m. In comparing the plots, averaging the data has the expected consequence of reducing the scatter in the data and pulling inward the tails of the data distribution.

The 15 m adjusted tape traverse data was next fitted to the more accurate angular traverse and panel map measurements of lithophysae abundance, and a new estimate of the variation of lithophysal cavities was made (details are in Appendix B, *Drift Deg AMR AF T-A-P Fit_V1_DBR.xls)*. A survey of large lithophysae (having a minimum cavity dimension of 50 cm) exposed in the wall of the ECRB from stations 14+44 to 25+35 was completed and used to produce an improved estimate of variation of lithophysal cavities. A histogram of this fitted cavity data and the fitted data including the 5 m averaged large-lithophysal inventory is shown in Figure 6.2-2. Table 6.2-1 lists the summary statistics for these various descriptions of lithophysal porosity, and a summary of panel map lithophysae (see examples in Figure 6.2-3).
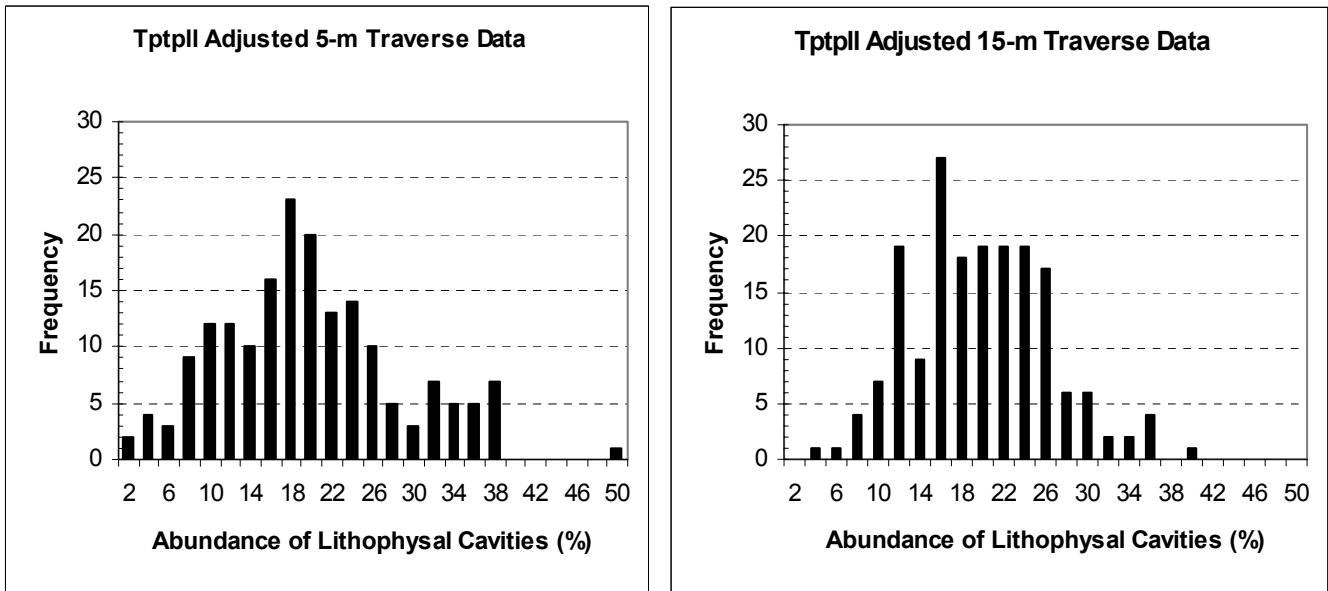
Source: Appendix B, Microsoft Excel file "Drift Deg AMR AF T-A-P Fit_*V1_DBR*.xls," Worksheet "T-A-P Cav Fit," cells O213 and AF213.

NOTE: Lithophysal porosity data are from ECRB Cross-Drift station 14+44 to 23+26, which includes the entire thickness of the Tptpll lithostratigraphic rock unit.

Figure 6.2-1. Histograms of Lithophysal Porosity for the Tptpll in the ECRB Cross-Drift Based on 5 m and 15 m Adjusted Tape Traverse Data
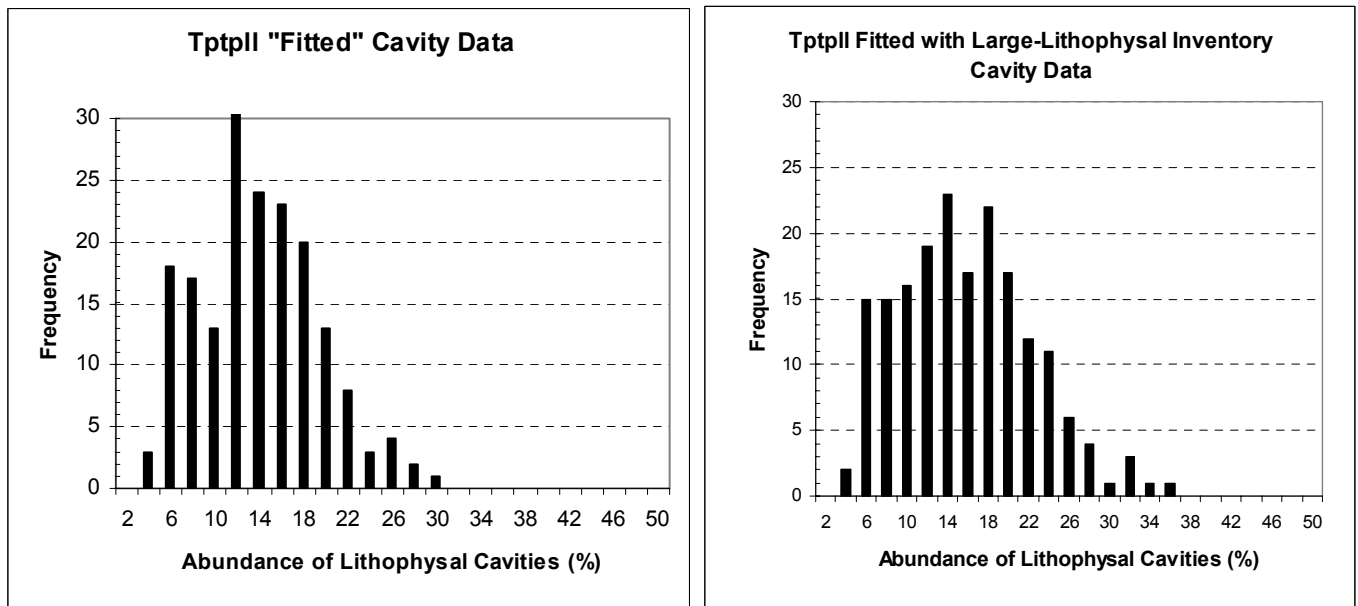
Source: Appendix B, Microsoft Excel file "Drift Deg AMR AF T-A-P Fit_*V1_DBR*.xls," Worksheet "Length – Fit and Stats," cells M216 and AX230.

NOTE: Lithophysal porosity data are from ECRB Cross-Drift station 14+44 to 23+26, which includes the entire thickness of the Tptpll lithostratigraphic rock unit.

Figure 6.2-2. Histograms of Lithophysal Porosity for the Tptpll in the ECRB Cross-Drift Based on Tape Traverse Fitted Cavity Data and Angular Traverse Data

Table 6.2-1. Descriptive Statistics of Tptpll Lithophysal Porosity Data

Type of Measurement	Count	Mean ± 1 SE	Mean ± 1 SE Percentage	Mean ± 1 SD	Mean ± 1 SD Percentage	Median	Minimum	Maximum	Range
5m Tape Trav	181	19 ± 1	19 ± 5%	19 ± 9	19 ± 50%	17.8	1.2	48.4	47.2
15m Tape Trav	181	19 ± 1	19 ± 5%	19 ± 7	19 ± 39%	18.2	3.3	39.0	35.7
Fitted Cavities	180	13 ± 1	13 ± 8%	13 ± 5	13 ± 40%	12.9	2.2	29.2	27.0
Fitted Cav+LL	185	15 ± 1	15 ± 7%	15 ± 7	15 ± 49%	14.5	2.5	34.6	32.1
Angular Trav	22	15 ± 2	15 ± 13%	15 ± 8	15 ± 54%	14.8	2.2	30.7	28.5
Panel Maps	18	13 ± 1	13 ± 8%	13 ± 5	13 ± 36%	13.4	5.3	19.0	13.7

Source: BSC 2003 [DIRS 166660], Attachment VII, Table VII-10; and Appendix B, Microsoft Excel file "Drift Deg AMR AF T-A-P Fit_*V1_DBR*.xls," Worksheet "Length – Fit and Stats," cells J244 to Z251.

NOTE: LL stands for the 5 m averaged large-lithophysae inventory. SE stands for the standard error rounded to nearest positive whole number. SD stands for standard deviation (including the uncertainty in the standard deviation). Lithophysal porosities in the table are reported as percent by volume. Since the field measurement uncertainty ranges from about 5 to 10 percent or higher (Section 6.2.1.1), one significant digit will be used to represent porosity uncertainty.

The rock mass porosity is spatially variable over a relatively small length scale, on the order of meters (Figure 6.1-2). The tape and angular traverse data represent average lithophysal porosity determinations over a 7 to 8 meter traverse length across the upper half of the tunnel. Local variations of lithophysae over a smaller scale may exceed the estimates shown in Figures 6.2-1 and 6.2-2, especially in areas where there are clusters of large lithophysae. The scale effect is illustrated by examining smaller portions of panel maps. Out of the 18 panel maps, the largest lithophysal porosity for the 1×3 m panel area was 19 percent (BSC 2003 [DIRS 166660], Attachment VII, Table VII-3). After each panel map was sliced into 1×1 m squares, some of the squares were determined to have a lithophysal porosity approaching 30 percent (Appendix B, Microsoft Excel file "LithophysalRockRanges_Calc.xls," worksheet "PFC"). Figure 6.2-4 shows an example of two 1×1 m slices that have lithophysal porosity of about 31 percent because of the presence of large lithophysal cavities.
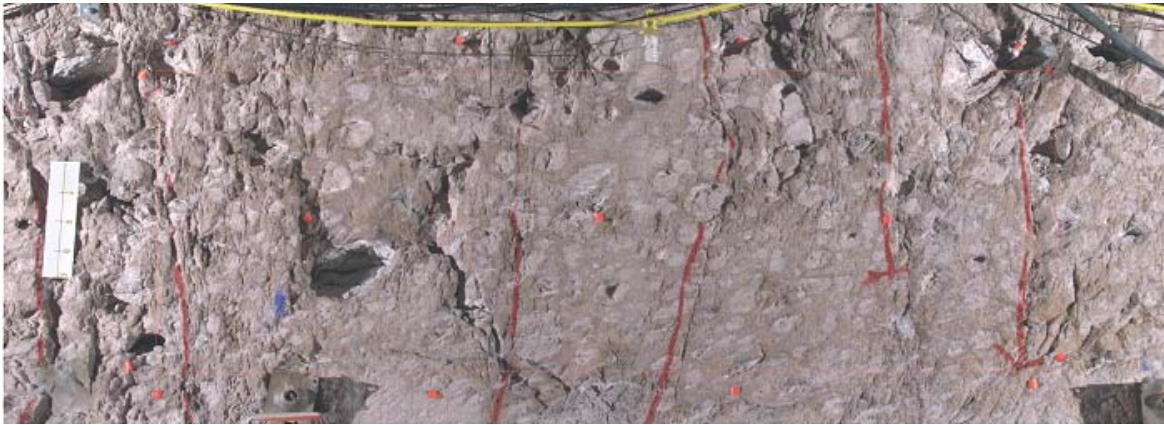
Source: BSC 2003 [DIRS 166660], Attachment VII, Figures VII-4 (top), VII-3 (center), and VII-8 (bottom). The respective lithophysal porosities for each panel map are given in BSC 2003 [DIRS 166660], Attachment VII, Table VII-3, p. VII-13.

Note: Section 16+41L (top), Section 14+93L (center) and Section 22+32L (bottom). The lithophysal porosity values come from abundance of lithophysal cavities for each panel map listed in Table VII-3 of BSC 2003 [DIRS 166660], Attachment VII). Panel Map 22+32L has an estimated 32.0% rim and spot material (Table VII-3).

Figure 6.2-3. Examples of Lithophysal Tuff Porosity Taken from 1×3 m Panel Maps: Maximum (top) With Lithophysal Porosity of Approx. 19.0%, Mean (center) With Lithophysal Porosity of 13.3%, and Minimum (bottom) With Lithophysal Porosity of 5.3%.

6.2.1.1   Uncertainty of the Lithophysal Porosity Field Characterization

BSC 2003 ([DIRS 166660], Attachment VII, Section VII.6.7) discusses the accuracy of the field characterization of lithophysal features for the Tptpll. There are three aspects of this uncertainty assessment: (1) the specific measurements made on features, (2) conditions that affect the measurements (e.g., human interpretation, backfilling of lithophysae, obscurity issues), and (3) how well the measurements and the summed and calculated values represent the three-dimensional distributions of the features. Total measurement uncertainty for angular and panel map data (including the first two aspects above) averages around ±5 percent for typical sizes of lithophysae and generally good conditions, but ranges up to approximately ±10 percent where conditions are less than optimal. Total measurement uncertainty for one-dimensional tape traverse data is larger, averaging around ±10 percent, and ranging up to 20 or even 30 percent.

The measured empirical data (DTNs: GS021008314224.002 and GS040608314224.001) indicate that the tape and angular measurement traverses often missed more abundant numbers of lithophysae observed nearby.   For example see Microsoft Excel file *Tptpll Litho Trav - Angle 1400-2200.xls* – "Comment 1" at the bottom of any worksheet with "-Laser" appended to the worksheet name, where the abundance of additional nearby lithophysae are recorded (DTN: GS021008314224.002, SEP Table S03045_002, "SEP Table 2 files.zip").

BSC 2003 [DIRS 166660], Section VII.6.7 discusses how representative the Tptpll one- and two-dimensional measurements may be of actual three-dimensional features and concludes that all measurement methods and final fit statistics underestimate the true measurements of features. In fact, "actual values at a specific location or the descriptive statistics probably represent minimum values" (BSC 2003 [DIRS 166660], Section VII.6.7, p. VII-44). This is a consequence of the limited number of lithophysae measured and the fact that many of the data measurements do not transect the center of lithophysae. A more rigorous theoretical point-counting and geometry analysis is needed to develop a defendable quantification of the uncertainty associated with the underestimate. However, considering the two-dimensional empirical underestimate in data mentioned in the previous paragraph, this additional three-dimensional under estimation may contribute 10 percent or higher uncertainty to the previously estimated total measurement uncertainty.

6.2.1.2   Simulation of Lithophysal Rock Porosity Over the Repository

The detailed study of the Tptpll lithostratigraphic features presented in BSC 2003 [DIRS 166660] Attachment VII and the analysis and simulation of spatial variability presented in Appendix A of this calculation shows that the lithophysal porosity varies systematically in layers of statistically higher and lower lithophysal porosity, parallel to the dip of the Tptpll unit. Mongano et al. (1999 [DIRS 149850], pp. 26) also divided the Tptpll into intervals with generally similar lithophysae size and abundance. Appendix A presents a model that produces a synthetic representation of the spatial variability of the lithophysal porosity in the Tptpll, based on field measurements as described in BSC 2003 [DIRS 166660] Attachment VII. The model is used to statistically represent lithophysal porosity in a series of 40 m long (along the axis of the ECRB Cross-Drift) by 50 m high (vertical) by 200 m wide parallelopipeds along the ECRB Cross-Drift axis from top to bottom of the Tptpll. The parallelopipeds are subdivided into a number of small (meter-scale) cubical grids within which the lithophysal porosity is estimated as

a function of vertical and horizontal position. Figure 6.2-5 presents examples of two vertical planes perpendicular to the drift axis centered at locations in the upper and lower portions of the Tptpll. These two planes correspond to the higher porosity subzone at the top of the Tptpll and the lower porosity material near the contact with the Tptpln (Appendix A, Section A.6).

6.2.2   Lithophysal Variability of the Repository Rock Beyond the Tptpll

Due to the current lack of suitable data describing the statistical variability of lithophysae outside the Tptpll lithostratigraphic zone, it is assumed that the Tptpll data adequately represent lithophysal rock in other repository rock zones. This assumption is discussed in more detail in Section 5.2. As noted earlier, the lithophysal survey data of Mongano et al. 1999 [DIRS 149850], p. 17) indicate higher lithophysal porosities in the Tptpul as compared with the Tptpll, so the assumption may not be valid.
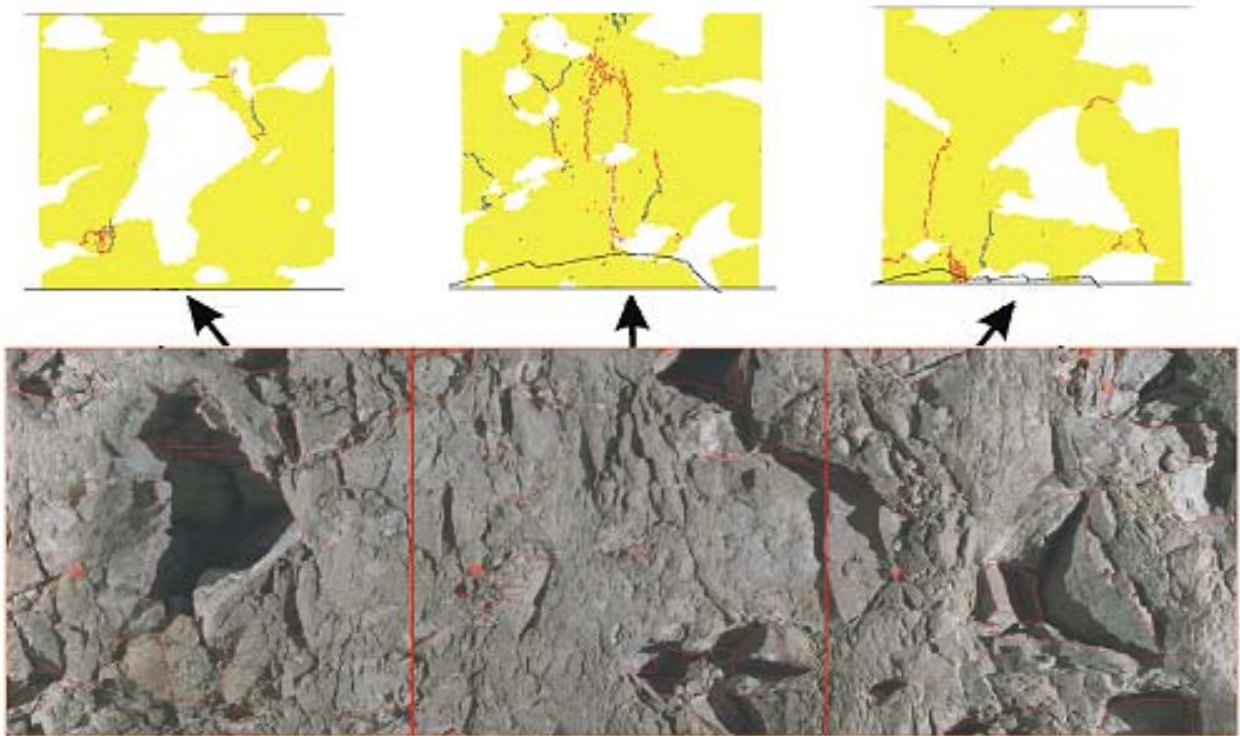
Source: BSC 2003 [DIRS 166660], Attachment V, Figure B-5

Note: Specimen A (top left) lithophysal porosity is 31%, Specimen B (top center) lithophysal porosity is 19%, and Specimen C (top right) lithophysal porosity is 31%. Porosity values can be found also in Appendix B, Microsoft Excel file "LithophysalRockRanges_Calc.xls," Worksheet "PFC."

Figure 6.2-4. PFC2D Stenciled-lithophysae Specimens Generated from Lithophysal Cavities of Panel Map at ECRB Cross-Drift Station 16+41 to 16+44 (Left Wall).
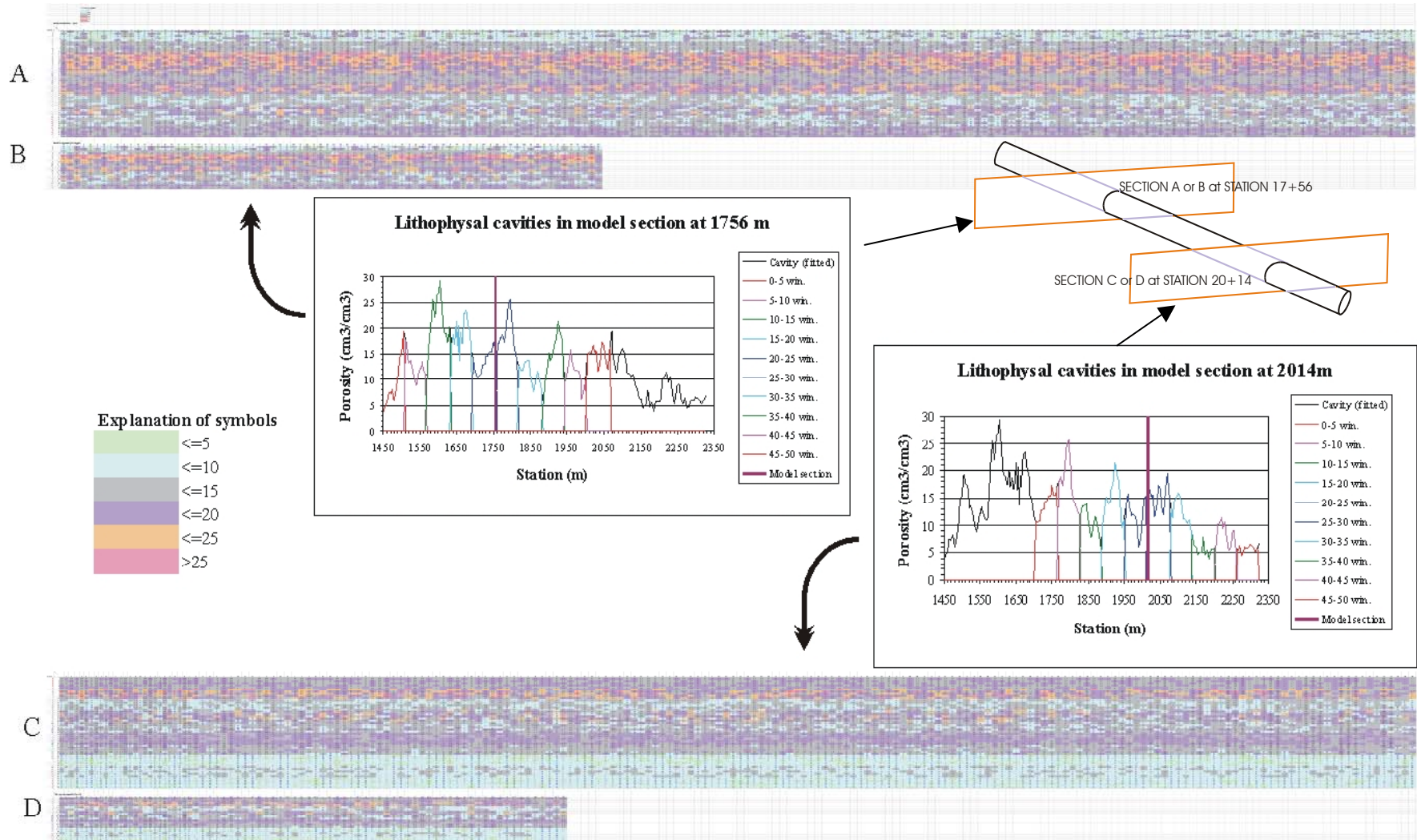
Source: Appendix A, Figure A-5

NOTE: Cross section A is a 50 × 200 cell table representing a 1 × 1 m grid and cross section B is a 20 × 80 cell table representing a 2.5 × 2.5 m grid for the simulated section at 17 + 56 in the ECRB Cross-Drift. Cross sections C and D represent a simulated section at 20 + 14 in the ECRB Cross-Drift. The upper cross sections (A and B) overlap the lower sections (C and D)

Figure 6.2-5. Schematic Illustration of the Process of Sampling and Modeling Spatial Variability Using Lithophysal Porosity Simulation Model Presented in Appendix A

6.3 MECHANICAL PROPERTIES OF LITHOPHYSAL ROCK BASED ON LABORATORY TESTING

A general description of the laboratory-testing program carried out to characterize the mechanical behavior of Yucca Mountain rock was provided in Section 1.1. Historically, most testing focused on traditional smaller-diameter cores, but recently the emphasis shifted to testing large samples of lithophysal tuff (Price 2004 [DIRS 170894]). A summary of what has been learned from small-core and large-core testing of Topopah Spring Tuff is provided in the following two sections.

6.3.1 Small-Diameter Core Mechanical Behavior

The bulk of the historical testing program, including characterization of Topopah Spring Tuff, consisted of compression and tension tests on small diameter (25 mm to 50 mm/1-in to 2-in) rock cores. These data are described in the *Subsurface Geotechnical Parameters Report* (BSC 2003 [DIRS 166660]), and additional analyses of these data are presented here. The DTNs for the 25 mm (1-in) specimen tests are SNL02030193001.019, SNSAND83164600.000, SNSAND84110100.000, and SNSAND85070300.000. The DTNs for the 50 mm (2-in) and 57 mm (2.2-in) specimen tests are SNL02030193001.001, SNL02030193001.002, SNL02030193001.004, SNL02030193001.012, SNL02030193001.014, SNL02030193001.016, SNL02030193001.018, SNL02030193001.019, SNL02030193001.020, SNSAND80145300.000, SNSAND83164600.000, SNSAND85070300.000, and SNL02040687003.001.

Testing on small-diameter cores from all of the formal lithostratigraphic units of the Topopah Spring Tuff indicates a distinct control of both compressive strength and elastic modulus based on the total porosity of the sample (Figure 6.3-1). The total porosity of these samples typically range from 8 to 19 percent, and due to the small specimen size, is primarily composed of matrix groundmass porosity, with additional porosity contributed by small amounts of rims, spots, and lithophysae.[*] It has been noted that rock containing a significant amount of lithophysae generally shows very poor drill-hole core recovery, which may significantly bias the sample suite in some intervals toward nonlithophysal samples (Brodsky et al. 1997 [DIRS 100653], Section 4.4.6, p. 56). However, some of these tested intact samples may contain structural defects such as small or partial lithophysae and rim or spot material that may result in lower values of compressive strength and elastic modulus. A histogram showing the frequency of total porosity of this set of 158 small-diameter core samples based on 5 percent intervals is shown in Figure 6.3-2. The histogram is close to being normally distributed with more than 50 percent of the specimens falling in the 11-15 percent porosity range and about 20 percent each in the proximate histogram bars. Almost 5 percent of the tested samples have a high porosity approaching 40 percent, however, these specimens are vitric rock and all come from nonwelded subzones located at the top and bottom of the tuff unit (Figure 1-2 and see note of Figure 6.3-1).

---

* Matrix groundmass porosity consists of pores generally less than 2μm in size, and totaling approximately 10 percent by volume (ranging from 8 to 12 percent) in densely welded tuffs (SGPR, BSC 2003 [DIRS 166660], Section 8.2.3.2, pp. 8-9 and 8-10). This porosity is assumed to be an intrinsic property of the matrix groundmass for all subunits of the Topopah Spring, and is distinguished from both rim/spot material (formed from the crystallization of vitric rock in the presence of vapor) and lithophysal porosity (formed from the local accumulation of gas in the vitric rock early in the cooling process). Rim and spot porosity averages 30 percent and typically ranges from 20 to 40 percent (SGPR, BSC 2003 [DIRS 166660], Table 8-3, p. 8-10).

Topopah Spring Units, Small Core (<51mm) Specimens, Saturated, L:D = 2.1, Rate = 10^{-5}
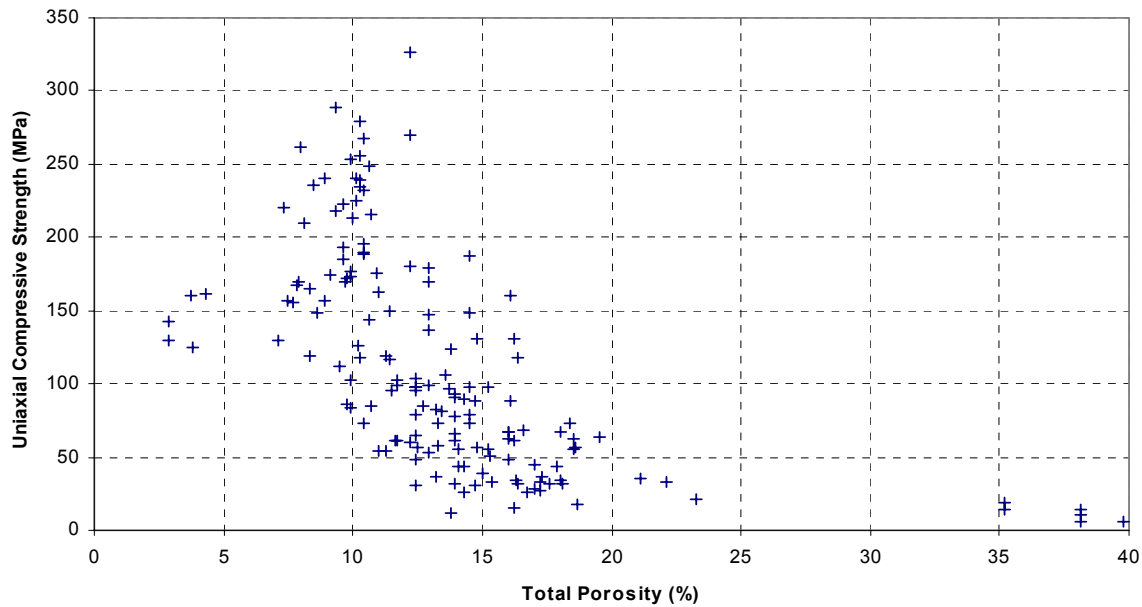
Topopah Spring Units, Small Core (<51mm) Specimens, Saturated, L:D = 2.1, Rate = 10^{-5}
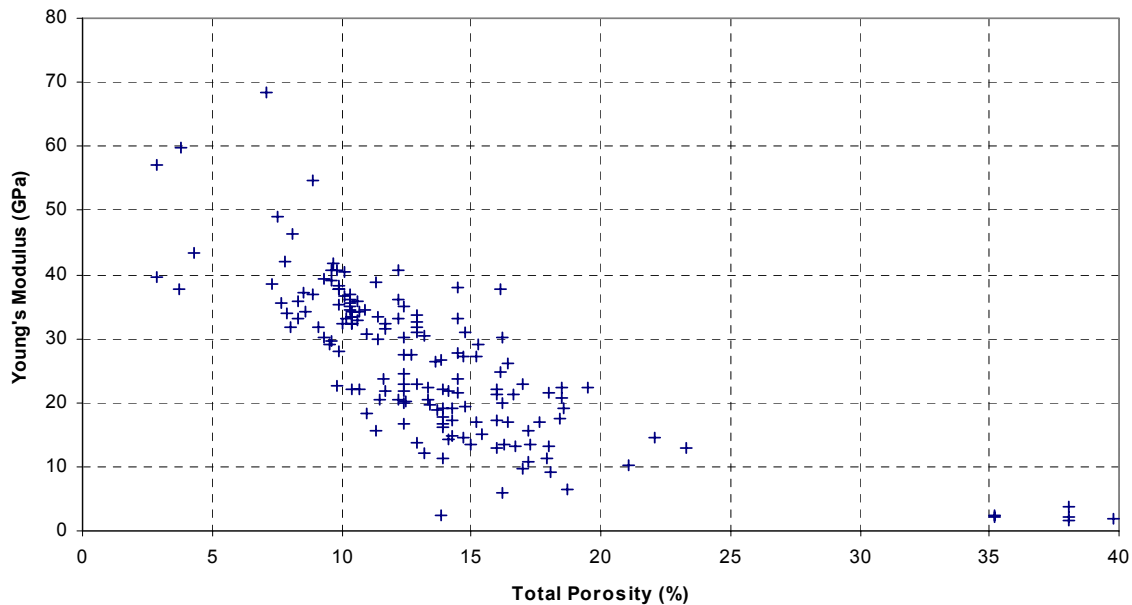
Source: Laboratory testing described in BSC 2003 [DIRS 166660], Section 8.4. Source DTNs are provided in Table 4-2. Plot from Appendix B, Microsoft Excel File "Compressive and Porosity Data REV00B_PorosityOnly_Tpt.xls," Worksheets "E v por" and "q v por." Plotted data from Worksheet "<=51mm," rows 11 through 168.

NOTE: Small-diameter cores generally contain only small amounts of lithophysal porosity, and thus the above tests are not indicative, in general, of properties of the lower and upper lithophysal units. The six specimens with 35-40% porosity come from unwelded vitric rock (subzones Tptrv3 and Tptpv1, see above Excel file, Worksheet "<=51mm," rows 13-14, 22-23, 45, and 113).

Figure 6.3-1. Intact Uniaxial Compressive Strength and Young's Modulus for Topopah Spring Tuff as a Function of Effective Porosity for Small Diameter Samples

Source: Laboratory testing described in BSC 2003 [DIRS 166660], Section 8.4. Source DTNs are provided in Table 4-2. Plot from Appendix B, Microsoft Excel File "Compressive and Porosity Data REV00B_PorosityOnly_Tpt.xls," Worksheet "Histogram." Histogram of small-diameter core specimen data includes 25 mm (1 in.) and 51 mm (2 in.) samples (Appendix B, Microsoft Excel File "Compressive and Porosity Data REV00B_PorosityOnly_Tpt.xls," Worksheet "<=51mm," rows 11 through 168). The six specimens with 35-40% porosity come from unwelded vitric rock (subzones Tptrv3 and Tptpv1).

Figure 6.3-2. Histogram of Total Porosity for Small Diameter Topopah Spring Tuff Specimens

The relationship between Uniaxial Compressive Strength and Young's Modulus for the same specimens of Figure 6.3-1 is shown in Figures 6.3-3 and 6.3-4. This relationship is seen to be approximately linear below a Young's Modulus of about 30 GPa, but is quite scattered above 30 GPa. In Figure 6.3-1, a Young's Modulus of 30 GPa corresponds to a total porosity range of about 9 to 13 percent, which is approximately the range of total porosity for matrix groundmass (see footnote). In other words, rock specimens containing lithophysae, spots, and rim material show a relatively strong linear correlation between specimen strength and elastic modulus (Figures 6.3-3 and 6.3-4), while the matrix groundmass rock has much more scatter in the data.

Topopah Spring Units, Small Core (<51mm) Specimens, Saturated, L:D = 2.1, Rate = 10^{-5}
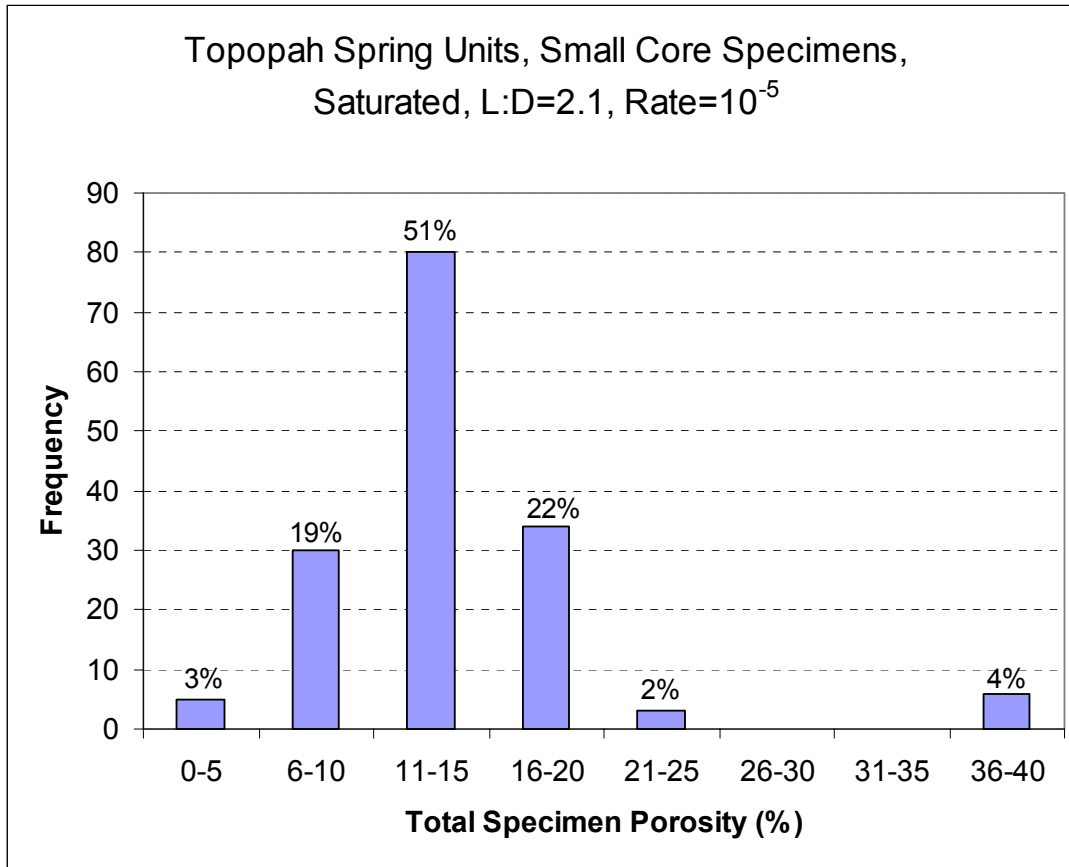

Source: Laboratory testing described in BSC 2003 [DIRS 166660], Section 8.4. Source DTNs are provided in Table 4-2. Plot from Appendix B, Microsoft Excel File "Compressive and Porosity Data REV00B_PorosityOnly_Tpt.xls," Worksheet "q v E" Plotted data from Worksheet "<=51mm," rows 11 through 168.

NOTE: Small-diameter cores from lithophysal rock generally contain only small amounts of lithophysal porosity, and thus the above tests are not indicative, in general, of properties of the Tptpll and Tptpul lithophysal zones.

Figure 6.3-3. Relationship of Intact Uniaxial Compressive Strength to Young's Modulus for Topopah Spring Tuff for Small Diameter Samples

Topopah Spring Units, Small Core (<51mm) Specimens, Saturated, L:D = 2.1, Rate = 10^{-5}
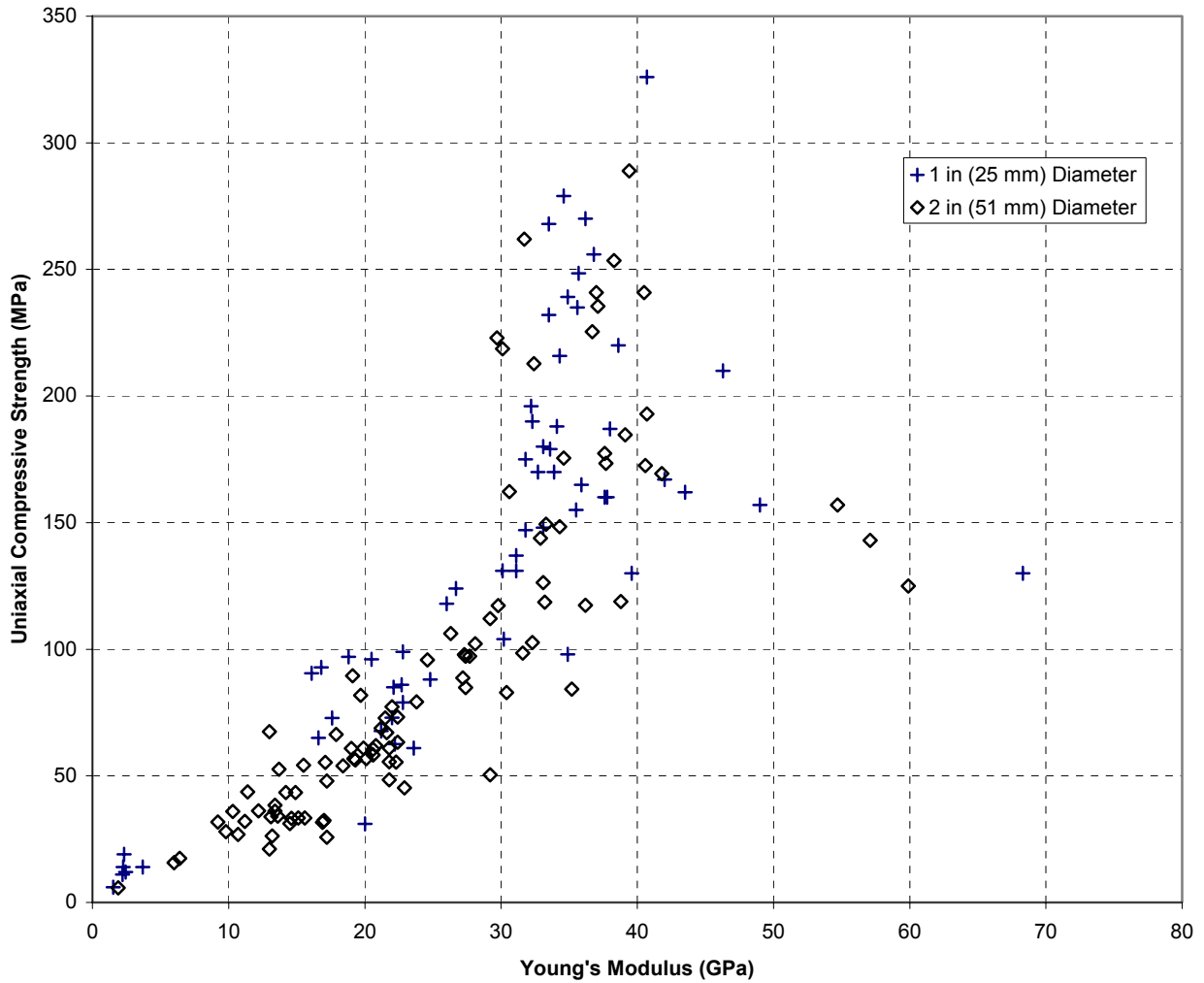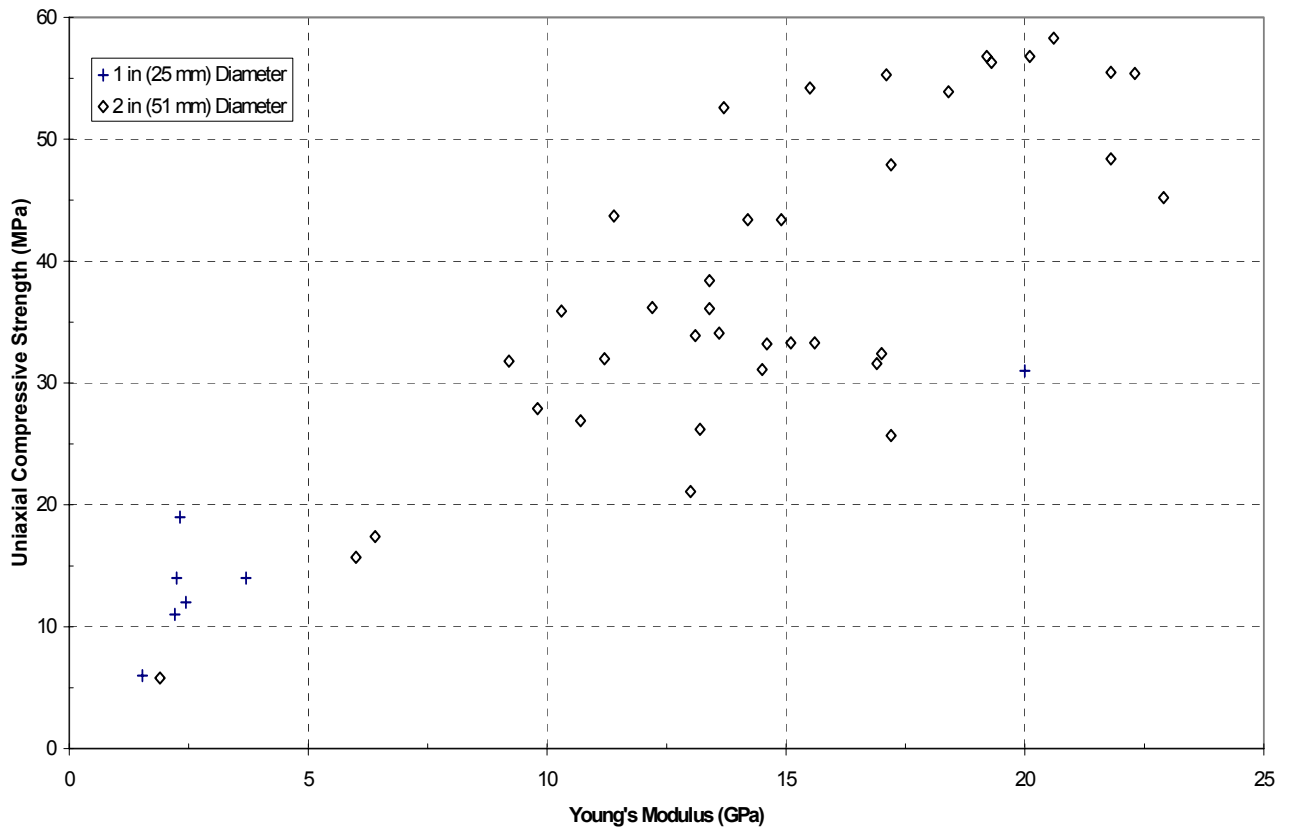

Source: Laboratory testing described in BSC 2003 [DIRS 166660], Section 8.4. Source DTNs are provided in Table 4-2. Plot from Appendix B, Microsoft Excel File "Compressive and Porosity Data REV00B_PorosityOnly_Tpt.xls," Worksheet "q v E (scale)"

NOTE: This figure is the same as Figure 6.3-3 except that it plots only the weaker rock of the data set (less than 60 MPa and less than 25 GPa). Small-diameter cores from lithophysal rock generally contain only small amounts of lithophysal porosity, and thus the above tests are not indicative, in general, of properties of the Tptpll and Tptpul lithophysal zones.

Figure 6.3-4. Relationship of Intact Uniaxial Compressive Strength to Young's Modulus for Topopah Spring Tuff for Small Diameter Samples (Expanded Scale)

On the scale of the emplacement drifts, the total porosity of the lower lithophysal zone (Tptpll) varies from 17 to 45 percent (average of 28 percent), lithophysal porosity values vary from 4 to 35 percent (average of 15 percent), and spot or rim porosity contributes 0 to 10 percent (average of 4 percent) (Figure 6.1-2b and Appendix B, file *Drift Deg AMR AF T-A-P Fit_V1_DBR.xls*, worksheet "Volume Percent – Stats," cells AQ208 to AT218).   The impact of lithophysal voids (and the inability to sample them) with small-diameter core samples is evident in Figures 6.3-1 and 6.3-2 as almost all total porosities of welded specimens are less than 20 percent.

After consideration of previous studies and recent testing, Price indicated it may be "appropriate to conclude that the fits of mechanical properties to porosity based on data from experiments on non lithophysal tuffs (over a range of porosities inclusive of the porosity levels in the lithophysal rocks) are applicable to the lithophysal tuffs" (Price 2004 [DIRS 170894], p. 6). In other words, the same physical relationship between porosity and certain mechanical properties (e.g., Figures 6.3-1, 6.3-3 and 6.3-4) governs in both nonlithophysal and lithophysal rock. In terms of uniaxial strength this relationship appears to have a bilinear nature in that at a rock porosity of approximately 10 percent there is a precipitous drop in strength that separates two UCS versus porosity slopes as seen in Figure 6.3-1. A similar bilinear relation is observed in Figure 6.3-3 where above a Young's modulus of 30 GPa a vertical relation is apparent, whereas below 30 GPa the relationship has a much lower slope. The bifurcation point occurs where nonlithophysal rock becomes lithophysal rock (total rock porosities greater than 10 percent).

Due to the voids often present in the outside surface of lithophysal rock specimens, it is not practical to perform triaxial testing of the specimens. As a result, no strength information as a function of increasing confining pressure is available to determine a Mohr-Coulomb failure envelope (friction angle and cohesion) or Hoek-Brown parameters. These properties will be explored using the numerical modeling of lithophysal rock specimens.

### 6.3.2   Large-Diameter Core Mechanical Behavior

6.3.2.1   Sample Gathering

As discussed above, the small diameter cores (about 51 mm or 2-in diameter and less) may not accurately reflect the true strength or elastic properties of the lithophysal rock since the diameter precludes a reasonable sampling of the lithophysal voids.   Therefore, to estimate ranges of lithophysal rock strength and elastic modulus, greater reliance is placed on measurements from large-diameter core samples that contain multiple lithophysal cavities within a given sample.

To this end, an extensive drilling program was undertaken in the ESF and ECRB Cross-Drift in 2002 to provide representative large-diameter (290 mm or 11.5-in. diameter) core samples of lithophysal rock from the Tptpul and Tptpll zones within the repository host horizon (discussed in Price 2004 [DIRS 170894], mechanical test results are reported in DTNs SN0208L0207502.001 and SN0211L0207502.002).   Figure 6.3-5 shows a plan view of the ESF and ECRB Cross-Drift facilities and the locations from which large-core samples were retrieved (Figures 6.3-6 and 6.3-7 for photographs of some core lengths obtained from the Tptpul and Tptpll in the ECRB Cross-Drift).   A total of 19 (290 mm or 11.5-in. diameter) cores with a length of at least 304 mm (12-in) were obtained.   Of these, 13 had a length to diameter (L:D) ratio of 1.7 or greater (Table 6.3-1).   These were felt to be sufficiently close to the recommended 2:1 length to diameter ratio to allow for uniaxial compressive strength testing.   Figure 6.3-6 shows a photograph of an uniaxial compressive strength test in progress.

However, great difficulty was encountered in recovering specimens of sufficient length for proper mechanical testing, and so sixteen specimens were under-cored (Figure 6.3-8) to provide 16 additional 146 mm (5.75-in) diameter samples.   These 146 mm diameter specimens were tested and the mechanical property results are discussed in Price 2004 [DIRS 170894] and available in DTNs SN0302L0207502.003 and SN0305L0207502.004], but unfortunately, porosity measurements are not yet available.   Although these samples are not judged to be sufficiently large to represent in situ properties, the data is nonetheless useful as additional information for establishing the relationship between strength and modulus and for estimating sample size effects.

This data was supplemented by previous testing by Price et al. 1985 [DIRS 106602] on 267 mm (10.5-in) diameter cores (Figure 6.3-9) taken from an outcrop of the Tptpul at Busted Butte (mechanical test results are reported in DTN: SNSAND84086000.000).   The boulders of tuff were collected from the southeastern flank of Busted Butte (Price et al. 1987 [DIRS 100173], pp. 7-8), located 5.5 km (3.4 mi) southeast of ESF Tptpul 290 mm diameter samples and 8 km (5 mi) southeast of ECRB Cross-Drift Tptpll 290 mm diameter samples (Figures 6.3-5 and 6.3-10). Other excavated specimens of Busted Butte tuff were shown to be petrologically and mineralogically equivalent to borehole samples from the same stratigraphic horizons (Price et al. 1987 [DIRS 100173]), however, the outcrop rock may be slightly weaker due to its proximity to the ground surface.   It will be assumed that the Busted Butte lithophysal samples exhibit the same mechanical behavior to samples of lithophysal tuff sampled from within Yucca Mountain.
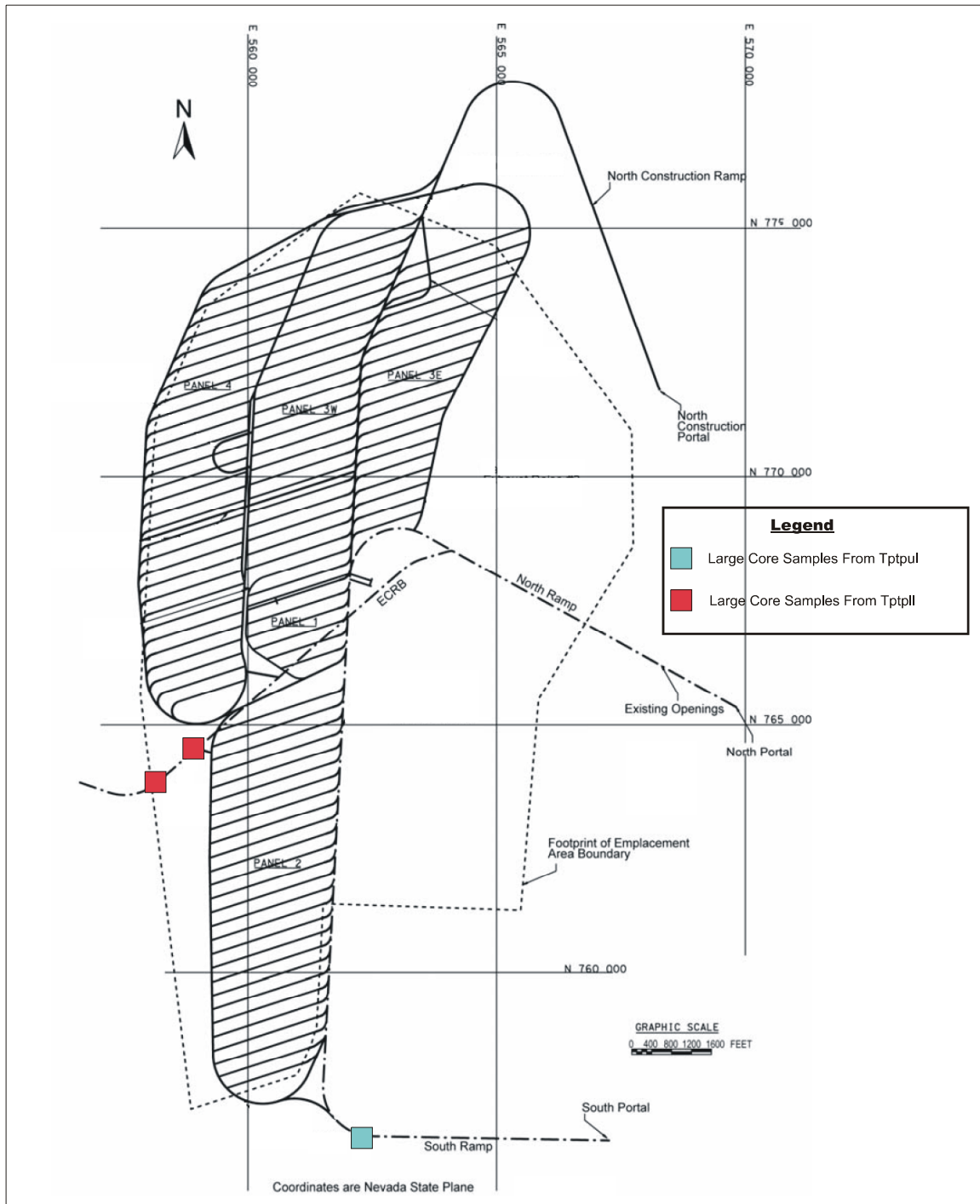
Source: Modified from BSC 2004 [DIRS 164519, Figure 1]. ESF or ECRB Cross-Drift Stationing from Figures 3 and 4 of BSC 2003 [DIRS 165572]. Specimen stationing locations taken from DTNs in Table 4-2, SN0302L0207502.003, and SN0305L0207502.004].

NOTE: Locations of 290 mm (11.5-in) diameter specimens: 9 near ESF 64+00 and 4 near ECRB 19+00. Locations of 146 mm (5.75-in) diameter specimens: 8 near ESF 64+00, 3 near ECRB 19+00, and 5 near ECRB 22+00.

Figure 6.3-5. Plan View of the ESF and ECRB Cross-Drift Facilities Showing the Locations Where Large-Diameter Lithophysal Samples (290 mm and 146 mm) Were Cored

Figure 6.3-6. Photographs of Large Lithophysal Core Samples (290 mm or 11.5-in. diameter) from the Tptpll and Tptpul Units (top) and a Sample in Uniaxial Compression (bottom)
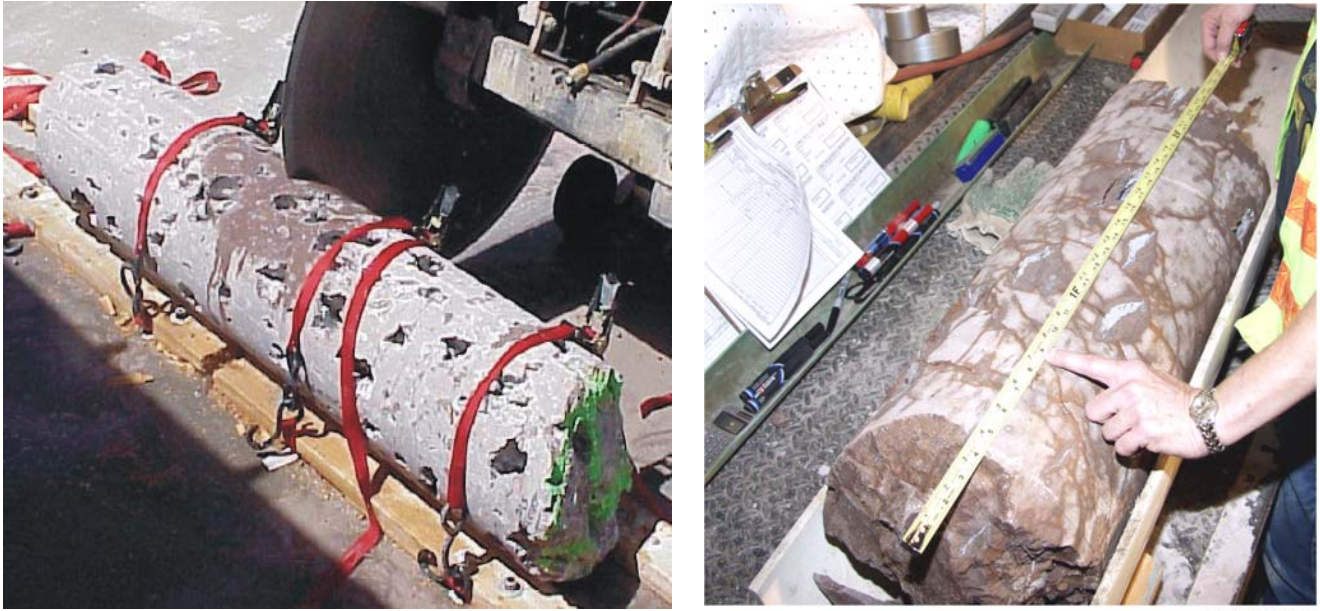
NOTE: Photographs of specimens from Tptpul (left) and from Tptpll (right). Moisture on specimen surface at right shows the intensive internal fracturing and lithophysae network.

Figure 6.3-7. Large (305 mm) Diameter Cores from Tptpul and Tptpll Units

NOTE: Lithophysae, white rims around lithophysae, and white spots are visible in these specimens.

Figure 6.3-8. Large (146 mm or 5.75-in) Diameter Subcores

NOTE: Lithophysae (voids), whitish rims around lithophysae, and white spots are visible in this specimen.

Figure 6.3-9. Large (267 mm or 10.5-in) Diameter Busted Butte Samples from the Tptpul Unit
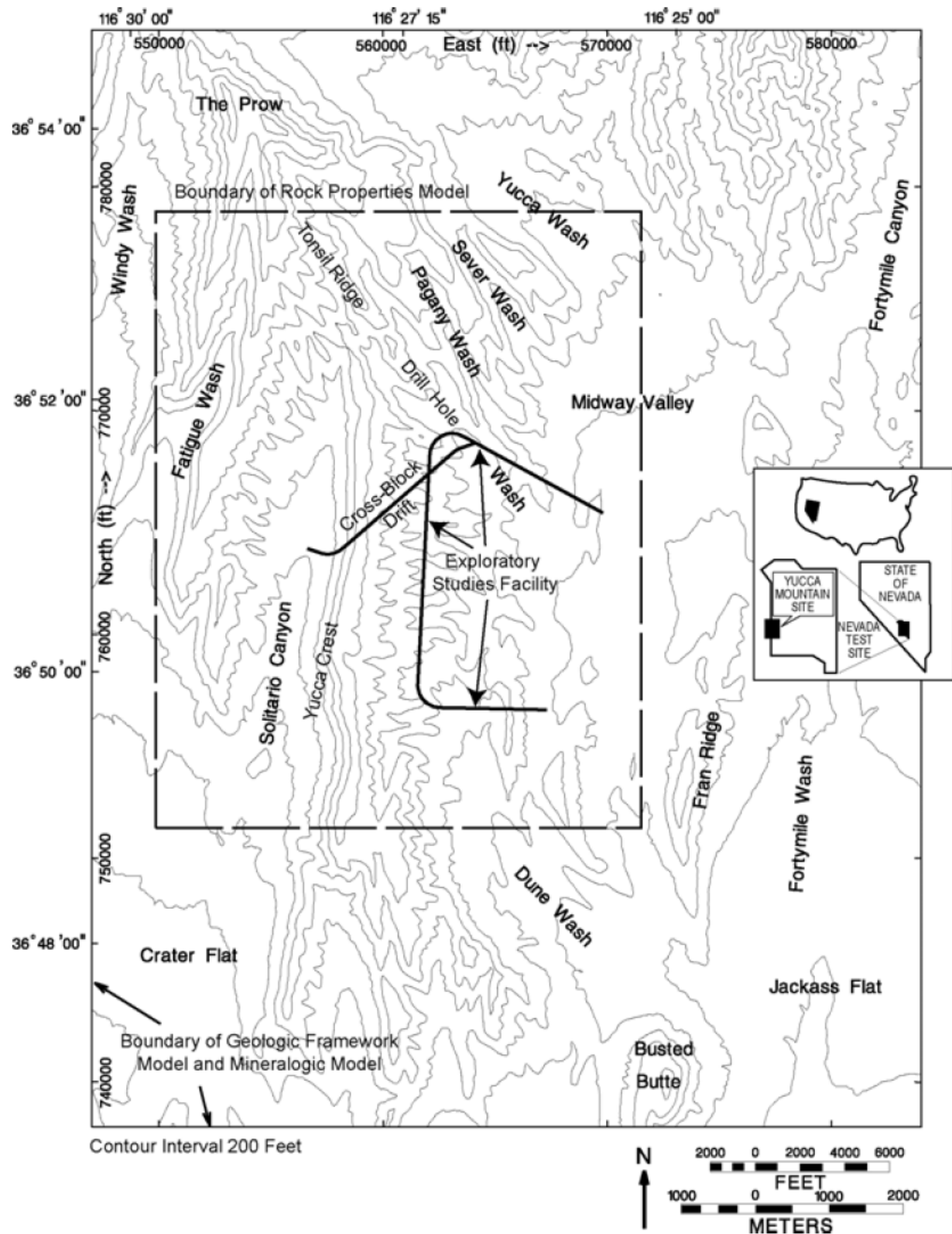
Source: Modified from BSC 2004 [DIRS 170029], Figure 1-1, p. 1-3.

NOTE: Busted Butte is visible on the southeast boundary of map.

Figure 6.3-10. Map Showing Topographical Features in the Vicinity of Yucca Mountain, the Location of Excavated Tunnels, and Various Project Modeling Boundaries

6.3.2.2 Large-Diameter Core Test Results and Analysis of Data

The results of compression testing on 290 mm (11.5-in) diameter samples from the Tptpul and Tptpll from the ESF main loop and ECRB Cross-Drift and 267 mm (10.5-in) diameter samples from the Tptpul at Busted Butte form the basis for the development of mechanical property ranges. The laboratory data from these tests are provided in Table 6.3-1. The test results used in this analysis excluded tests conducted at high temperatures (greater than 100 ºC) and specimen results where the length to diameter (L:D) ratio is 1.5 or less. This left ten Busted Butte samples and thirteen ESF or ECRB Cross-Drift samples (nine tested under room dry conditions and 4 tested saturated).

The combined instrument uncertainty involved in determining uniaxial compressive strength of these samples of lithophysal rock are approximately ± 3 percent, and ± 3.5 percent for determination of Young's moduls (Price 2004 [DIRS 170894], p. 3). The lithophysal porosity for each of the large-diameter specimens was estimated by conducting four vertical line surveys down the length of each specimen and involves significant uncertainty, probably as much as 15 to 20 percent. The source of the lithophysal porosity estimates is DTN: SN0305L0207502.005 and a quantification of associated uncertainty may be available later. The contribution to uncertainty due to the small number of samples (based on the standard error, Appendix B, Microsoft Excel file "LithophysalRockRanges_Calc.xls," Worksheet "rock-props") is for the ten Busted Butte samples: ±10 percent (strength), ±6 percent (Young's modulus), and ±7 percent (lithophysal porosity). The limited sample uncertainty for all 13 ESF or ECRB Cross-Drift 290 mm diameter samples is: ±11 percent (strength), ±15 percent (Young's modulus), and ±9 percent (lithophysal porosity). Total porosity was estimated by summing: (1) the volume fraction of lithophysae (lithophysal porosity), (2) the volume fraction of the matrix groundmass multiplied by the average matrix porosity, and (3) the volume fraction of rims and spots multiplied by the average rim or spot porosity (Price 2004 [DIRS 170894], p. 4 and DTN: SN0305L0207502.006).

An example of a stress-strain curve obtained during laboratory testing is shown in Figure 6.3-11. The initial non-linear portion of the curve up to about 0.15 percent strain is not due to non-linear material behavior at low stress levels but, rather, a consequence of imperfect contacts between the sample and loading platens. It is likely that the first micro-fractures begin to occur during linear elastic loading. With additional loading, the linear elastic strain response transitions into a nonlinear specimen response as more micro-fractures are created in the specimen's matrix-groundmass (prior to point A). Failure begins to occur at yielding (approximately point A) when localized micro-fractures begin to coalesce into macro-fractures and permanent (plastic) strains begin to be measured in the specimen. Local failure can be physically described as that portion of the rock that is structurally supporting a significant portion of the load fails, possibly leading to a substantial redistribution in stresses across the specimen, and an observed temporary drop in stress or as seen in Figure 6.3-11, an increase of strain at more or less constant stress. Further loading beyond point A creates additional micro-fractures, development of more macro-fractures that often connect lithophysae, and more plastic strains. The uniaxial compressive strength of a rock specimen represents the specimen failure strength for the purposes of this calculation, and is defined as that stress representing the peak or maximum uniaxial stress experienced by the specimen during its loading history (point C, or 0.4 percent of axial strain). However, from the stress-strain curve, it is clear that the sample is already in an active state of failure at point B, or

0.36 percent of axial strain. If it is not possible for the specimen to further redistribute the applied level of stresses after local failure, then the peak stress has been reached (corresponding to the maximum compressive strength of the specimen) and the sample of tuff may fail catastrophically. For the case of nonlithophysal Topopah Spring Tuff, this entire response is typically brittle, meaning the progression from linear elastic behavior to macro-fractures and ultimate failure occurs very rapidly. For lithophysal tuff the response tends to be less brittle since the presence of lithophysae allow for local failure and redistribution of stresses before peak failure is reached. The state of failure for the idealized elastic-plastic model occurs at point A', which is the assumed transition point between linear elastic behavior and plastic failure.
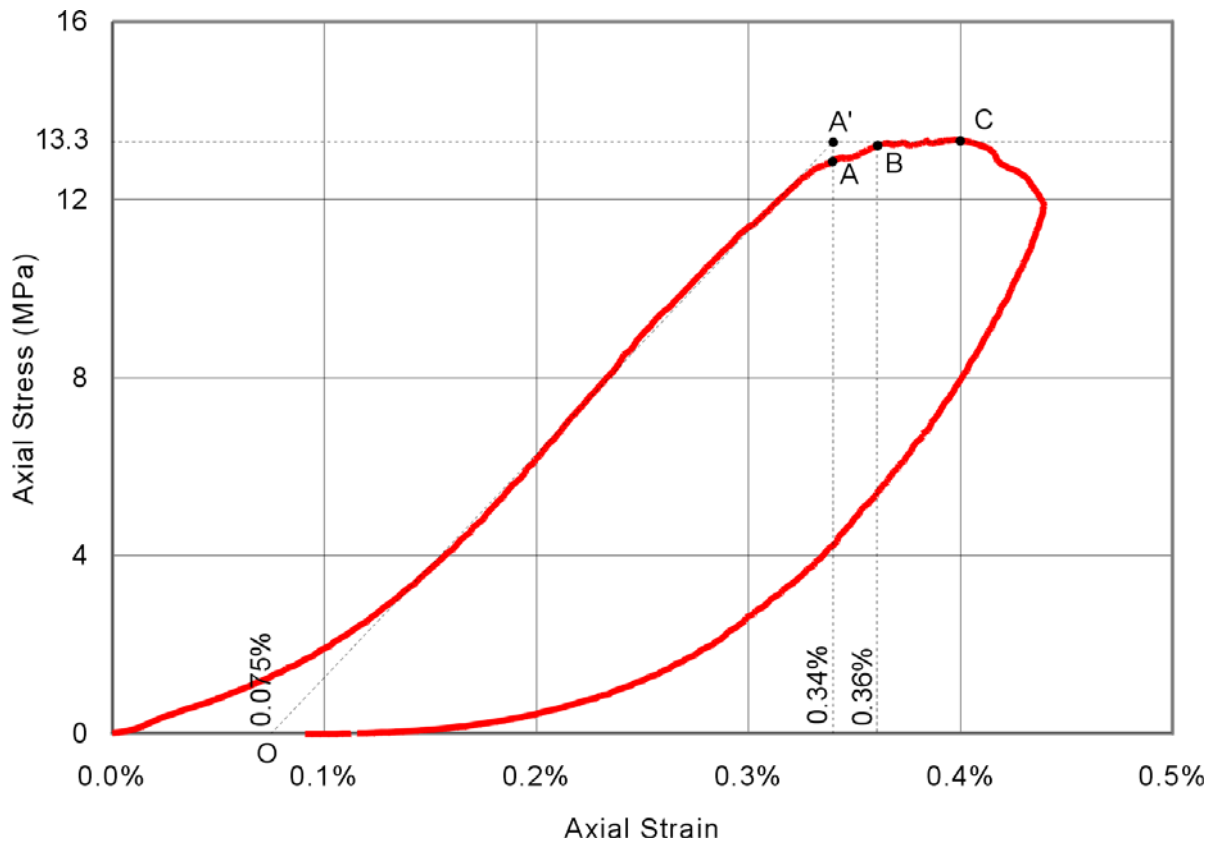
Source: Stress-strain data for test taken from DTN: SN0211L0207502.002, *Supporting Information for Mechanical Properties of Lithophysal Tuff, Batch #2* (MOL.20030214.0179), Section 6 "Reduced Data Tables and Plots," pp. 207-215.

NOTE: This sample is cored from the Tptpll unit in the ECRB Cross-Drift with test ID is ECRB-GTEC-CS1928-02-0.0'-2.5'-01023424-SNL-A (Batch #2, YMPLL24A). From Table 6.3-1 it is reported that the sample was tested in a room dry condition, length to diameter ratio is 1.8, the lithophysal porosity is 22.2 %, uniaxial compressive strength is 13.3 MPa, Young's modulus is 5.0 GPa, and the axial strain at failure is 0.4%.

Figure 6.3-11. Experimental Stress-Strain Curve for Tptpll 290 mm Diameter Sample YMPLL24A
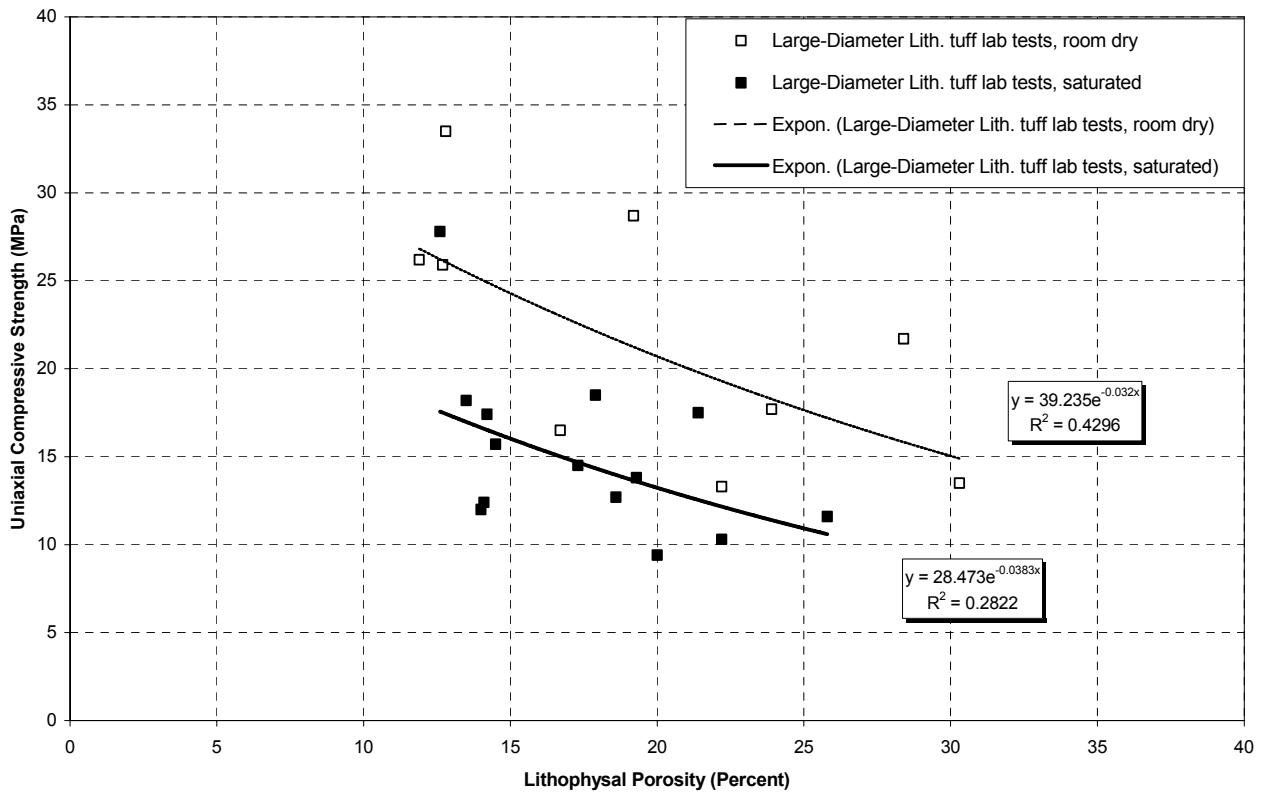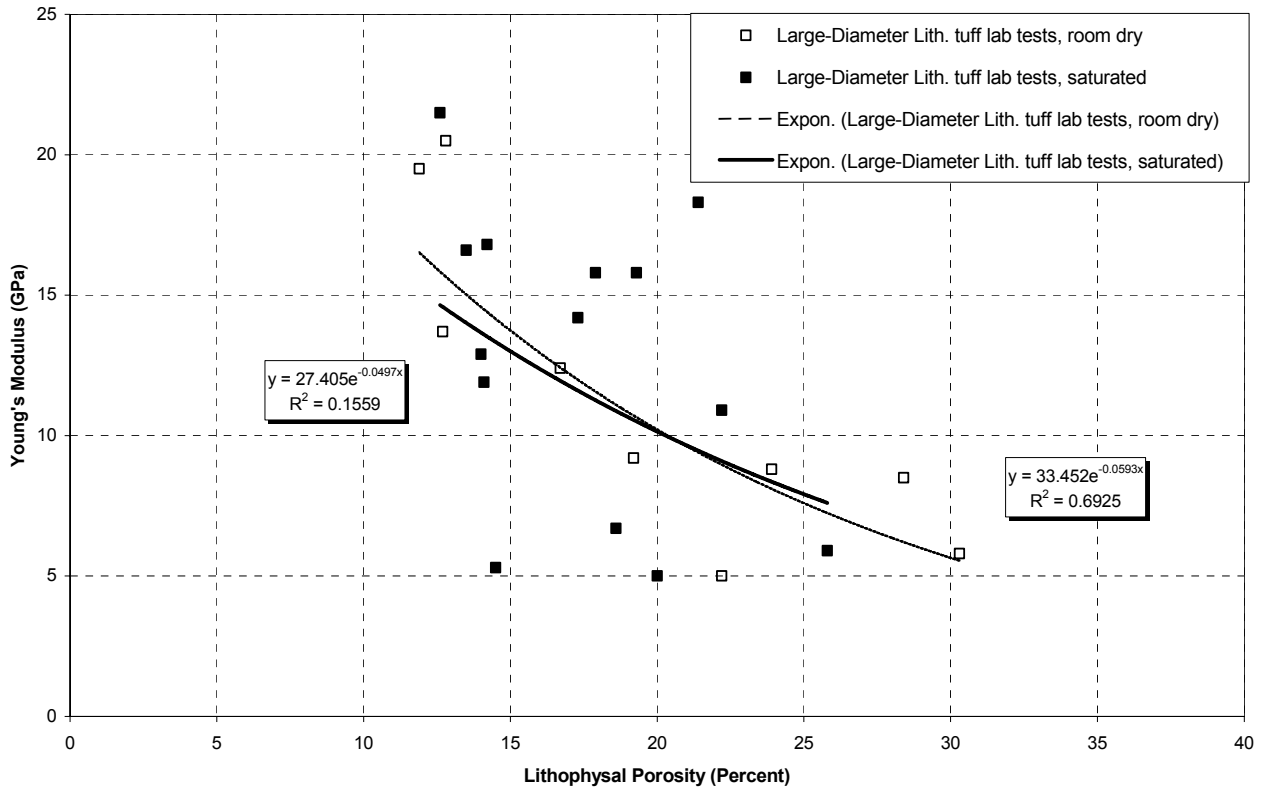
The uniaxial compressive strength and Young's modulus are shown as functions of approximate lithophysal porosity for the 267 mm (10.5-in) and 290 mm (11.5-in) diameter samples of the Tptpll and Tptpul in Figure 6.3-12. Although significant scatter exists in the data, a best-fit exponential function has been superimposed on the data for both room dry and saturated sample conditions. These data show little impact of saturation level on Young's Modulus, but results in a general reduction in uniaxial compressive strength (UCS) with the saturated samples tending to form a lower bound to the room dry strengths. Histograms of the distribution of UCS and Young's Modulus are presented in Figure 6.3-13. A mean strength of 17.8 MPa and a mean modulus of 12.2 GPa were calculated based on large-diameter samples (Appendix B, Microsoft Excel file "LithophysalRockRanges_Calc.xls," Worksheet "histograms.").

It is useful to define the relationship of the UCS and Young's Modulus in a fashion that is independent of the lithophysal porosity. The UCS and Young's Modulus are the primary mechanical input properties, and representing their interrelationship on a single diagram allows one to more easily develop a base set of input properties that will define the pairing of these parameters across the entire range of potential in situ porosity conditions. The UCS and modulus data for each large-diameter core test, presented in Figure 6.3-12, is plotted by core saturation level in the form of UCS vs Young's modulus in Figure 6.3-14. These data show that a reasonably linear relationship exists between these mechanical properties, which was the case also for the small-diameter core data (Figures 6.3-3 and 6.3-4). The large core data have been subdivided into two sets – the room dry and saturated data – and linear relations fit to each set. As seen in this plot, the saturated samples tend to form a lower bound to the room dry strengths. On the average, small-diameter core UCS values are slightly higher than large-diameter core UCS values for corresponding Young's moduli less than 25 GPa (Figure 6.3-4).

An alternative way to plot the large-diameter core test results is by sample location (Figure 6.3-15). The Busted Butte sample tests appear to comprise a lower strength subgroup in the figure, as do the saturated ESF or ECRB Cross-Drift sample tests, which, on average, yield lower strength results than the ESF or ECRB Cross-Drift sample room-dry results.

As in small samples, due to the voids often present in the outside surface of lithophysal rock specimens, it is not practical to perform triaxial testing of the specimens. As a result, no strength information as a function of increasing confining pressure is available for large diameter specimens to determine a Mohr-Coulomb failure envelope (friction angle and cohesion) or Hoek-Brown parameters. These properties will be explored using the numerical modeling of lithophysal rock specimens.

Source: Appendix B, Microsoft Excel file "LithophysalRockRanges_Calc.xls," Worksheets "LC E-por" and "LC q-por"
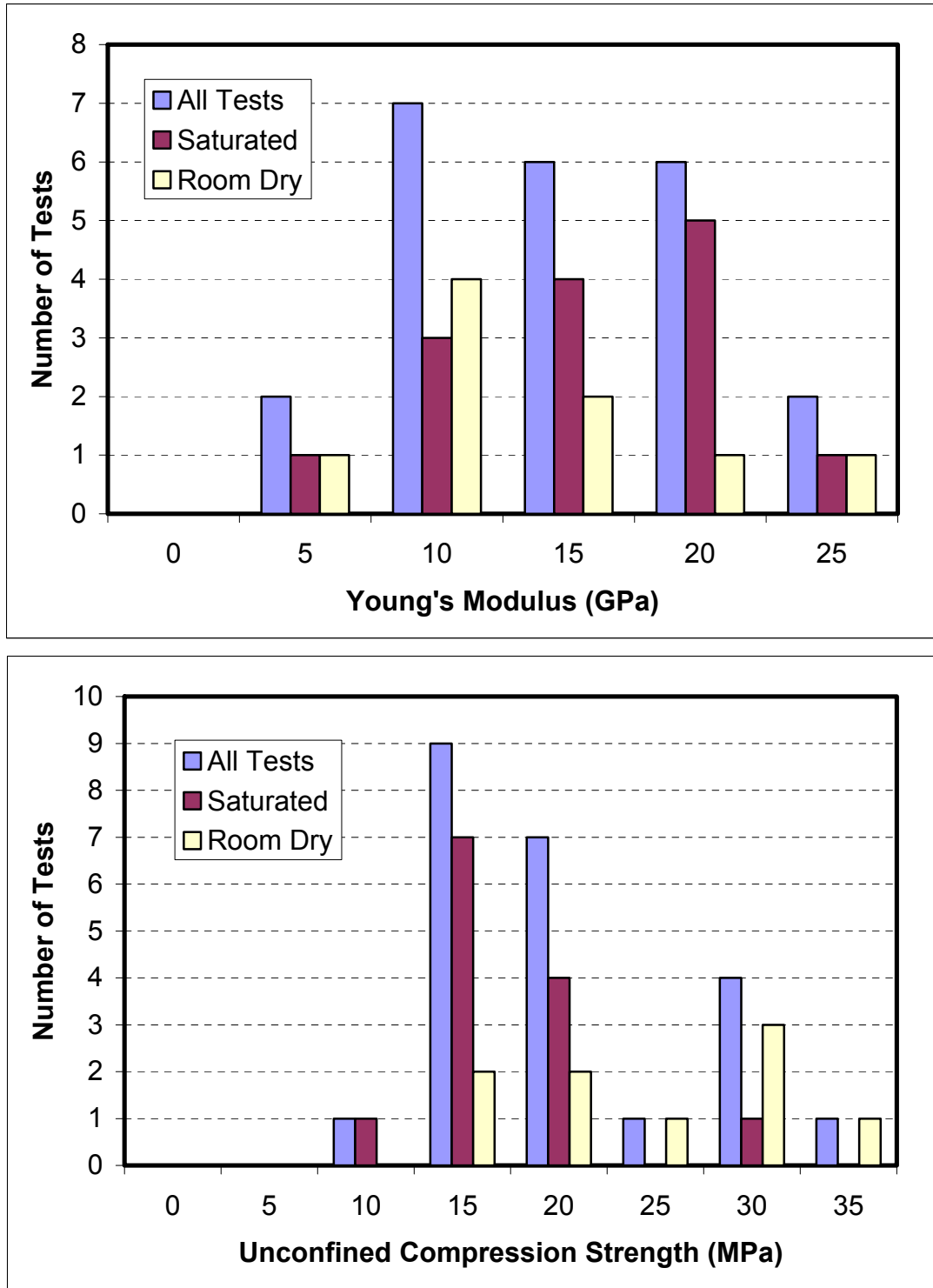
Figure 6.3-12. Variation in Young's Modulus (top) and Uniaxial Compressive Strength (bottom) as a Function of the Lithophysal Void Porosity for 10.5 and 11.5-in. Diameter Cores from the Tptpul and Tptpll Units.

Table 6.3-1. Mechanical Test Results of Lithophysal Tuff from 267 and 290 mm-Diameter Samples

Test ID	Lithostratigraphic Unit	L:D Ratio	Saturation	Temperature (ºC)	Uniaxial Strength (MPa)	Young's Modulus (GPa)	Poisson's Ratio	Estimated Lithophysal Porosity	Estimated Total Porosity	DTN
YMPLL49A	Tptpll	1.1 : 1	Dry	195	32.2	7.1	—	11.7	23.6	SN0211L0207502.002*
YMPLL43A	Tptpll	1.1 : 1	Dry	200	31.1	6.5	—	20.3	29.2	SN0211L0207502.002*
YMPLL23A	Tptpll	1.8 : 1	Room Dry	24	28.7	9.2	—	19.2	30.6	SN0211L0207502.002*
YMPLL24A	Tptpll	1.8 : 1	Room Dry	24	13.3	5.0	—	22.2	32.4	SN0211L0207502.002*
YMPLL46A	Tptpll	1.8 : 1	Room Dry	24	21.7	8.5	—	28.4	37.4	SN0211L0207502.002*
YMPLL87A	Tptpll	1.9 : 1	Saturated	24	15.7	5.3	—	14.5	25.7	SN0211L0207502.002*
YMPUL59B	Tptpul	1.2 : 1	Dry	190	19.6	7.3	—	39.4	56.8	SN0208L0207502.001*
YMPUL67A	Tptpul	1.3 : 1	Dry	190	34.8	9.9	—	6.2	25.3	SN0208L0207502.001*
YMPUL62B	Tptpul	1.0 : 1	Dry	200	37.0	13.7	—	19.3	42.8	SN0208L0207502.001*
YMPUL50A	Tptpul	1.5 : 1	Room Dry	24	22.1	14.9	0.21	28.5	40.9	SN0211L0207502.002*
YMPUL59A	Tptpul	2.0 : 1	Room Dry	24	13.5	5.8	0.39	30.3	51.7	SN0208L0207502.001*
YMPUL61A	Tptpul	1.9 : 1	Room Dry	24	17.7	8.8	—	23.9	38.2	SN0208L0207502.001*
YMPUL62A	Tptpul	1.8 : 1	Room Dry	24	25.9	13.7	—	12.7	32.2	SN0208L0207502.001*
YMPUL64A	Tptpul	1.7 : 1	Room Dry	24	33.5	20.5	—	12.8	31.0	SN0208L0207502.001*
YMPUL65A	Tptpul	2.0 : 1	Room Dry	24	26.2	19.5	—	11.9	25.6	SN0208L0207502.001*
YMPUL66A	Tptpul	1.7 : 1	Room Dry	24	16.5	12.4	—	16.7	31.0	SN0208L0207502.001*
YMPUL60A	Tptpul	1.8 : 1	Saturated	24	12.7	6.7	—	18.6	38.7	SN0208L0207502.001*
YMPUL63A	Tptpul	1.9 : 1	Saturated	24	9.4	5.0	0.24	20.0	38.7	SN0208L0207502.001*
YMPUL68A	Tptpul	2.1 : 1	Saturated	24	11.6	5.9	0.03	25.8	39.3	SN0208L0207502.001*
1B	Tptpul	2.0 : 1	Saturated	22	14.5	14.2	0.14	17.3	32.7	SNSAND84086000.000
1D	Tptpul	2.0 : 1	Saturated	22	10.3	10.9	0.14	22.2	33.3	SNSAND84086000.000
2A	Tptpul	2.0 : 1	Saturated	22	12.4	11.9	0.16	14.1	30.9	SNSAND84086000.000
3A	Tptpul	2.0 : 1	Saturated	22	12.0	12.9	0.14	14.0	40.0	SNSAND84086000.000
8A	Tptpul	2.0 : 1	Saturated	22	18.2	16.6	0.14	13.5	38.2	SNSAND84086000.000
8B	Tptpul	2.0 : 1	Saturated	22	17.4	16.8	0.18	14.2	32.0	SNSAND84086000.000
8C	Tptpul	2.0 : 1	Saturated	22	18.5	15.8	0.13	17.9	34.4	SNSAND84086000.000
8D	Tptpul	2.0 : 1	Saturated	22	17.5	18.3	0.13	21.4	37.9	SNSAND84086000.000
8E	Tptpul	2.0 : 1	Saturated	22	13.8	15.8	0.21	19.3	35.5	SNSAND84086000.000
8F	Tptpul	2.0 : 1	Saturated	22	27.8	21.5	0.21	12.6	37.2	SNSAND84086000.000

Source DTNs are also listed in Table 4-2. For DTNs listed above and marked with an (*), the estimate of lithophysal porosity is given in DTN: SN0305L0207502.005 as volume fraction of lithophysae, and the estimate of total porosity is given in DTN: SN0305L0207502.006. The associated qualified DTN of compressive strength values is MO0311RCKPRPCS.003 and qualified DTN of Young's Modulus values is MO0402DQRIRPPR.003.

Note: Not all DTNs above are used in Section 6. Excluded are test results conducted at high temperatures (greater than 100 ºC) and specimen results where the length to diameter (L:D) ratio is 1.5 or less.

Source: Appendix B, Microsoft Excel file "LithophysalRockRanges_Calc.xls," Worksheet "histograms."

Figure 6.3-13. Histograms of Young's Modulus (top) and Uniaxial Compressive Strength (bottom) for the 10.5 and 11.5-in. diameter core samples of Topopah Spring lithophysal tuff.
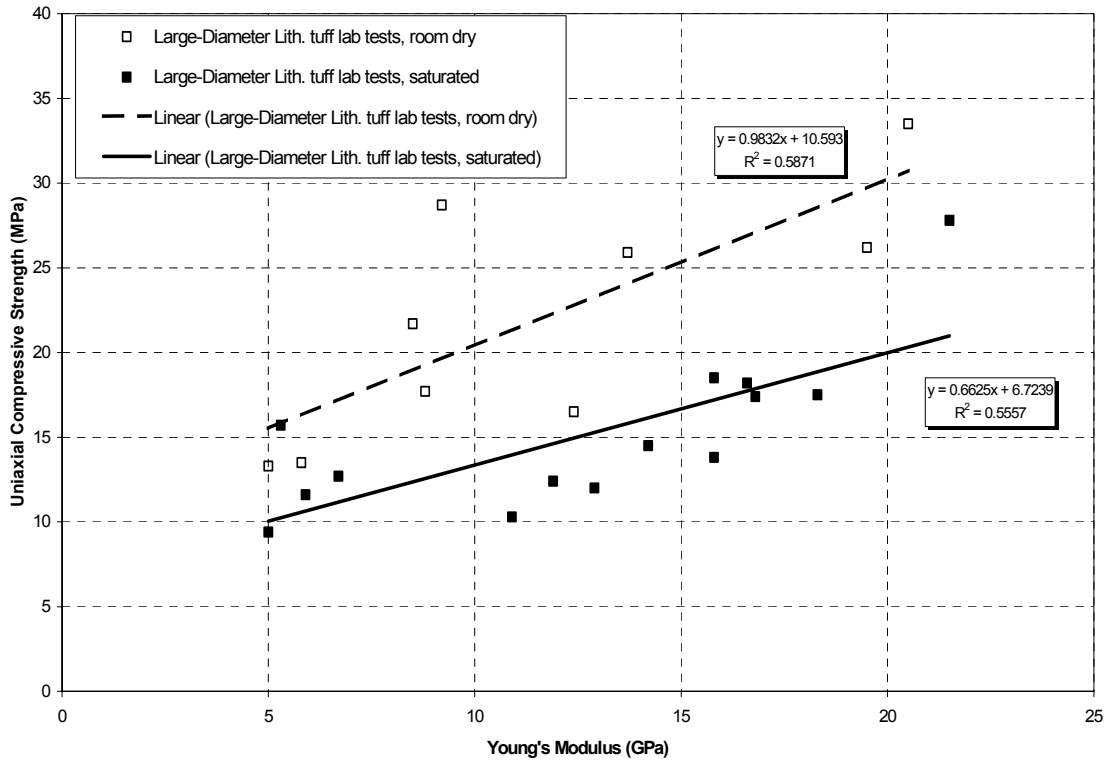
Source: Appendix B, Microsoft Excel file "LithophysalRockRanges_Calc.xls," Worksheet "LC q-E."

Figure 6.3-14. Uniaxial Compressive Strength as a Function of Young's Modulus and Saturation Level for 10.5 and 11.5-in. Diameter Cores from the Tptpul and Tptpll Units.
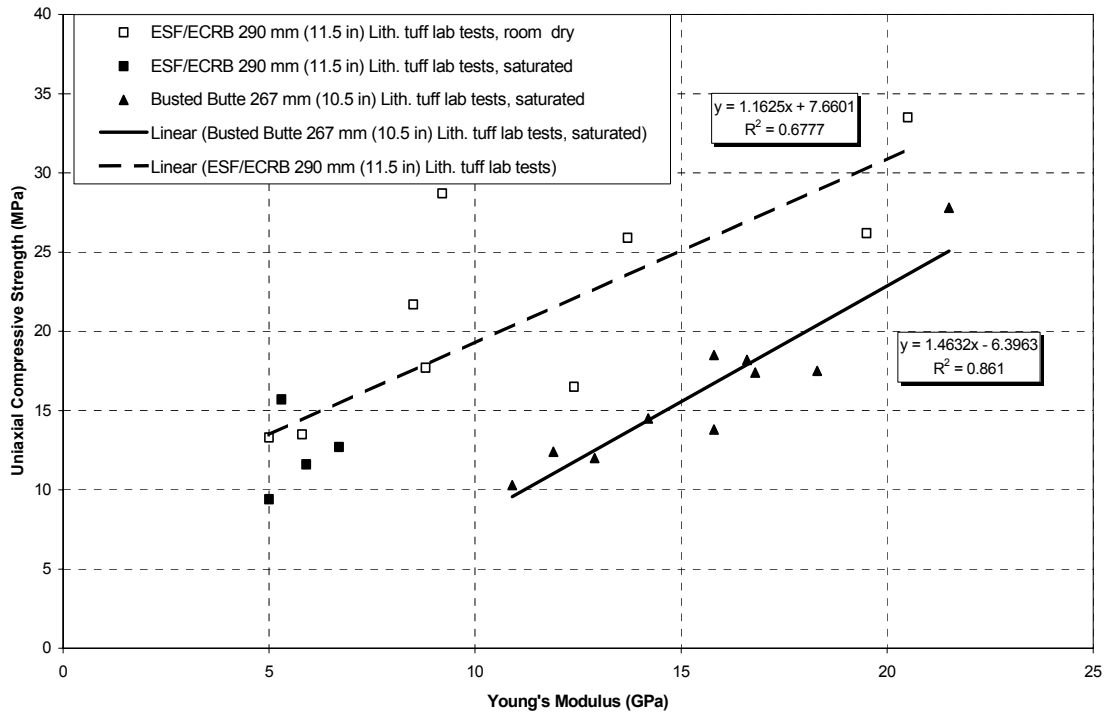
Source: Appendix B, Microsoft Excel file "LithophysalRockRanges_Calc.xls," Worksheet "LargeCores."

Figure 6.3-15. Uniaxial Compressive Strength as a Function of Young's Modulus and Sample Location for 10.5 and 11.5-in. Diameter Cores from the Tptpul and Tptpll Units.

6.3.3   Size Effect Study for Lithophysal Rock

A significant sample-size effect on mechanical rock properties is revealed when test results of various diameter samples of Topopah Spring Tuff are compared. Figure 6.3-16 shows the sample-size effect portrayed in a plot of compressive strength versus Young's modulus for medium to large-sized ESF or ECRB Cross-Drift lithophysal rock specimens. This figure also shows that saturated samples sometimes yield strengths higher than unsaturated samples of similar rock at equivalent Young's modulus values (compare with Figure 6.3-15). Figure 6.3-17 combines the test results of Sections 6.3.1 and 6.3.2 and shows the sample-size effect in a plot of compressive strength versus Young's modulus between small and large-sized Topopah Spring Tuff specimens. When the same mechanical test results are plotted versus total sample porosity on a log-log scale the sample-size effect is again observed (Figure 6.3-18). As is expected, the lithophysal rock large-core samples generally have higher porosity since they are able to contain lithophysae and parts of lithophysae within their volume.

A recent program of laboratory compression testing (Price 2004 [DIRS 170894]) was carried out to examine several important effects, including sample size, orientation (anisotropy), and saturation of the Tptpll (and comparison to previous testing in the Tptpmn). Four large boulders were removed from the southeast flank of Busted Butte from the outcrop of the lower portion of the Tptpll zone.   This Busted Butte lithophysal tuff is similar to lithostratigraphic zones identified within the central block of Yucca Mountain, however, Busted Butte Tptpll rock has far fewer lithophysae (about 2 percent) compared to the 5 to 25 percent in the central block. The rock block was collected and initially cut into samples of manageable size (Figure 6.3-19).

A total of one hundred twenty-five (125) samples with sizes ranging from 1 to 8.8-in. (26 to 223 mm) diameter were cut and tested to examine the size effect. Of the 125 samples tested, 120 were right-circular cylinders with nominal diameters of 26, 51, 82 and 121 mm (1, 2, 3.2 and 4.7-in), with all L:D ratios very close to 2:1 (with a range of from 1.9:1 to 2.1:1). The remaining five (5) samples were 200 mm (8-in) square-sided parallelepipeds with an average L:D ratio of 2:1. This series of tests comes from DTN: SN0306L0207502.008 [DIRS 165015].

The results of the sample size on UCS are shown in Figure 6.3-20. In this figure, the UCS is plotted as a function of the sample volume (as a log-log plot), and is compared to the test data for the Tptpmn given in Price 1986 [DIRS 106589]. The vertical offset of the two lines is indicative of the slightly different average strength of the Tptpll and Tptpmn matrix material, although the size effect is virtually identical. These results are consistent with the slight drop in strength observed between small-diameter core specimens (from drill holes) and large-diameter core specimens (from ESF and ECRB Cross-Drift tunnel wall borings) sampled from Topopah Spring Tuff near the repository rock (compare between Figures 6.3-4 and 6.3-14).

Lithophysal Rock Medium and Large-Core Specimens

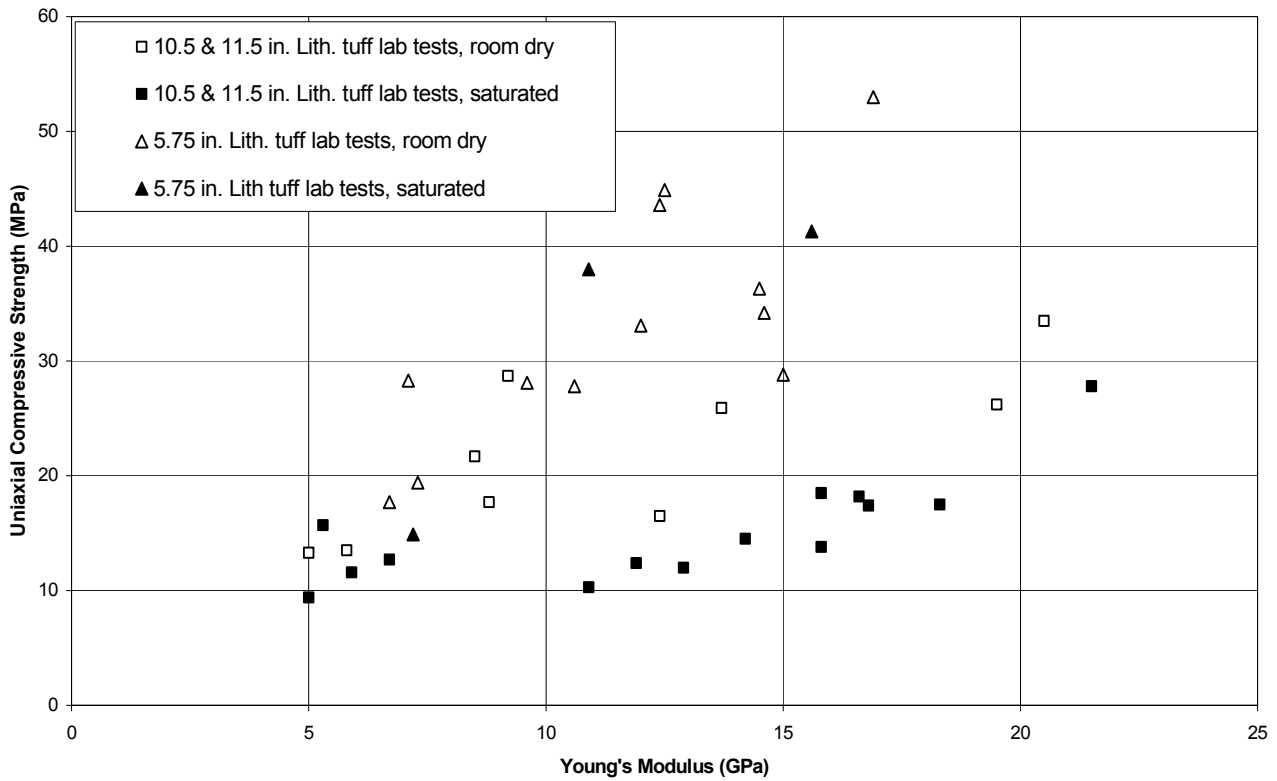Source: Appendix B, Microsoft Excel file "LithophysalRockRanges_Calc.xls," Worksheet "6-in cores."

NOTE: Results from the testing of Tptpul or Tptpll large-core samples (DTNs in Table 4-2, SN0302L0207502.003, and SN0305L0207502.004]). The 146 mm (5.75-in) diameter samples (triangles) generally have higher strengths than the larger samples (squares), as is expected due the sample size effect (no sample porosity data is currently available for 146 mm diameter samples).

Figure 6.3-16. Results of Intact Uniaxial Compressive Strength to Young's Modulus for Medium and Large-Core Specimens of Lithophysal Rock
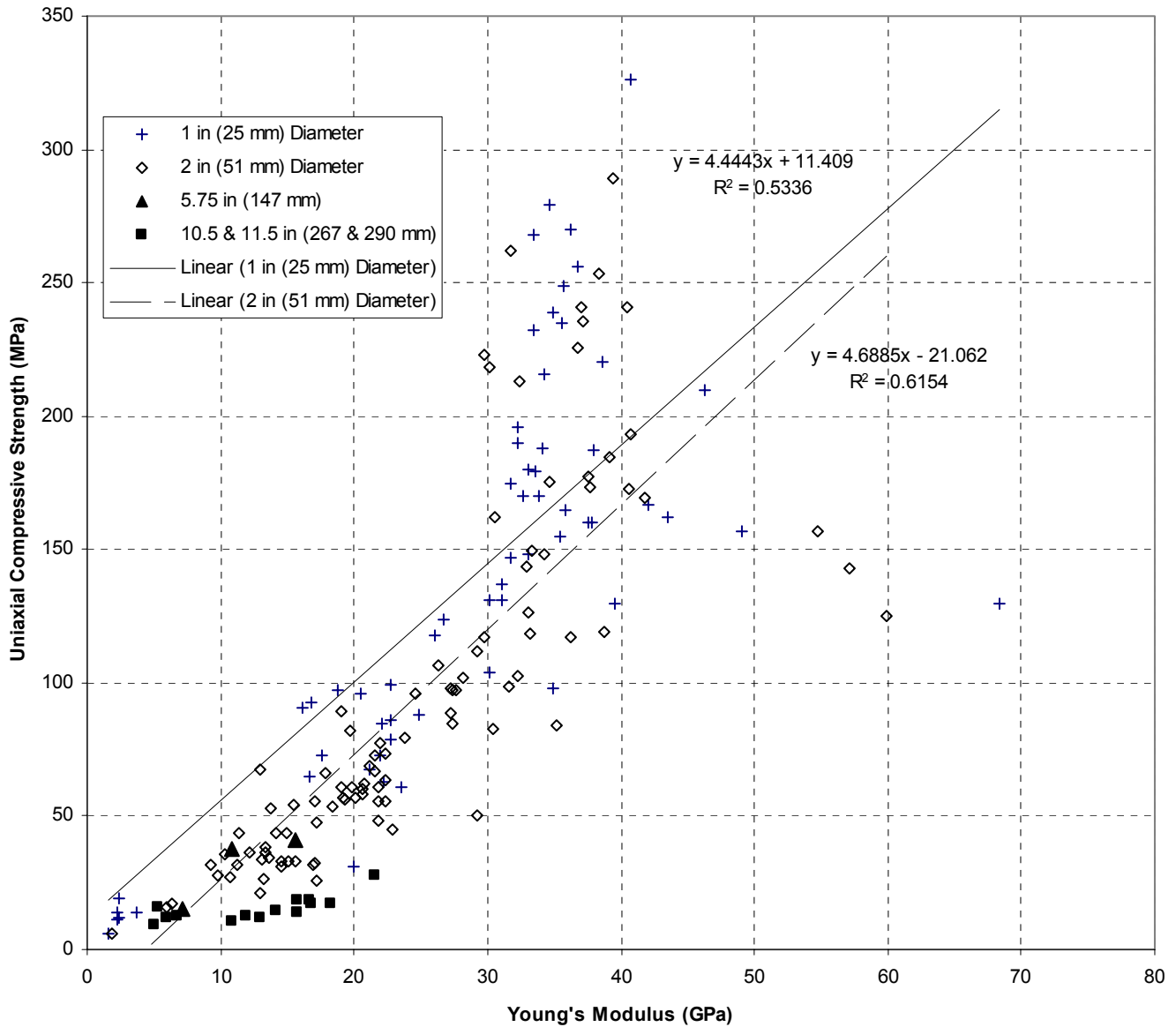
Source: Appendix B, Microsoft Excel file "Compressive and Porosity Data REV00B_PorosityOnly_Tpt.xls," Worksheet "Plots."

NOTE: From the best fit lines to the 25 mm and 51 mm diameter test data shows that for the same Young's moduls the 25 mm diameter samples are on the average about 25 MPa stronger. The 147 mm diameter test data plots near the 51 mm data, but at greatly reduced strength and modulus levels. The large-core data (267 and 290 mm diameter) has the least strength of all sample sizes for similar Young's modulus values.

Figure 6.3-17. Results of Intact Uniaxial Compressive Strength to Young's Modulus for Saturated Small and Large-Core Specimens of Topopah Spring Lithophysal Rock
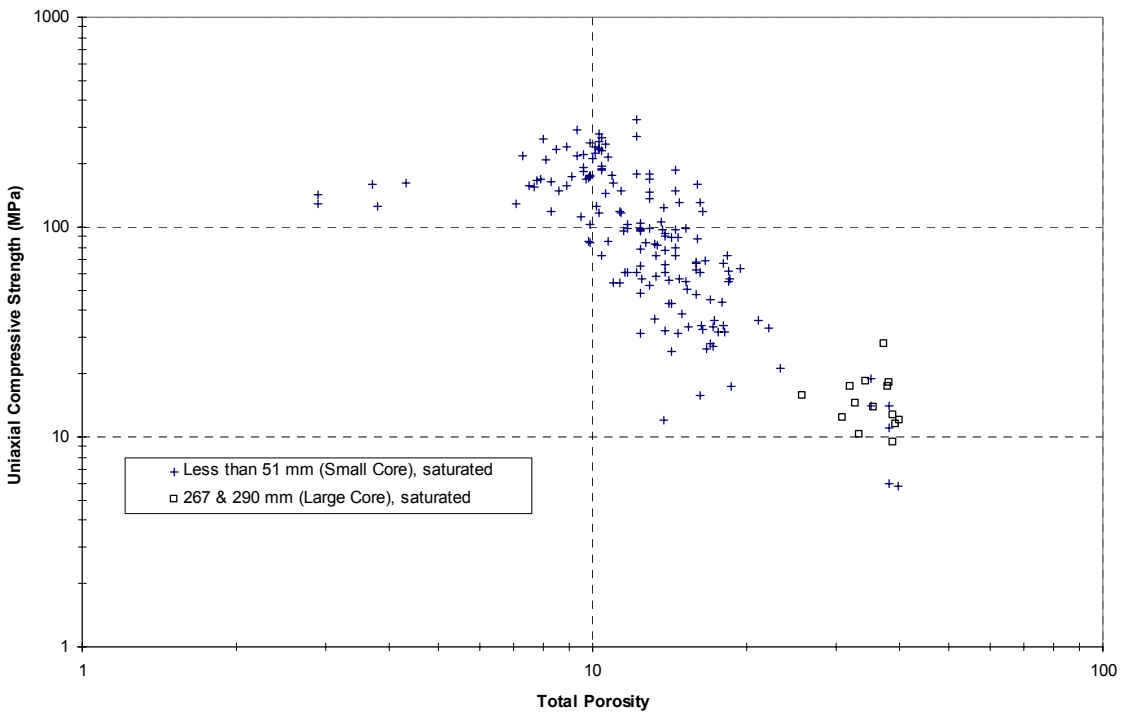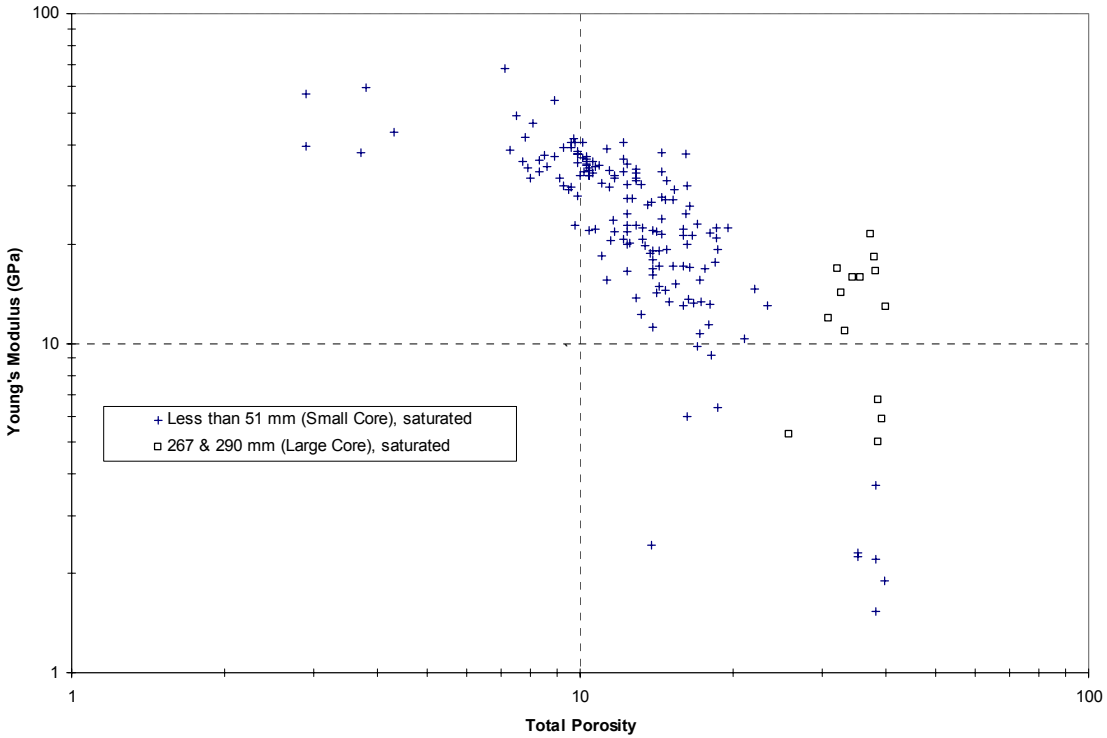
Source: Appendix B, Microsoft Excel file "Compressive and Porosity Data REV00B_PorosityOnly_Tpt.xls," Worksheet "Plots."

Figure 6.3-18. Variation in Young's Modulus (top) and Uniaxial Compressive Strength (bottom) as a Function of the Total Porosity for Small and Large-Diameter Cores of Topopah Spring Tuff

NOTE: The rock block is from the Tptpll zone near its lower boundary with the Tptpln, Busted Butte.

Figure 6.3-19. Rock block being removed from Busted Butte (left) and Development of Rectangular
Specimens for Matrix Size Effect Study (right)
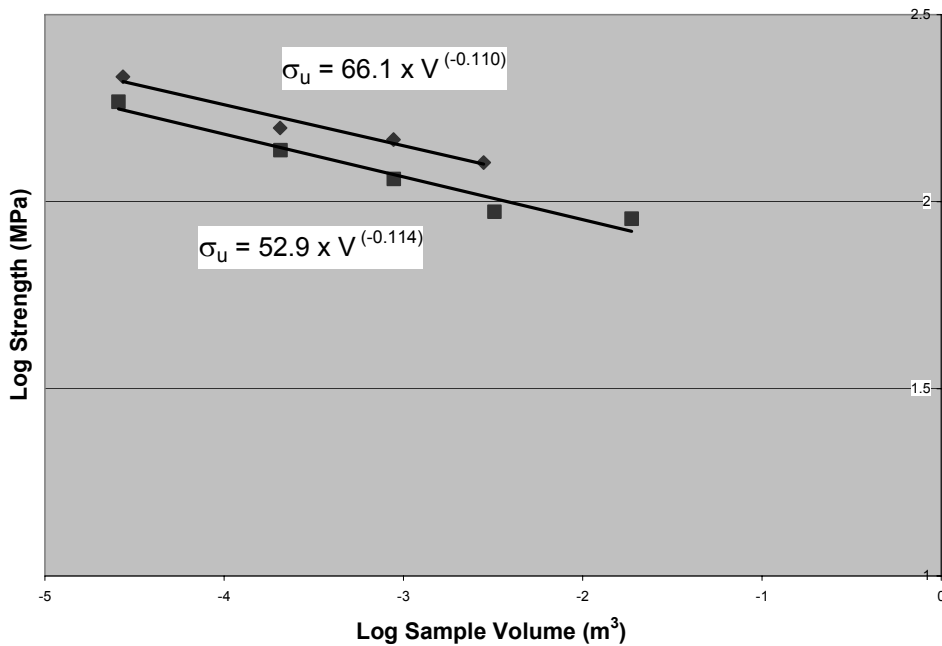
Source: Figure 2 from Price 2004 [DIRS 170894]. Plotted results are from the 2003 testing of Tptpln or Tptpll
samples (the diamond-shaped data, DTN: SN0306L0207502.008 [DIRS 165015]) are compared to previous testing
of samples from the Tptpmn (the square-shaped data, Price 1986 [DIRS 106589]).

NOTE: The plot of Log Ultimate Strength (the mean of the data at a given volume) versus Log Sample Volume using
Tptpll Busted Butte outcrop (room dry) samples (the diamond-shaped data) and the Tptpmn Busted Butte
outcrop (saturated) samples (the square-shaped data). Experiments were run in uniaxial compression at
room temperature and a nominal constant axial strain rate of 10^{-5} s^{-1}.

Figure 6.3-20. Results of Size Effect Study Showing Variation in Sample Uniaxial Compressive Strength
as a Function of Sample Volume

6.3.4 Effect of Rock Saturation on Mechanical Rock Properties

Laboratory testing of welded Topopah Spring Tuff specimens (51 mm to 290 mm diameters) at room temperature and three saturation conditions (saturated, room dry and oven dry) have been conducted. Testing indicates possible slight trends of increasing Young's modulus (Price 2004 [DIRS 170894], Section 5.2.1.3; BSC 2003 [DIRS 166660], Section 8.4.2.1, p. 8-65 and Figure 8-15) and increasing mean uniaxial compressive strength (Price 2004 [DIRS 170894], Section 5.2.1.3; BSC 2003 [DIRS 166660], Section 8.4.4.2, pp. 8-93, 8-95 and Figures 8-27 and 8-28) with decreasing sample water content. The magnitude of the saturation effects on mechanical properties is on the order as the natural scatter observed in tested specimens (Price 2004 [DIRS 170894], Section 5.2.1.3.3). Furthermore, the precise level of saturation for a given sample is relatively unknown since the percentage of internal rock pores that become saturated during the vacuum saturation procedure is uncertain.

6.3.5 Effect of Rock Temperature and Geochemical Alteration on Mechanical Rock Properties

A number of detailed geological studies have been conducted at the Yucca Mountain site to define the basic mineralogy of the rocks, and the petrologic and geochemical processes that occurred during the formation of the Topopah Spring Tuff, and that have continued over time. These studies have included a detailed description of the mineralogy of the repository host horizon from samples and observations developed from surface-based core holes through the repository block, as well as from the ESF and ECRB Cross-Drift. From the standpoint of potential geochemical alteration of the rock by water, these studies show (BSC 2003 [DIRS 164670], Table 6.2; BSC 2004 [DIRS 166107], Section 6.3.1.5; and BSC 2004 [DIRS 170137], Section A1.1.1.2):

- The Topopah Spring Tuff is largely composed of fine-grained feldspars and silicate-based rocks rocks that formed during the cooling of the rock mass shortly after deposition. Clay-forming minerals were typically not formed during the petrogenesis of the repository host horizon.

- Clay is not common in the crystallized rocks of the repository host horizon, nor is clay a volumetrically significant fracture-coating material.

- It is not likely that, even over the postclosure period, mineral alteration will occur to form clay in any significant amount in repository rocks and fractures due to the lack of suitable environmental conditions.

The most likely pathway of potential geochemical alteration for welded Topopah Spring Tuff is related to the phase change of certain component minerals (tridymite and cristobalite) with increased temperature. Phase transitions in synthetic tridymite occur at approximately 117°C and 163°C, and in synthetic cristobalite at approximately 272°C, and involve notable changes in volume (Brodsky et al. 1997 [DIRS 100653], Section 4.2.2.2, p. 41). Tests on Topopah Spring welded tuff show that beginning at a transition temperature of approximately 175°C to 225°C, strains in a strain-versus-temperature curve increase in a highly nonlinear fashion until they level off above 300°C (Brodsky et al. 1997 [DIRS 100653], Section 4.2.2.2, pp. 41-44). Between

temperatures of approximately 150˚C and 175˚C, peaks in specific heat are observed in welded Topopah Spring Tuff specimens, which are also suspected to be a result of phase changes in the rock mineralogy (Brodsky et al. 1997 [DIRS 100653], Section 4.3.1, pp. 49, 52-53). Conservative modeling of drift wall temperature during the preclosure period results in a maximum estimated drift wall rock temperature less than approximately 85˚C (BSC 2004 [DIRS 169862], Section 6.6.2, Figure 6-5c). From the above observations it is expected that no significant affect on the elastic or strength properties of welded Topopah Spring Tuff due to mineral phase changes will result during preclosure.

Actual testing of welded Topopah Spring Tuff specimens (51 mm diameter) up to tested temperatures of 200˚C indicates a slight to marginal decrease in Young's modulus (BSC 2003 [DIRS 166660], Section 8.4.2.1, p. 8-64 and Figure 8-14) and inconclusive results for uniaxial compressive strength (BSC 2003 [DIRS 166660], Section 8.4.4.2, p. 8-93 and Figures 8-25 and 8-26). Due to the limited number of samples tested under similar conditions and as can be observed in the above figures, the magnitude of the temperature effects on mechanical properties is within the range of natural scatter on specimens tested under base conditions (saturated, room temperature, and constant strain rate of 10^{-5} s^{-1}).

6.3.6 Limitations of the Lithophysal Rock Property Estimates

Users of this laboratory summary of the mechanical properties of lithophysal rock should be aware of a number of limitations:

- Much of the porosity data associated with each tested specimen is currently unqualified and the large-core porosity estimates have a large uncertainty.

- There are only a limited number of large-diameter uniaxial compressive strength tests upon which the property correlations are based.

- Figures 6.3-17 and 6.3-18 indicate a clear sample size or scaling effect. However, other than the scaling information available in Figures 6.3-16 to 6.3-19, no attempt is made extrapolate laboratory data to even larger scales (see the assumption discussed in Section 5.4).

6.4 DEVELOPMENT OF LITHOPHYSAL ROCK MASS CATEGORIES AND BOUNDS

The development of lithophysal rock mass mechanical parameters and rock mass quality categories is based on the laboratory tuff behavior described in Section 6.3. The project approach for assessment of the mechanical stability of drifts uses parametric analyses based on the assumption of a homogenous rock mass characterized by constant rock properties. To represent the inherent variability of the rock mass, a series of discrete constant property levels, linked to lithophysal porosity, are used to represent (approximately) the lowest, highest and median in situ conditions. The likelihood of occurrence of these particular conditions is based on the percentage of a given rock mass category to exist in the lithophysal rock.

The rock mass porosity is spatially variable over a relatively small length scale, on the order of meters (BSC 2003 [DIRS 166660], Attachment VII). Therefore, the rock mass rarely consists of uniformly weak or strong material, but consists of small regions of varying strength and modulus. Accordingly, an assumption of a homogenous rock mass will tend to *underestimate* the stability of drifts in the weakest rock mass classifications and will *overestimate* the drift stability in the highest rock mass classifications. The impact of actual lithophysae geometry and spatial variability on the rock mass properties and the relation to conservatism in the rock mass category bounding methodology is discussed below.

6.4.1 Development of Rock Mass Categories Based on Laboratory Testing

The best site-specific data available for the determination of rock mass categories are the large-core 290 mm (11.5-in.) diameter test samples of Tptpul and Tptpll lithophysal rock taken from the ESF and ECRB Cross-Drift tunnels. This data includes test results from both room dry and saturated specimens. For the purposes of developing empirical lithophysal rock mass categories, a linear fit to the site-specific large-diameter core data is adopted from Figure 6.3-14 and shown also in Figure 6.4-1. Test results from 267 mm (10.5-in.) diameter saturated specimens taken from Busted Butte are also shown in the figure, but are not used for choosing the various base-case rock categories since: (1) these specimens come from several kilometers away from the repository site (Section 6.3.2.1), (2) the outcrop rock was near the surface so could have been weakened due to weathering, and (3) the geometrical pattern of the lithophysae may be different from that seen in the host rock (more and smaller size lithophysae). However, the Busted Butte test results are accounted for in characterizing the uncertainty in mechanical property data (determining the range of observed behavior).

It is desirable to define a convenient number of rock mass quality categories for lithophysal rock based on the volume percentage of lithophysal porosity. The 290 mm (11.5-in.) diameter sample values of UCS and Young's modulus are plotted in Figure 6.4-1 and a linear best fit is applied to the data. Since a relatively linear relationship exists between the UCS and Young's modulus and both of these key parameters are dependent on the volume percentage of lithophysal porosity (Section 6.3), the best fit line in Figure 6.4-1 is defined as the theoretical base-case relationship. The base-case line is subdivided into five successive categories of 5 MPa (uniaxial compressive strength), starting at 10 MPa (weakest rock) and ending at 30 MPa (strongest rock). Consequently, the entire range of useful UCS values is subdivided into a series of five evenly distributed lithophysal rock mass "categories" that reflect the approximate range of lithophysal

rock mechanical behavior, based on the range of lithophysal porosity observed in the detailed Tptpll field study. The Young's modulus corresponding to each base-case uniaxial compressive strength value is determined from the linear fit of the 11.5-in. data in Figure 6.4-1 and values are given in Table 6.4-1. The validity of this approach to represent lithophysal rock mass is discussed over the remaining subsections of Section 6.

Each of the mechanical property pairs (uniaxial compressive strength and Young's modulus) share a common lithophysal porosity. By examining the large-diameter test data (including Busted Butte results) in terms of Young's modulus versus lithophysal porosity (Figure 6.3-11), estimates of lithophysal porosity associated with these rock categories can be established. Since exponential best fits have been historically applied to laboratory data (Section 6.3.2.2), exponential curve bounding-estimates of rock behavior were estimated in Figures 6.4-2 through 6.4-4 using the criteria of including all test result scattering between the bounding curves. Since moving from the mechanical properties and porosity relationships (Figures 6.4-2 and 6.4-3) to uniaxial strength versus Young's modulus (Figures 6.4-5) involves a nonlinear transformation, some judgment and a trial-and-error approach is used to estimate the bounds shown in Figures 6.4-2 and 6.4-3. The upper and lower bounds shown in Figure 6.4-4 derive automatically from the bounds set in the previous two figures. A summary of the rock mass categories for lithophysal rock (from Figure 6.4-1) and their estimated ranges of lithophysal porosity are given in Table 6.4-1. For each lithophysal rock mass category there corresponds an estimated uniform distribution of Young's modulus and trapezoidal (upper to lower bound) distribution of uniaxial compressive strength.

Figure 6.4-5 shows how the lithophysal porosity ranges were developed for the five lithophysal rock mass categories. In brief, first a linear fit was made to the 267 and 290 mm (10.5 and 11.5-in) diameter large-core test data, both under dry and saturated conditions. Second, all the 23 large-core test results from Appendix B, Microsoft Excel file "LithophysalRockRanges_Calc.xls," Worksheet "rock-props" were copied into the statistical software JMP 5.1 and analyzed to obtain 95 percent confidence intervals around the linear fit line. The steps involved in creating confidence intervals are: (1) open the JMP file "LargeCoreLithophysalData.JMP;" (2) select the "Fit Y by X" icon; (3) select "Modulus" as the "Y, Response," select "Lithophysal Porosity" as the "S, Factor" and then "OK" to create a bivariate plot of the data; (4) select the red triangle on the plot and select "Fit Line" to create a linear best to the data; (5) select the red triangle next to "Linear Fit" just below the plot and select "Confid Curves Fit" to create the 95 percent confidence intervals around the linear fit line.

Third, uncertainty ranges of lithophysal porosity for each of the rock mass categories were subjectively determined. Using the 95 percent confidence curves as a starting point, engineering judgment was applied along with several constraints to determine the porosity ranges: (1) lithophysal porosities must be greater or equal to zero, (2) establish constant plus and minus ranges on either side of the base case value (blue triangles in Figure 6.4-5), and (3) uncertainty should increase away from the center of data (category 3) as shown by the confidence curves.

Finally, these ranges of laboratory lithophysal porosity (established for each rock mass category, Table 6.4-1) and their correlation with companion mechanical properties, are considered to be applicable to the lithophysal porosities determined by field mapping techniques (Section 5.4). Accordingly, field lithophysal porosities and their simulation over the repository area can be

correlated to rock mass mechanical properties (Section 5.5). Examples of lithophysal rock that roughly correspond to the rock mass categories are shown in Figures 6.4-6 and 6.4-7.

Lithophysal Rock Quality Categories
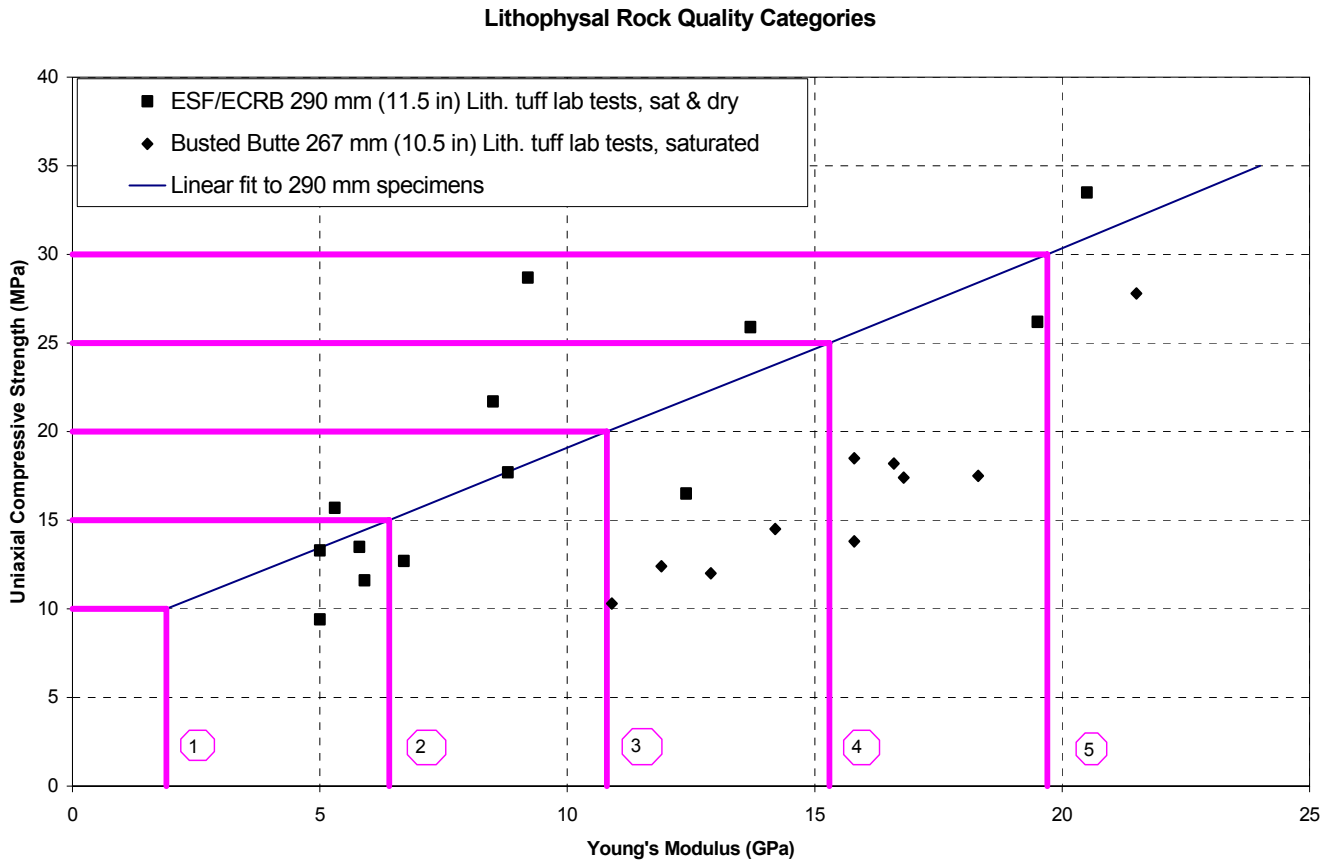
Source: Appendix B, Microsoft Excel file "LithophysalRockRanges_Calc.xls," Worksheet "Categories." Source DTNs SNSAND84086000.000, SN0208L0207502.001, SN0211L0207502.002, SN0305L0207502.005, SN0305L0207502.006, MO0311RCKPRPCS.003, and MO0402DQRIRPPR.003.

NOTES: Plot of large-diameter test results of Tptpll and Tptpul specimens from the ESF and ECRB Cross-Drift. Linear Relationship given is of Uniaxial Compressive Strength to Young's Modulus for 290 mm (11.5 in) diameter core samples. See Table 6.4-1 for numerical values associated with proposed rock mass categories.

Figure 6.4-1. Proposed Rock Mass Categories Based on Unconfined Compressive Strength as a Function of Young's Modulus Based on Large-Core Tests of Lithophysal Rock
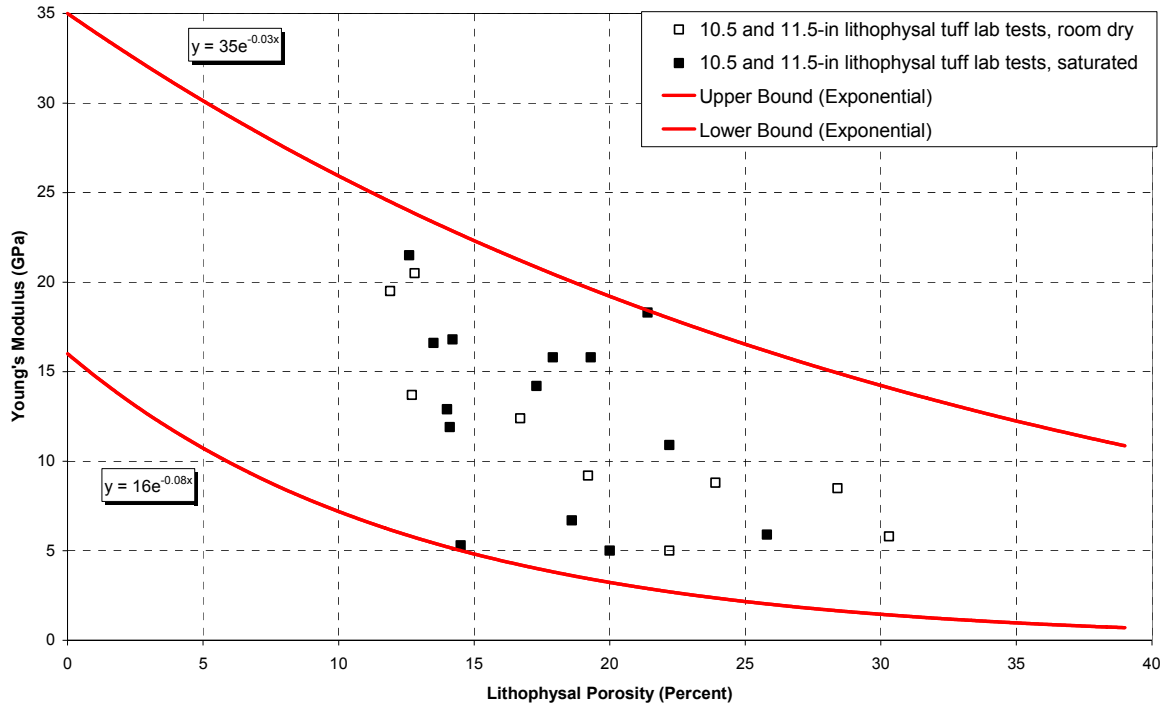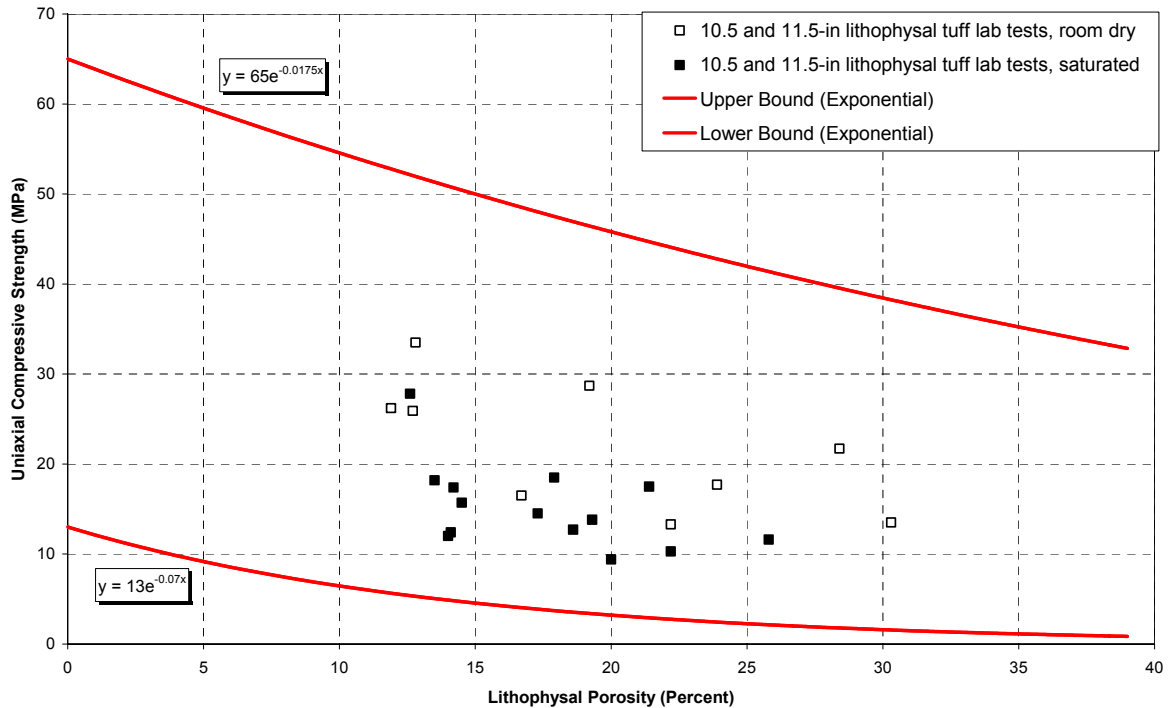
Source: Appendix B, Microsoft Excel file "LithophysalRockRanges_Calc.xls," Worksheet "LC E-por (B)"

Figure 6.4-2. Determination of Upper and Lower Bounds of the Young's Modulus versus Lithophysal Porosity Relationship for 10.5 and 11.5-in. Diameter Cores from the Tptpul and Tptpll Units

Source: Appendix B, Microsoft Excel file "LithophysalRockRanges_Calc.xls," Worksheet "LC q-por (B)"

Figure 6.4-3. Determination of Upper and Lower Bounds of the Uniaxial Compressive Strength versus Lithophysal Porosity Relationship for 10.5 and 11.5-in. Diameter Cores from the Tptpul and Tptpll Units
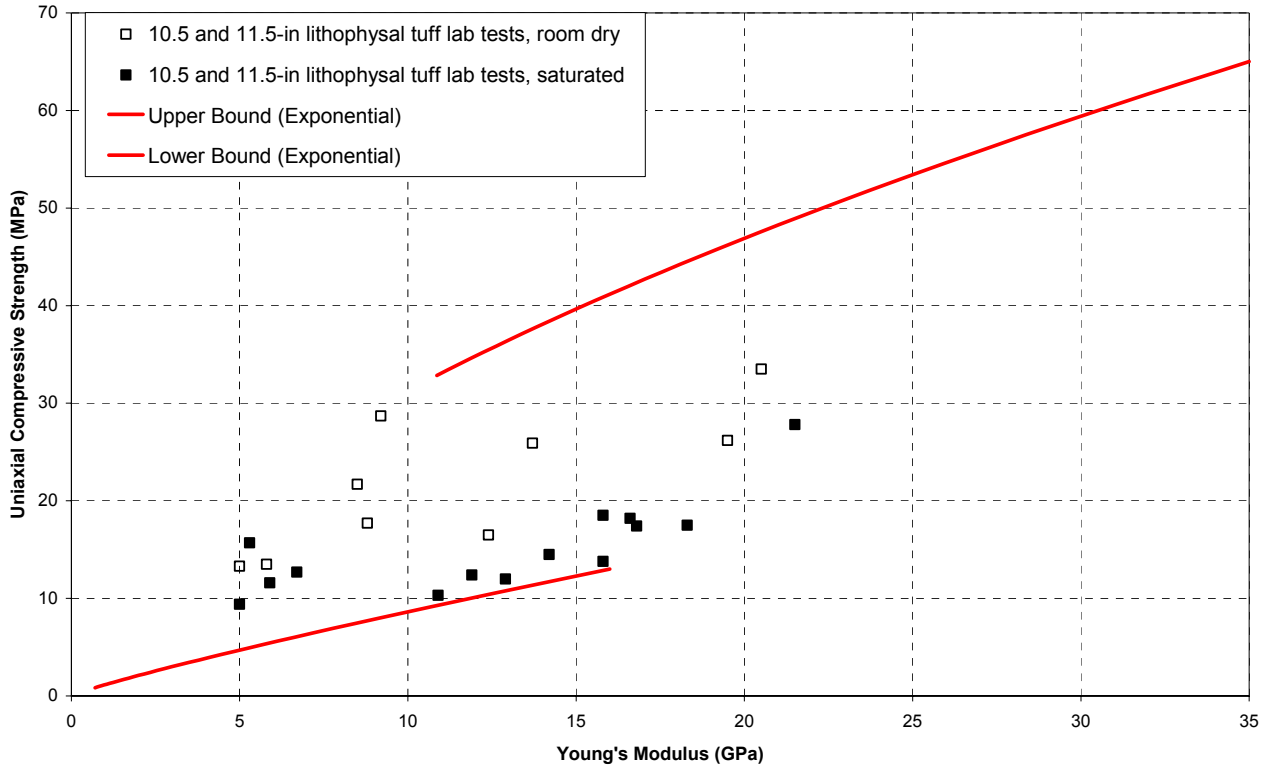
Source: Appendix B, Microsoft Excel file "LithophysalRockRanges_Calc.xls," Worksheet "LC q-E (B)"

Figure 6.4-4. Resulting Upper and Lower Bounds of the Uniaxial Compressive Strength versus Young's Modulus Relationship for 10.5 and 11.5-in. Diameter Cores from the Tptpul and Tptpll Units

Table 6.4-1. Suggested Range of Mechanical Properties Developed from ESF or ECRB Cross-Drift Large-Core Testing

Rock Mass Category	Base-Case Uniaxial Compressive Strength (MPa)	Base-Case Estimated Young's Modulus[a] (GPa)	Approximate Lithophysal Porosity From Laboratory Tests[b] (%)	Lithophysal Porosity Ranges for Rock Mass Categories[c] (%)
1	10	1.9	35 +/- 8	greater than 25
2	15	6.4	28 +/- 6	20-25
3	20	10.8	21 +/- 4	15-20
4	25	15.3	13 +/- 5	10-15
5	30	19.7	7 +/- 7	less than 10

Source: DTNs SN0208L0207502.001, SN0211L0207502.002, SN0305L0207502.005, SN0305L0207502.006, and SNSAND84086000.000. See Appendix B, Microsoft Excel file "LithophysalRockRanges_Calc.xls" for further explanation and supporting calculations.

[a]Young's Modulus estimated from linear fit to 290 mm (11.5-in) diameter core data in Figure 6.4-1

[b]Estimated from correlation of Young's modulus to lithophysal porosity in Figure 6.4-5

[e]For convenience the lithophysal porosity ranges (column five) will be used based on an approximate correlation with the laboratory lithophysal porosity determinations (column four).
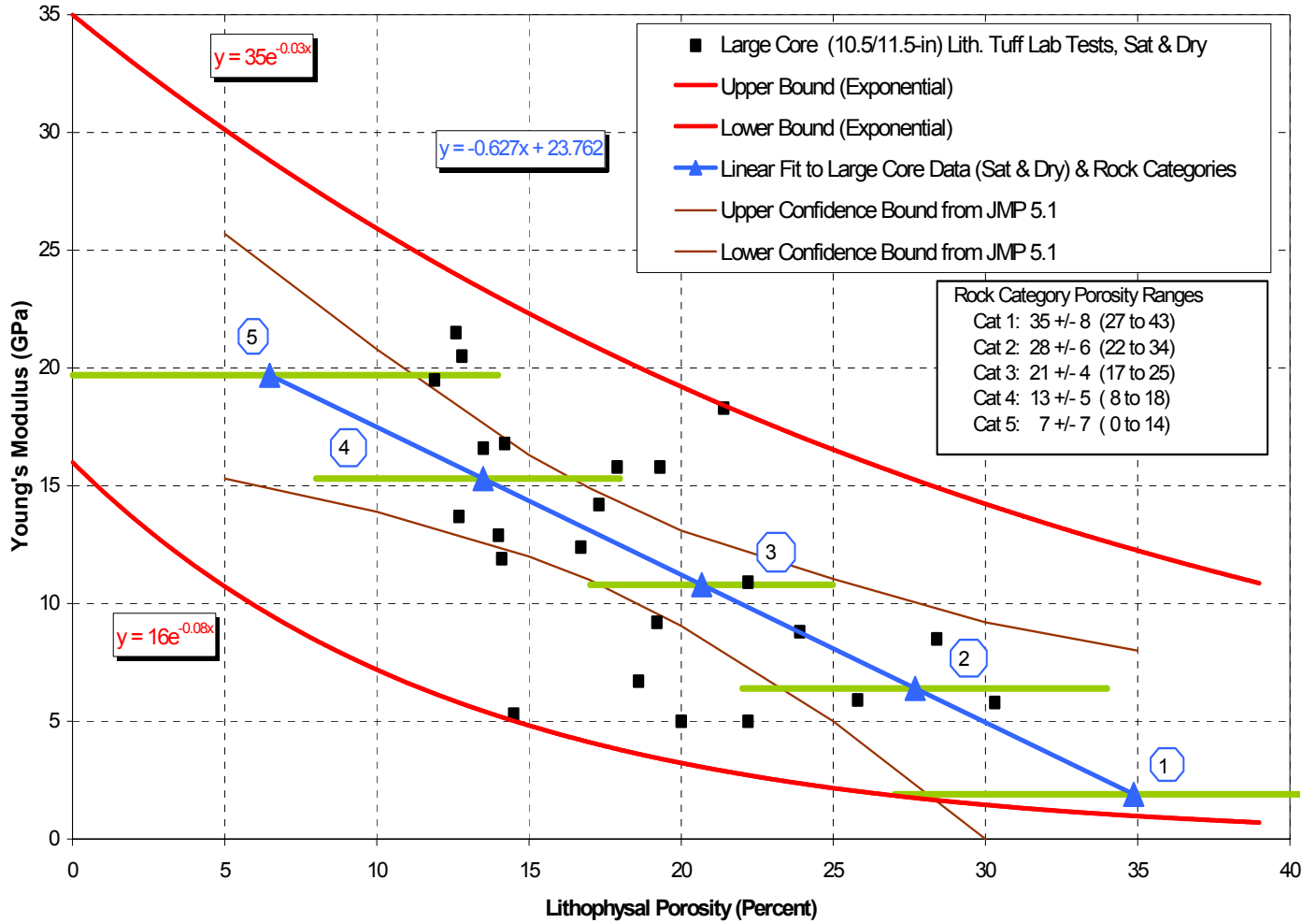
Source: Appendix B, Microsoft Excel file "LithophysalRockRanges_Calc.xls," Worksheet "LC E-por (Range)"

NOTE: First a linear fit was made to the 267 and 290 mm (10.5 and 11.5-in) diameter large-core test data, both under dry and saturated conditions (blue line). Second, the large-core data was placed in the statistical software JMP 5.1 and analyzed to obtain 95% confidence intervals around the linear fit line (brown lines, Appendix B, JMP file "LargeCoreLithophysalData.JMP"). Third, uncertainty ranges of lithophysal porosity for each of the rock mass categories was subjectively determined (green lines). More details of this process are provided in Appendix B, Microsoft Excel file "LithophysalRockRanges_Calc.xls," Worksheet "Fits."

Figure 6.4-5. Development of the Lithophysal Porosity Ranges that Correspond to Each of the Lithophysal Rock Mass Categories
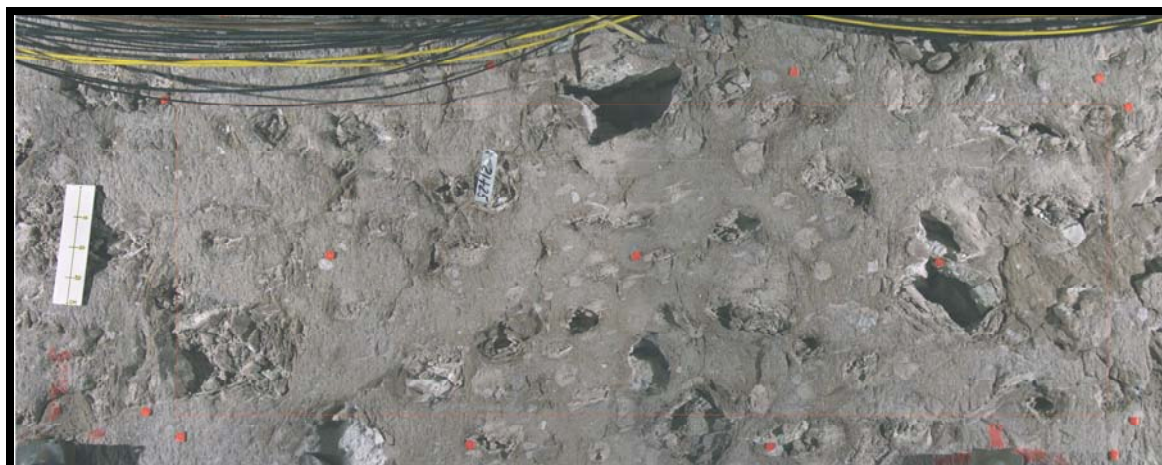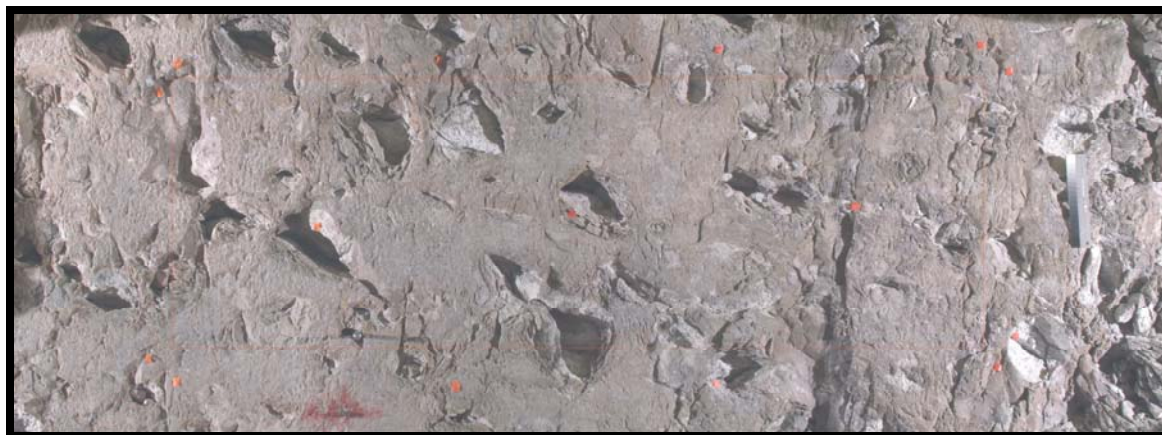
Source: BSC 2003 [DIRS 166660], Attachment VII, Section VII.2, Figures VII-4 (top), VII-3 (center), and VII-7 (bottom).

Note: Section 16+41L (top), Section 14+93 (center) and Section 21+24 (bottom)

Figure 6.4-6. Examples of Approximate Rock Mass Category Levels Taken from 1×3 m Panel Maps: Category 3 (top) With Lithophysal Porosity of Approx. 19%, Category 4 (center) With Lithophysal Porosity of 13.3%, and Category 5 (bottom) With Lithophysal Porosity of 8.5%.

(a) Rock Category 1 (31.3 %)

(b) Rock Category 2 (22.5 %)

(c) Rock Category 3 (18.7 %)

(d) Rock Category 4 (13.0 %)

(e) Rock Category 5 (6.9 %)
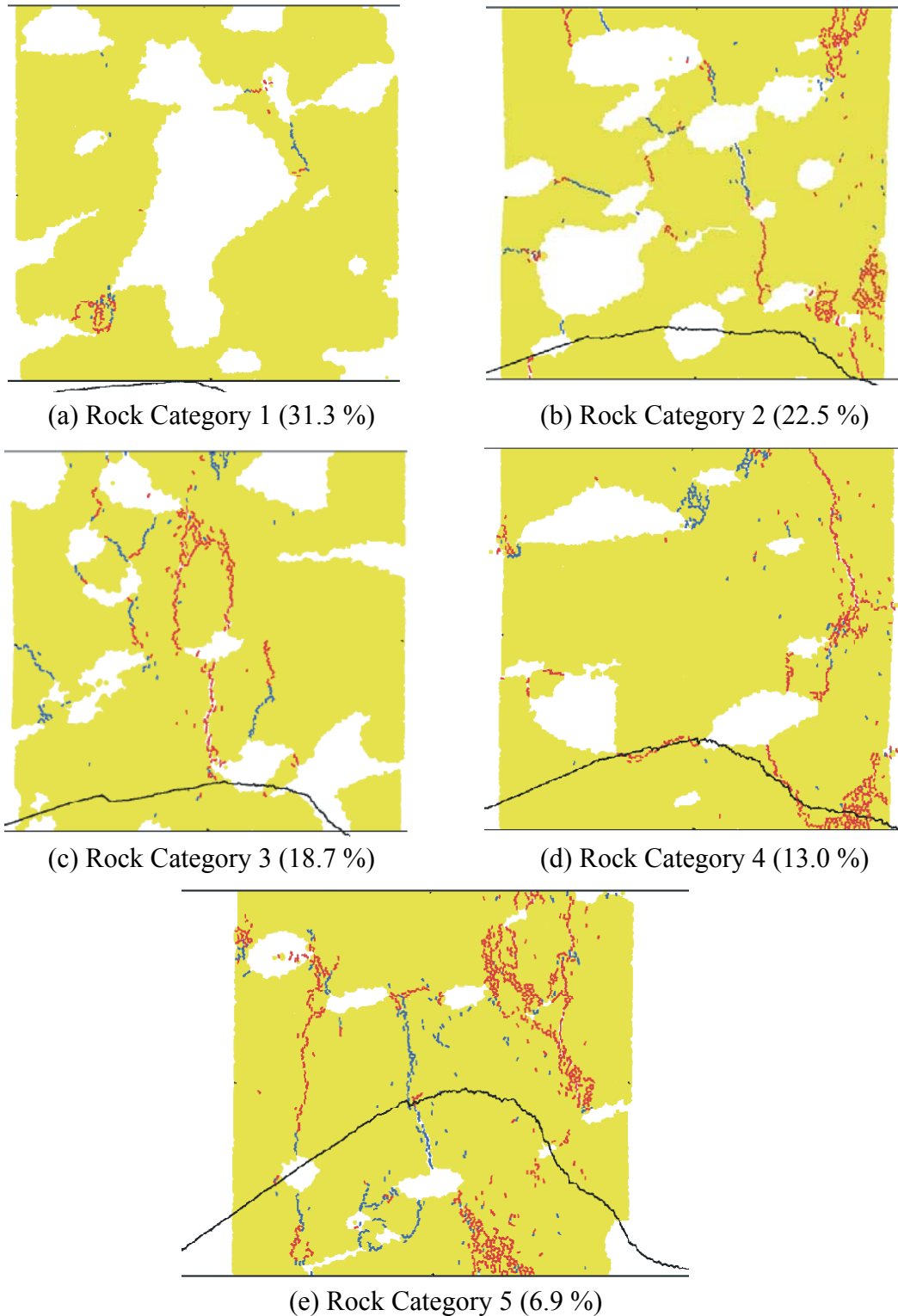
Source: BSC 2003 [DIRS 166660], Attachment V, Appendix B. Porosity values can be found in Appendix B of this calculation, Microsoft Excel file "LithophysalRockRanges_Calc.xls," Worksheet "PFC" column K using the locations given in the note below.

NOTE: PFC2D stencil specimen locations: (a) 16+41LA, (b) 19+19LC, (c) 16+41LB, (d) 16+56LA, and (e) 20+69LA. Quantities in parentheses are volume percent lithophysal porosity. See Section 6.5.5 for specimen and test details.

Figure 6.4-7. Examples of Rock Mass Category Porosities Taken from 1×1 m Stencils of Panel Maps

6.4.2 Field Distribution of Lithophysal Porosity for Rock Mass Categories

An estimate of the overall distribution of these rock mass categories within the Tptpll can be obtained indirectly from the detailed field study of Tptpll lithophysal features conducted in the ECRB Cross-Drift (Section 6.2). The histogram given in Figure 6.4-8 shows the abundance (frequency) of lithophysal porosity in the ECRB Cross-Drift from stations 14+44 to 23+26 (essentially from the top to the bottom of the Tptpll). This plot subdivides the abundance of lithophysal porosity into 5 percent intervals that roughly correspond to lithophysal porosity ranges for the rock mass categories given in Table 6.4-1. The lowest quality categories (1 and 2) represent the rock mass with 20 percent or greater lithophysal porosity, and make up approximately 20 percent of the repository host rock. Category 1, which represents the lowest quality and highest porosity rock, makes up less than 10 percent of the rock mass and represents localized conditions of high porosity rock found primarily near the top of the Tptpll, observed along ECRB Cross Drift stations 15+50 to 16+00. Rock mass categories 3, 4, and 5 consist of higher geomechanical quality rock and are representative of approximately 80 percent of the lithophysal rock mass.
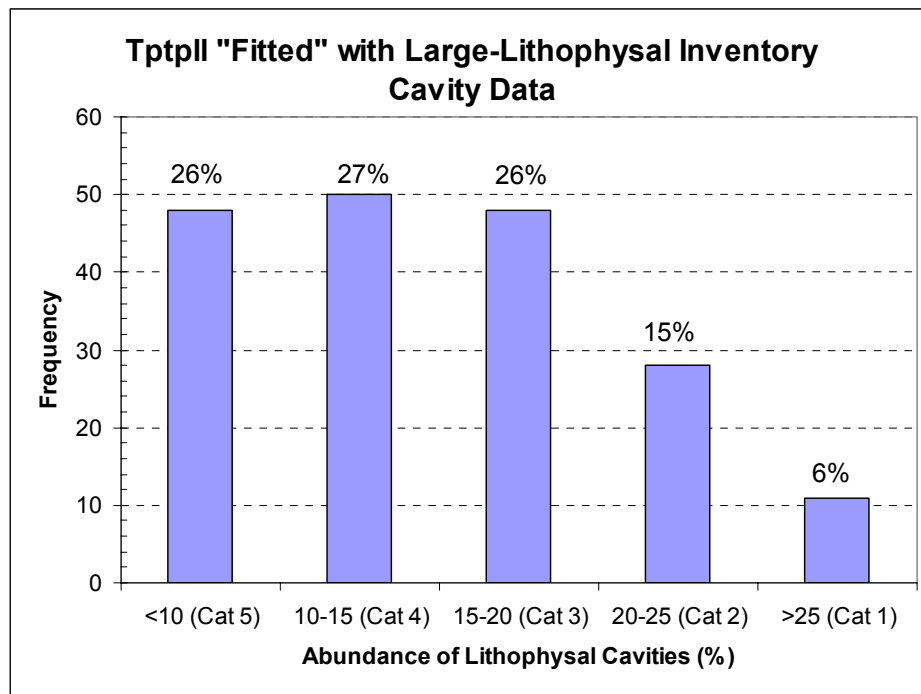
Source: Appendix B, Microsoft Excel file "Drift Deg AMR AF T-A-P Fit_*V1_DBR*.xls," Worksheet "Length – Fit and Stats," cell AF268.

NOTE: The percent value given above each histogram bar represents the percent of measured Tptpll rock corresponding to each rock mass quality category (Cat). Lithophysal porosity data are from ECRB Cross-Drift stations 14+44 to 23+26, which includes the entire thickness of the Tptpll lithostratigraphic rock unit.

Figure 6.4-8. Distribution of Lithophysal Porosity and Estimated Rock Mass Categories for the Tptpll Unit in the Enhanced Characterization of the Repository Block Cross-Drift

6.5 NUMERICAL MODELING OF LITHOPHYSAL ROCK

Laboratory testing procedures recommend that the test-sample dimensions should be at least 10 times the size of any mineral grains or other inclusions. The typical range of observed lithophysal void sizes (Sections 6.2 and 6.3) would dictate that very large samples would need to be tested; the representative elementary volume of lithophysal rock is on the order of cubic meters to cubic decameters depending on the size of lithophysae. In order to develop an adequate correlation between lithophysal porosity and mechanical properties of lithophysal rock, sufficient numbers of laboratory tests on large-size rock samples are desired that cover the expected range of lithophysal porosity. But as a consequence of the size of rock samples required, the lack of high-capacity equipment needed to test such large samples and the cost and time that would be required to produce an adequate statistical database, a suitable laboratory testing effort was impractical to carry out. The presence of voids intersecting the sample surface also makes standard triaxial testing difficult or impossible.

It is apparent that the uniqueness of lithophysal rock poses formidable challenges to obtaining data directly by the process of testing larger rock specimens. The problem, therefore, is how to characterize the uncertainty and spatial variability of the mechanical properties of this material. To overcome the inability to conduct adequate physical testing, numerical modeling was used to supplement the existing intact rock property database and to confirm the mechanical property estimates of lithophysal rock.

This section presents a systematic method of creating a numerical model of the material, calibrating that model against existing laboratory data, and then conducting numerical biaxial and triaxial tests to supplement existing test data. The supplemental data can be used to predict the more representative larger-scale behavior of the repository.

An essential part of the resolution strategy is the development of numerical modeling approaches that are capable of simulating the mechanics of deformability and yielding of the actual lithophysal rock. One of the advantages of conducting numerical tests on synthetic models of rock is the ability to monitor evolution of the damage more precisely than can be done with laboratory samples. Numerical modeling allows direct monitoring of the formation and propagation of macro cracks by coalescence of micro cracks.

6.5.1 Computational Models Adopted

Different discontinuum numerical modeling approaches, the PFC and UDEC models, are used to examine the basic mechanisms of how lithophysae affect the failure characteristics and moduli of the Tptpul and Tptpll. These models were chosen because of their ability to represent physical voids in a material and for their capability to model complex failure mechanisms, such as fracture initiation and propagation between voids. The physics-based discontinuum numerical modeling programs—PFC2D (BSC 2004 [DIRS 169930]), PFC3D (BSC 2004 [DIRS 169931]), and UDEC (BSC 2002 [DIRS 161949])—are used as numerical "laboratories" to simulate and test the basic deformation and failure response mechanisms of lithophysal tuff. These programs were chosen due to their ability to simulate the physics of deformation and fracture of a bonded granular matrix that contains void space of varying shape, size and porosity. Using two different approaches provides a check and greater confidence in the modeling. The UDEC program is

additionally used as it allows constituent grains that are nonspherical in shape, and thus overcomes some simplifications used in the PFC approach. Specifically, it allows greater flexibility in modeling failure mechanisms under biaxial compression.

The large-diameter core laboratory testing is a relatively small sampling of the lithophysae conditions that exist in the field, although the approximate porosities of the cores encompass the range of most field-measured conditions. To extend the laboratory data base to account for the in situ variability in lithophysal porosity - i.e., shape, size and distribution - a numerical study was conducted using the calibrated Particle Flow Code (PFC) model.

The basic calibration and validation of the PFC model is described in detail in the *Subsurface Geotechnical Parameters Report* (BSC 2003 [DIRS 166660], Attachment V, Appendix A, Section A.5.1). In this calibration, lithophysae were represented in simulated tuff samples as circular holes that were randomly distributed to produce a given porosity. The model matrix (containing no voids or fractures) behavior was first calibrated through comparison of the model response (Young's modulus and UCS) to the results from laboratory testing of nonlithophysal rocks. The models were then validated for lithophysal rocks by assuming the same matrix as the nonlithophysal case, but adding voids of varying size to replicate the lithophysal porosity of the rock mass. Simulated uniaxial compression tests were then carried out and compared to laboratory and field testing results of lithophysal rock to verify the general predictability of the approach.

It was shown that the numerical model was able to reasonably account for the failure mechanisms of lithophysal and nonlithophysal rock specimens as observed in the laboratory, and could reproduce the general effect of lithophysal porosity on UCS and Young's modulus. An outcome of this process was an explanation for the mechanisms of strength and modulus reduction that accompanies additional porosity. Numerical biaxial compression experiments were used to develop estimated yield criteria and dilation angles for lithophysal rocks as a function of porosity.

The above-calibrated model was used to conduct a "shape study" in which the impact of lithophysal porosity, shape, size and distribution on rock property variability were examined.[*] The variability of rock mechanical properties due to lithophysae shape and spatial distribution is studied by randomly creating voids of simple shape (e.g., circle, triangle, or star) in the matrix material and by modeling realistic void shapes and distributions corresponding to lithophysal cavities identified in ECRB Cross-Drift panel maps (1 × 3 m). In the latter case, simulated samples of the lithophysal rock mass were developed directly from field panel map lithophysae distributions (BSC 2003 [DIRS 166660], Attachment VII) by overlaying (stenciling) the panel map directly onto the PFC model to create the void geometry.

Finally, the laboratory and field data are integrated with the computational property variability estimates to establish the range of strengths and moduli that represent the rock mass properties in the ECRB Cross-Drift and, especially, the Tptpll. A bounding approach based on parametric modeling over the entire range of estimated rock mass properties is used for conducting drift

---

[*] This study is documented in detail in the *Subsurface Geotechnical Parameters Report* (BSC 2003 [DIRS 166660], Section 9.1 and Attachments V and VIII).

degradation analyses (BSC 2004 [DIRS 166107], Section 6.4.1.2). These rock parameters ranges are then used as a basis for excavation stability calculations.

6.5.2 Particle Flow Code (PFC) and Universal Distinct Element Code (UDEC) Model Descriptions

The PFC approach represents rock as a number of small, rigid, spherical grains that are bonded together at their contacts with shear and tensile strength, as well as a grain-to-grain friction angle after the "contact bond" has been broken (Figure 6.5-1). Note that the corners of the triangles and stars are rounded in the PFC2D material, and thus, do not induce the infinite stresses that would occur if the exact geometry were present to a linear elastic body. Details on the mechanisms of the PFC and UDEC programs are provided in Itasca Software–Cutting Edge Tools for Computational Mechanics (Itasca Consulting Group 2002 [DIRS 160331]). The deformability of the contacts between particles is represented by a normal and shear stiffness at the contact point. Porosity is developed naturally in the model by control of the shape and size of void space between chains of bonded grains. The contact properties and porosity distribution are referred to as "microstructural" properties. Thus, the input conditions necessary for the model are very simple, only contact strength and stiffness. However, extremely rich constitutive behavior may develop naturally based on void porosity and the few straightforward input properties and their variability throughout the rock.
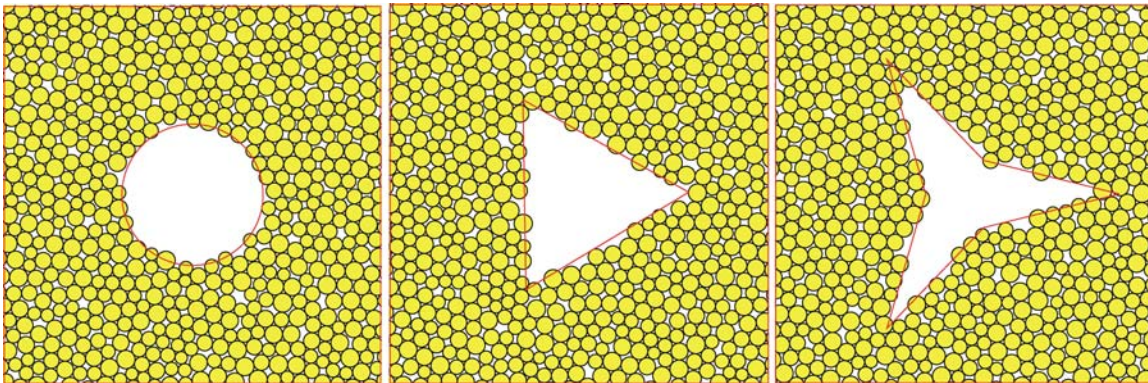
Source: BSC 2003 [DIRS 166660], Attachment V, Figure 2, p. V-8.

Figure 6.5-1. Resolution of Voids in PFC2D Specimens of Circular-, Triangular- and Star-Shaped Voids

When load is applied to the grain assembly, forces are transmitted across particle contacts. If the shear or tensile strength of the contact is reached, failure will occur, and the adjacent particles are free to slide past one another, or to separate. In either case, a fracture is formed and the forces must reorient in some fashion, thus redistributing loads. Realistic failure mechanisms may then develop, which can be compared to those observed in the laboratory. Calibration of the model against laboratory testing is necessary via sensitivity studies in which the contact strength and stiffness values are varied and the macroscopic stress-strain response is compared to that monitored.

Both PFC and UDEC models for lithophysal tuff (Figures 6.5-2 and 6.5-3) represent the rock as a cemented granular material. The grains in the PFC material are circular [two-dimensional computational model PFC2D (Itasca Consulting Group, 2002)] or spherical [three-dimensional computational model PFC3D (Itasca Consulting Group, 2003)] and rigid, while the grains in the two-dimensional computational model UDEC (Itasca Consulting Group, 2000) material are polygonal and deformable. The grain contacts in the PFC material exist at a point (at which the two circles or spheres touch) and grains are joined with bonds that approximate brittle elastic cement.

The simulated rock is represented in UDEC as a number of intact "grains" that are separated by contact interfaces whose mechanical behavior is represented by a standard Coulomb slip criterion. The grain contacts in the UDEC material exist along contact interfaces (or finite-length segments along which the two polygons touch), and grains are joined with bonds that approximate a frictional and cohesive contact (Figure 6.5-3).[*] Note that the UDEC approach, although similar to PFC, is different specifically in that the grains may be of any arbitrary shape, and the contacts between grains are not point force contacts, but linear interface contacts of finite length. Additionally, the UDEC grains may be deformable rather than rigid. The importance of this distinction will be described later. The UDEC program provides the capability to allow contact points along a fracture trace to be assigned a particular material property. In other words, portions of a contact interface could be assigned a standard Coulomb slip behavior (linearly elastic-perfectly plastic constitutive model), whereas others could be bonded to the opposing grain with the strength of the adjacent rock grains. The elastic behavior of fractures is controlled by constant normal and shear stiffness, which is consistent with the Young's modulus of the intact rock blocks. Potential fractures can occur when a finite tensile failure stress is reached, or when Coulomb slip occurs, functions of interface cohesion and friction angle, respectively. If a potential fracture occurs, either in tension or shear, tensile strength and cohesion are set to zero, whereas the friction angle is set to the residual value. As a result grain boundaries act as "potential or incipient fracture" locations and are "invisible" to the model until yielding begins when the Coulomb shear or tensile failure stresses are exceeded. In this manner, it is possible to allow for the progressive fracturing of intact rock.

The *UDEC* program is used to generate a 1 m × 1 m rock "sample" composed of a large number of random, irregular, and interconnected blocks or "grains" with average dimension of 0.017 m (BSC 2003 [DIRS 166660], Section 9.2.2.2). It is important that the sample contain blocks that are sufficiently small such that they do not dictate where and how fractures can form and propagate. The blocks in the model are defined by randomized Voronoi tessellation, which is controlled by supplying a Voronoi seed value. Veronoi tessellation is a term describing the discretization technique used to construct a material model that is composed of a sufficient number of small blocks to allow a realistic propagation of fractures in the model. A plane strain assumption is used in the modeling so that each simulated rock specimen is considered to have an infinite depth. Several different tessellations were used to insure that the results were not particular to a specific geometry.

---

* The PFC and UDEC models for lithophysal tuff are described in BSC 2003 [DIRS 166660] Sections 9.1 and 9.2, Attachments V and VI, respectively. The calculation input, output, and associated Excel calculation files are recorded on report CD-ROMs listed in SGPR, Attachment VIII. A thorough description of the PFC code and its application to modeling rock is found in the SGPR as Attachment V, Appendix C.

Both models represent lithophysal tuff as a well-connected base material with discrete voids. In the lithophysal tuff, most of the porosity is concentrated in lithophysae and the surrounding rim or spot material. The base material represents both the matrix and the rim or spot material in a smeared fashion, and the discrete voids represent the lithophysae. The PFC base material has an inherent porosity (approximately 0.17 and 0.36, for PFC2D and PFC3D, respectively) that does not correspond with that of the tuff; the tuff microstructure at this small-scale is not reproduced by the PFC material (BSC 2003 [DIRS 166660], Attachment V, Appendix A, Section A.3). The void or lithophysal porosity (equal to the ratio of void volume over total specimen volume) is the same as the volume fraction of lithophysae.

Physics of PFC Model for Rock
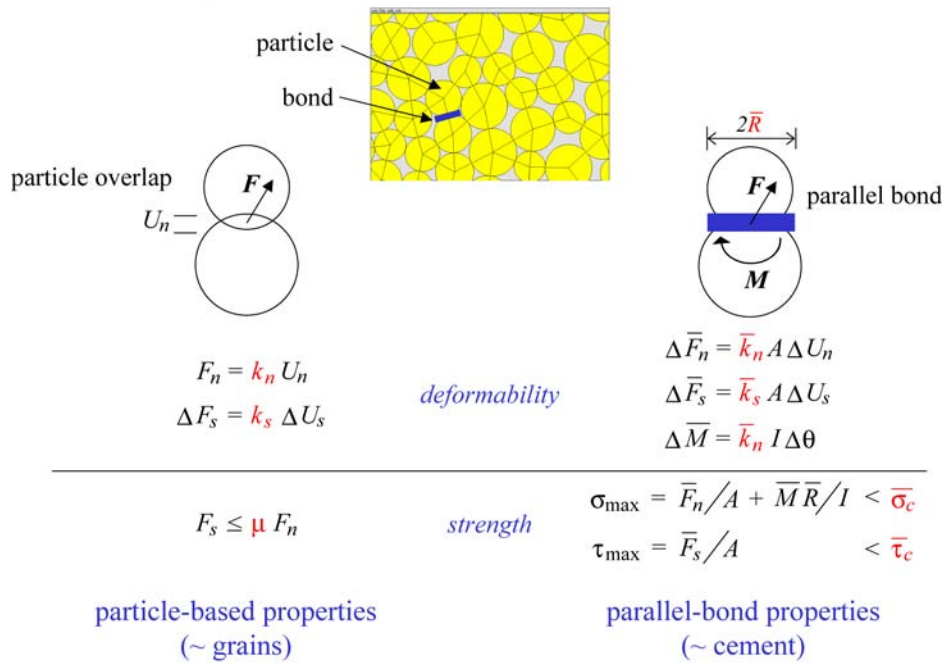
Source: Modified from BSC 2003 [DIRS 166660], Attachment V, Appendix C, Figure 3, p. V-75.

NOTE: Mechanical response in the PFC program is governed by the strength and deformability relationships of the bonds between rigid particles. Two bond types are provided: a simple contact bond (left), and a parallel bond (right), which simulates cement between particles that resists moments as well as shear and normal loads.

F_n = normal contact force

k_n = normal stiffness

U_n = relative normal displacement

ΔF_s = shear contact force increment

k_s = shear stiffness

ΔU_s = relative shear displacement increment

$\Delta \overline{F}_n$ = axial-directed force increment for bond

$\overline{k}_n$ = bond normal stiffness

A = area of bond cross-section

ΔU_n = relative normal displacement increment

$\Delta \overline{F}_s$ = shear-directed force increment for bond

$\overline{k}_s$ = bond shear stiffness

ΔU_s = relative shear displacement increment

$\Delta \overline{M}$ = bending moment increment for bond

I = moment of inertia of the bond cross-section

$\Delta \theta$ = increment of rotational angle

F_s = shear contact force

μ = contact friction coefficient

σ_{max} = maximum tensile stress acting on the bond periphery

τ_{max} = maximum shear stress acting on the bond periphery

$\overline{R}$ = particle radius

$\overline{F}_n$ = axial-directed force for bond

$\overline{F}_s$ = shear-directed force for bond

Figure 6.5-2. The Basic Mechanics of the PFC Program
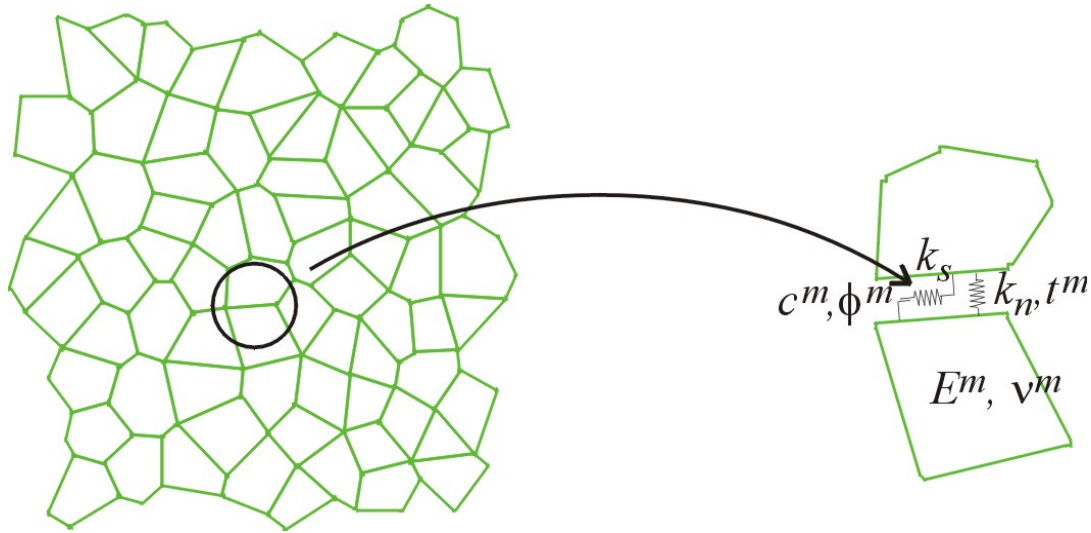
Source: BSC 2003 [DIRS 166660], Attachment VI, Figure VI-1, p. VI-2.

NOTE: The following parameters characterize the mechanical behavior of the UDEC model: The plastic interface parameters are functions of shear and tensile plastic strains. In the simulations presented in this calculation, it is considered that cohesion and tensile strength soften to zero at the onset of yield.

Elastic properties of blocks (Young's modulus, E^m and Poison's ratio, v^m).

Interface properties: both elastic (normal stiffness, k_n, and shear stiffness, k_s) and plastic (tensile strength, t^m, cohesion, c^m, and friction, ϕ^m).

Figure 6.5-3. Micro Properties of the UDEC Voronoi Model

6.5.3   Numerical Model Calibration

Both models are calibrated by inserting randomly distributed circular (PFC2D and UDEC) or spherical (PFC3D) voids (Figures 6.5-4 and 6.5-5)[*] and matching the Young's modulus and strength measured from uniaxial compression tests on large-diameter (approximately 12") specimens. Although the PFC and UDEC models were calibrated to the same laboratory results, there are slight differences in calibration such that the modeled UDEC strength is slightly less and UDEC stiffness is larger than the corresponding PFC modeled results. Sample *numerical* compression experiments were conducted for zero-void and lithophysal tuffs using the same numerical matrix properties.
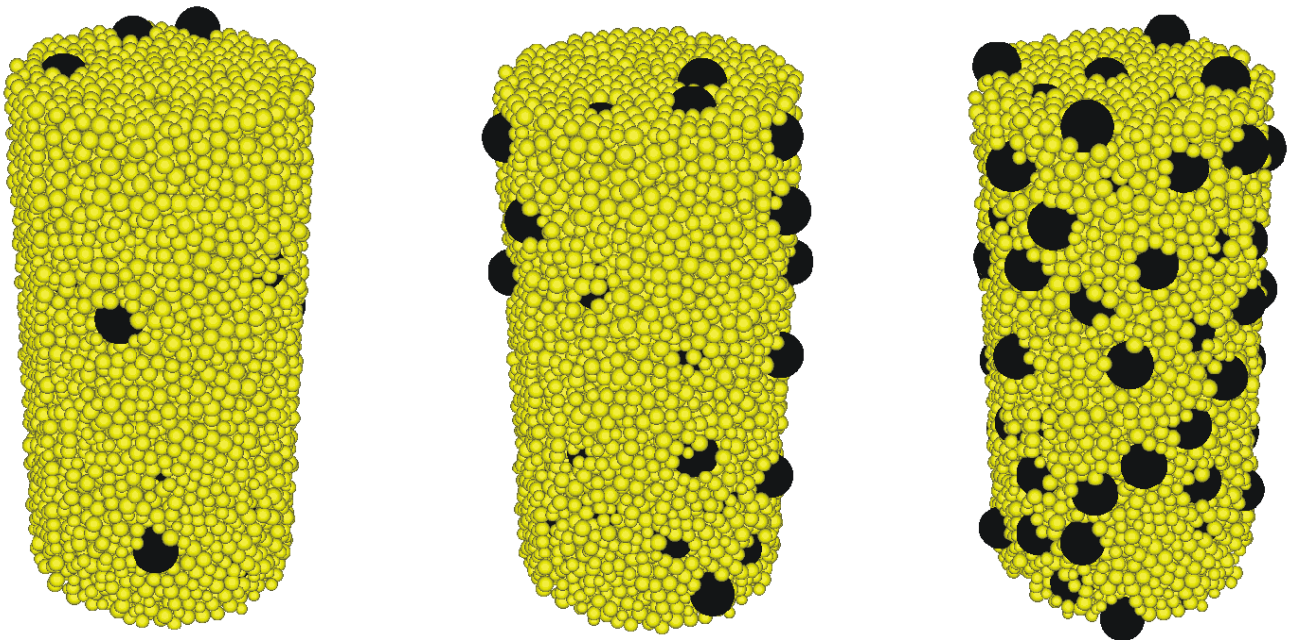
---

[*] The voids may intersect the specimen boundary, and the length of bridging material between any two voids is greater than 41.5 mm (SGPR, BSC 2003 [DIRS 166660], Attachment V, Section 2.2, p. V-7).
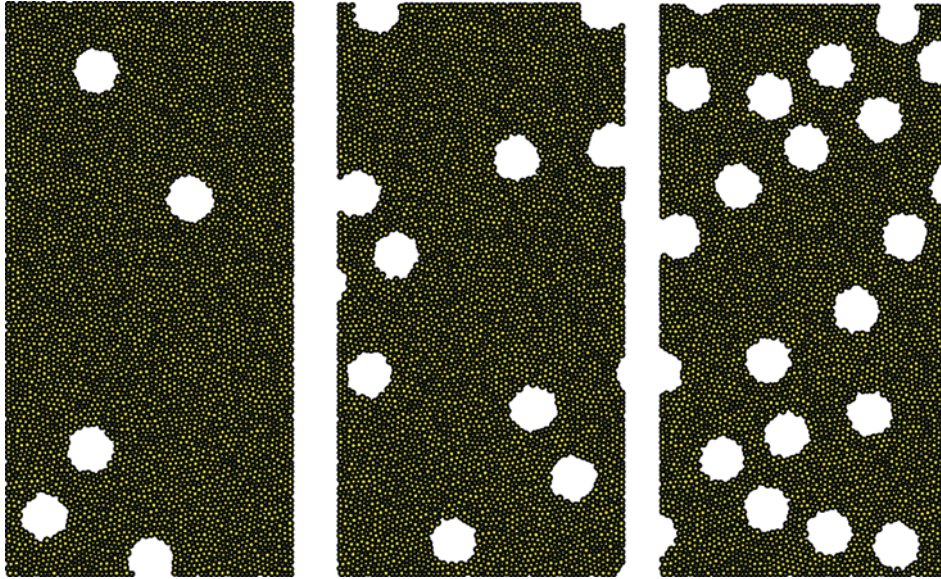
Source: BSC 2003 [DIRS 166660], Attachment V, Figure A-3, p. V-29.

a. PFC2D UCS Test Specimens of Lithophysal Tuff (Void Porosities of 0.05, 0.10 and 0.20)

Source: BSC 2003 [DIRS 166660], Attachment V, Figure A-4, p. V-30.

b. PFC3D UCS Test Specimens of Lithophysal Tuff (Void Porosities of 0.05, 0.10 and 0.19)

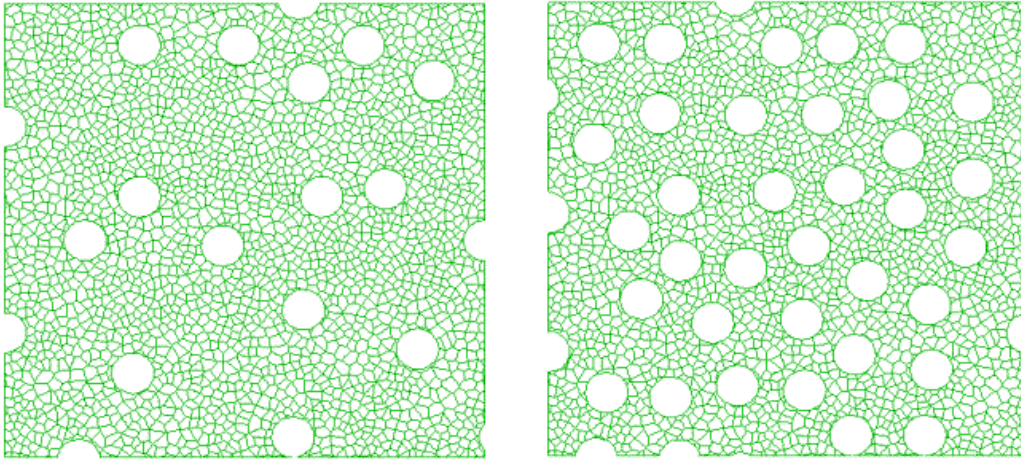Figure 6.5-4. PFC2D and PFC3D Test Specimens of Lithophysal Tuff

Figure 6.5-5. UDEC Test Specimens of Lithophysal Tuff (Void Porosities of 0.10 and 0.24)

6.5.3.1 PFC Model Calibration

A number of PFC uniaxial compression tests were run on simulated tuff with and without lithophysal voids (Figure 6.5-6). The samples with no lithophysal voids show a typical shear failure mechanism as evidenced by the coalescence of extension cracks to form major shear fractures (discussed in more detail in Section 6.5.4, Figure 6.5-18). The model also shows highly linear (elastic) response just to the point of rock failure, followed by a brittle post–peak failure response due to the uniformity of bond strength set in the samples (Figure 6.5-19). This replicates the observed stress-strain laboratory behavior of samples with no lithophysal voids (Figure 6.3-12).

The PFC model of lithophysal rock was next calibrated to the laboratory test results of specimens averaging 15 to 20 percent lithophysal porosity. First, circular holes were added to the zero-voids model using a random spatial distribution to represent the lithophysal rock (Figure 6.5-4). Next, the PFC models of simulated lithophysal rock were run and the correspondence between numerical and laboratory-derived strengths, Young's modulus and porosity were examined. PFC micro-properties were adjusted until PFC model results matched the laboratory data at a void porosity of approximately 0.17 (Figures 6.5-7, where the exponential best fits of 290 mm laboratory data (Section 6.3.2.2), PFC2D, and PFC3D results all intersect), and produce a reasonable variation of modulus and strength with lithophysal volume fraction (Figures 6.5-7 to 6.5-9)[*]. Besides lithophysae, the effects of other inherent structural weaknesses in actual lithophysal rock such as rims, spots, and short trace-length fractures were taken into account in a smeared way (during calibration) by reducing the mechanical properties of the synthetic (matrix) material to match the laboratory large-core data. This is the reason why PFC synthetic material at zero lithophysal porosity converges to strength and stiffness values smaller than those typical of Topopah Spring nonlithophysal rock. [†]

---

[*] All specimens are 1 m wide; the aspect ratio is the ratio between specimen length to diameter and is denoted by "AR." The average particle or block size is denoted by "Davg."

[†] The microproperties of the base material are kept constant for all void porosities. The effect of the varying abundance of rim/spot material could be incorporated into the models in a direct (by assigning different microproperties to a region surrounding each void) or a smeared (by modifying the microproperties of the base material as a function of void porosity) fashion, but this was beyond the scope of the present study.
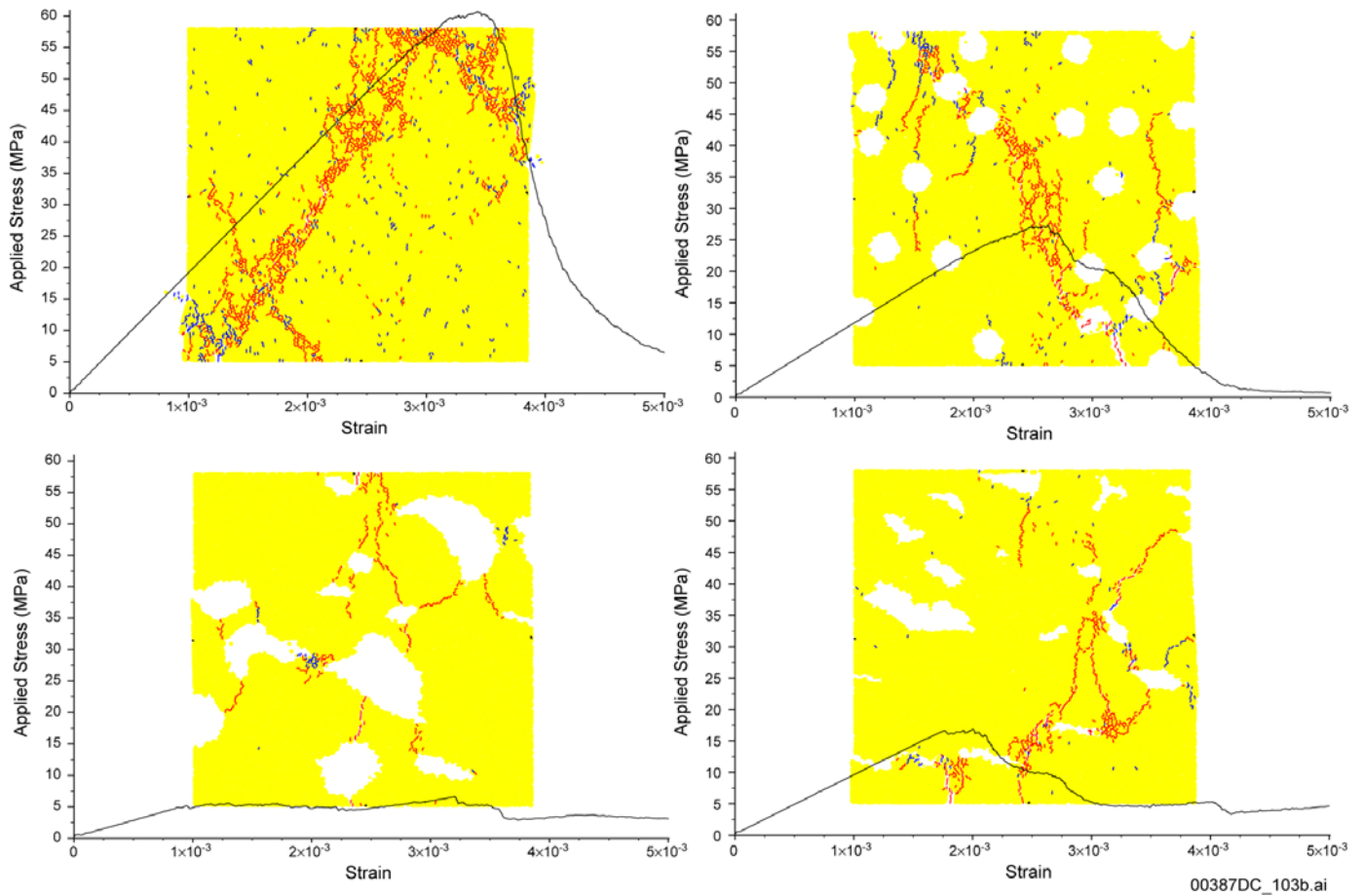
Source: Various PFC simulation models from BSC 2003 [DIRS 166660], Attachment V.

NOTE: Zero void welded tuff (upper left) is calibrated to provide matrix properties. Circular holes (upper right) provide a simple model of lithophysae, whereas lower models provide more realistic (hand-stenciled and digitized) shapes from Tptpll panel maps. Rock with no lithophysal voids fails in a brittle fashion through propagation of a major shear fracture (composed of small tensile fractures) through the sample. Samples with lithophysal voids fail due to tensile splitting (each red line is a bond breakage between small particles) and shear fractures between holes. Variability in lithophysal strength arises due to abundance, shape, and distribution of the holes throughout the sample.

Figure 6.5-6. PFC Calibration Experiment Samples and their Respective Uniaxial Compressive Stress–Strain Curves for Cases of Circular and Stenciled Lithophysae Shapes
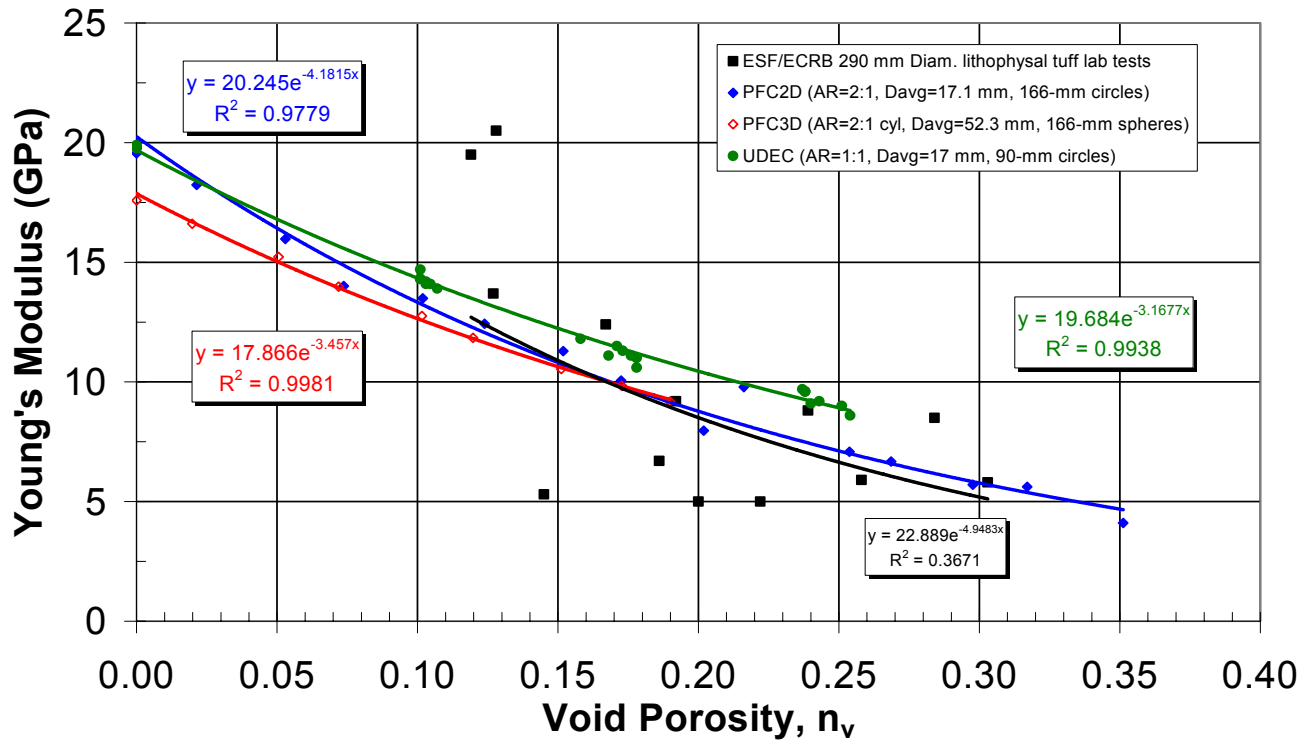
Source: Appendix B, Microsoft Excel file "PFC&UDEC_Plots.xls," Worksheet "mpl-E(bf4)."

Figure 6.5-7. Young's Modulus (E) vs Void Porosity (n_v) for Lithophysal Tuff and Models of Randomly Distributed Circular and Spherical Voids
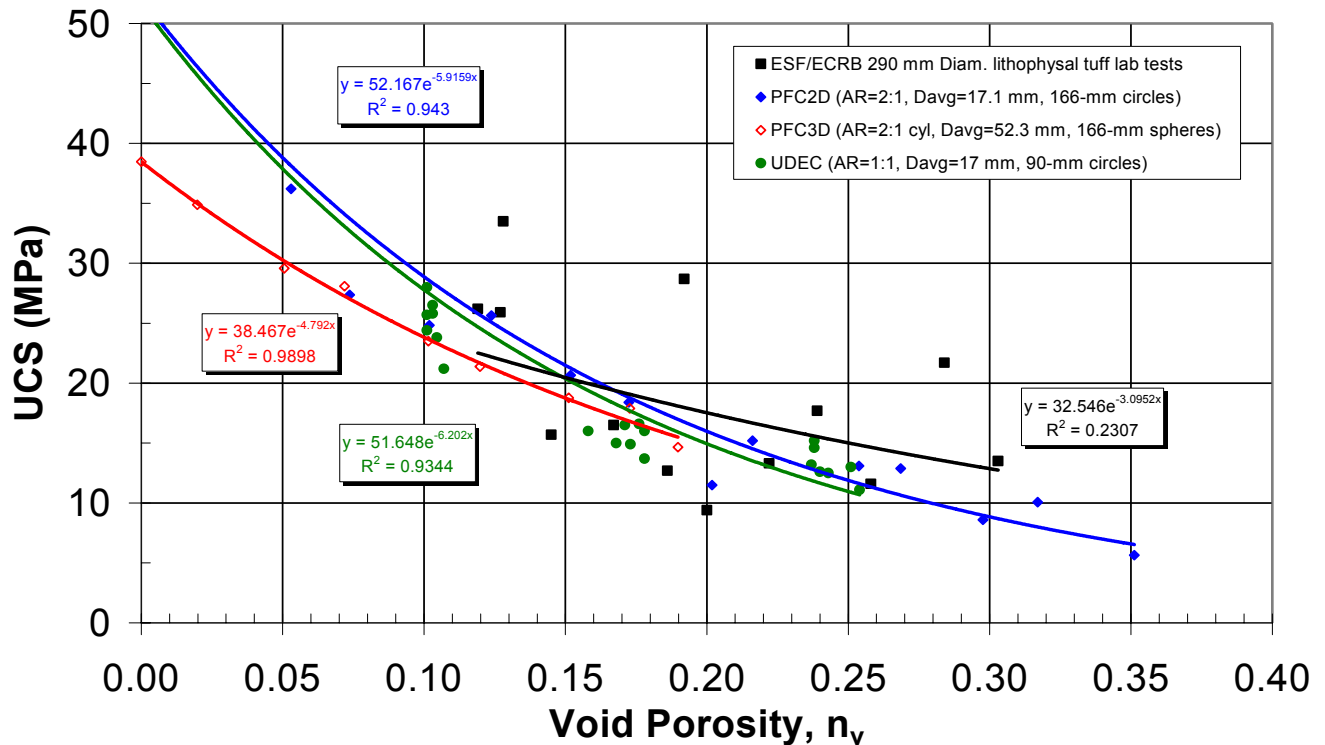
Source: Appendix B, Microsoft Excel file "PFC&UDEC_Plots.xls," Worksheet "mpl-qu(bf4)."

Figure 6.5-8 Uniaxial Compressive Strength vs. Void Porosity for Lithophysal Tuff and Models of Randomly Distributed Circular and Spherical Voids
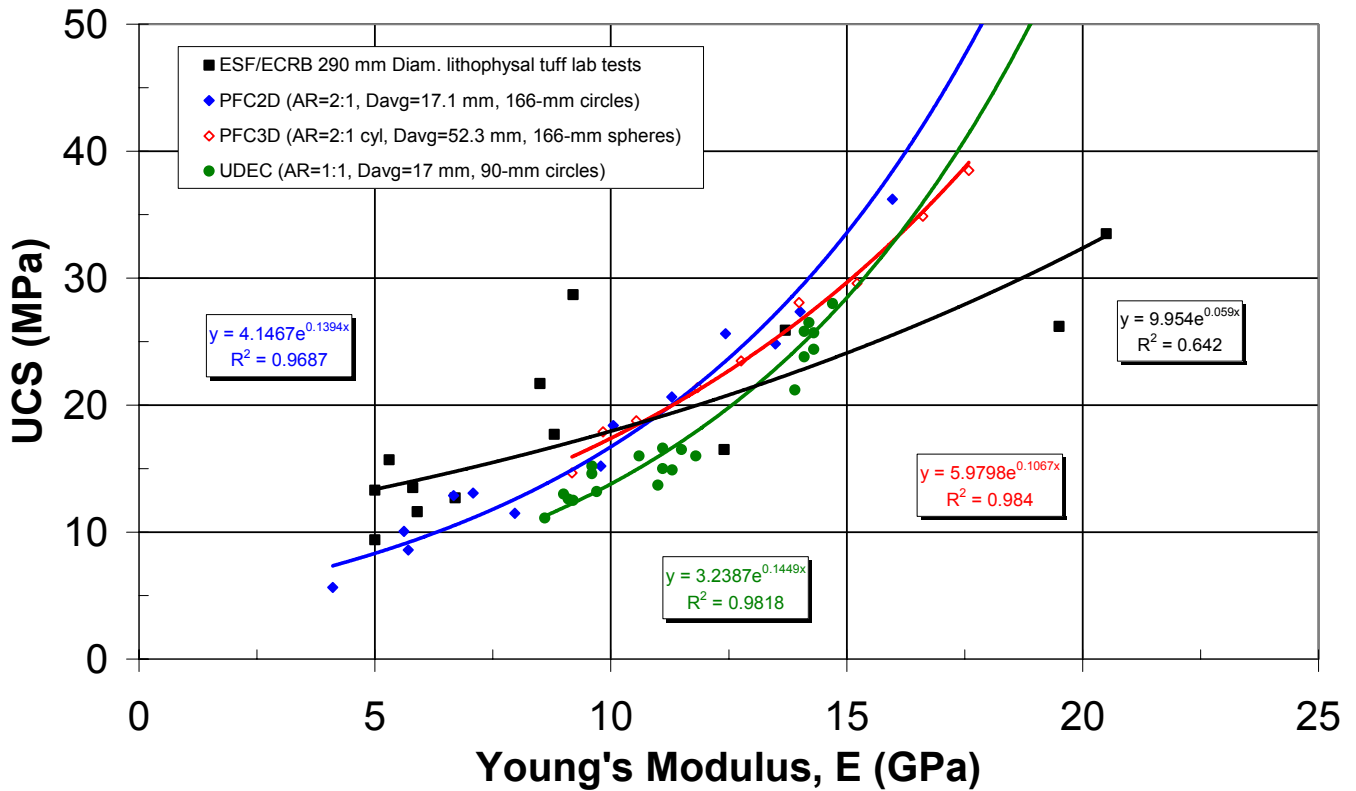
Source: Appendix B, Microsoft Excel file "PFC&UDEC_Plots.xls," Worksheet "mpl-que(bf4)."

Figure 6.5-9. Young's Modulus (E) vs. Uniaxial Compressive Strength (UCS) for Lithophysal Tuff and Models of Randomly Distributed Circular and Spherical Voids

The PFC material properties are obtained by testing PFC specimens in a polyaxial cell and in a direct-tension device. The polyaxial cell loads a parallelepiped specimen between pairs of opposing walls. The walls are made frictionless and assigned a stiffness equal to that of the PFC particles in order to eliminate frictional effects. The top and bottom walls act as loading platens, and the velocities of the lateral walls are controlled to maintain a constant confining stress. Uniaxial compression tests are performed by removing the lateral walls. The polyaxial cell inhibits specimen bulging because the lateral walls remain straight. The polyaxial cell does not simulate a triaxial test in which a specimen is encased in a membrane and confined by fluid pressure.

The direct-tension device controls the velocities of a thin layer of boundary particles on the top and bottom specimen faces to apply uniaxial strain. The rotations and non-axial translations of the boundary particles are constrained to zero; thus, the test mimics a complete gluing of a rigid platen to each face such that the specimen is not allowed to contract at the platen-specimen interface. The total out-of-balance force acting on each set of boundary particles is monitored during the test, and the average of this force is divided by the initial specimen cross-sectional area to compute the applied stress.

The numerical models were observed to reproduce the failure mechanisms observed in the laboratory lithophysal rock test specimens. A conclusion of this initial work with a simplistic void porosity model is that the primary strength-decreasing effect of the lithophysae is due to the formation of tensile splitting between neighboring lithophysae under uniaxial compressive load. As porosity increases, the spacing between lithophysae decreases, and thus a greater propensity for tensile splitting at lower applied forces exists. The tensile splitting mechanism results in increasingly less-brittle post–peak response with increasing porosity. Additionally, the same matrix strength provides a reasonable fit to both nonlithophysal and lithophysal laboratory data because the void porosity is the primary driver in the mechanical properties reduction and not mineralogical differences in lithophysal and nonlithophysal rocks (BSC 2003 [DIRS 164670], Table 6.2).

6.5.3.2 UDEC Model Calibration

The cohesion and friction angle of the UDEC micro-joints are used to control the sample's uniaxial compressive strength. The normal and shear stiffness of micro-joints as well as the bulk and shear modulus of the intact rock (blocks) are used to control the sample modulus.

The elastic and strength properties can be decoupled during the iteration process (i.e. model deformability and strength can be calibrated separately). It is common to calibrate model elastic parameters first. Clearly, calibration of the elastic properties is a problem with a non unique solution. The two elastic macro-properties (E and v) are functions of block size and four micro properties (k_n, k_s, E^m, and v^m). The average block size is determined based on having a sufficient number of blocks to allow for consistent and repeatable results in the two-dimensional synthetic sample given the sample size and lithophysal void size (so that fracture development and propagation is independent of grain size and orientation). The Poisson's ratio of the blocks is selected to be equal to the macro Poisson's ratio, such that $v^m = v$. The additional requirement needed to match the macro Poisson's ratio is that the ratio between normal and shear joint stiffness is greater than 1. Simulations confirmed that a Poisson's ratio of 0.2 is matched when $k_n / k_s \approx 2$. It is reasonable that the contribution of joints to model deformability is larger than the contribution of blocks, but it is desirable, from the perspective of convergence of the numerical model, that the stiffnesses of the blocks and joints are of the same order of magnitude. Therefore, based on guidance in the *UDEC* User's Guide Manual (Itasca Consulting Group 2002 [DIRS 160331], Manuals/UDEC/User's Guide/Section 3: Problem Solving, Section 3.2.3), it was selected that (BSC 2003 [DIRS 166660], Attachment VI, Eq. 16)

$$5 < \frac{K^m + \frac{4}{3}G^m}{b\,k_n} < 10 \qquad (6\text{-}1)$$

where b is the average block size, and K^m and G^m are the bulk and shear moduli of the blocks, respectively. With these considerations, there is a single independent elastic micro-parameter (k_n). The proper macro deformability of the model was then matched by rescaling of the elastic micro-properties (k_n, k_s, K^m, and G^m).

Calibration of strength micro-properties involves matching the macro (laboratory scale) failure-envelope and postpeak behavior by adjusting strength micro-properties. Note that model plastic deformation appears to be a function of the size and shape of blocks. The failure envelope, which is a surface in the principal stress space, reduces to a line in $\sigma_1 - \sigma_3$ space if it is assumed that the failure envelope is not a function of the intermediate principal stress. Numerical test runs have shown that the micro friction angle, which is initially equal to 35° and softens to 15°, results in the desired postpeak behavior and strength increase as a function of confinement. In order to match the observed mode of failure for lithophysal tuff with no cavities under uniaxial loading conditions (i.e. axial splitting), the micro tensile strength is assigned to be less than or equal to 50 percent of the micro cohesion. After these relations are established, the proper peak strength is matched by rescaling micro cohesion and tensile strength.

Each sample was tested with a loading condition that simulated either tensile, uniaxial compressive strength (UCS) or triaxial compression (with confinement pressures of 1 MPa, 3MPa, and 5 MPa). The loading of each sample was controlled by a FISH function (LT.FIS) that adjusts the axial loading velocity to limit the axial stress difference between the top and the bottom of the sample. This insures that the sample is loaded almost quasi-statically, and dynamic effects are relatively small.

In all cases the tests simulated a frictionless platen at the top and bottom of the sample. The axial stresses are generated in response to a controlled velocity condition on the top of the sample. In the case of triaxial compression, a constant lateral confining stress is applied to the sample edges prior to the axial loading of the sample. The applied confining stress does not extend into lithophysal voids that intersect the edges. The lateral confining stresses were adjusted based on the actual loaded surface area to insure that the total force was equal on both sides of the sample.

The axial stress is defined by the sum of the reaction forces at the loading 'platen' divided by the original sample width. The axial strain is defined as the change in distance between the 'platens' divided by the original sample height. The volumetric strain is calculated by integrating the current sample width over the current sample height and dividing by the original sample volume. These quantities are automatically calculated and recorded at regular intervals during the test.

The target modulus and uniaxial compressive strength were selected to match the lithophysal tuff properties derived in the *PFC* lithophysal study (Section 6.5.3.1). The values of 20 GPa for Young's modulus (Figure 6.5-7) and 60 MPa for uniaxial compressive strength (Figure 6.5-13) were used as the target values for the calibration of large-core lithophysal tuff with zero percent lithophysal porosity. The lithophysal porosity is defined as the lithophysal volume fraction (ratio of volume of inserted voids to total sample volume). There is an inherent matrix porosity included in the numerical rock model since the calibration is based on intact rock specimens having a matrix groundmass porosity of about 10 percent. The calibration process produced the micro- and fracture properties given in Table 6.5-1. The average values from five model samples (with different Voronoi seeds) were 19.8 GPa and 58.7 MPa for the modulus and UCS, respectively (BSC 2003 [DIRS 166660], Section 9.2, Table 9-3).

Table 6.5-1. Calibrated *UDEC* (Micro) Fracture Properties to Reproduce Average Intact Strength and Deformability of Lithophysal Rock with No Cavities.

Micro-Fracture Parameter	Value	Unit
Intact Bulk Modulus	23.0	GPa
Intact Shear Modulus	17.2	GPa
Joint Normal Stiffness	2360.0	GPa/m
Joint Shear Stiffness	1180.0	GPa/m
Joint Cohesion	22.0	MPa
Joint Friction	35.0	Degrees
Joint Tension	9.0	MPa
Residual Cohesion	0.0	MPa
Residual Friction	15.0	Degrees
Residual Tension	0.0	MPa

Source: BSC 2003 [DIRS 166660], Section 9.2, Table 9-2.

The generation of the lithophysal samples resulted from cutting 90 mm diameter holes in the non lithophysal samples. The position of the holes was controlled using one of two techniques. Some of the samples were created so as to match specific simulated samples used in the *PFC* lithophysal study (Section 6.5.4).   The rest of the samples were generated using a Fish function with a random number generator that specified the location of the holes. Successive holes are introduced until the total area of the removed material matches the desired lithophysal porosity.

In both techniques, there were some simple rules that were used for the placement of holes (BSC 2003 [DIRS 166660], Attachment VI, Section VI.2). These rules are necessary to ensure that the bridges between voids contain more than one block and to ensure that the collapse of voids does not affect the applied boundary conditions. The first rule is the distance between the edges of adjacent holes can never be less than 0.041 m. The second rule is there must be at least a 0.045 m distance between the edge of a hole and the sample sides (unless the hole intersects the side). If the hole intersects the sample side then the intersection is limited to half of the diameter or less.

Several samples were generated for three target nominal lithophysal porosities of 10, 17 and 24 percent. In each case the placement of the holes was varied. Because of the placement rules it was not possible to generate samples with lithophysal porosity greater than approximately 26 percent. Figure 6.5-6 show typical samples representing lithophysal porosities of 10 and 24 percent.

6.5.3.3 Determination of the PFC and UDEC Material Properties

For each PFC or UDEC synthetic sample tested, histories of the axial stress, axial strain, and volumetric strain were recorded. The history data points were transferred to Excel spreadsheets for post processing. The Excel spreadsheet contains the raw history data points of axial strain, volumetric strain and axial stress. Based on that raw data, Young's modulus, Poisson's ratio, dilation angle, UCS, internal angle of friction, cohesion, and the Hoek Brown factors σ_{ci} and m_i can be calculated. For two-dimensional models the specimen height is parallel with the global y-axis and the lateral dimension lies along the global x-axis.

Several assumptions are made when obtaining material properties from PFC polyaxial-cell tests. First, stresses and strains are computed using the specimen dimensions at the start of the test. Stresses in the PFC2D models are computed assuming that each particle is a disk of unit thickness. Finally, strains are computed from the wall displacements.* These assumptions and further details regarding the determination of PFC material properties are described in BSC 2003 [DIRS 166660], Attachment V, Appendix A, Section A.2

Since the UDEC model uses a plane strain assumption, each simulated rock specimen is considered to have an infinite depth (i.e., the specimen is constrained in along the global z-axis). Stresses and strains are computed using the specimen dimensions at the start of the test.

Peak Compressive Strength. The value of peak compressive strength was taken as the greatest axial compressive stress (σ_y) achieved during the test.

Young's Modulus. Young's modulus is defined as the ratio of the axial stress to axial strain (ε_y) in the plane strain material (slope of the axial stress-strain curve) and is calculated at a stress equal to 50 percent of the UCS value (secant method).

$$E = \frac{\sigma_y}{\varepsilon_y} \qquad (6\text{-}2)$$

Poisson's Ratio.   Poisson's ratio (υ) is defined as the ratio of lateral contraction ($-\varepsilon_x$) to longitudinal extension (ε_y) for the plane strain material and is calculated (at 50 percent of UCS) using the following formula, which can be derived from elastic theory for plane strain (Appendix C, Eq. C-5):

$$S_e = \frac{elastic \quad volumetric \quad strain}{elastic \quad axial \quad strain}$$

$$\upsilon = -\frac{\varepsilon_y}{\varepsilon_x} = \frac{1 - S_e}{2 - S_e} \qquad (6\text{-}3)$$

Dilation Angle. The dilation angle (ψ) is calculated from the slope of the expansive (plastic) portion of volumetric strain versus axial strain curve. The slope is calculated by a linear fit to the data from the greatest volumetric contraction to the end of the test. The calculation is performed using the internal LINEST function in Excel. The slope is then used to calculate the dilation angle (in degrees) using the following formula (Appendix C, Eq. C-15):

---

* Void collapse and non-homogeneous deformation in the post-peak region produce a large scatter in both the measurement-based (using the average of three measurement regions lying along the specimen axis) and the specimen-based (using gage particles on the specimen surface) deformation measurements. Note that the wall-based modulus is slightly less than the specimen-based modulus, because of the ball-wall overlap that makes the wall-based strain greater than the specimen-based strain.

$$S_p = \frac{plastic \quad volumetric \quad strain}{plastic \quad axial \quad strain}$$

$$\psi(\text{deg}) = \arcsin\left(\frac{S_p}{S_p + 2}\right) \times \frac{180}{\pi} \tag{6-4}$$

Angle of Internal Friction. The angle of internal friction (ϕ) is calculated from the slope of the σ_1 (axial stress) versus σ_3 (confining pressure) graph. The slope (S_ϕ) is calculated by a linear fit to the data using the internal trend function in Excel. The peak friction angle is determined using the peak applied compressive stresses. The friction angle (in degrees) is calculated by the following formula (Brown 1981 [DIRS 102003], pp. 125-127):

$$\phi(\text{deg}) = \arcsin\left(\frac{S_\phi - 1}{S_\phi + 1}\right) \times \frac{180}{\pi} \tag{6-5}$$

Cohesion. The cohesion (c) is calculated from the friction angle and the UCS using the following formula (Brown 1981 [DIRS 102003], pp. 125-127):

$$c = UCS \times \frac{1 - \sin\phi}{2\cos\phi} \tag{6-6}$$

6.5.4 Effect of Void Shape on Mechanical Properties

The effect of void shape on mechanical properties is studied using the PFC2D model by inserting randomly distributed voids of simple shape (circle, triangle and star) and by inserting voids corresponding with lithophysal cavities identified in panel maps of the walls of the ECRB Cross-Drift (Figures 6.5-10 and 6.5-11).[*] The simple-shape results demonstrate that the void shape does significantly affect Young's modulus and uniaxial compressive strength depending upon void porosity (Figures 6.5-12 and 6.5-13). However, when the void porosity is removed from explicit reference by plotting compressive strength versus Young's modulus, the data set for all three shapes falls into nearly the same curve (Figure 6.5-14).

Additional insight into the softening and weakening effects is provided by the following analysis. The results for triangular- and star-shaped voids can be superposed onto the curves for circular shapes by introducing an effective porosity that accounts for the "effective span" of the void (Figures 6.5-15 to 6.5-17). This suggests that an effective circle can be associated with any shape and that effective porosity can be used to relate the response to that of circular shapes. The area of the noncircular voids is given by the following equation (BSC 2003 [DIRS 166660], Attachment V, Eq. (1), p. V-7)

---

[*] The specimens are 1 m by 1 m, and the average particle diameter of the PFC2D material is 9.9 mm.

$$A_v = \left(\frac{3\sqrt{3}}{8}\right)\beta D^2, \qquad \beta = \begin{cases} 0.50, & \text{triangle} \\ 0.25, & \text{star} \end{cases} \tag{6-7}$$

where D is the bounding-circle diameter and β is a geometric constant. An effective circle is defined for the triangular- and star-shaped voids by

$$D_{\mathrm{eff}} = \lambda D, \;\; A_{v(\mathrm{eff})} = \frac{\pi D_{\mathrm{eff}}^2}{4} \tag{6-8}$$

where λ is an unknown scaling parameter that, in general, will differ for each shape and cannot be rigorously defined and $A_{v(\mathrm{eff})}$ is the effective-circle area of a void. Instead, λ is determined by trial-and-error until the Young's modulus or uniaxial compressive stress versus void porosity relationship (Figures 6.5-16 and 6.5-17) for triangles (or stars) match as closely as possible the same curves for circular voids. The various best-fit values of λ for the different shaped voids are given in Figures 6.5-15 to 6.5-17. The effective void porosity, $n_{v(\mathrm{eff})}$, is defined as the ratio of effective-circle volume of a voids, $V_{v(\mathrm{eff})}$, to total specimen volume, V,

$$n_{v(\mathrm{eff})} = \frac{V_{v(\mathrm{eff})}}{V} = \frac{A_{v(\mathrm{eff})}}{A} \tag{6-9}$$

which is also the ratio of effective-circle area of voids, $A_{v(\mathrm{eff})}$, to total specimen area, A. By combining Eqs. 6-7, 6-8, and 6-9, the void porosities are related by

$$n_{v(\mathrm{eff})} = \left(\frac{V_{v(\mathrm{eff})}}{V_v}\right)n_v = \left(\frac{A_{v(\mathrm{eff})}}{A_v}\right)n_v = \left(\frac{2\pi\lambda^2}{3\sqrt{3}\,\beta}\right)n_v \tag{6-10}$$

Substituting the appropriate values of λ and β into Eq. 6-10 and rearranging gives

$$A_{v(\mathrm{eff})} = \begin{cases} 1.22\,A_v, & \text{triangle} \\ 1.92\,A_v, & \text{star} \end{cases} \tag{6-11}$$

The superposition of the uniaxial compressive strength data for all void shapes onto nearly the same curve (Figure 6.5-17) is surprising, and suggest either that the stress concentrations created by sharp void angles in actual rock do not produce a significant weakening effect, or that the PFC model used cannot duplicate the effect, perhaps due to the rounded representation of the sharp corners in the PFC material.
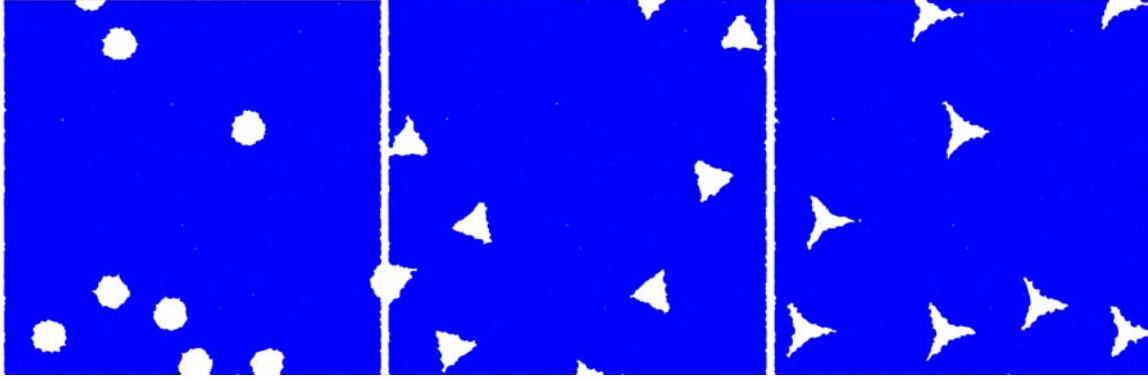
Source: BSC 2003 [DIRS 166660], Attachment V, Figure 3, p. V-8.

Figure 6.5-10. PFC2D Specimens of Circular-, Triangular- and Star-Shaped Voids With Void Porosities of Approximately 0.05
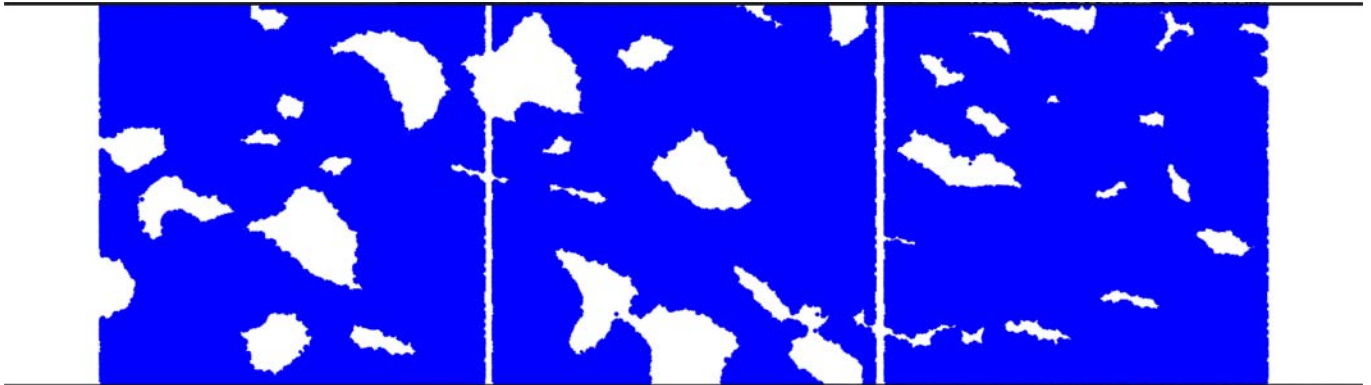
Source: BSC 2003 [DIRS 166660], Attachment V, Figure 13, p. V-14.

Figure 6.5-11. PFC2D Stenciled Lithophysae Specimens (Left, Middle and Right) Generated from Lithophysal Cavities of Panel Map 14+93R
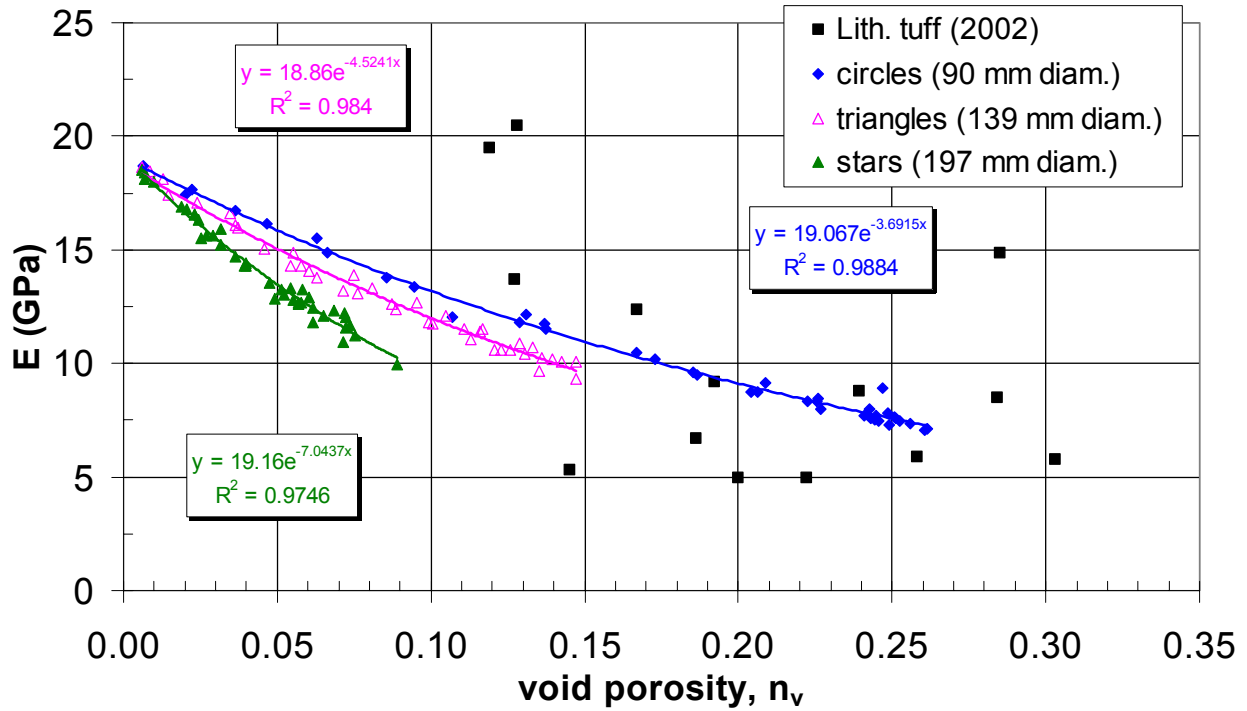
Source: BSC 2003 [DIRS 166660], Attachment V, Figure 4, p. V-9. Tuff is from 290 mm diameter tests.

Figure 6.5-12. Young's Modulus (E) vs. Void Porosity (n_v) for Lithophysal Tuff and PFC2D Models of Randomly Distributed Circular-, Triangular- and Star-Shaped Voids
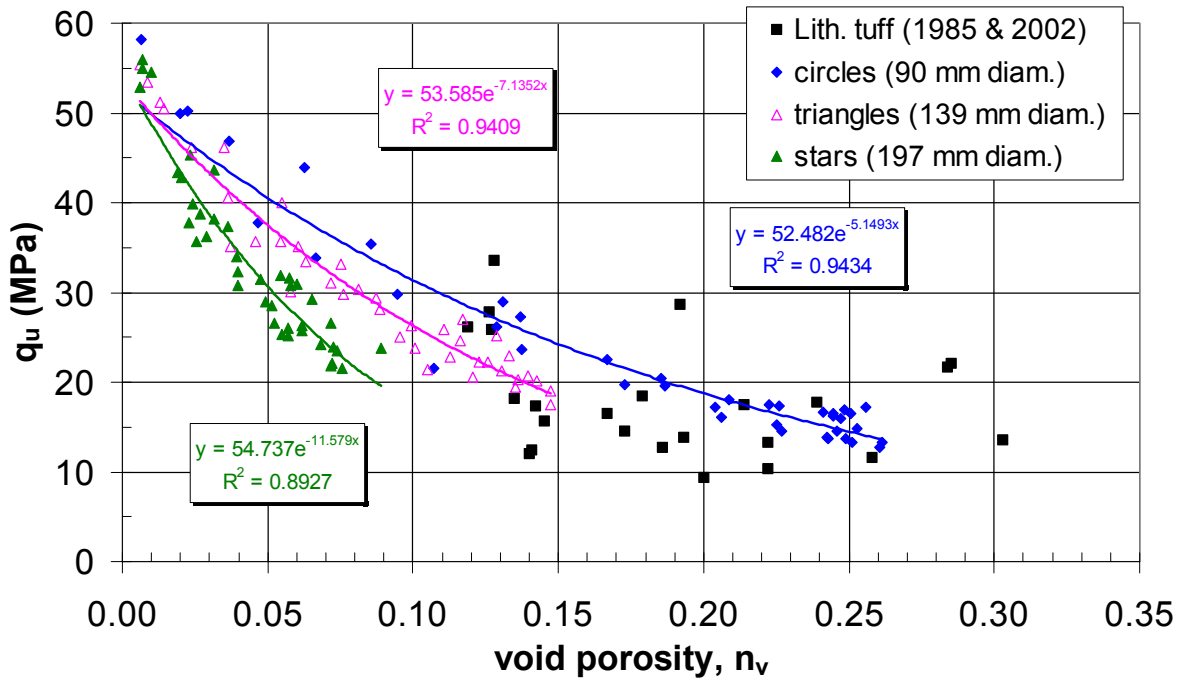
Source: BSC 2003 [DIRS 166660], Attachment V, Figure 5, p. V-10. Tuff is from 267 and 290 mm diameter tests.

Figure 6.5-13. Uniaxial Compressive Strength (q_u) vs. Void Porosity (n_v) for Lithophysal Tuff and PFC2D Models of Randomly Distributed Circular-, Triangular- and Star-Shaped Voids
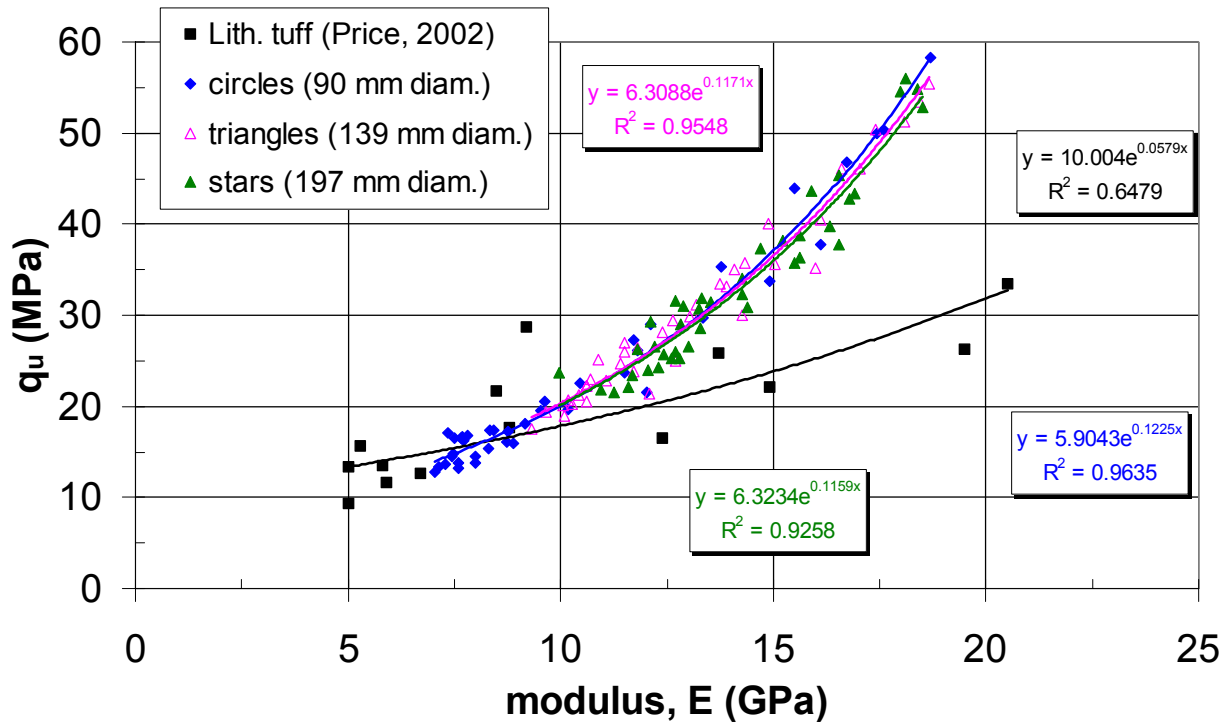
Source: BSC 2003 [DIRS 166660], Attachment V, Figure 9, p. V-12. Tuff is from 290 mm diameter tests.

Figure 6.5-14. Uniaxial Compressive Strength (q_u) vs. Young's Modulus (E) for Lithophysal Tuff and PFC2D Models of Randomly Distributed Circular-, Triangular- and Star-Shaped Voids
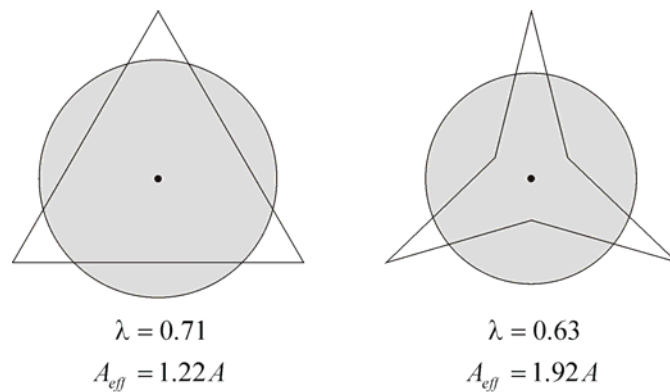
Source: Modified from BSC 2003 [DIRS 166660], Attachment V, Figure 1.

NOTE: Lambda, λ, is an scaling parameter that varies with void shape and A_{eff} is the effective-circle area of a void (shaded circle in the figure).

Figure 6.5-15. Effective Circles Used to Compute Effective Void Porosity for Triangular and Star Shapes
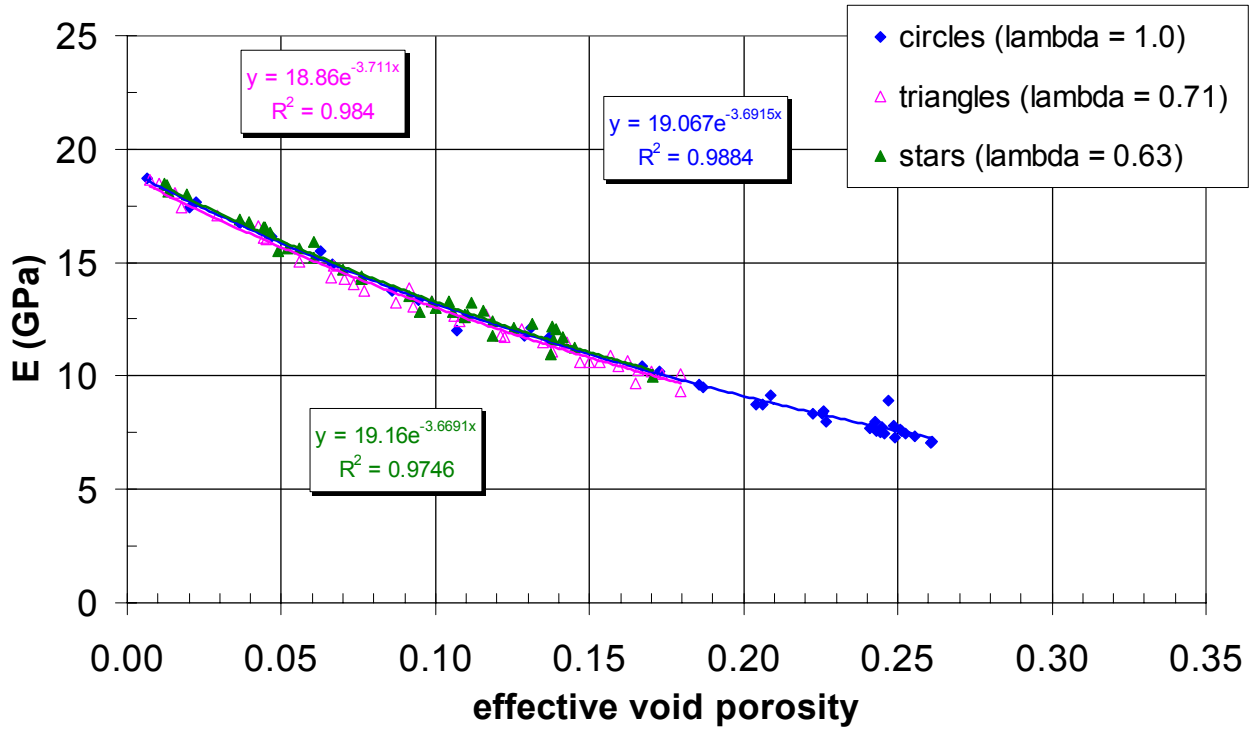
Source: Appendix B, Microsoft Excel file "ShapeStudy.xls," Worksheet "E(c-t-s) Aeff."

Figure 6.5-16. Young's Modulus (E) vs. Effective Void Porosity (n_v) for PFC2D Models of Randomly Distributed Circular-, Triangular- and Star-Shaped Voids
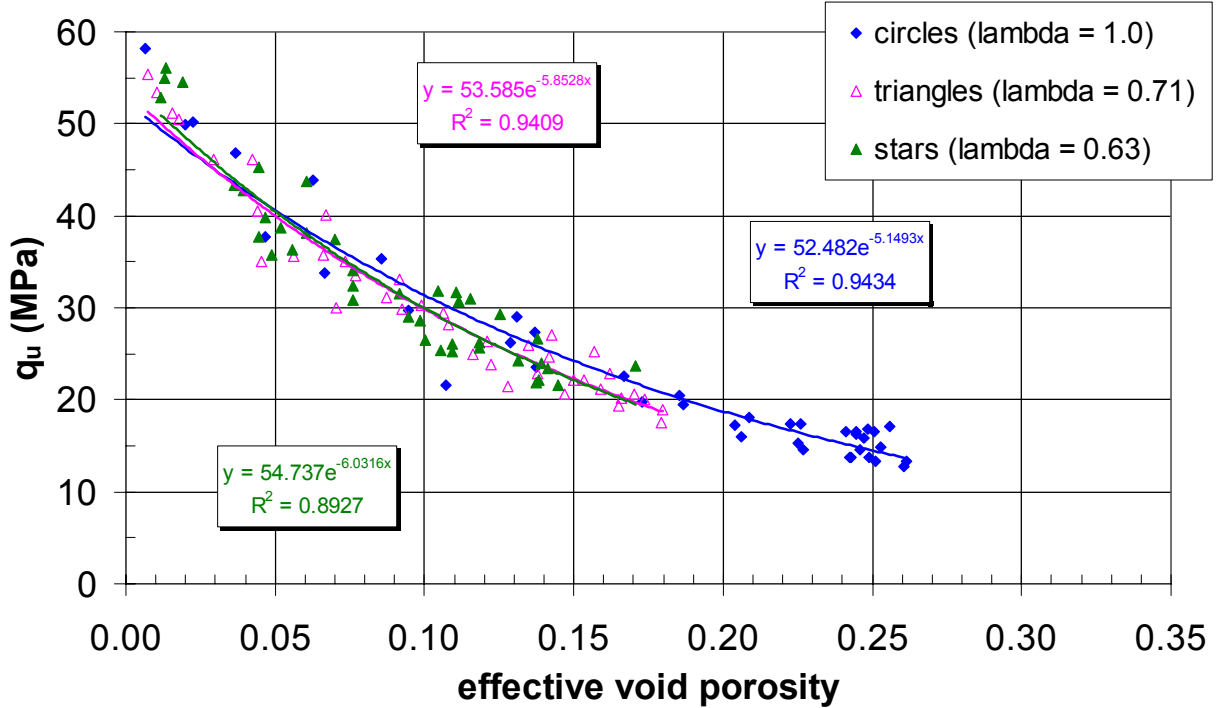
Source: Appendix B, Microsoft Excel file "ShapeStudy.xls," Worksheet "q(c-t-s) Aeff."

Figure 6.5-17. Uniaxial Compressive Strength vs. Effective Void Porosity for PFC2D Models of Randomly Distributed Circular-, Triangular- and Star-Shaped Voids

Figures 6.5-18 to 6.5-22 illustrate typical fracturing that occurs in PFC samples with voids. The PFC particles are drawn in yellow, the platens are drawn as black lines, and the stress-strain curves (black lines) plotted in Figures 6.5-20 to 6.5-22 use the same scales (stress ranges from 0 to 55 MPa and strain ranges from 0 to 0.5 percent). Each fracture is depicted as a line lying between the two previously bonded particles with a length equal to the average diameter of the two previously bonded particles. The line is oriented perpendicular to the line joining the centers of the two previously bonded particles. The cracks are colored such that blue indicates failure of pre-peak grain bond failures and red indicates failure of grain bonds after the specimen's peak compressive strength was reached.

The PFC and UDEC computational models develop tensile splitting and shear failure mechanisms that generally characterize a progressive failure of the rock material between lithophysal voids and specimen boundaries. The stress-strain behavior is initially linear elastic until fractures begin to appear prior to reaching the peak stress. As can be seen in the numerical specimen tests (e.g., Figure 6.5-18), initially, tensile failure cracks develop along more or less vertical failure paths, and often originate from void boundaries. Subsequently, the growth of micro-cracks in the rock matrix material is often observed to coalesce into macro-fractures exhibiting tensile (vertical fracture orientation) or shear (diagonal fracture orientation) failure of the specimen (Figure 6.5-18). At the peak stress point, there usually is considerable damage in the specimen (blue fractures in Figure 6.5-18) and most of the stress-induced macro-fractures connect lithophysae. For example, the stress-strain curves and the damage existing at an axial strain of 0.5 percent of the PFC2D specimens with void porosities of approximately 0.05 are shown in Figures 6.5-19 and 6.5-21. Examination of similar synthetic specimen damage plots in the *Subsurface Geotechnical Parameters Report* (BSC 2003 [DIRS 166660], Attachment V, Appendix B) reveals the same general failure pattern (Figures 6.5-20 to 6.5-22), which is analogous to the evolution to failure observed in experimental laboratory testing of large-core lithophysal tuff samples (Figure 6.3-12). For each damage plot, a graph of the axial stress (in units of Pa) versus axial strain (Figure 6.5-19) is overlaid that correspond with the state at an axial strain of 0.5 percent.
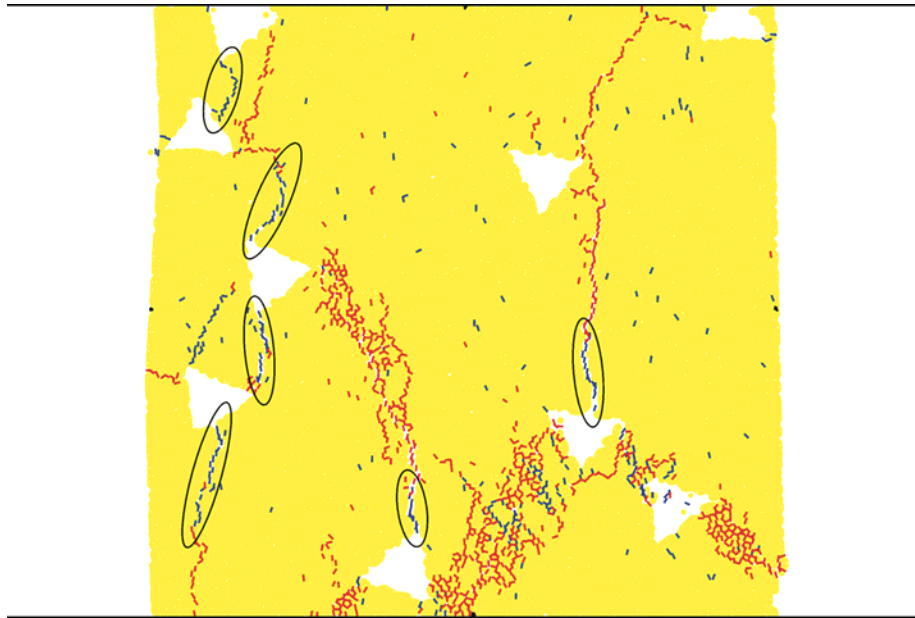
Source: BSC 2003 [DIRS 166660], Attachment V, Figure 8, p. V-11

NOTE: In the figure, blue indicates failure of pre-peak grain bond failures and red indicates failure of grain bonds after the specimen's peak compressive strength was reached. The initial prepeak damage has initiated three distinct vertical failure paths across the specimen. At the lower right two postpeak shear failure paths can be observed between voids and the specimen edges.

Figure 6.5-18. Damage at an Axial Strain of 0.5% in PFC2D Specimen with Triangular-Shaped Voids Showing Six Sites of Critical Damage
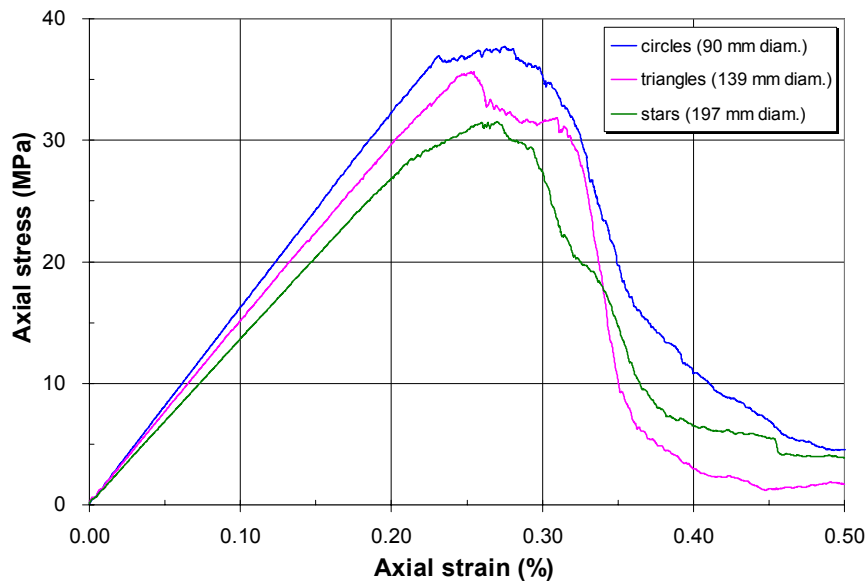
Source: BSC 2003 [DIRS 166660], Attachment V, Figure 7, p. V-11

Figure 6.5-19. Stress-Strain Curves of PFC2D Specimens of Circular-, Triangular- and Star-Shaped Voids with Void Porosities of Approximately 0.05
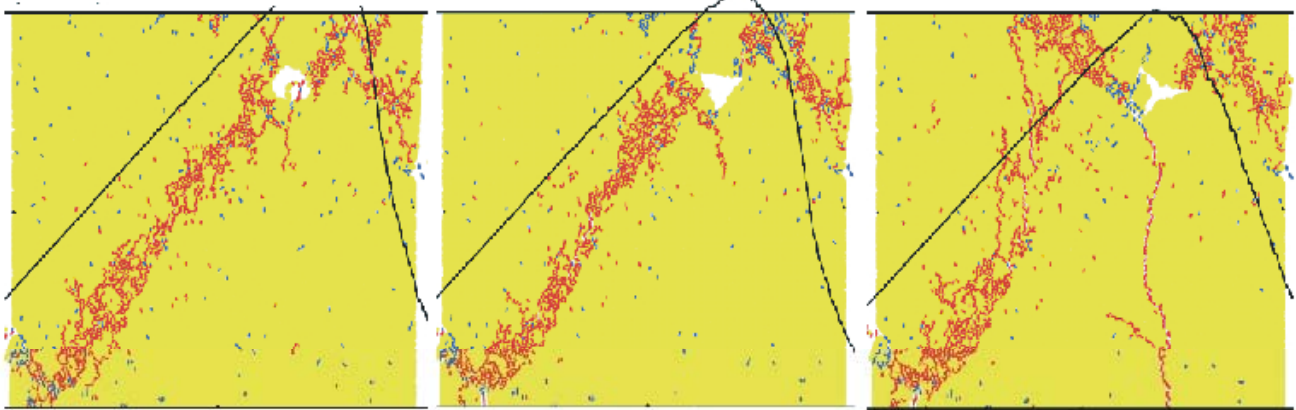
Source: BSC 2003 [DIRS 166660], Attachment V, Appendix B, Figure B-19, p. V-60

Figure 6.5-20. Damage at an Axial Strain of 0.5% in PFC2D Specimens of Circular-, Triangular- and Star-Shaped Voids with Void Porosities of Approximately 0.006
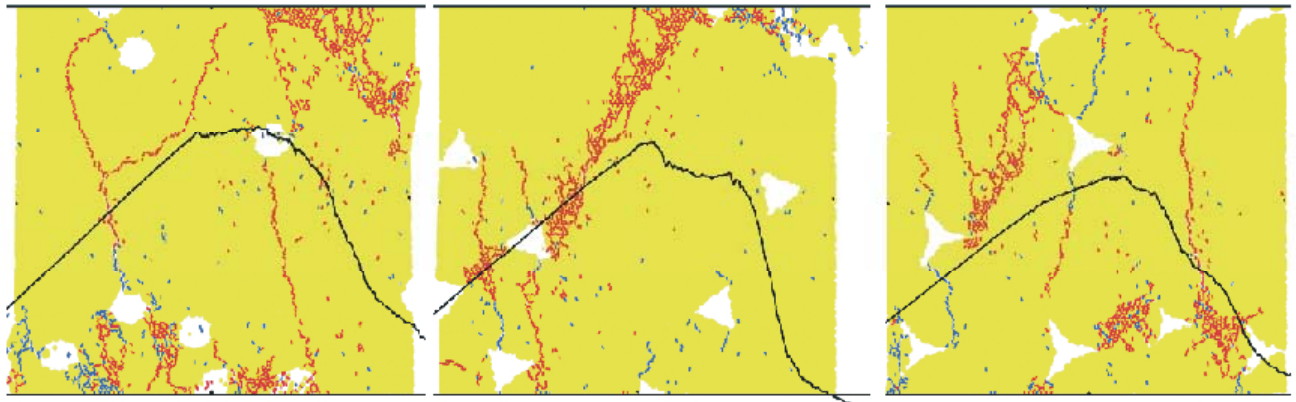
Source: BSC 2003 [DIRS 166660], Attachment V, Appendix B, Figure B-21, p. V-62

Figure 6.5-21. Damage at an Axial Strain of 0.5% in PFC2D Specimens of Circular-, Triangular- and Star-Shaped Voids with Void Porosities of Approximately 0.05
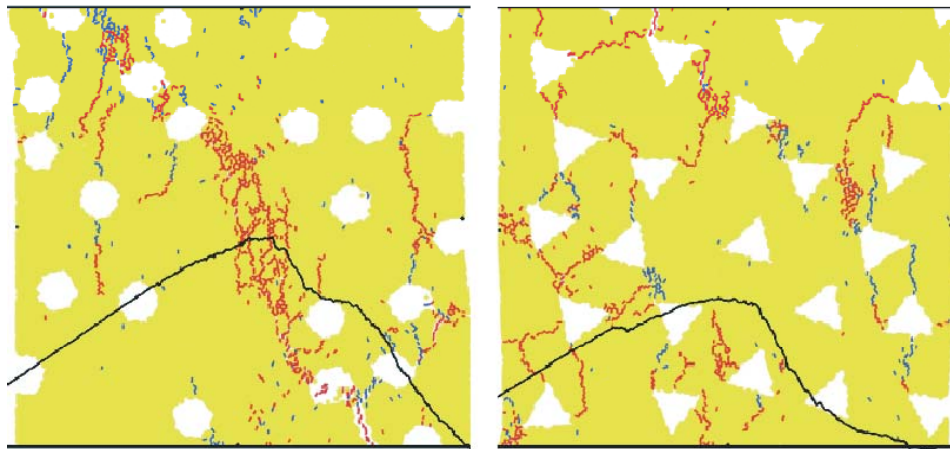
Source: BSC 2003 [DIRS 166660], Attachment V, Appendix B, Figure B-23, p. V-64

Figure 6.5-22. Damage at an Axial Strain of 0.5% in PFC2D Specimens of Circular- and Triangular-Shaped Voids with Void Porosities of Approximately 0.14

6.5.5   Modeling of Realistic Shaped Voids and Distributions of Voids

The variability of rock mechanical properties due to lithophysae shape and spatial distribution is studied by modeling realistic void shapes and distributions corresponding to lithophysal cavities identified in ECRB Cross-Drift panel maps (1×3 m).   By modeling a simulated PFC rock specimen with actual patterns of holes, stress concentrations and fracturing between the holes can be represented in a realistic way, allowing detailed examination of deformation and failure mechanisms.

A series of simulated samples of the lithophysal rock mass were developed directly from field panel map lithophysae distributions (BSC 2003 [DIRS 166660], Attachment VII) by overlaying (stenciling) the panel map directly onto the PFC model to create the void geometry.   A typical panel map is shown in Figure 6.5-23.   Each panel map defines a 1×3 meter area within which lithophysal cavities, rims, spots and lithic clasts have been identified as separate features.   The lithophysal cavities (excluding the rims) are used to define the voids in the PFC2D specimens as follows.   First, the cavity features (Figure 6.5-24) are used to produce a bitmap image with a resolution of 100 cells per meter. Next, the location of the PFC2D specimen is specified relative to the panel map system.   Then, all PFC2D particles with centroids lying within each void-cell of the bitmap are deleted.   So for the synthetic panel-map models the total void porosity arises only from the stenciled voids.   Actual panel map rock total porosity is composed of natural matrix porosity and the porosity of rim or spot material in additional to the lithophysal voids.

A set of three non overlapping PFC2D specimens (left, middle and right) was then extracted from each panel map (Figure 6.5-25).   A total of 18 panel maps located from approximately stations 15+00 to 23+00 (Tptpll unit) were used to produce a total of 54 PFC2D stenciled-lithophysae specimens that were then subjected to numerical uniaxial compression testing.

Numerical testing was performed in which the available lithophysal panel maps generated in the ECRB Cross-Drift were discretized and used as compression test "specimens" for the calibrated model.   As seen in Figures 6.4-7 and 6.5-26, the complex shape, size and distribution of lithophysal voids results in the same general failure mode (tensile splitting between voids) and same general trend of decreased compressive strength and Young's modulus with increasing void porosity (compare to Figures 6.5-21 and 6.5-22); however, the variability tends to be greater primarily due to the nonuniform shapes and distributions of voids.   A few large voids or an aligned distribution of voids within a sample can result in significantly lower uniaxial compressive strength (Figure 6.5-27) than widely spaced and more uniformly distributed voids in a sample of the same size.   The tests shown in Figure 6.5-27 illustrate cases of low strength and modulus values due to fortuitous alignments of lithophysae, lithophysae intersecting numerical specimen boundaries, and the presence of large-lithophysal cavities relative to the sample dimensions, all indicative of inadequate sample size.

The conclusions from the PFC model calibration are that a viable tool has been developed for simulation of the mechanical response of lithophysal tuff to stressing and that this tool can be used, in addition to field and laboratory testing, to study variability in material response.
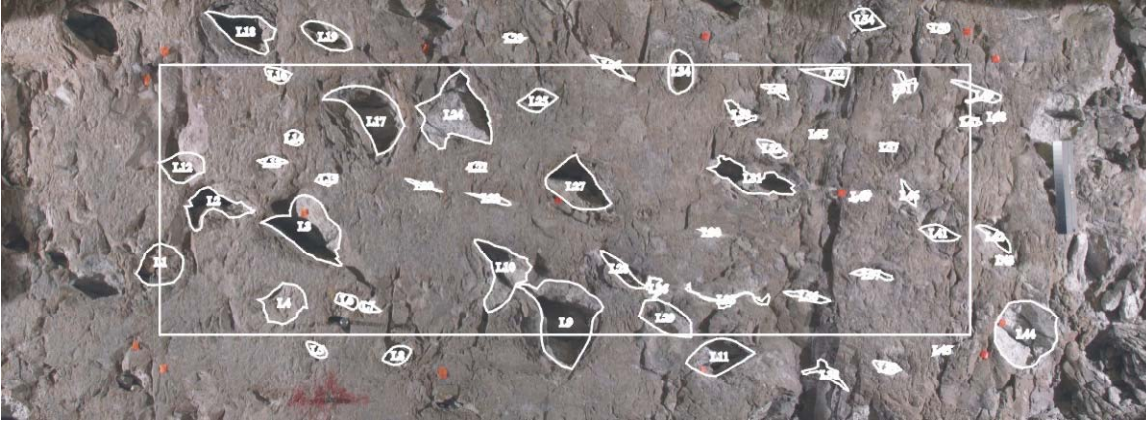
Source: BSC 2003 [DIRS 166660], Figure 9-19, p. 9-19

Figure 6.5-23. Panel Map at ECRB Cross-Drift Station 14+93 to 14+96 (Right Wall)

Source: BSC 2003 [DIRS 166660], Figure 9-20, p. 9-19

Figure 6.5-24. Cavity Features from Panel Map at ECRB Cross-Drift Station 14+93 to 14+96 (Right Wall)

Source: BSC 2003 [DIRS 166660], Figure 9-21, p. 9-19

Figure 6.5-25. PFC2D Stenciled-lithophysae Specimens (Left, Middle and Right) Generated from Lithophysal Cavities of Panel Map at ECRB Cross-Drift Station 14+93 to 14+96 (Right Wall)
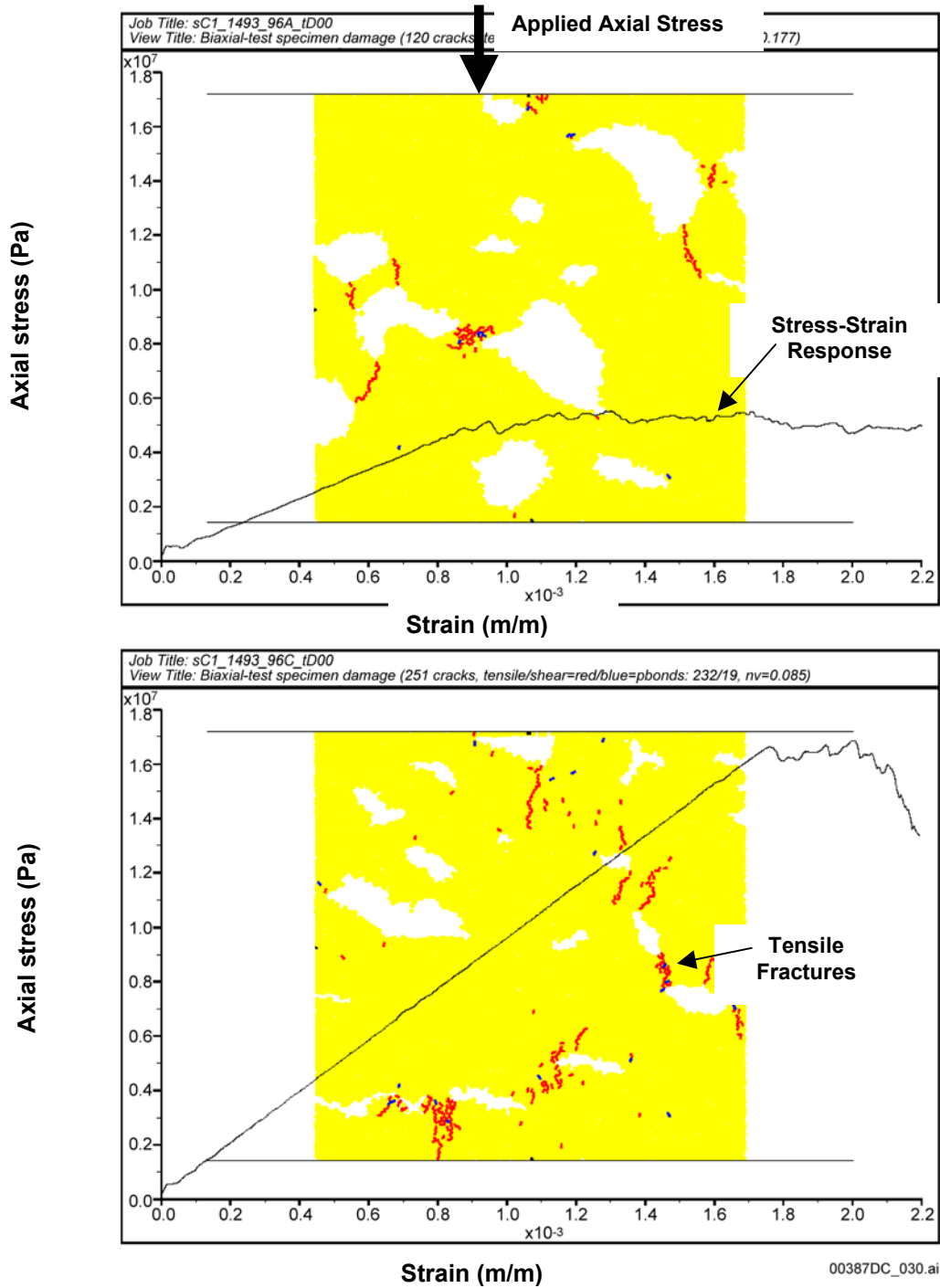
Source: BSC 2003 [DIRS 166660], Attachment V, Appendix B, Figure B-1, p. V-42, left and right specimens (Plots are at an earlier time in the loading history and scales are modified)

NOTE: Specimen is composed of several thousand bonded particles. Red lines are tensile fractures that have propagated between lithophysae to ultimately form a failure mechanism. Superimposed stress-strain curve illustrates impact of lithophysae distribution on uniaxial compressive strength, Young's modulus and postpeak failure mechanism. Vertical axis is axial stress in Pa; horizontal axis is strain in m/m.

Figure 6.5-26. Examples of Particle Flow Code Compression Tests Using Simulated Rock Specimens Developed by "Stenciling" Field Panel Maps in the ECRB Cross-Drift
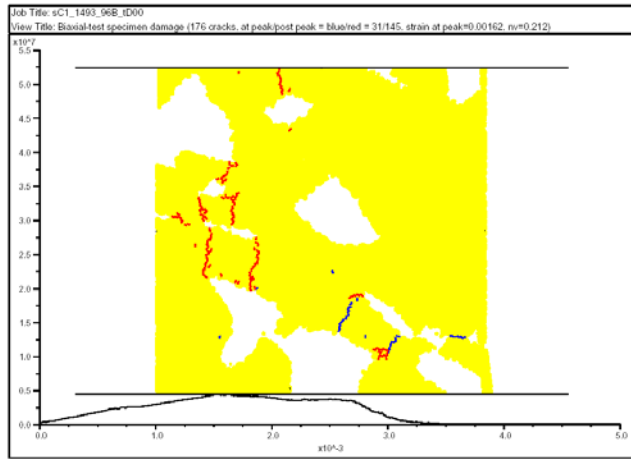
14+93 to 14+96 Right Wall, Middle Section
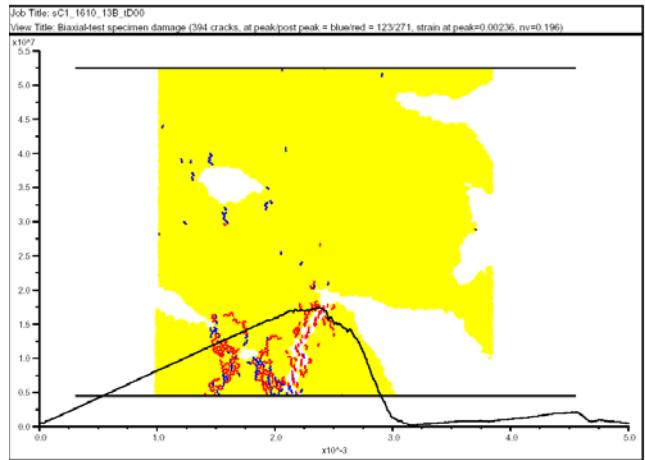
16+10 to 16+13 Right Wall, Middle Section
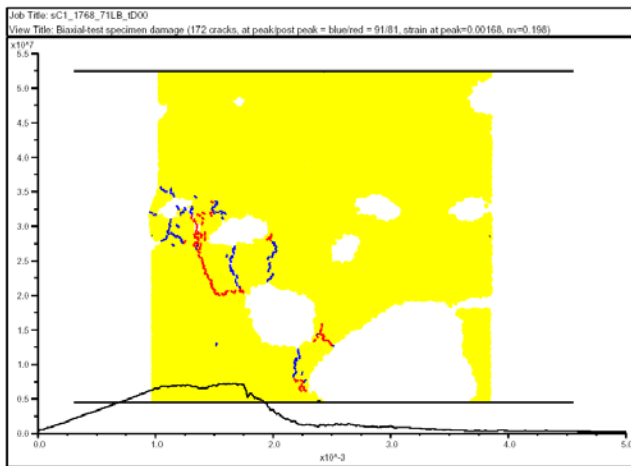
17+68 to 17+71 Left Wall, Middle Section
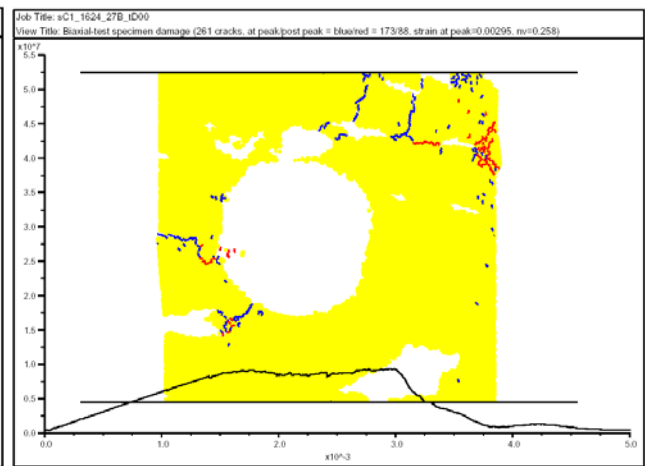
16+24 to 16+27 Right Wall, Middle Section
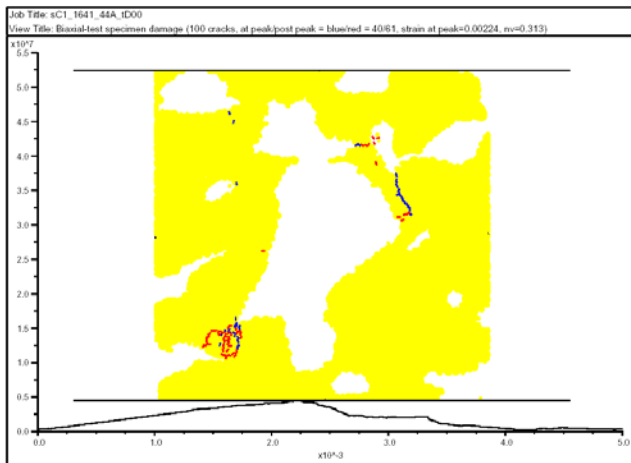
16+41 to 16+44 Left Wall, Left Section
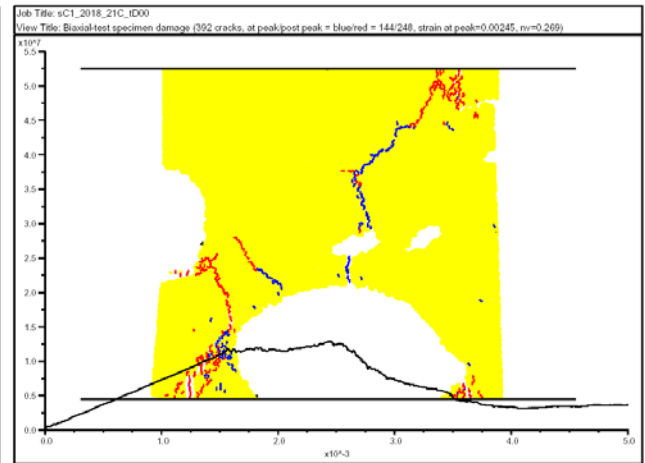
20+18 to 20+21 Left Wall, Right Section

Source: BSC 2003 [DIRS 166660], Figure 9-27, p. 9-27.

Figure 6.5-27. PFC2D Stenciled-lithophysae Specimens Showing Insufficient Sample Size at the 1 m Scale due to Presence of Large Lithophysae and Lithophysal Geometry

The panel map results demonstrate that:

1. The stenciled lithophysae material is softer and weaker and exhibits greater property variability when plotted with lithophysal porosity than the material with randomly distributed circular voids (Figures 6.5-28 and 6.5-29).

2. The property variability of the stenciled lithophysae material is similar to the scatter of the laboratory data (Figures 6.5-28 and 6.5-29). Scatter is slightly larger for laboratory data since the laboratory specimen lithophysal porosity is uncertain, whereas it is known with certainty for numerical specimens.

3. The variability of the correlated uniaxial compressive strength and Young's modulus data (Figure 6.5-30) is considerably less than property correlations with lithophysal porosity (Figures 6.5-28 and 6.5-29).

4. Finally, the strength-versus-modulus relationship of modeled panel map specimens is similar to that of the model material with populated with randomly distributed voids of simple shape, suggesting that the strength-versus-modulus curve is independent of void geometry (Figure 6.5-31).

The large scatter observed when plots are made with lithophysal porosity is likely due to the variation in structural weakness (unequal distribution of stresses and bending moments in the material) that is not reflected in the raw porosity measurement. However, when uniaxial compressive strength versus Young's modulus specimen data are plotted, the inherent structural weaknesses of an individual specimen is reflected in the corresponding strength-modulus data pair. For example, this dependence between parameters means that a specimen with a significant structural weakness can be expected to result in both a lower compressive strength and a softer Young's modulus.

The divergence in the fits of numerical results and large-diameter core laboratory results (for specimens with smaller void porosity) in Figure 6.5-30 appears to indicate that the numerical material should be recalibrated. Recalibration to a lower strength would fit the laboratory data better and yield better predictions, especially for strength results corresponding to Young's Modulus values above 15 GPa (roughly a void porosity less than 10 percent). Although the small-diameter core laboratory results (Figure 6.3-4) provide a closer fit to the numerical data, the PFC simulations still overpredict small-diameter uniaxial compressive strengths corresponding to values of Young's Modulus values greater than 15 GPa.
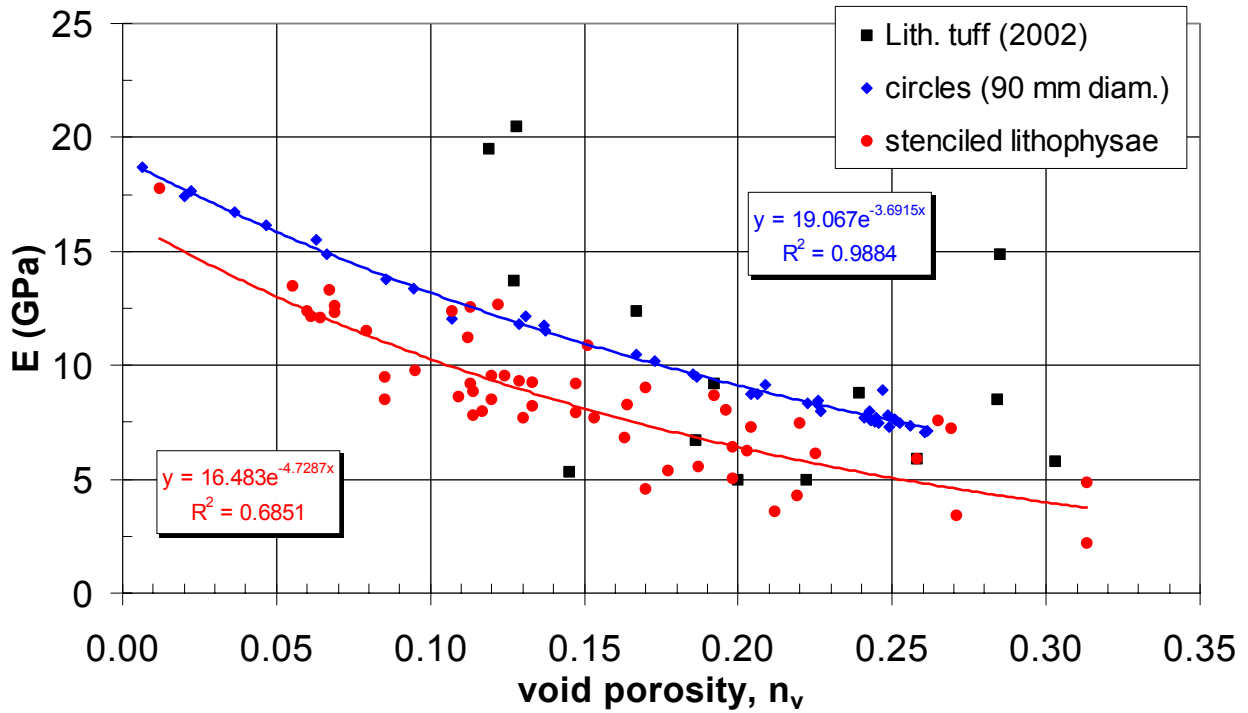
Source: BSC 2003 [DIRS 166660], Attachment V, Figure 14, p. V-16. Tuff is from 290 mm diameter tests.

Figure 6.5-28. Young's Modulus (E) vs. Void Porosity (n_v) for Lithophysal Tuff and PFC2D Models of Randomly Distributed Circles and Stenciled Lithophysae
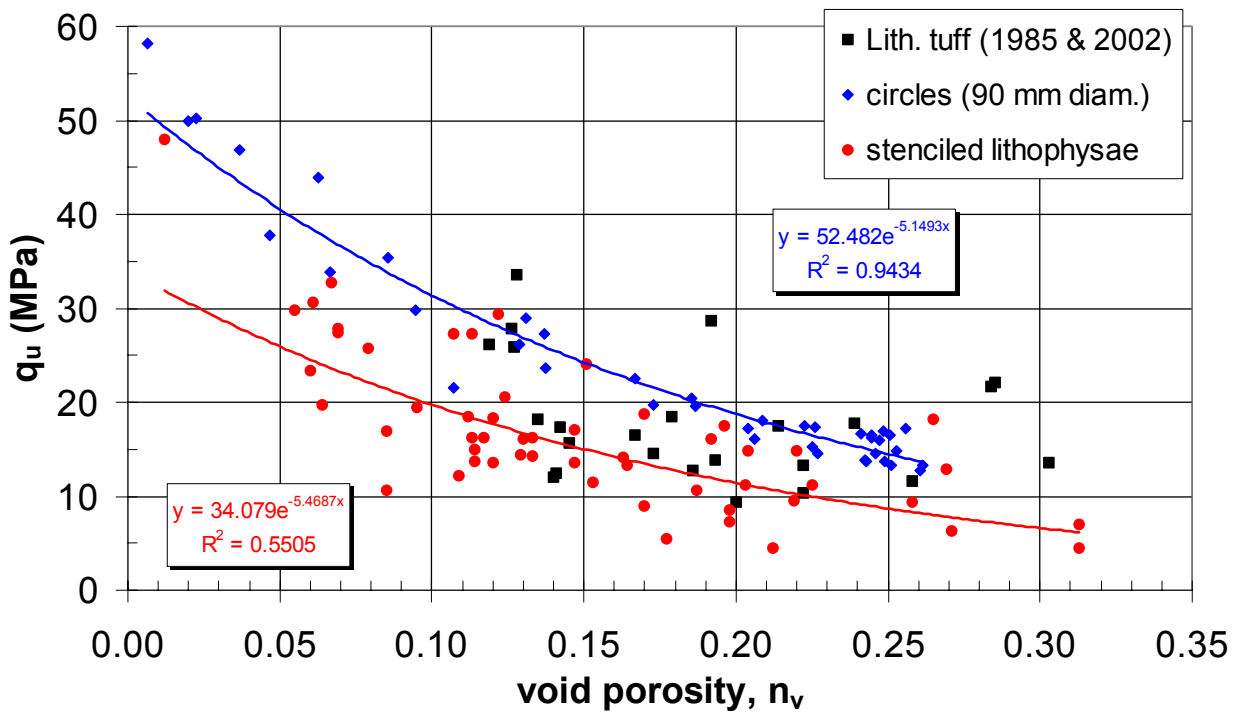
Source: BSC 2003 [DIRS 166660], Attachment V, Figure15. Tuff is from 267 and 290 mm diameter tests.

Figure 6.5-29. Uniaxial Compressive Strength (q_u)vs. Void Porosity (n_v) for Lithophysal Tuff and PFC2D Models of Randomly Distributed Circles and Stenciled Lithophysae
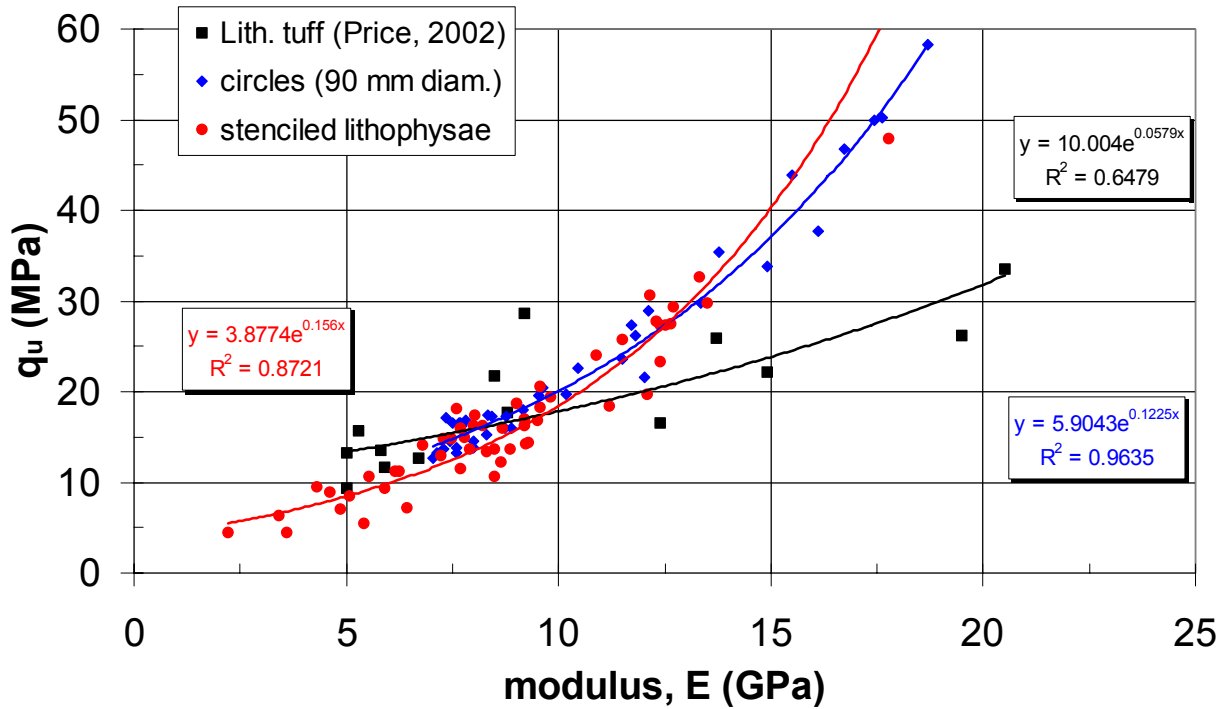
Source: BSC 2003 [DIRS 166660], Attachment V, Figure.17, p. V-17. Tuff is from 290 mm diameter tests.

Figure 6.5-30. Uniaxial Compressive Strength (q_u) vs. Young's Modulus (E) for Lithophysal Tuff and PFC2D Models of Randomly Distributed Circles and Stenciled Lithophysae
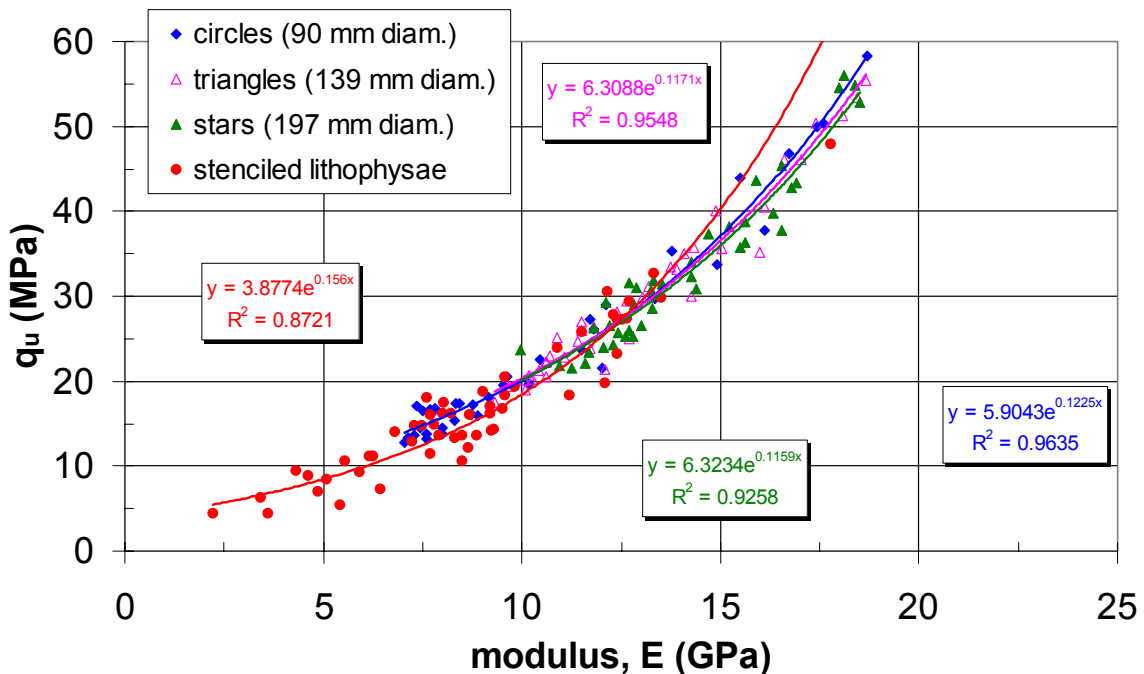
Source: BSC 2003 [DIRS 166660], Attachment V, Figure 18, p. V-18

Figure 6.5-31. Uniaxial Compressive Strength vs. Young's Modulus for PFC2D Models of Randomly Distributed Voids of Simple Shape and Stenciled Lithophysae

6.5.6   Confined Biaxial Behavior of Synthethic Lithophysal Material

The previous PFC calibration and analyses describe simulated compression tests on lithophysal rocks. As discussed earlier, triaxial laboratory experiments have not been conducted on actual representative lithophysal samples due to the size of the sample and the associated difficulties in obtaining pressure vessels and confining jacketing systems for samples with cavities.

An understanding of the confining pressure response is necessary for verification or determination of a proper yield criterion for the lithophysal rocks and understanding how the basic rock mass failure parameters (rock mass strength and dilatancy) are affected by lithophysal porosity. UDEC is the primary tool used for this purpose since the PFC model appears to lack the ability to realistically predict post–peak failure mechanisms due to a rotational degree of freedom in the circular particle model, which activates when the PFC particle bonds fail. As a result of these particle rotations need lithophysal holes, postpeak strength is underpredicted.

The confined and tensile properties of the synthetic materials are measured by performing polyaxial-cell and direct-tension tests; the equivalent Mohr-Coulomb and Hoek-Brown yield parameters are determined for the UDEC material. A series of uniaxial (extension and compression) and biaxial compression, as well as extensional experiments is conducted on the modeled samples, with circular lithophysal voids added randomly to create porosities of 10.3, 17.8 and 23.8 percent. Figures 6.5-32 to 6.5-35 show samples of the stress strain curves from each of the nominal lithophysal porosity groups.

The stress strain response for tensile testing and compression at a number of confining pressures are shown. Adjacent to each of the stress-strain curves is a figure of the sample (with displacement field in green and fracture indicators in red) in the failed state. From Figures 6.5-32 to 6.5-35 it is observed that the material becomes more ductile as the confining pressure is increased. The figures also show that failure occurs by fractures forming in the rock bridges between the voids. Rock failure results from fracturing between the voids in a similar fashion as that demonstrated previously for the PFC modeling. The general behavior is typical for brittle rock materials – increasing strength with confinement and conversion of the failure mode from axial splitting (unconfined) to shear failure as the confining pressure increases. The material response is elastic-brittle at low confinement and elastic-plastic at higher confining levels.

The numerical results showing the calculated properties from the uniaxial and biaxial tests on simulated lithophysal specimens are presented in Table 6.5-2. In the above series of numerical biaxial tests performed on the UDEC models (Figures 6.5-32 to 6.5-35), it was observed that, as the void porosity increases, the material becomes more ductile. This is a result of internal redistribution of loads during failure. The stiffest path through the sample will fail, and the load will transfer to another path.   It also is apparent from the data summary of Table 6.5-2 presented in Table 6.5-3 that, as the void porosity increases, the strength is reduced.   This strength reduction likely results because with larger or an increased number of voids there is less material to break through. These "material bridges" between voids tend to be loaded uniaxially (due to the absence of confining material), which also tends to reduce the compressive strength compared to material that is more confined. The overall strength reduction observed in the numerical tests occurs mainly as a drop in the cohesion component of the strength, and the internal angle of friction remains nearly constant (until the void porosity exceeds 17 percent).
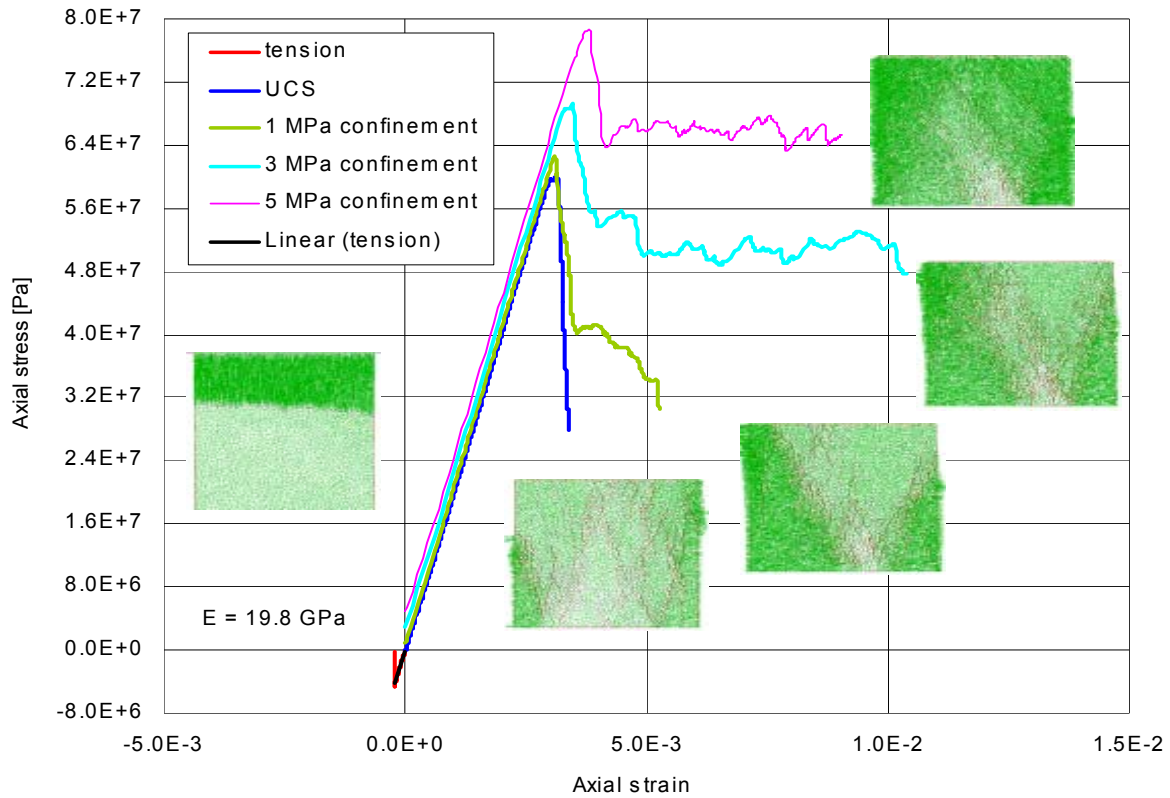
Source: BSC 2003 [DIRS 166660], Section 9.2.3, Figure 9-30, p. 9-33.

Figure 6.5-32. Stress-strain response and failure mechanisms for lithophysal porosity of 0.0%
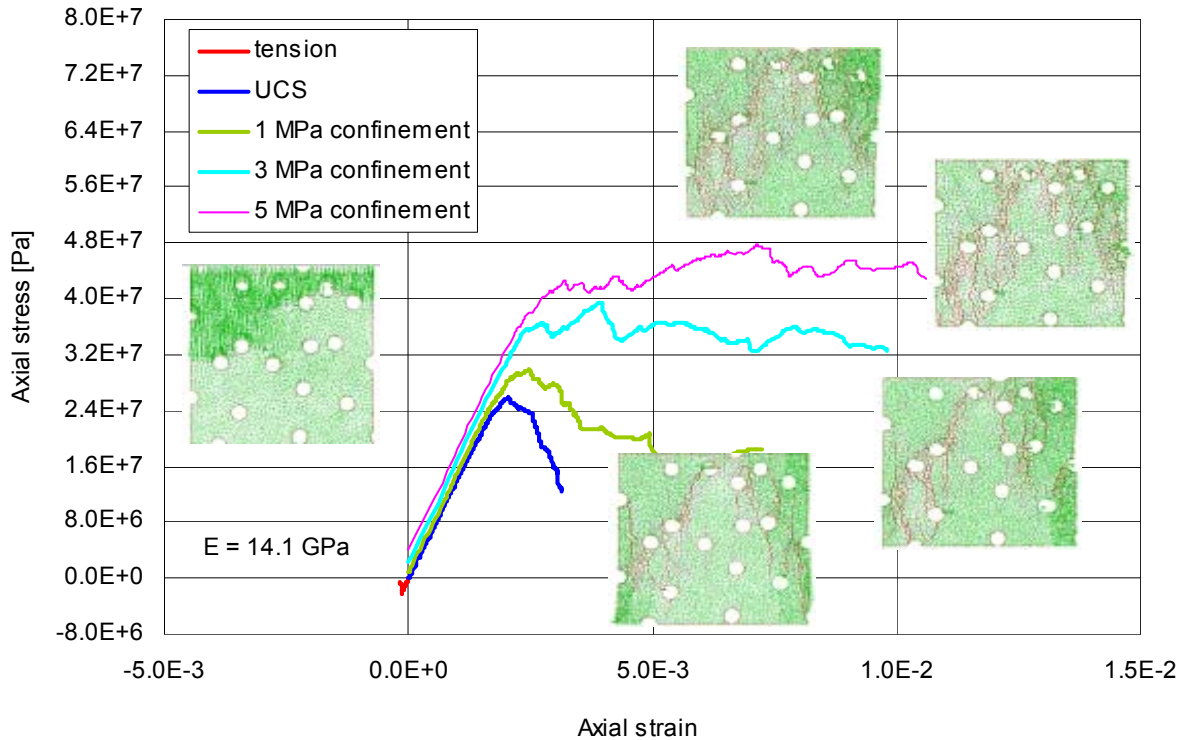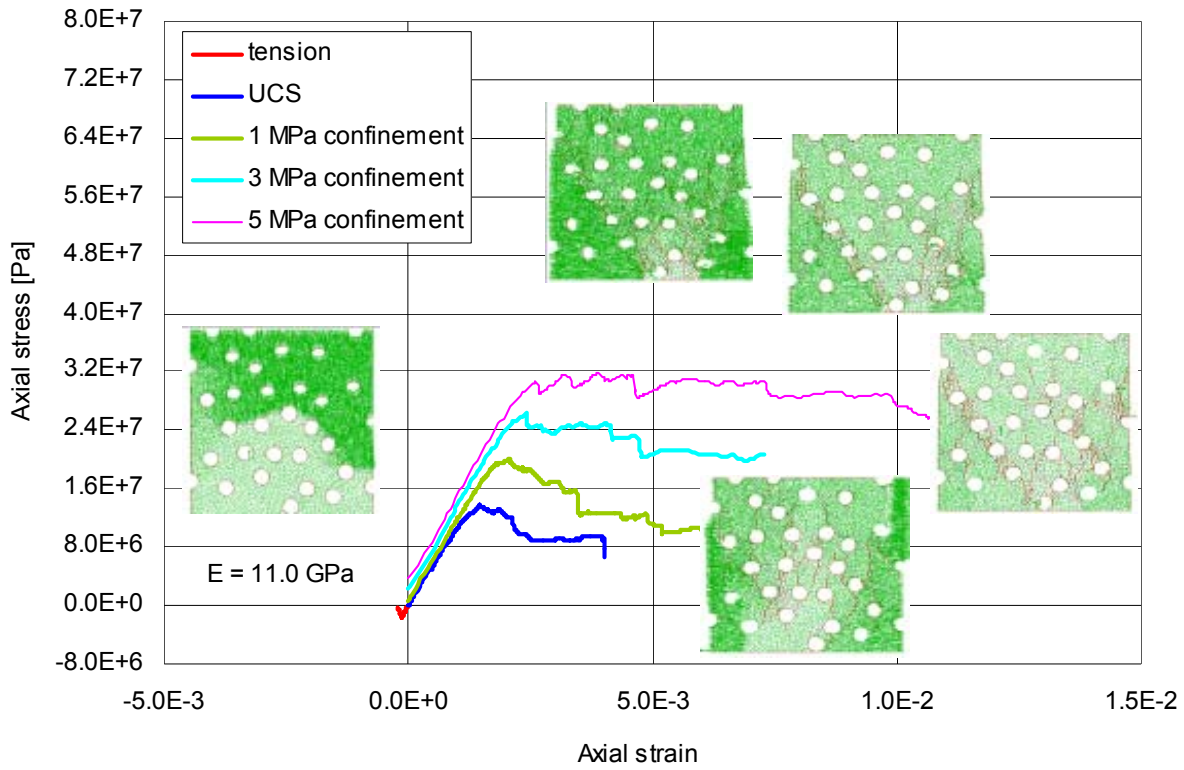

Source: BSC 2003 [DIRS 166660], Section 9.2.3, Figure 9-33, p. 9-37.

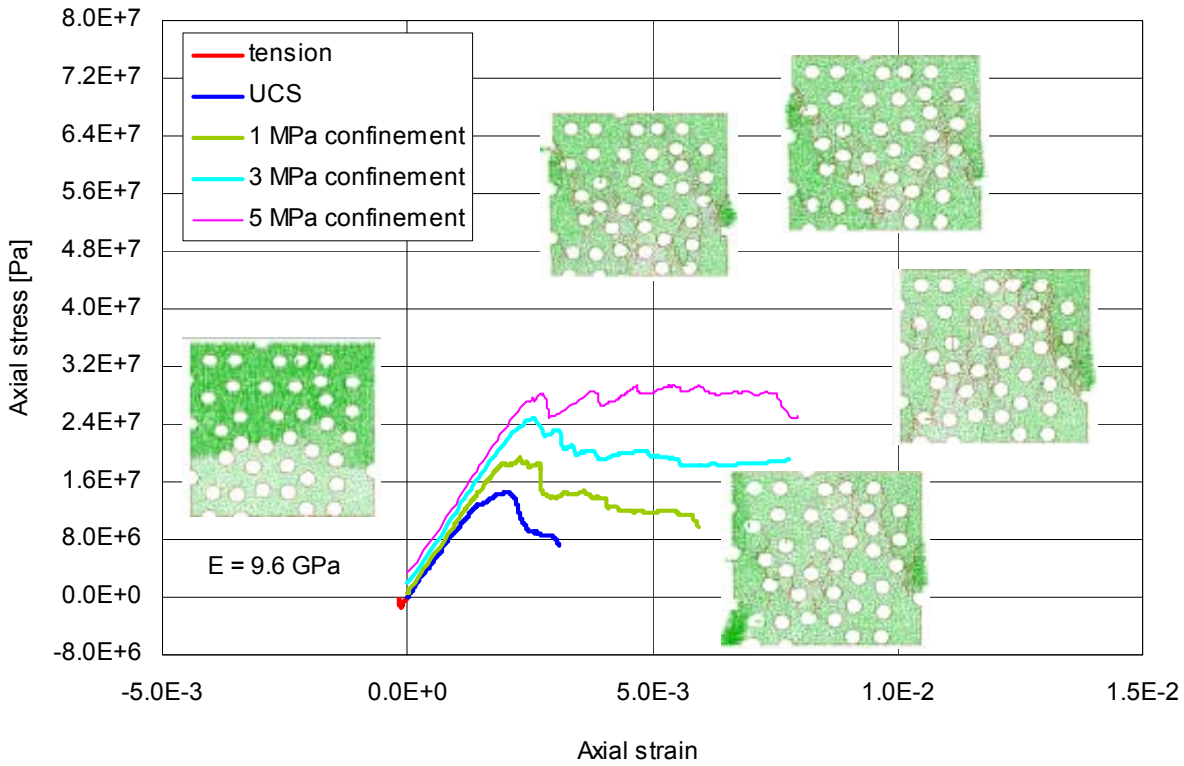Figure 6.5-33. Stress-strain response and failure mechanisms for lithophysal porosity of 10.3%

Source: BSC 2003 [DIRS 166660], Section 9.2.3, Figure 9-34, p. 9-37.

Figure 6.5-34. Stress-strain response and failure mechanisms for lithophysal porosity of 17.8%

Source: BSC 2003 [DIRS 166660], Section 9.2.3, Figure 9-35, p. 9-38.

Figure 6.5-35. Stress-strain response and failure mechanisms for lithophysal porosity of 23.8%

Table 6.5-2. Physical Property Results from UDEC Numerical Modeling on Simulated Lithophysal Tuff

Lith. Porosity (%)	Elasticity		Tensile Strength (MPa)	Compressive Strengths				Dilation			Mohr-Coulomb Strength Parameters		Hoek Brown Strength Parameters	
	E	ν		Confining Pressure (MPa)				Confining Pressure (MPa)			φ	c (MPa)	σ_{ci} (MPa)	m_i
				0	1	3	5	1	3	5				
0.000	19.8	0.16	4.66	60.1	62.7	69.3	78.7	48°	39°	35°	35°	15.6	59.1	6.2
0.000	19.9	0.16	4.86	59.7	63.4	71.9	78.1	55°	40°	34°	35°	15.4	59.7	6.1
0.000	19.8	0.17	3.91	58.7	62.5	70.5	78.4	49°	42°	36°	37°	14.8	58.4	6.7
0.000	19.8	0.16	4.52	59.9	64.2	72.2	79.0	52°	44°	37°	36°	15.3	60.1	6.3
0.000	19.8	0.16	4.26	55.1	60.1	69.2	76.5	45°	38°	32°	38°	13.3	55.4	7.5
0.103	14.1	0.19	2.11	25.8	30.0	39.5	47.8	42°	32°	27°	39°	6.1	25.2	9.4
0.101	14.3	0.19	1.96	24.4	29.1	33.3	39.8	35°	30°	14°	29°	7.1	24.9	4.6
0.101	14.7	0.18	2.17	28.0	33.0	40.0	48.0	37°	29°	22°	36°	7.1	28.1	7.4
0.101	14.3	0.22	2.16	25.7	32.5	41.4	47.0	38°	30°	29°	38°	6.3	27.0	8.1
0.105	14.1	0.17	2.09	23.8	28.7	34.7	42.3	40°	32°	28°	34°	6.3	23.9	6.7
0.107	13.9	0.18	1.95	21.2	27.0	35.5	40.0	39°	32°	29°	39°	5.0	21.2	9.9
0.103	14.2	0.19	2.09	26.5	29.9	37.0	46.0	37°	38°	25°	36°	6.7	25.6	7.6
0.178	11.0	0.20	1.70	13.7	20.1	26.4	32.0	40°	30°	25°	34°	3.7	15.0	6.9
0.176	11.1	0.19	1.84	16.6	22.6	29.8	35.0	39°	28°	26°	35°	4.4	17.7	7.0
0.171	11.5	0.19	1.74	16.5	22.2	28.9	32.1	35°	29°	25°	31°	4.7	18.1	5.1
0.158	11.8	0.18	1.89	16.0	23.0	31.3	38.7	39°	27°	22°	39°	3.8	16.8	10.3
0.168	11.1	0.19	1.72	15.0	21.4	26.7	31.2	36°	25°	21°	31°	4.3	16.6	5.2
0.173	11.3	0.18	1.62	14.9	20.5	28.5	35.7	34°	27°	21°	37°	3.7	15.1	9.5
0.178	10.6	0.23	1.65	16.0	21.1	28.1	34.6	35°	26°	27°	35°	4.2	16.3	7.4
0.238	9.6	0.21	1.52	14.6	19.4	25.0	29.4	35°	29°	23°	29°	4.3	15.5	4.8
0.254	8.6	0.19	1.46	11.1	15.9	20.9	24.6	35°	19°	13°	27°	3.4	12.2	4.2
0.237	9.7	0.17	1.62	13.2	17.8	24.1	29.0	32°	19°	15°	31°	3.7	13.8	5.8
0.251	9.0	0.18	1.52	13.0	17.0	24.7	29.3	37°	24°	18°	32°	3.6	13.3	6.5
0.240	9.1	0.20	1.55	12.6	17.1	21.7	27.7	30°	27°	18°	29°	3.7	13.0	5.2
0.243	9.2	0.19	1.53	12.5	18.5	23.0	28.0	37°	27°	21°	29°	3.7	13.9	4.9
0.238	9.6	0.19	1.55	15.2	20.0	25.5	28.7	34°	21°	15°	27°	4.7	16.4	3.9

Source: Appendix B, Microsoft Excel file "summary2_newest.xls," Worksheet "UDEC"

Table 6.5-3. Summary of Average Compressive Strength, Young's Modulus, Mohr-Coulomb, and Hoek-Brown Failure Law Parameters Derived from UDEC Simulations

Lithophysal Porosity (%)	UCS (MPa)	Young's Modulus (GPa)	Friction Angle (degree)	Cohesion (MPa)	Tensile Strength (MPa)	Hoek Brown σ_{ci} (MPa)	Hoek Brown m_i
0	58.7	19.8	36	14.9	4.4	58.5	6.6
10	25.1	14.2	36	6.4	2.1	25.1	7.7
17	15.5	11.2	35	4.1	1.7	16.5	7.3
24	13.2	9.3	29	3.9	1.5	14.0	5.0

Source: BSC 2003 [DIRS 166660], Section 9.2.4, Table 9-3, p. 9-42.

The synthetic lithophysal tuff clearly exhibits large dilation angles for uniaxial compressive testing. Such behavior is expected because micro damage of the material during uniaxial compressive strength testing is predominantly tensile fracturing, which results in large amount of dilation. Figure 6.5-36 and Table 6.5-4 shows the effect of increasing lithophysal porosity on the dilation angle. As the void porosity increases, the dilation angle decreases. The presence of the lithophysae allows some of the yield dilation to be accommodated internally. This reduces the expansion that is measured on the external boundaries. The dilation angle also decreases with increasing confining pressure. This is due to the greater lateral restraint.

The following general observations can be made from the numerical tests:

- Reduction of peak compressive strength with increased lithophysal porosity

- Reduction of Young's modulus with increased lithophysal porosity

- Less brittle postpeak response, leading to elastic-plastic response for the higher confining pressures

- Reduction in tensile strength with increased lithophysal porosity.

Table 6.5-4. UDEC Simulation Summary of Dilation Angles for Various Confining Pressures

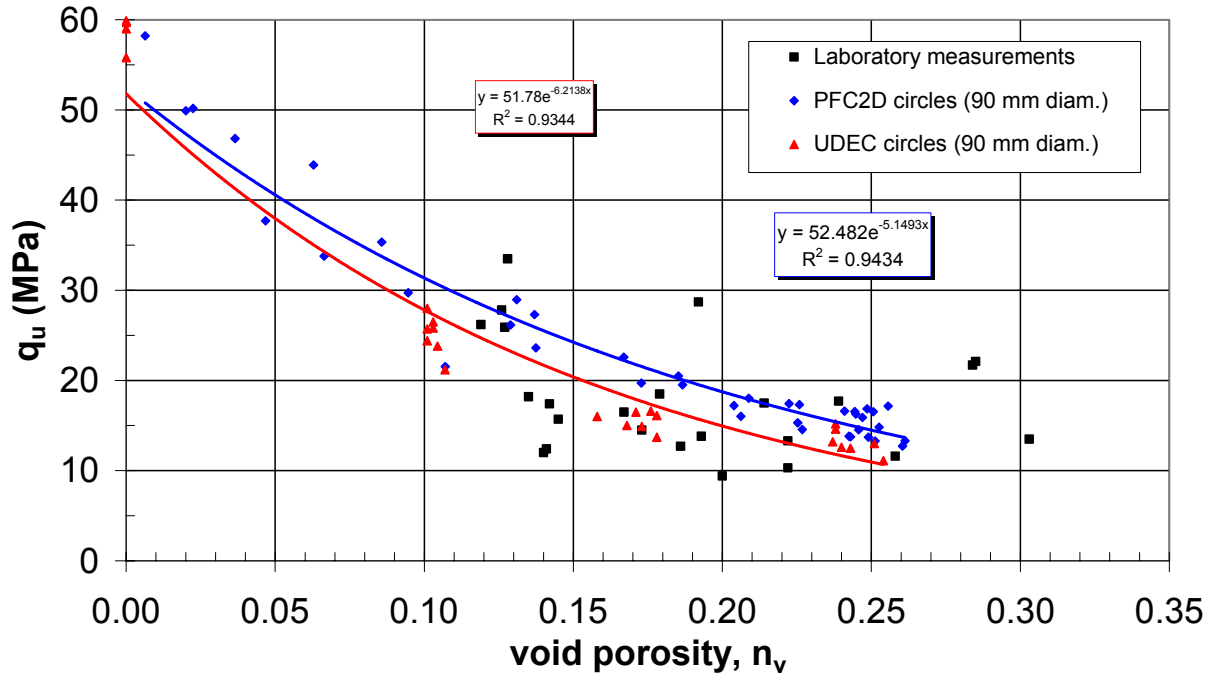| Lithophysal Porosity	Dilation (degrees)		
	1 MPa	3 MPa	5 MPa
0%	50°	41°	35°
10%	38°	32°	25°
17%	37°	27°	24°
24%	34°	24°	18°

Source: Computed from Table 6.5-2 data in Appendix B, Microsoft Excel file "summary2_newest.xls," Worksheet "UDEC"
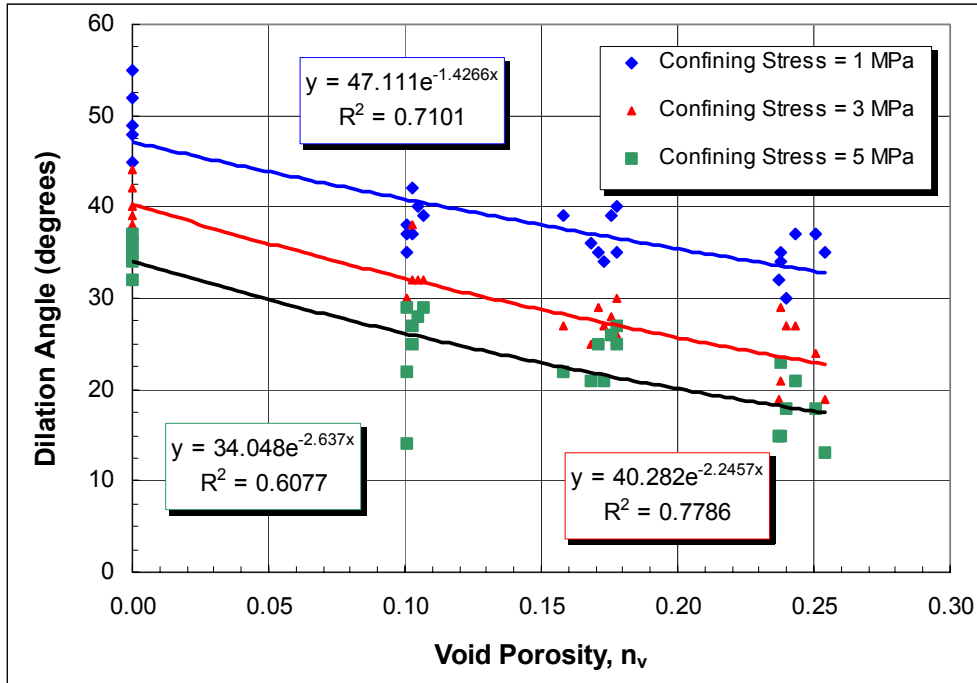
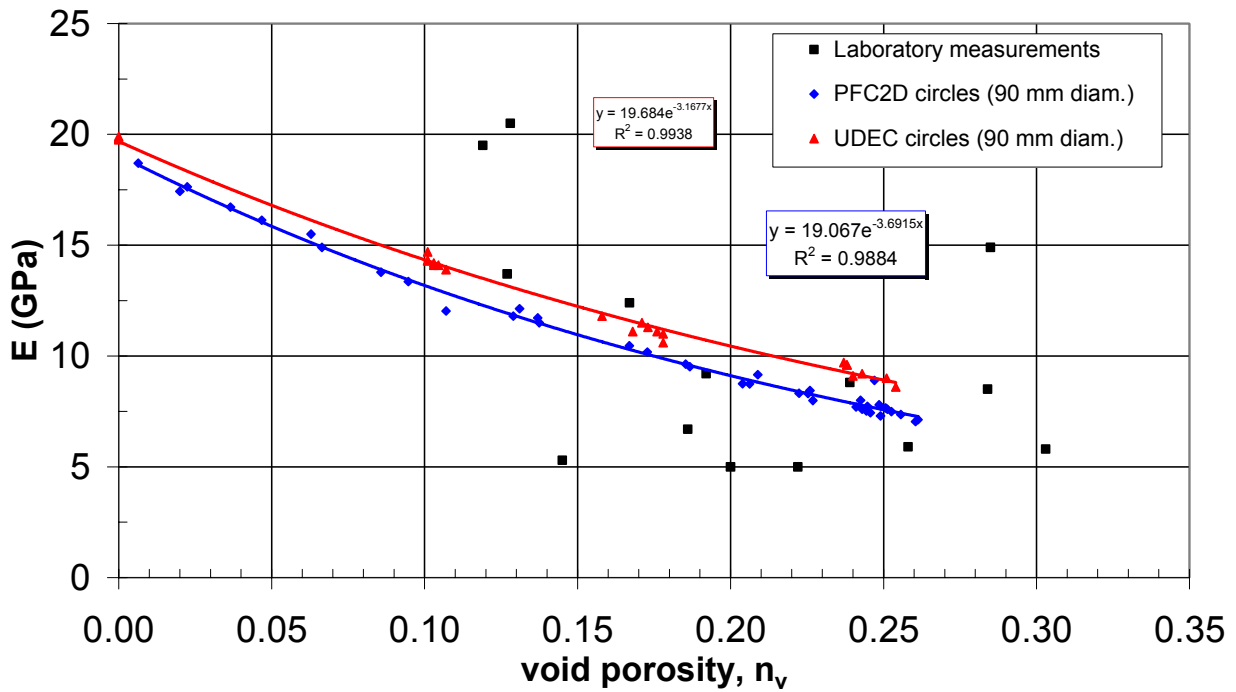Source: BSC 2003 [DIRS 166660], Section 9.2.3, Figure 9-39, p. 9-40.

Figure 6.5-36. Dilation Angles Versus Void Porosity at Various Confining Stresses from UDEC
Simulations for Lithophysal Tuff

The relationships of uniaxial compressive strength and Young's modulus to lithophysal porosity
are shown in Figures 6.5-37 and 6.5-38 respectively, indicating good agreement with laboratory
compression tests on large diameter (0.27 to 0.29 m/10.5 to 11.5 in.) cores samples of lithophysal
tuff. The correlation of uniaxial compressive strength and Young's modulus is shown in Figure
6.5-39. The UDEC results shown are in good agreement with the PFC simulations, but give
higher uniaxial compressive strength values than the laboratory test data, especially when the
void porosity is low (Young's modulus greater than 15 MPa). This is because the UDEC model
was calibrated for the zero percent porosity case with a uniaxial compressive strength of 60 MPa
and a Young's modulus of 20 GPa. A recalibration of the UDEC model may allow a better fit to
the laboratory UCS versus Young's modulus data, but the resulting fits to plots of laboratory
UCS and Young's modulus with lithophysal porosity may worsen.

Source: BSC 2003 [DIRS 166660], Section 9.2.3, Figure 9-36, p. 9-39.

Figure 6.5-37. Comparison of UDEC Simulations of Lithophysal Porosity Effects on Uniaxial Compressive Strength (q_u) to Laboratory Measurements on Large Samples and to PFC Simulations

Source: BSC 2003 [DIRS 166660], Section 9.2.3, Figure 9-37, p. 9-39.

Figure 6.5-38. Comparison of UDEC Simulations of Lithophysal Porosity Effects on Young's Modulus (E) to Laboratory Measurements on Large Samples and to PFC Simulations
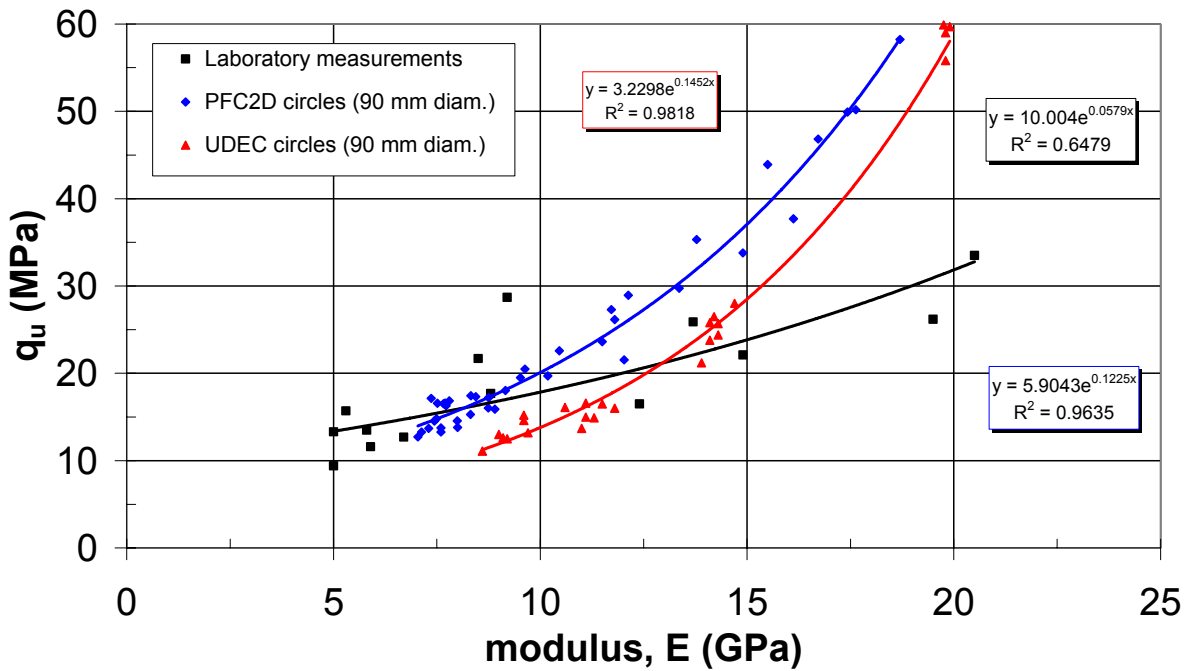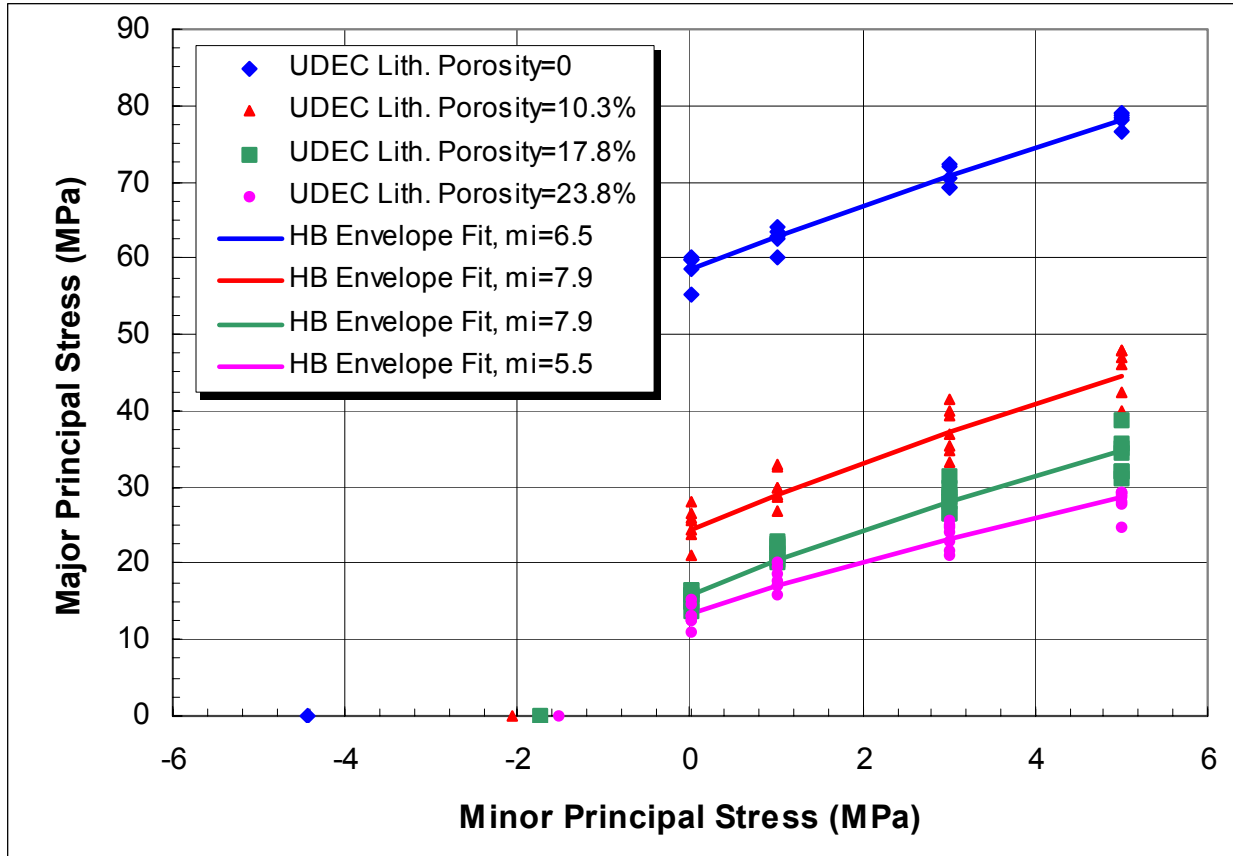
Source: BSC 2003 [DIRS 166660], Section 9.2.3, Figure 9-38, p. 9-40.

Figure 6.5-39. Comparison of UDEC Simulations of Uniaxial Compressive Strength (q_u) vs. Young's Modulus (E) to Laboratory Measurements on Large Samples and to PFC Simulations

6.5.7 Estimation of Linear and Nonlinear Failure Envelopes

The *UDEC* peak strength values from the results shown in Figures 6.5-32 to 6.5-35 can be used to construct traditional failure envelopes for the lithophysal samples. Figure 6.5-40 shows the failure stress values plotted in principal stress space with Hoek-Brown envelopes fit to the results (Hoek 2000 [DIRS 160705], p. 179). In each case, multiple simulations were made for each confining stress level in which different random distributions of *UDEC* block structures and void placements were used. The Mohr-Coulomb and Hoek-Brown strength parameters derived from the fits to this data are given in Table 6.5-5.

As seen in Figure 6.5-40, the primary effect of increasing lithophysal porosity is a significant reduction in the compressive and tensile strength components, with minor strength reduction when the lithophysal porosity is raised above 17.8 percent. The value of cohesion behaves in a similar way. There is little apparent impact of lithophysal porosity on peak friction angle until porosity exceeds 20 percent.

Source: BSC 2003 [DIRS 166660], Section 9.2.4, Figure 9-40, p. 9-41.

Figure 6.5-40. Major Principal Stress Versus Minor Principal Stress from UDEC Simulations as well as Hoek-Brown Non-Linear Failure Envelope Fits for Various Lithophysal Porosities

Table 6.5-5. Average UCS, Young's Modulus, Mohr-Coulomb (Linear) Parameters, and Hoek-Brown (Nonlinear) Parameters from UDEC Biaxial Test Simulations of Lithophysal Tuff

Lithophysal Porosity (%)	Estimated UCS (MPa)	Estimated Young's Modulus (GPa)	Estimated Friction Angle (deg)	Estimated Cohesion (MPa)	Estimated Hoek-Brown UCS (MPa)	Estimated Hoek-Brown m_i
0	58.7	19.8	36	14.9	58.5	6.6
10	25.1	14.2	36	6.4	25.1	7.7
17	15.5	11.2	35	4.1	16.5	7.3
24	13.2	9.3	29	3.9	14.0	5.0

Source: BSC 2003 [DIRS 166660], Table 9-3, p. 9-42.

The values of UDEC simulated friction angle and cohesion determined in Table 6.5-5 can be compared to similar determinations made for laboratory triaxial tests on small (51 mm and less) diameter rock specimens. Tptpul rock tests (saturated, room temperature) yielded 60 degrees and 7.5 MPa for friction and cohesion, while Tptpll rock tests (saturated, room temperature) resulted in 50 degrees and 21 MPa (BSC 2003 [DIRS 166660], Table 8-40, p. 8-123). The laboratory values are indicative of a stronger strength envelope than the simulated rock strength envelope using the 0 percent lithophysal porosity case (values of 36 degrees and 14.9 MPa), which is expected since small laboratory specimens are biased toward nonlithophysal rock samples (Section 6.3.1). The Hoek-Brown Geologic Strength Index (GSI), based on geotechnical characterization indices such as Barton's Q index and Bieniawski's rock mass rating (RMR), is often used for estimation of equivalent Mohr-Coulomb linear strength parameters (cohesion and friction angle) or Hoek-Brown nonlinear strength properties (material constants m and s). The Mohr-Coulomb and Hoek-Brown strength properties are typically used as input to numerical models in which the rock mass mechanical constitutive model is based on these failure laws. A great deal of literature and case examples exist, in which these models have been compared to deformation measurements in a wide variety of rock types and rock qualities. Although little experience in tunneling in lithophysal tuff is available, it is instructive to use the results of the UDEC simulations to estimate, from the Hoek-Brown strength parameters, the approximately equivalent values of GSI as a function of lithophysal porosity.

To perform such an estimate, the 0 percent lithophysal porosity case discussed above is assumed to represent the rock matrix, and the cases of 10.3, 17.8, and 23.8 percent lithophysal porosity are considered to be 'degraded' quality rock in the same sense as fracturing is used in the typical case as a means of degrading intact rock strength. Using Hoek's empirically derived relation for rock mass modulus, E_m, based on GSI (e.g., Hoek et al. 2002 [DIRS 162204], Eq. 11a):

$$E_m(GPa) = \left(1 - \frac{D}{2}\right)\left(\frac{\sigma_{ci}}{100}\right)^{0.5} \times 10^{[(GSI-10)/40]}$$

(6-12)

Where D is a rock mass disturbance index, which in this case we set to zero, and solving for GSI we get:

$$GSI = 10 + \left(\frac{40}{\ln 10}\right)\left[\ln E_m - 0.5\ln\left(\frac{\sigma_{ci}}{100}\right)\right]$$

(6-13)

Using Eq. 6-13 with σ_{ci} (58.7 MPa) for 0 percent porosity and the moduli from Table 6.5-5 we find the relation between GSI and porosity as shown in Table 6.5-6.

Table 6.5-6. Relationship Between GSI and Porosity

Porosity (%)	GSI
10	61
17	57
24	53

This relationship, also shown in Figure 6.5-41, is preliminary in nature and is given simply to illustrate the possible impact of lithophysal porosity in terms of the typical rock mass characterization parameters used in industrial practice.
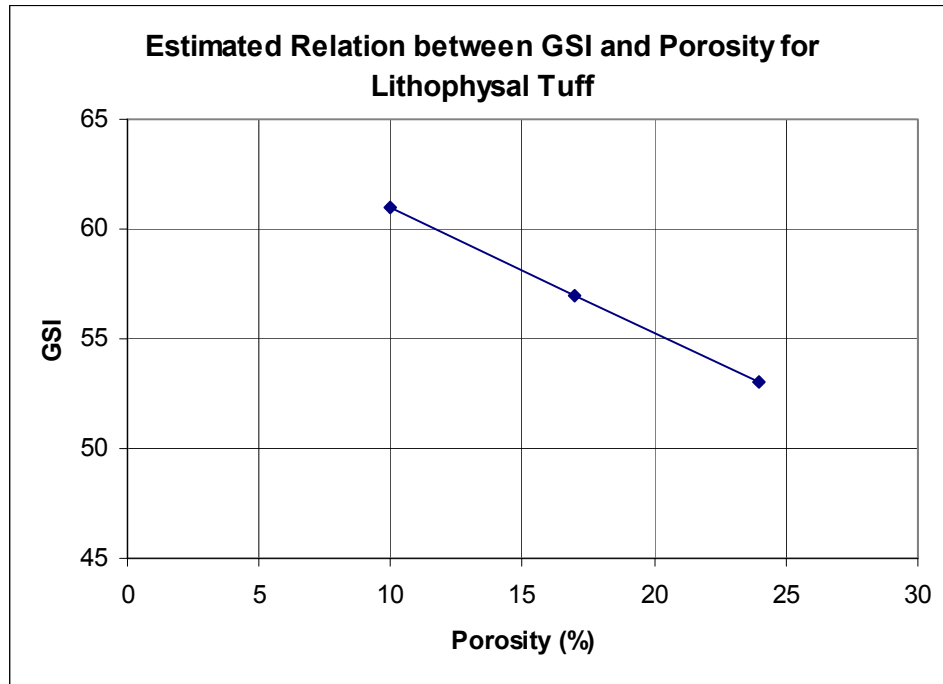
Source: BSC 2003 [DIRS 166660], Section 9.2.5, Figure 9-41, p. 9-43.

Figure 6.5-41. Estimated Relationship Between GSI and Porosity for Lithophysal Tuff

6.5.8 Limitations and Uncertainty Analysis of the Numerical Modeling

The following limitations are inherent in the PFC modeling study and are summarized and described as follows:

- Both the panel maps and the PFC2D analyses are two-dimensional slices, whereas the true lithophysal geometries are three-dimensional. An assessment should be made of the limitations of this two-dimensional approach. It is a straightforward process to map true lithophysal geometries into the PFC3D model; however, current computing capabilities make it impractical to run PFC3D models of sufficient resolution to resolve the voids adequately. Such computational limitations are being addressed in the development of a scheme called AC/DC (Adaptive Continuum/DisContinuum), which supports parallel processing and replaces elastic regions remote from cracks by a continuum formulation, represented by a linear matrix, thus achieving economies in computation time. It may be possible to simulate true lithophysal geometries in PFC3D models using the AC/DC methodology.

- The void geometries from the panel maps (on the scale of a meter) may not be representative of the laboratory specimens (on the scale of a foot). The effect of specimen size on material properties has not been addressed in this work. PFC2D modeling of the slot tests is expected to give a better understanding of such scaling issues.

- The PFC material does not contain fractures already present in the matrix material of some of the lithophysal tuff. The effect of such fractures could be added in a smeared sense by reducing the stiffness and strength of the PFC base material or in a direct sense by adding discrete fractures to the PFC material between the voids. Such discrete fractures could take the form of reduced strength and stiffness of the particles and bonds lying within a specified thickness of each fracture surface.

- The effect of rims, spots and lithic clasts on the material properties are not accounted for directly by the PFC model, because it only provides a base material to which voids can be added. One could define additional regions for rims, spots and lithic clasts and assign them appropriate stiffnesses and strengths; however, these properties are not available at present.

The following uncertainties and limitations are inherent in the UDEC modeling study.

- The effect of lithophysal cavity shape and size on lithophysal rock properties has not been addressed in this study. In the current study, the shape of cavity is circular and the size is fixed at 0.09 m. In reality, both the shape and the size vary with location. These may be important non-conservative factors that affect lithophysal rock properties and contribute to its behavior.

- The *UDEC* analyses are two-dimensional, whereas the true lithophysal cavities are three-dimensional. The two-dimensional plane-strain models with their infinitely long voids may underestimate compressive strength values, since the third dimension is not available for support and stress redistribution. This aspect of the two-dimensional *UDEC* analyses should be considered conservative.

- The effect of specimen size on lithophysal rock properties has not been addressed in this study. The specimen size of 1 m × 1 m used is small compared to that of a representative volume appropriate for modeling a repository drift. This may or may not affect the derived lithophysal rock Young's modulus and compressive strength properties.

- Preexisting fractures in the matrix material of lithophysal rock are not accounted for directly by the *UDEC* model. The effect of such fractures may be included in a smeared sense by reducing the contact stiffness and strength between interconnected particles.

- Comparisons of the *UDEC* simulations are made to actual large-core laboratory tests under uniaxial compressive loading conditions only. Though the two-dimensional *UDEC* models were used to simulate triaxial compressive tests, no comparisons have been made due to the lack of actual triaxial test data on rock specimens with typical-sized lithophysae. The small diameter laboratory test results (limited lithophysal porosity) give higher UCS values and strength envelopes than predictions from UDEC biaxial simulations of lithophysal tuff. This is likely because smaller samples are biased by containing fewer rims, spots, and fractures (the presence of these structural weaknesses

are more likely to result in unusable broken cores); furthermore, calibration against large-core samples with these rock features resulted in synthetic matrix properties with lower mean modulus and strength values than those exhibited by actual small-diameter intact rock samples.

- The current *UDEC* study uses the average large-core laboratory values of Young's modulus and uniaxial compressive strength to calibrate the *UDEC* base-case models and does not account for the effect of variations across lithophysal rock mass categories or rock condition. The derived lithophysal properties may be sensitive to these variations. Additional analysis on this sensitivity is considered valuable for further understanding the effect of lithophysal porosity on rock mass properties.

6.5.9 Summary and Conclusions Relative to Lithophysal Rock Behavior

The PFC model has been calibrated against the laboratory testing data discussed above. Numerical compressive strength experiments were conducted first for zero-void welded tuff to derive strength properties of the matrix (Figure 6.5-6). In subsequent analyses, simple uniformly distributed circular (and later triangular) holes were added to the model, and the relationship between laboratory-derived strengths, modulus, and porosity was examined. The modeling results showed good agreement with laboratory data (Figures 6.5-7 to 6.5-9), although the modeling could be improved with a new calibration to the laboratory data. Results indicated that the primary strength-decreasing effect of the lithophysae is due to initiation and propagation of tensile splitting between lithophysae under compressive load. As porosity increases, the spacing between lithophysae decreases, and rock acquires a greater propensity for tensile splitting at the lower applied stresses.

Further PFC numerical testing was performed during which lithophysal panel maps (Figures 6.2-4 and 6.5-23) were discretized and used as 1.0×1.0 m compressive test specimens (Figures 6.5-26 and 6.5-6) for the model. As shown in Figures 6.5-28 and 6.5-29, the simple models containing circular holes display less variability in results than similar analyses that utilize actual lithophysae shapes. Actual shapes result in greater variability in test results (particularly at low porosities) and a lower estimate of mean compressive strength and Young's modulus.

Variability in the rock response and size effect appears to be a function primarily of the distribution of the lithophysae (i.e., percentage porosity and how evenly distributed it is through the rock mass), and, to a lesser extent, the deviation of the shape of true voids from circular voids. The property scatter apparent at given values of lithophysal porosity reduces significantly when the data are plotted in terms of uniaxial compressive strength versus Young's modulus, suggesting that this correlation is independent of void geometry.

Approximately 80 simulated uniaxial compression tests of actual lithophysae distributions were modeled, and the results in terms of UCS and Young's Modulus as functions of the lithophysal porosity and UCS versus Young's Modulus were discussed in Section 6.5.5 (Figures 6.5-28 to 6.5-31). The introduction of actual (from tunnel mapping) lithophysae shapes and distributions has two distinct effects compared to using circular voids:

1. The actual lithophysae shapes and distributions introduce significant variability into the uniaxial compressive strength or Young's modulus for a given porosity. This variability is a function of the distribution of solid bridge length between lithophysae that is, in turn, a function of the porosity and nature of the distribution of that porosity.

2. The actual lithophysae shapes and distributions appear to provide a lower bound to the uniaxial compressive strength and Young's modulus to that given by the circular lithophysae shapes and to the laboratory data.

Standard forms of yield conditions for rock masses – Mohr-Coulomb and Hoek-Brown – were fit to the laboratory and model extrapolation data, and their standard strength parameters were determined. The best-fit Hoek-Brown envelopes for the UDEC lithophysal rock simulations yield strength envelopes that are weaker than those derived from laboratory tests on Topopah Spring small-diameter lithophysal rock specimens. Again, this is likely an artifact of the bias against rims, spots, and fractures in actual small-diameter specimens.

The conclusion drawn from the PFC and UDEC modeling is that this approach provides a viable methodology for simulating the mechanical response of lithophysal welded tuff to stressing and that this tool can be used to study variability in material response in addition to laboratory and field testing. These numerical results will be added to the bounding analyses in the next section.

The introduction of voids within rock produces a distinctly different mechanical failure mechanism from that active in nonlithophysal rock. Both the PFC (Figures 6.5-6 and 6.5-20 to 6.5-22) and UDEC (Figures 6.5-32 to 6.5-35) modeling approaches predict a traditional shear-plane failure response with zero or one void. With the presence of only a few voids the uniaxial compressive strength experiences a significant drop from the nonlithophysal case and micro-fractures in the rock matrix are observed to coalesce and form observable inter-lithophysal macro-fractures. In such instances the lithophysae and fracturing tend to produce nonuniform stresses within the sample, isolating portions of the rock that support most of the applied vertical load. With increasing load and shear strains a network of inter-lithophysal fractures and patterns is developed, which is more pervasive when there are many lithophysae. The failure patterns most commonly observed are groups of more or less vertical tensile macro-fractures, but shear macro-fractures are also common connecting lithophysae. This failure mechanism is consistent with observations of lithophysal rock fracturing observed in the underground (Sections 5.4, 6.1, and 6.2), and laboratory tests of actual large-core samples (Section 6.3.2).

6.6 UPDATED LITHOPHYSAL ROCK MASS MECHANICAL PARAMETERS AND BOUNDING ANALYSIS

The development of rock mass mechanical behavior and estimate of property ranges for the lithophysal rock is based on actual tests on lithophysal rock and is described in Section 6.4. The laboratory-based property summary is then supplemented by numerical model extrapolation using the PFC and UDEC discontinuum programs. As discussed earlier, numerical modeling of lithophysal rock is a valuable tool in light of the sparse laboratory-testing database, limited in both number of specimens tested and the available porosity range and size of specimens. This integration of the laboratory data with the computational property variability estimates form the basis of the predicted range of strengths and moduli that represent the rock mass properties in the ECRB Cross-Drift and, especially, the Tptpll. The general strategy is illustrated in Figure 1-5.

The approach to use numerical modeling data has two steps. First, the PFC and UDEC numerical model predictions are compared against the existing laboratory compression data, where it is demonstrated specifically that a detailed understanding of the basic physical mechanisms of the rock mass behavior can be obtained without resorting to empiricism or complex constitutive modeling. Next, the model is used to extend the laboratory data by conducting numerical experiments on simulated samples of lithophysal tuff at various physical conditions of porosity, lithophysae shape and distribution, as well as various levels of confinement and applied stress. The outcomes of the modeling are potential added confidence in the estimates of the range of rock mass strength and stiffness for varying conditions of lithophysal porosity, size, shape, and distribution. Additionally, the results provide a means of understanding the size-scaling and variability issues introduced by lithophysae shape and distribution and their impact on rock mass properties and failure criteria.

The numerical laboratory testing of lithophysal rock was presented in Section 6.5. These simulated tests were performed with three sophisticated discontinuum programs (PFD2D, PFC3D, and UDEC), and involved the study of actual (from tunnel lithophysal mapping) geometries of lithophysal cavities. The numerical results are added to the 267 and 290 mm (10.5-in and 11.5-in) diameter large-core laboratory test data in the next section to see how well the numerically derived test results fit the rock mass categories and bounding estimates.

### 6.6.1 Numerical Mechanical Property Bounding Analysis

The PFC and UDEC simulated uniaxial compression test results are superimposed on the previous figures (Figures 6.4.2 to 6.4-4) of laboratory UCS versus Young's Modulus and bounding estimates in Figures 6.6-1 to 6.6-3). As seen in these plots, the results of the calibrated PFC simple shape-studies, simulations of the ECRB Cross-Drift panel map specimens, and UDEC simulations are overlaid on the large-core 267 and 290 mm (10.5-in 11.5-in) diameter laboratory data. The previously estimated upper and lower strength bounds are also given on the plots. As can be seen, the upper and lower bounds encompass the laboratory and numerical data with the exception of the highest values of numerically predicted uniaxial compressive strength and Young's modulus as shown in Figure 6.6-3.
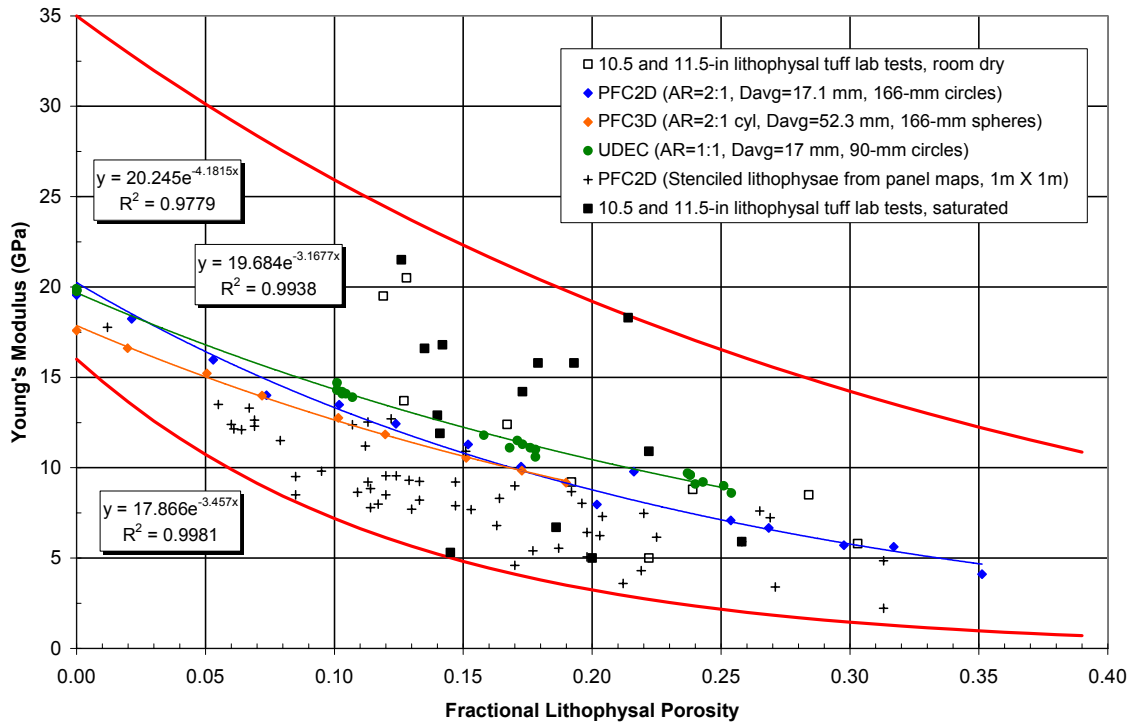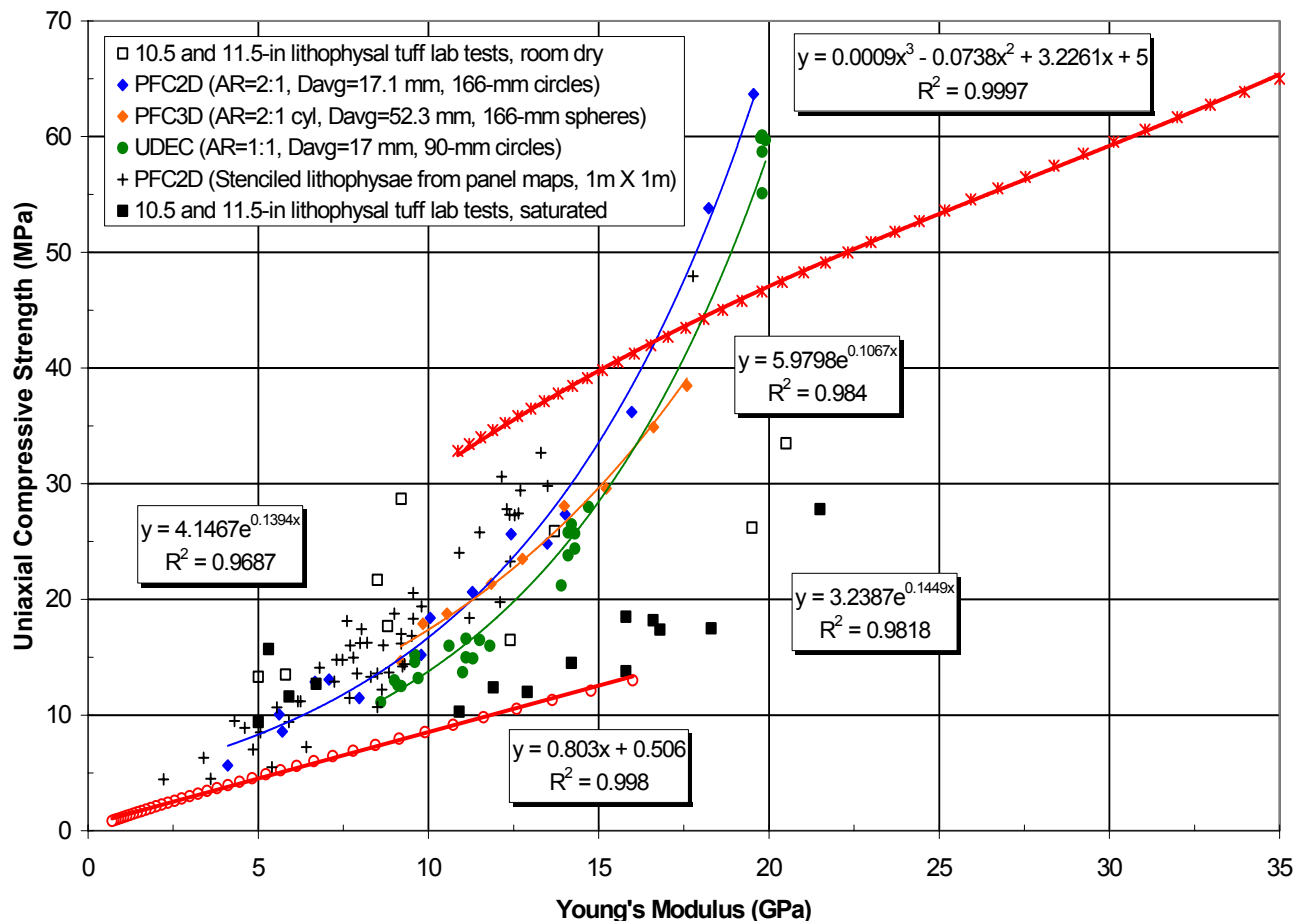
Source: Appendix B, Microsoft Excel file "LithophysalRockRanges_Calc.xls," Worksheet "E-por"

Figure 6.6-1. Upper and Lower Bounds of the Young's Modulus versus Lithophysal Porosity Relationship for 10.5 and 11.5-in Diameter Cores and Simulated Numerical Test Results
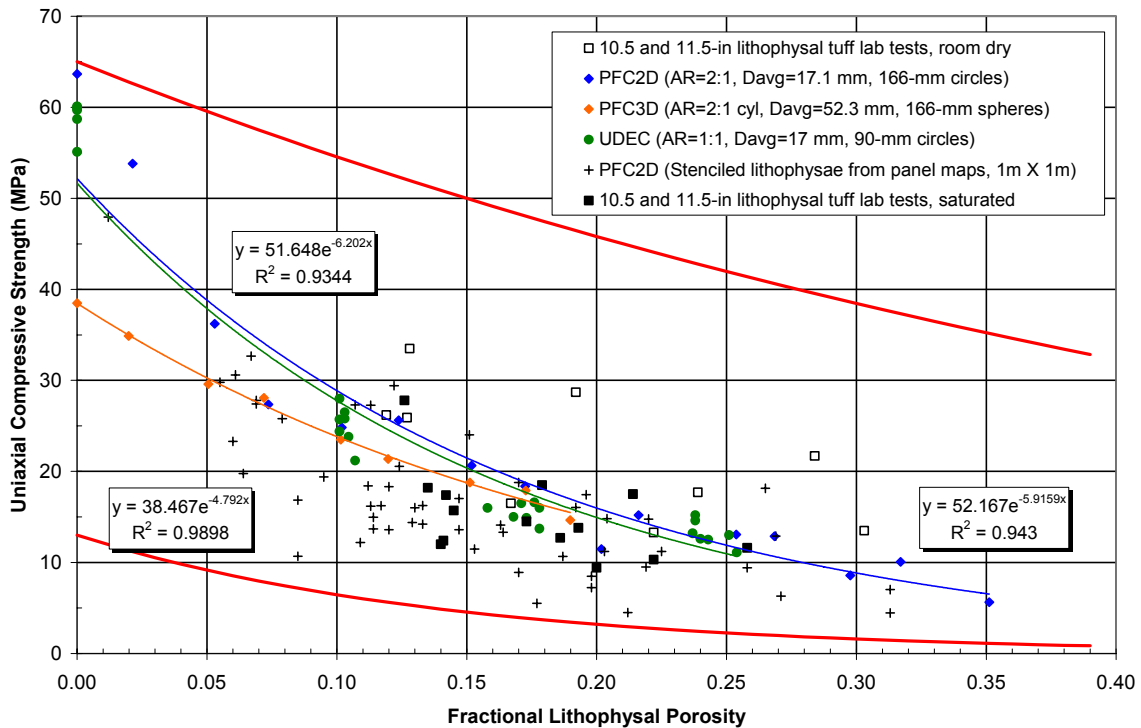
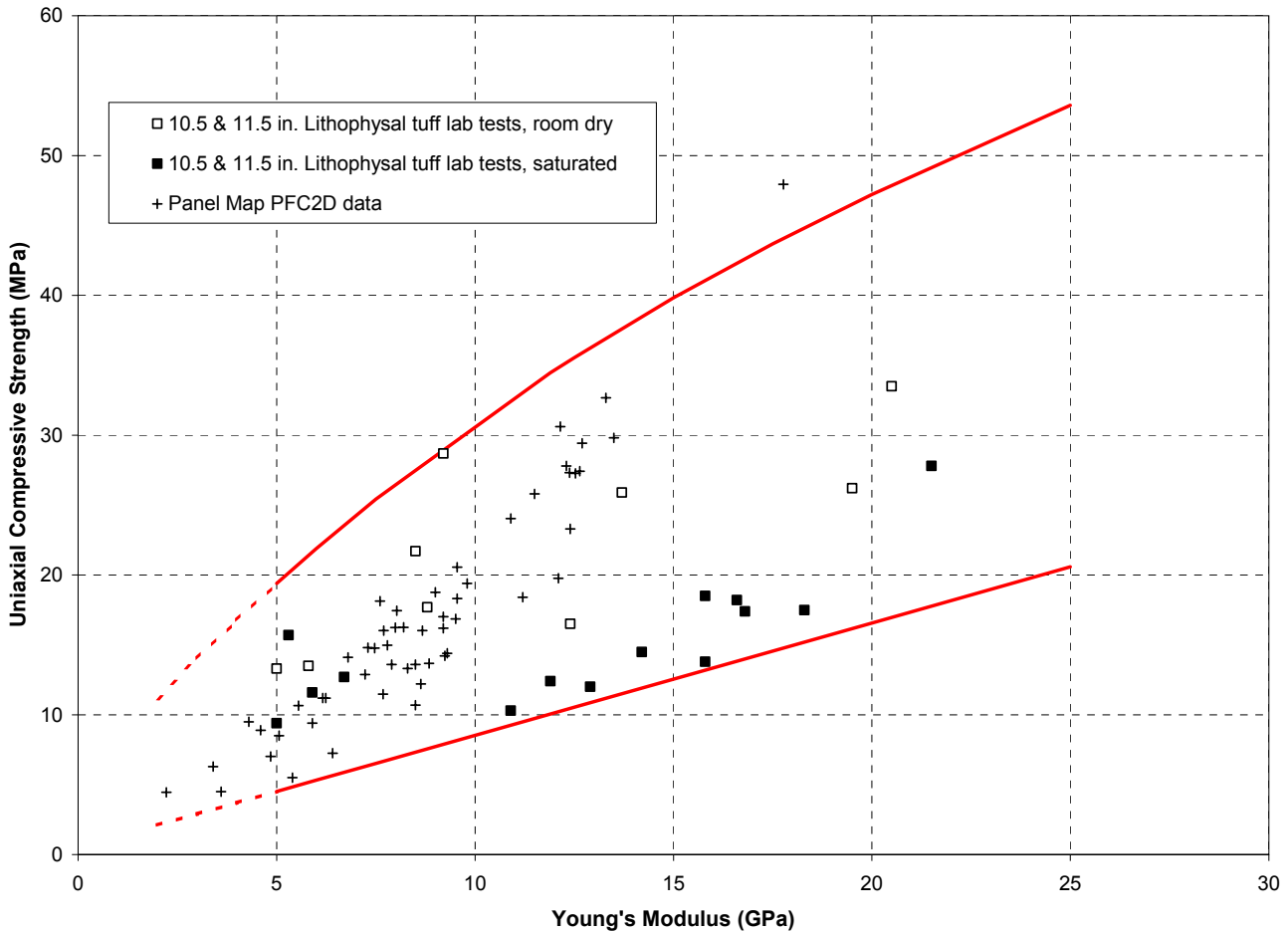Source: Appendix B, Microsoft Excel file "LithophysalRockRanges_Calc.xls," Worksheet "q-por"

Figure 6.6-2. Upper and Lower Bounds of the Uniaxial Compressive Strength versus Lithophysal Porosity Relationship for 10.5 and 11.5-in Diameter Cores and Simulated Numerical Test Results

Source: Appendix B, Microsoft Excel file "LithophysalRockRanges_Calc.xls," Worksheet "q-E"

NOTE: The plotted points making up the upper and lower bounds are from the estimated exponential equations. The solid lines are polynomial best-fit lines constructed for ease of extrapolation using the standard "Add Trendline" function of Microsoft Excel. The extrapolated polynomial upper and lower bounds are plotted subsequently in Figures 6.6-4 and 6.6-5.

Figure 6.6-3. Upper and Lower Bounds of the Uniaxial Compressive Strength versus Young's Modulus Relationship for 10.5 and 11.5-in Diameter Cores and Simulated Numerical Test Results

The upper and lower bounds in Figure 6.6-3 (produced using exponential fits) have been refit to polynomials as shown in the figure in order to more easily extend the range of the bounds in subsequent figures. A simplified version of Figure 6.6-3 is given in Figure 6.6-4, where the polynomial upper and lower bounds have been plotted for the full range of depicted properties. Since no laboratory large core data is available below a Young's Modulus of 5 GPa, the lines representing the bounding values are dashed. Some of the PFC simulations of the ECRB Cross-Drift panel-map specimens plot within the dashed low modulus and low strength range in Figure 6.3-4, which also shows that the low Young's modulus and uniaxial compressive strength results of available small-diameter core tests of Topopah Spring Tuff largely plot within the dashed bounds range. The range of data generated by the PFC extrapolations for size, shape, and distribution variability generally fall within the range of the laboratory testing. It is seen that the uniaxial compressive strength of saturated specimens generally forms the lower bound of the laboratory data range, with a minimum strength value of approximately 10 MPa.

Source: Appendix B, Microsoft Excel file "LithophysalRockRanges_Calc.xls," Worksheet "Bounds"

NOTE: The upper and lower bounds that are dashed lines represent bounds that are outside the range of measured values. Some of the PFC simulations of the ECRB Cross-Drift panel map specimens plot within this range.

Figure 6.6-4. Upper and Lower Bounds of the Uniaxial Compressive Strength versus Young's Modulus Relationship with Large-Core Laboratory and PFC Panel Map Lithophysae Shape Study Results

In Figure 6.6-5, the base-case rock mass property categories are now added to Figure 6.6-4, illustrating the estimated upper and lower bounding values of UCS associated with each value of the base-case Young's modulus (Table 6.6-1). The linear line of base-case Young's modulus and uniaxial compressive strength pair are also added to the diagram and compared with the nonlinear line (blue) forming the means between the upper and lower bounds. Figure 6.6-5 shows that the base-case line and means line are close to one another, however, the trend of the bounds is to converge toward the origin. This nonlinear bounds converging at the origin is more realistic than the base-case property prediction, which yields a positive uniaxial compressive strength of about 8 MPa for a Young's modulus of zero.
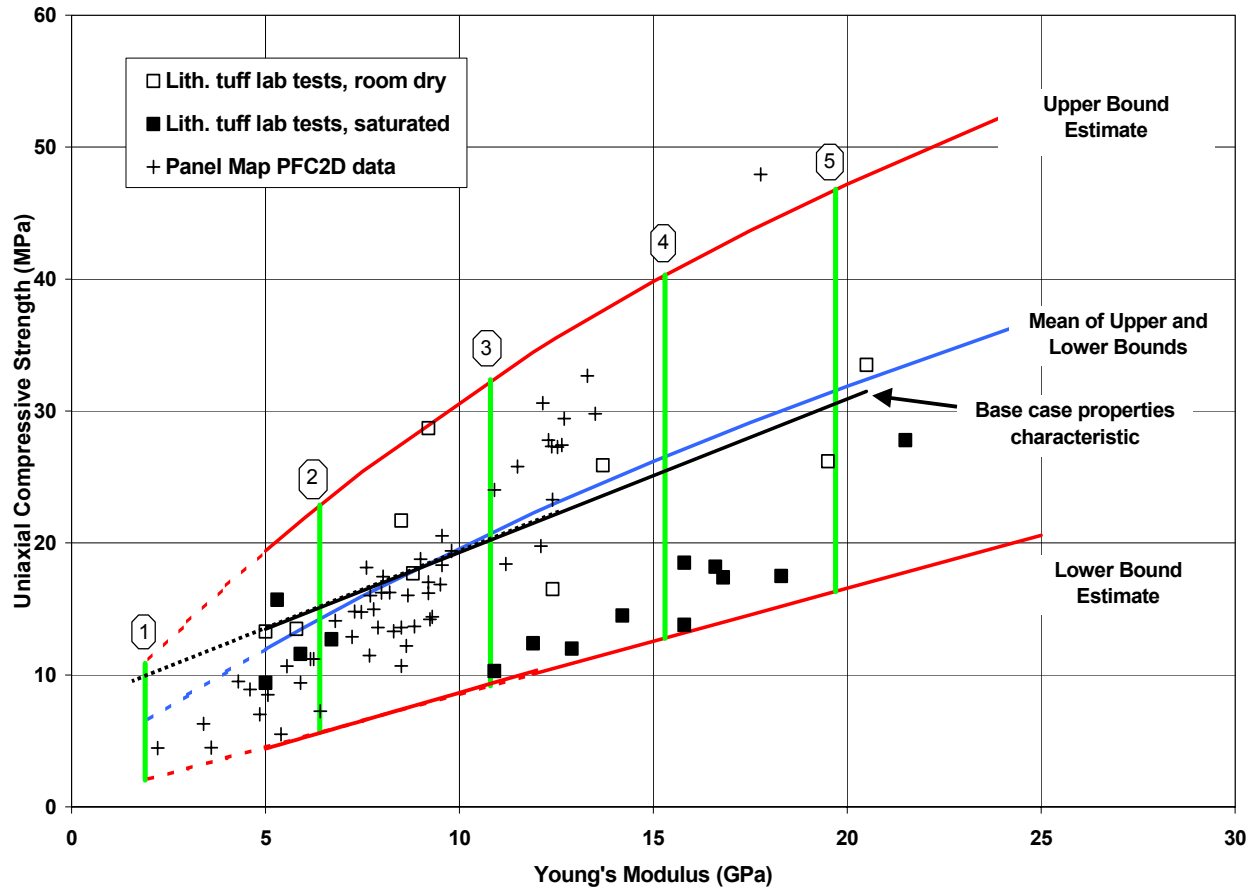
Source: Modified from Appendix B, Microsoft Excel file "LithophysalRockRanges_Calc.xls," Worksheet "Bounds (cat)"

Figure 6.6-5. Uniaxial Compressive Strength vs. Young's Modulus Showing Approximate UCS Upper and Lower Bounds

Table 6.6-1. Base Case, Upper and Lower Bound Strength Values for the Five Lithophysal Rock Mass Categories

Rock Mass Category	Uniaxial Compressive Strength (MPa)			Estimated Young's Modulus (GPa)	Lithophysal Porosity Ranges for Rock Mass Categories (%)
	Base Case	Lower Bound	Upper Bound		
1	10	2.0	10.9	1.9	greater than 25
2	15	5.6	22.9	6.4	20-25
3	20	9.2	32.4	10.8	15-20
4	25	12.8	40.3	15.3	10-15
5	30	16.3	46.8	19.7	less than 10

Source: Modified from Table 6.4-1 with information from Figure 6.6-5.

From Sections 6.3.4 and 6.3.5 the effect of rock saturation and increased temperature (up to approximately 200°C) is small and can be neglected in estimating the mechanical properties of intact rock. Since the ground matrix part of lithophysal rock is considered to control the elastic and strength behavior of lithophysal rock mass, it is expected that rock saturation and increased temperature can also be neglected in estimating the rock mass mechanical properties.

6.6.2 Impact of Bounds Applied to Yield and Performance of Numerical Simulations of Tuff and Observations at the Drift Scale

It is desirable to simulate the expected behavior of tuff at the drift scale for each of the lithophysal rock-mass categories of rock. These simulations can then be compared to observations of the actual ESF and ECRB Cross-Drift tunnels. In these numerical studies, the rock mass was assumed to be homogeneous with constant rock mass mechanical properties. For each rock mass category simulated, the lower bound estimate of strength and corresponding value of Young's modulus were used (i.e., the intersection of the vertical category bar and the lower bound line in Figure 6.6-5, Table 6.6-1). The analyses were carried out with the UDEC program and involved examination of stability of the emplacement drifts under in situ and thermal loading for the lower bound values for all categories. The modeling results showed that UCS values less than approximately 10 MPa result in predicted extensive sidewall failure of emplacement tunnels under in situ stresses only (Figure 6.6-6). This is obviously not observed in the ECRB Cross-Drift or ESF where tunnels are in stable and excellent condition with minimal ground support in the crown and generally no ground support in the sidewalls. The laboratory tests on small-diameter tuff also shows that typical minimum UCS values, even for total porosities in excess of 30 percent, are approximately 10 MPa (Figure 6.3-1, out of the six test results only two are slightly less than 10 MPa). Further, laboratory tests on large-diameter tuff yielded UCS values of about 10 MPa or higher (Figure 6.3-12).

An explanation of why the rock mass UCS may have a lower bound of approximately 10 MPa is that one does not find Category 1 and 2 rock at the drift scale (corresponding to lithophysal porosities greater than 20 percent). At the 5 m or smaller scale there may be instances of locally mapped high porosity, but it is probable that at this same location the inherent spatial variability of lithophysal voids will diminish the porosity in the third dimension. Consequently, the assumption of a homogeneous, high porosity rock mass, as assumed in the Category 1 and 2 cases is conservative, since the spatial variability of porosity will result in overall lower rock porosities and a corresponding higher rock mass strength. The application of the lower bound 10 MPa strength cutoff line is shown in Figure 6.6-7. Note that the few PFC2D panel map strength values that plot below 10 MPa in Figure 6.6-7 typically have high values of lithophysal porosity (Figure 6.5-29). The upper and lower bounds for the various lithophysal rock mass categories with the 10 MPa strength cutoff are summarized in Table 6.6-2.

UCS = 4.5 MPa, E=5 GPa   UCS = 5.9 MPa, E=6.7 GPa

extensive sidewall shear failure and fall-out

minor yield along sidewall

UCS = 7.2 MPa, E=8 GPa   UCS = 9.9 MPa, E=11.7 GPa
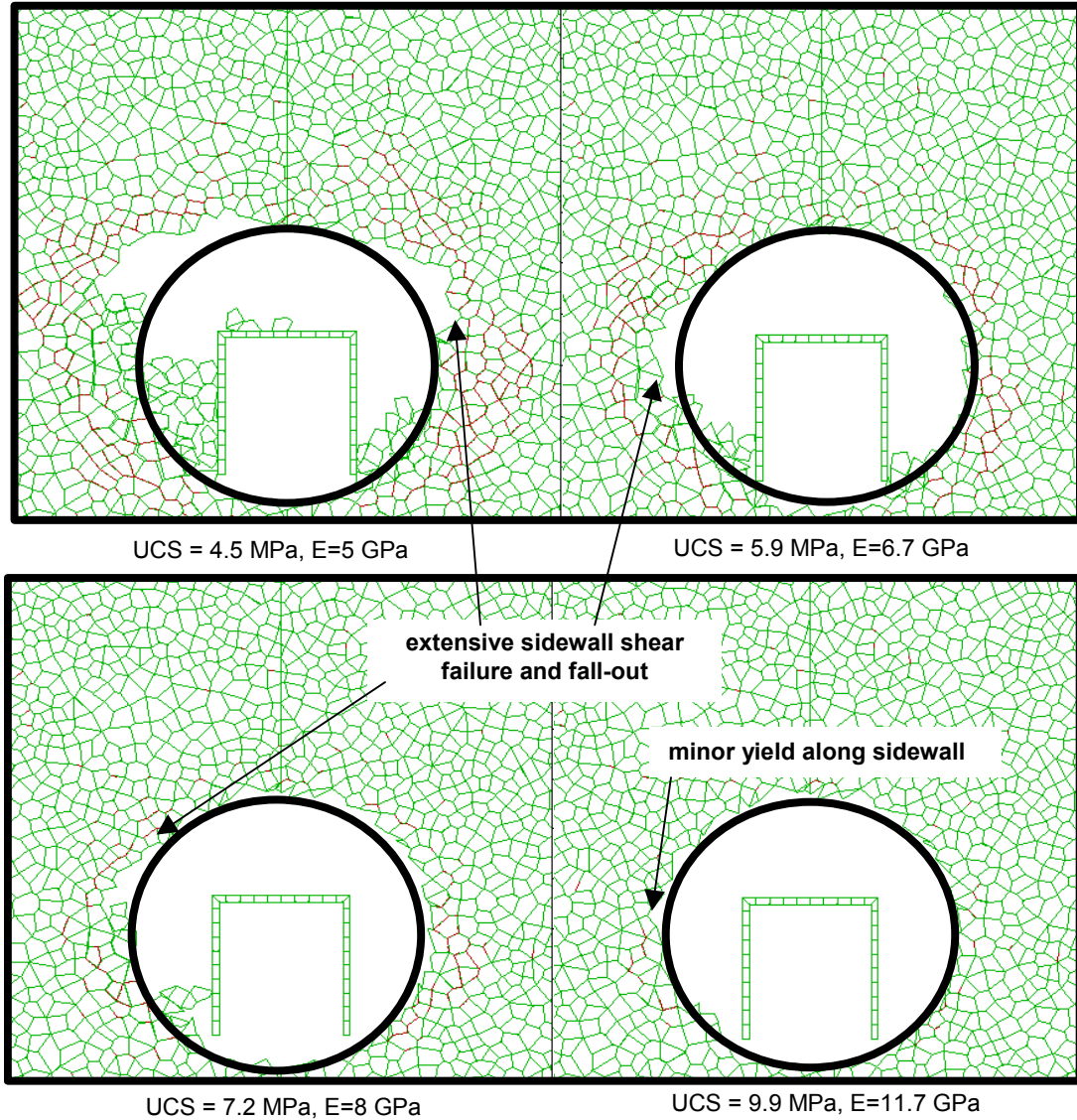
Source: *Drift Degradation Analysis* (BSC 2004 [DIRS 166107], Appendix E, Figure E-14, p. E-36).

Note: The lower bound properties line is shown in Figure 6.6-5. Drift exhibits extensive sidewall failure under in situ load only for UCS values less than approximately 10 MPa. This behavior is not observed in the ESF or ECRB Cross-Drift and so lower bound properties (UCS less than approx. 10 MPa) under predict the actual in situ strength values.

Figure 6.6-6. UDEC Emplacement Drift Stability Analysis Under In Situ Loading for Combinations of UCS and Young's Modulus Along the Lower Bound Properties Line
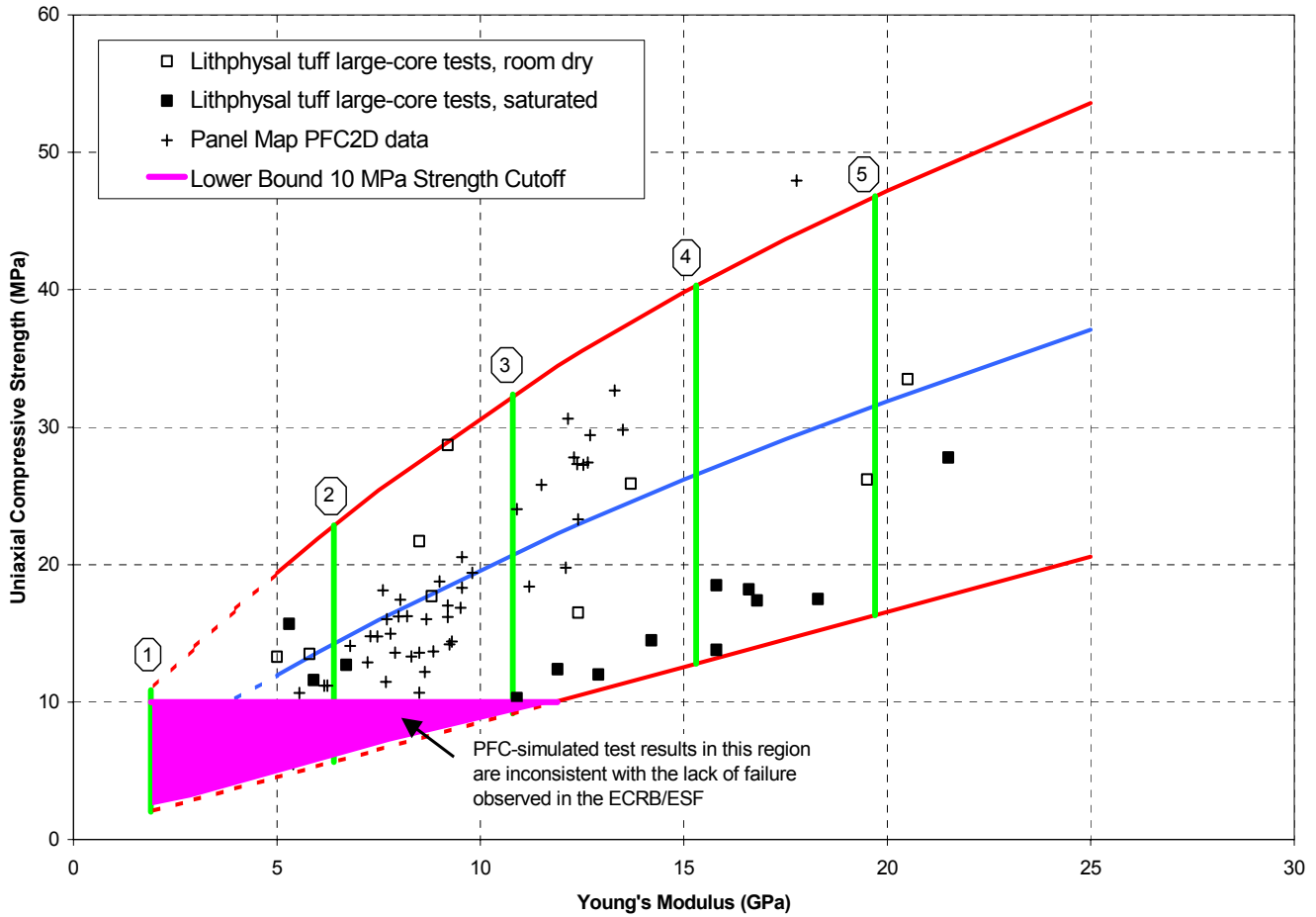
Source: Appendix B, Microsoft Excel file "LithophysalRockRanges_Calc.xls," Worksheet "Bounds (cutoff)"

NOTE: Base-case average properties defined for each category are the mean and the upper and lower bounds of each range. Category 1 is highest porosity, lowest quality rock and category 5 is lowest porosity, highest quality rock. The strength cutoff applies for the assumption of a homogeneous rock mass and is based on numerical UDEC simulations at drift scale.

Figure 6.6-7. Uniaxial Compressive Strength vs. Young's Modulus Showing Approximate Upper and Lower Bounds with 10 MPa Strength Cutoff

Table 6.6-2. Base Case, Upper and Lower Bound Strength Values for the Five Lithophysal Rock Mass Categories with 10 MPa Strength Cutoff

Rock Mass Category	Uniaxial Compressive Strength (MPa)			Estimated Young's Modulus (GPa)	Lithophysal Porosity Ranges for Rock Mass Categories (%)
	Base Case	Lower Bound	Upper Bound		
1	10	10	10.9	1.9	greater than 25
2	15	10	22.9	6.4	20-25
3	20	10	32.4	10.8	15-20
4	25	12.8	40.3	15.3	10-15
5	30	16.3	46.8	19.7	less than 10

Source: Modified from Table 6.6-1 with information from Figure 6.6-7.

To investigate the impact of spatial variability of porosity on the lower bound and mean rock mass properties, a numerical investigation was carried out using the calibrated UDEC Voronoi drift scale model in the *Drift Degradation Analysis* (BSC 2004 [DIRS 166107], Appendix E, Section E4.1.4.2). The purpose of the analyses was to determine the rock mass stress-strain response for an inhomogeneous rock mass composed of spatially varying lithophysal porosity, and thus spatially varying rock mass UCS and Young's Modulus. The goal of the modeling was to conduct numerical compression tests on simulated rock mass "samples" that are sufficiently large to contain the variability of lithophysal porosity affecting the emplacement drift scale. This requires a geometric model of the spatial variability of lithophysal porosity as a function of position within the Tptpll as well as the UDEC model.

Appendix A of this document presents a methodology for simulating the spatial variability of lithophysal porosity based on field measurements in the Tptpll in the ECRB Cross-Drift. The model is used to statistically represent lithophysal porosity in a series of 40 m long (along the axis of the ECRB Cross-Drift) by 50 m high (vertical) by 200 m wide parallelopipeds along the ECRB Cross-Drift axis from top to bottom of the Tptpll. The parallelopipeds are subdivided into a number of small (meter-scale) cubical grids within which the lithophysal porosity is estimated as a function of vertical and horizontal position. Figure 6.6-8 presents an example of a vertical plane perpendicular to the drift axis within the Tptpll.

Thirty rock mass "samples" measuring 10 m high by 5 m wide (drift scale) were randomly selected both vertically and horizontally within each of the parallelopipeds (Figure 6.6-8). Each of the porosity grids of the parallelopiped that are found within the boundaries of each of these 10×5 m rock mass samples have a value of lithophysal porosity associated with them. This porosity is used to assign the associated rock mass category and, in turn, its associated UCS and Young's modulus (and the calibrated cohesion, friction angle and stiffness representing the strength and modulus) to the elements within that particular grid. The resulting sample thus contains spatially variable UCS and Young's modulus that represents the in situ variability of lithophysal porosity. Figure 6.6-8 shows an example of one of the 10×5 m UDEC "samples" composed of Voronoi blocks and the contours of the resulting lithophysal porosity captured from the simulated Tptpll parallelopipeds. The mean, maximum and minimum lithophysal porosities in each of the samples are plotted in Figure 6.6-9, showing that the samples from the upper block, as expected, contain a greater proportion of lithophysal material with porosities in excess of 25 percent. The means of all the samples show average lithophysal porosity of 15.3 percent and 12.8 percent, for the upper block and the lower block, respectively. These are consistent with the field measurements presented in Section 6.2 and the *Subsurface Geotechnical Parameters Report* (BSC 2003 [DIRS 166660] Attachment VII).
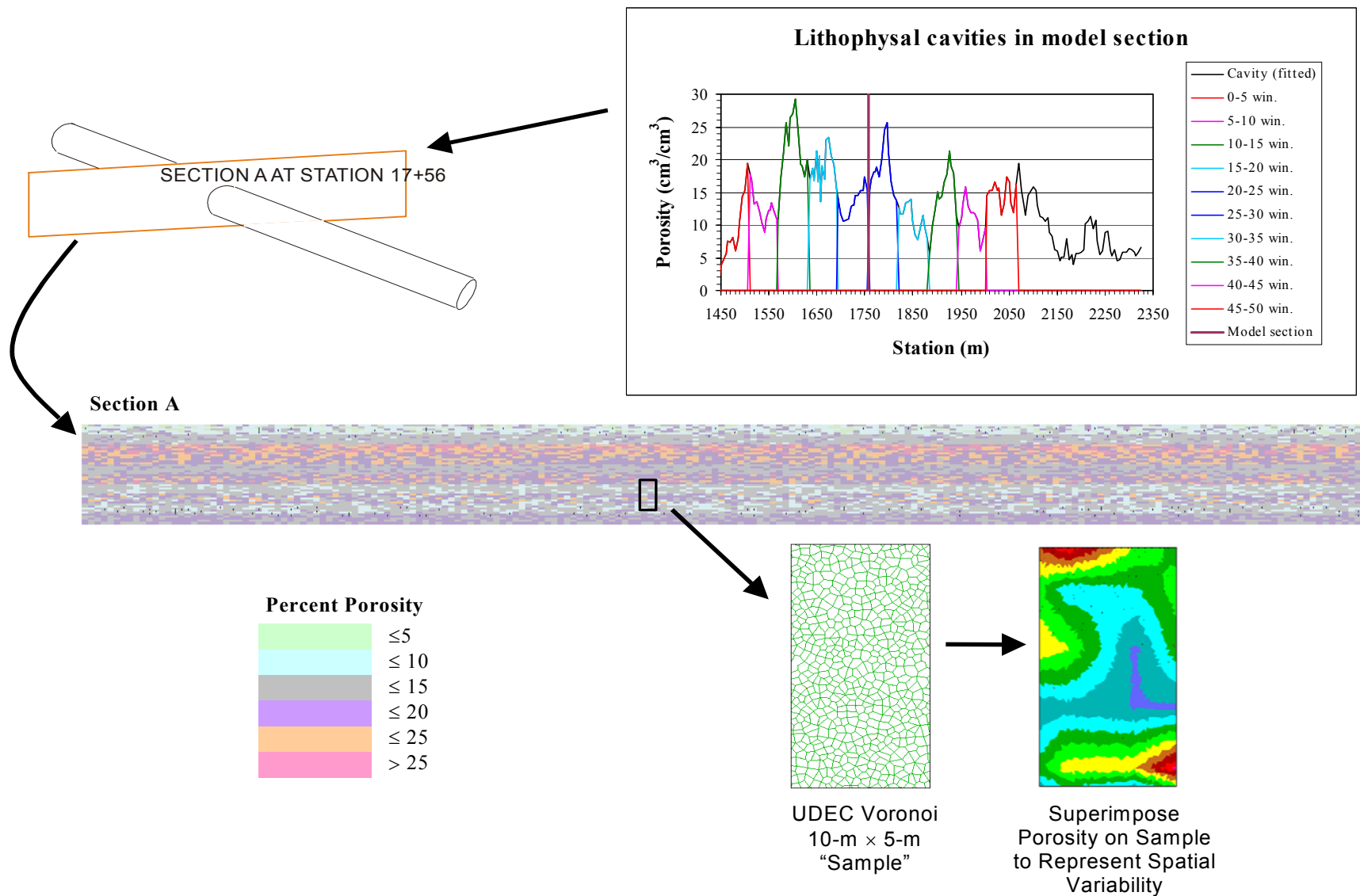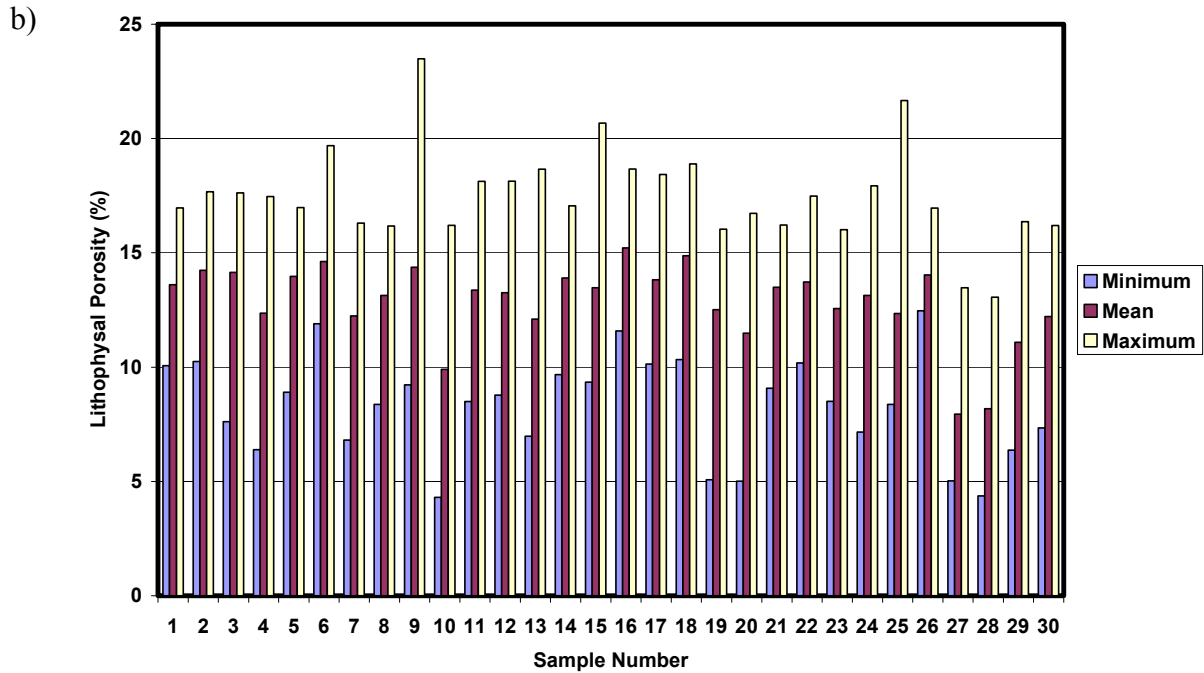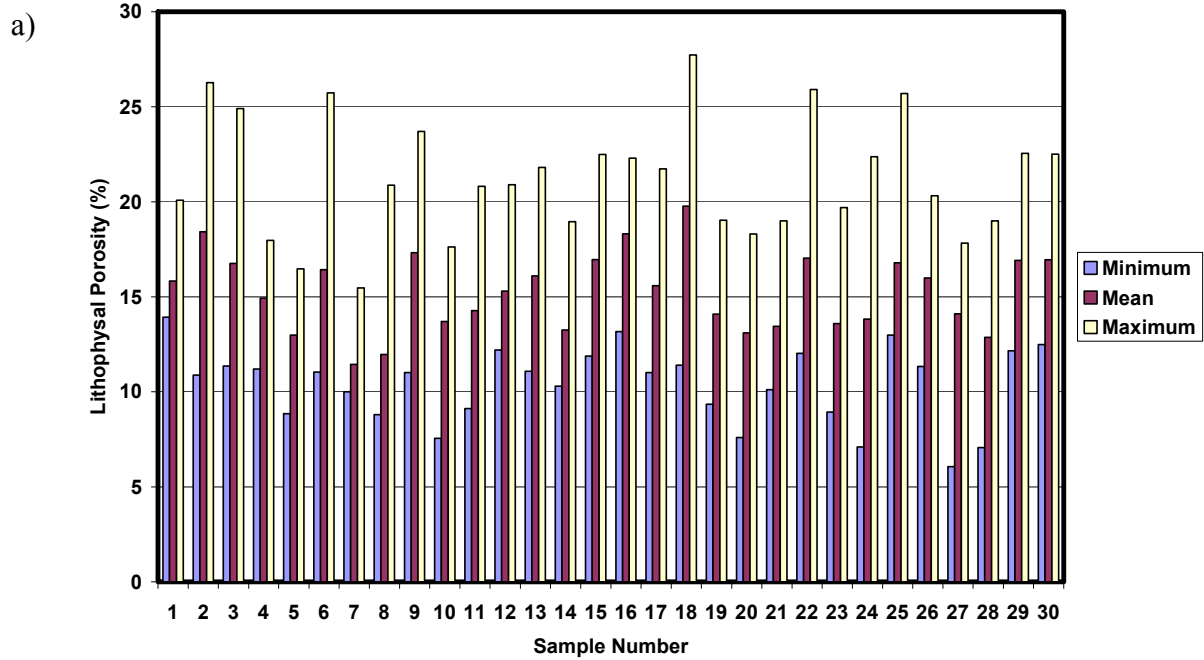
Source: Appendix A, Figure A-5

NOTE: Cross section A is a 50 × 200 cell table representing a 1 × 1 m grid for the simulated section at 17 + 56 in the ECRB Cross-Drift.

Figure 6.6-8. Schematic Illustration of the Process of Sampling and Modeling Spatial Variability Using Lithophysal Porosity Simulation Model

Source: *Drift Degradation Analysis* (BSC 2004 [DIRS 166107], Appendix E, Figure E-16, p. E-40)

NOTE: Mean, minimum, and maximum refer to those values of lithophysal porosity in the particular sample. (a) the upper cross section; (b) the lower cross section of the Tptpll

Figure 6.6-9. Spatial Variability in Lithophysal Porosity in Each of 30 Samples

UDEC simulations of compression tests were conducted for 30 samples from each of the upper and lower cross sections of the Tptpll. No explicit voids are modeled in the drift-scale numerical samples, rather equivalent rock mass properties are identified and used. For each synthetic sample, the rock mass uniaxial compressive strengths adopted for each lithophysal rock mass category were defined by two sets of values – the base-case mechanical properties, and the lower bound rock properties (Figure 6.6-7 and Table 6.6-2). The upper bound values are not examined as they are irrelevant since the base-case analyses of drift stability presented in Section 6.4 are conservative – higher strengths will only result in greater stability. These results and the conclusions below are documented in *Drift Degradation Analysis* (BSC 2004 [DIRS 166107], Appendix E, Section E4.1.4.2).

The UDEC numerical uniaxial compression tests of drift scale samples typically show that the samples fail as expected in an axial splitting mode (Figure 6.6-10). Two sets of numerical tests were carried out, the first using base-case mechanical properties and the second using lower bound properties. The results of these simulated compression tests are plotted in Figure 6.6-11 in terms of the relationship of UCS and Young's Modulus. Several conclusions from this work can be made, including:

1. The variability in porosity distribution inherent in the samples results in UCS values that roughly equal or exceed 10 MPa. As seen in Figure 6.6-11, the spatial variability in rock mass compressive strength results in sample strengths that are grouped nearest rock mass category 4, which correspond to an average porosity of 10-15 percent (Table 6.6-2). It is difficult, considering variable rock mass porosity, to produce average rock mass strength values that are at the low end of the category range. This agrees with observations in the ESF main loop and ECRB Cross-Drift of stable, lightly supported excavations in the lithophysal units that show little or no signs of instability.

2. The distribution of sample UCS and Young's moduli for both the base case and lower bound properties naturally fall within the range of lithophysal rock mass categories 3 to 4. This is in agreement with the in situ distribution of lithophysal porosities (Section 6.2.1 and Figure 6.4-8) that show the most common values lie in the Category 3 to 4 ranges. This confirms the consideration that the typical rock mass properties for the lithophysal units lie in the Category 3 to 4 ranges, and that the occurrence of Category 1 or 2 rocks is typically as localized regions of high porosity, potentially accompanied by large lithophysae.

3. The results verify that the consideration of homogenous rock mass properties used in the base-case lithophysal rock mass categories is conservative in nature.

Based on these calculations, the range of lithophysal rock mass properties are considered to have a lower bound strength of 10 MPa, with the lower bound following the saturated rock strength estimate for strengths greater than 10 MPa.
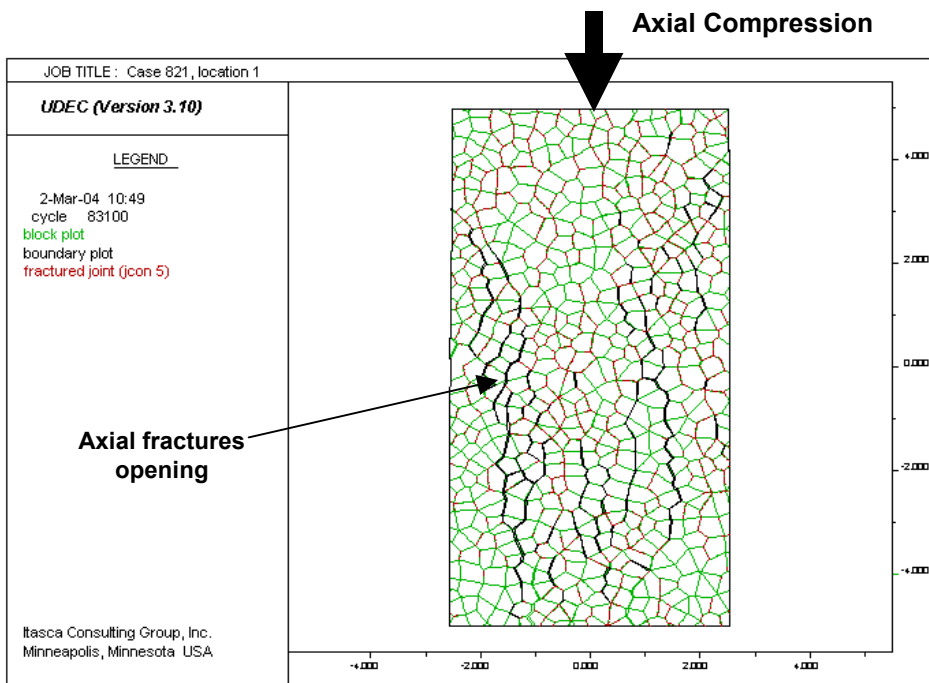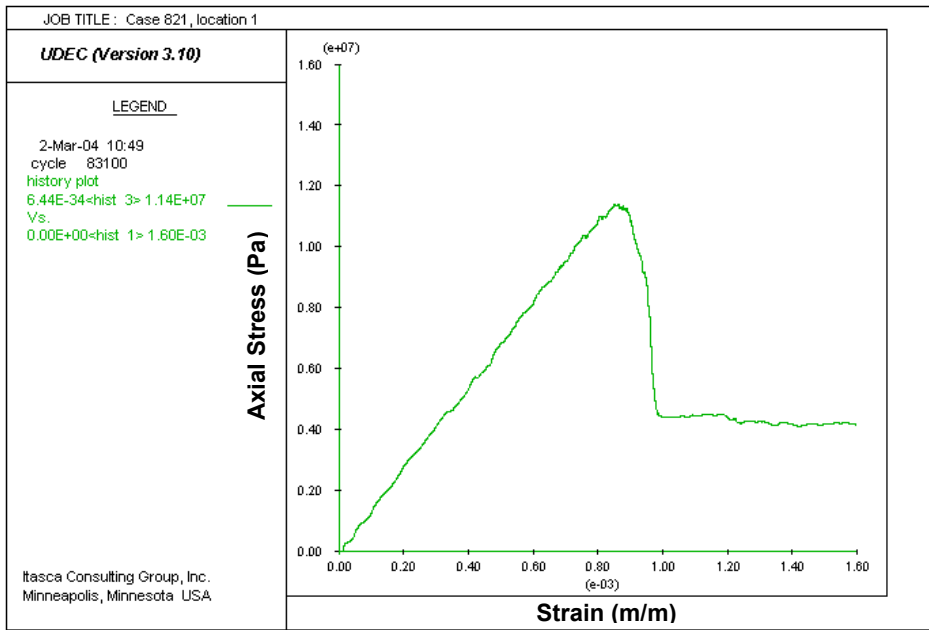
Source: *Drift Degradation Analysis* (BSC 2004 [DIRS 166107], Appendix E, Figure E-17, p. E-41)

NOTE: Estimated modulus and peak strength are determined from stress-strain curve. Sample fails in axial splitting mode as seen by black, axially oriented macro-fractures. Red block contacts indicate yield in either tension or shear.

Figure 6.6-10. Example of Uniaxial Compressive Strength Test Results on 10 m × 5 m Rock Mass Sample Containing Spatially Variable Lithophysal Porosity
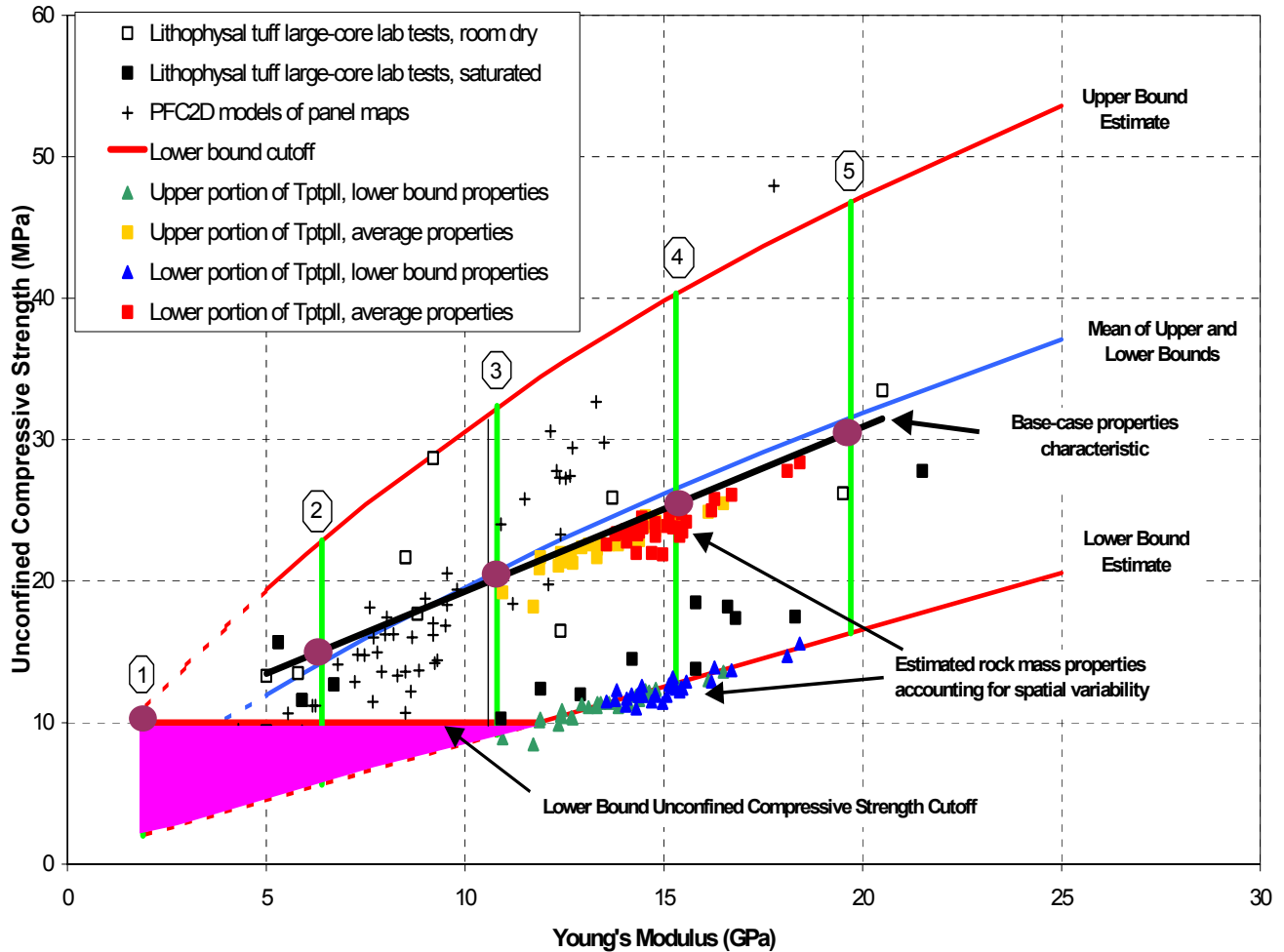
Source: Appendix B, Microsoft Excel file "LithophysalRockRanges_Calc.xls," Worksheet "Bounds (NLS)"

NOTE: Base-case average properties defined for each category are the mean and the upper and lower bounds of each range. Category 1 is highest porosity, lowest quality rock and category 5 is lowest porosity, highest quality rock.

Figure 6.6-11. Lithophysal Rock Strength and Modulus Range Divided into Five Rock Mass Categories Covering the Large-Diameter Core Laboratory Testing and PFC Extrapolation Lithophysal Shape Extrapolation Studies

6.7 CONFIRMATION OF THE LITHOPHYSAL ROCK MECHANICAL MODEL AND PROPERTY BOUNDS

This section describes the activities conducted to validate the mechanical behavioral model of lithophysal rock and the estimated range of properties associated with the assigned rock mass categories. The validation activities consist of:

- Comparison of the numerical mechanical material failure mechanisms in lithophysal rock to observations in laboratory specimens.

- Comparison of the prediction of drift scale fracturing in the Tptpll at ECRB Cross-Drift depth to observations of tunnel sidewall fracturing in the ECRB Cross-Drift

- Comparison of the rock mass property ranges to preliminary results from in situ slot tests

The details of the validation comparisons are given in the *Drift Degradation Analysis* (BSC 2004 [DIRS 166107], Sections 7.6.5.1 and 7.6.5.2).

6.7.1 Comparison of Predicted Numerical Failure Modes to Laboratory Observations

The UDEC "potential fracture" model is formulated to allow fractures to form as the stresses dictate. An initial and simple validation is to compare the predictions of the model to observations and common knowledge from laboratory testing. In uniaxial compression, with 2:1 length-to-diameter specimens, the failure mode is typically in the form of axial splitting, or coalescence of axially oriented fractures observable on the surface of the sample. Figure 6.7-1 presents a typical UDEC plot of predicted fracturing (red tensile cracks) that forms axial to the sample axis. The UDEC grain structure of the sample is not shown so that the formed cracks are clearly seen. The typical laboratory failure response is shown (Figure 6.7-1) in the associated photograph of a large core sample from the Tptpul after testing. The axial fractures are clearly visible in this photo.

Realistic predictions of damage, stress redistribution, deformation, and other constitutive behavior are obtained in simulated compression tests using the UDEC Voronoi block model. The micro properties of the joints and blocks in the UDEC model are calibrated to the stiffness and strength of lithophysal rock mass, Category 1, as determined from uniaxial compressive strength tests (Section 6.5.3.2 and Table 6.6-2). The resulting constitutive behavior of the UDEC Voronoi block model is very complex, as illustrated by plots of failure envelope, stress-strain curves for different confinements and volumetric strain as a function of axial strain, shown in Figures 6.5-32 to 6.5-35. Unfortunately, the number and types of laboratory and in situ experiments was insufficient to describe the complete constitutive behavior of the lithophysal tuff with a high level of confidence, particularly in the post-peak strain range and for confined conditions. The mechanical behavior exhibited by the synthetic Voronoi block model seems to be quite reasonable and typical for hard, brittle rocks like the Topopah Spring tuff. For unconfined conditions, the UDEC synthetic model softens in a rather brittle manner after reaching the peak stress. As confinement increases, the post-peak behavior becomes more ductile; for 3 MPa confinement, it is almost perfectly plastic (i.e., there is no strength decrease for a considerable plastic strain). The perfectly plastic Mohr-Coulomb model most likely will represent a lower bound of damage and deformation for the uniaxial compression case.

Applied Axial Load
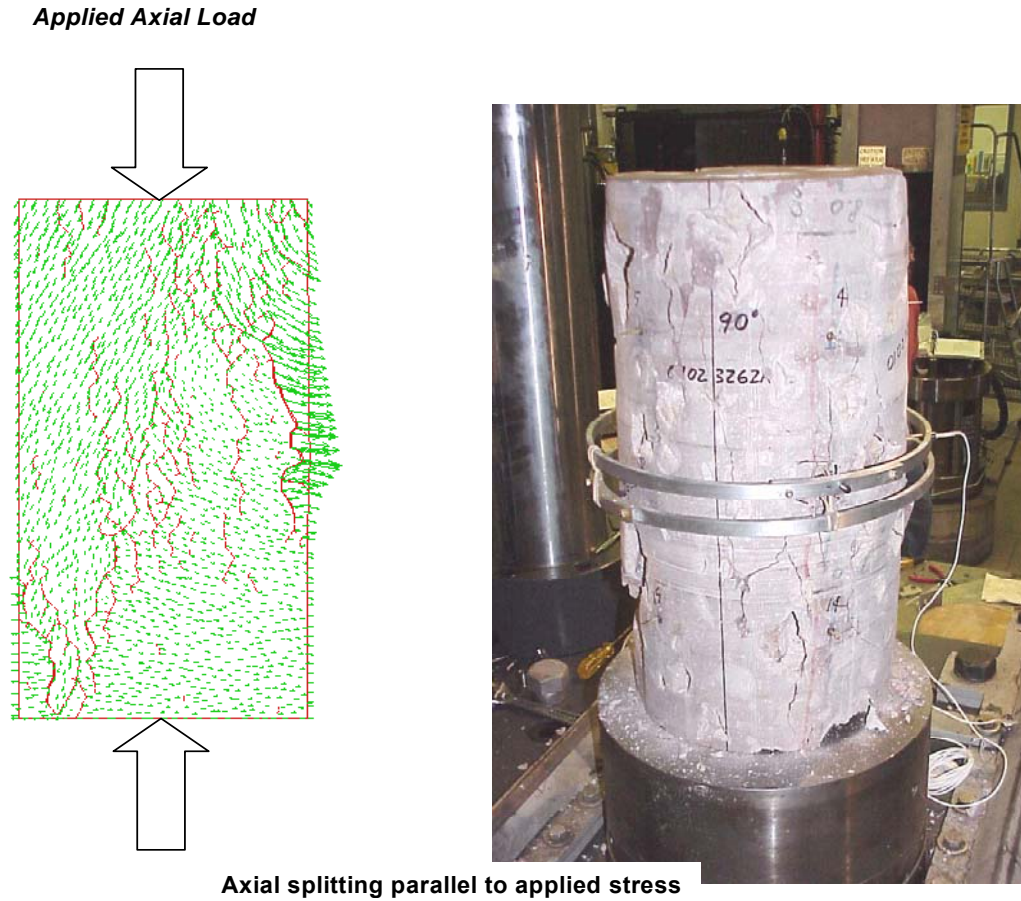
Axial splitting parallel to applied stress

Source: *Drift Degradation Analysis* (BSC 2004 [DIRS 166107], Figure 7-23, p. 7-42)

NOTE: The model predicts axial splitting when no confinement is applied as seen by the red tensile block boundary breakages (fractures) formed and by the velocity vectors that show the sidewall spalling. Core photo shows a similar axial splitting phenomenon.

Figure 6.7-1. UDEC Discontinuum Model of Failure of Lithophysal Tuff Specimen Under Uniaxial Compression

6.7.2   Comparison of UDEC Model Predictions to Field Observations

The proposed modeling approach was verified by comparison of predicted in situ stress-induced damage to the minor damage observed in sidewalls of ESF main loop and ECRB Cross-Drift in the lowest quality Tptpll. Additionally, no sidewall damage is observed in drifts in higher quality Tptpul at shallower depth. Tunnels in all modeled lithostratigraphic zones are stable after excavation, regardless of depth or rock quality. However, some damage, in the form of wall parallel fractures (opening of existing fracture fabric) at the springline, can be observed in the sidewalls of the tunnels at greater depth in the Tptpll. Figure 6.7-2 shows the formation or opening of wall-parallel fractures observed in 12-in. diameter boreholes drilled for geomechanical sampling in the sidewalls of the ESF main loop and ECRB Cross-Drift at the tunnel springline. The wall-parallel fractures are typical of stress-induced yield in tunnels. The boreholes drilled in the relatively low quality Tptpll at depths of 300 to 350 m show sidewall fracturing to depths of approximately 0.5 to 0.6 m. Holes drilled into relatively high quality Tptpul at depths of approximately 200 to 250 m show no fracturing.

Source: *Drift Degradation Analysis* (BSC 2004 [DIRS 166107], Figure 7-25, p. 7-44)

NOTE: Top photo shows sidewall fracturing or opening of preexisting wall-parallel fractures in a 12" diameter horizontal borehole drilled in the springline of the ESF in low quality Tptpll (approximately Category 1). Overburden depth is approximately 325 m. Depth of fracturing is approximately 1.5 to 2 ft (0.46 to 0.61m). The bottom photo shows a horizontal, 12-in diameter borehole drilled in the springline in good quality Tptpul (approximately Category 5) in ESF near site of slot test 2 showing no sidewall damage. The depth of overburden is approximately 250 m.

Figure 6.7-2. Observed Rock Mass Conditions at the Tunnel Springline in Lithophysal Rock in the ESF

The presence of these fractures and their depth into the drift wall, observed in large hole drilling, is a convenient feature from which an estimate of the rock mass strength properties and validation of the model can be made. A parametric study of drift stability and rock yield depth was conducted using the UDEC lithophysal model for the five lithophysal rock mass categories (Table 6.6-2) and imposed overburden depths of 250, 300, and 350 m, corresponding to the Tptpll and Tptpul (BSC 2004 [DIRS 166107], Section 7.6.5.2). As seen in Figures 6.7-3 and 6.7-4, the model reproduces the approximate depth and orientation of drift wall-parallel fractures observed underground for rock mass Category 1. The model results indicate that the rock adjacent to the drift wall yields in a state of uniaxial compression since the minimum stress at or near the drift wall is zero or small since the radial stress component is zero. The depth of fracturing is clearly visible in these models as that portion of the rock where stress relaxation has occurred. The models also show that, for the range of potential lithophysal rock properties, there is no drift wall yield at the depth of the Tptpul from rock mass Category 1.
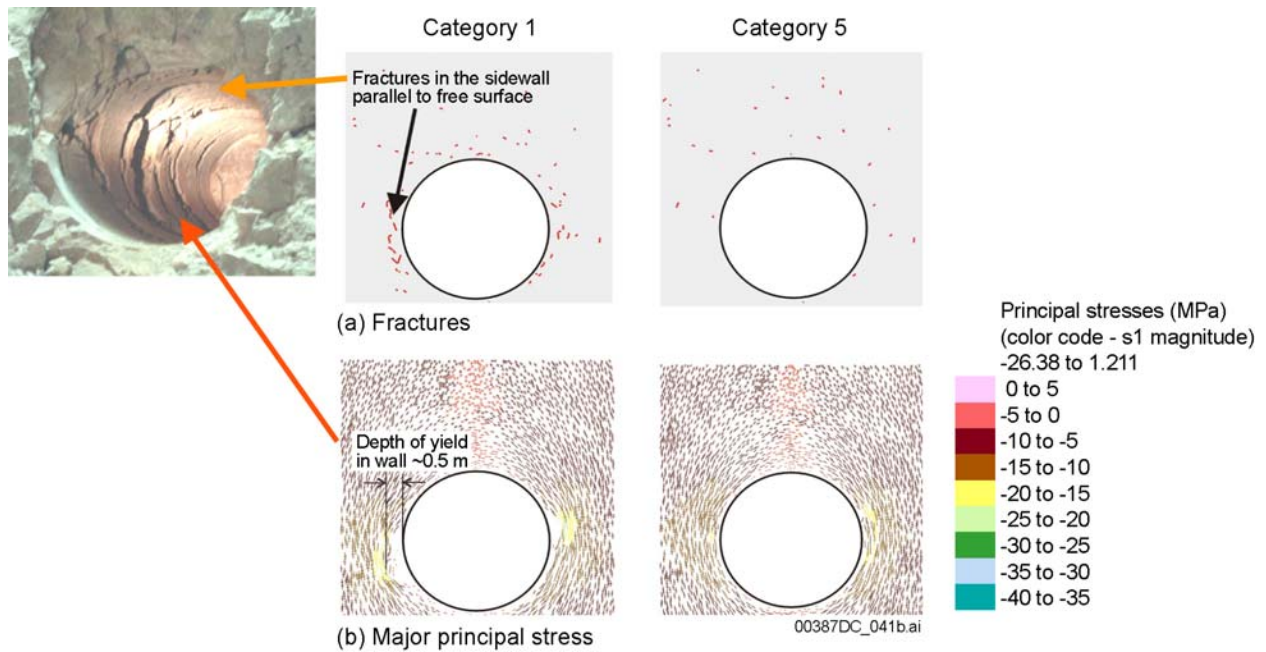
Source: UDEC model results are from *Drift Degradation Analysis* (BSC 2004 [DIRS 166107], Figure 7-26, p. 7-46)

NOTE: Upper figure for Category 1 shows predicted fracturing to a depth of approximately 0.5 m in the sidewall of ECRB Cross-Drift. Lower picture shows stress vectors (in Pa) colored by the magnitude of the stress component. Depth of yield for Category 1 is limited to about 0.5 m in the immediate springline area. The model for Category 5 shows elastic rock mass response (i.e., no yield). Stress vectors in lower figure also shows elastic stress distributions with no readjustment due to yielding.

Figure 6.7-3. Estimate of Rock Mass Fracturing and Stress State Under In Situ Loading Only, Depth of 300 m, Tptpll, Rock Mass Category 1 (Low-Strength Characteristics) and 5 (High-Strength Characteristics)
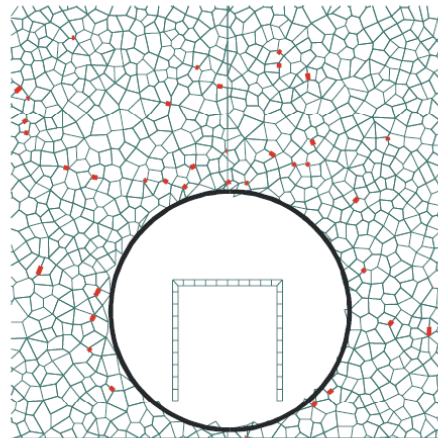
(a) Overburden at 250 m
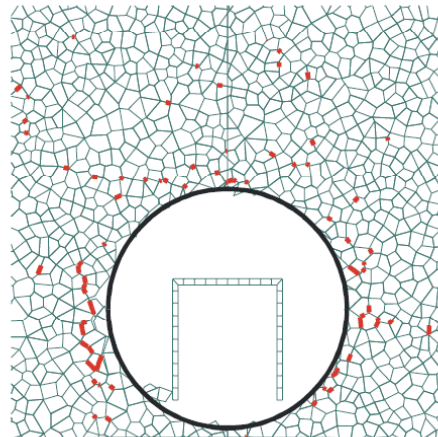
(b) Overburden at 300 m
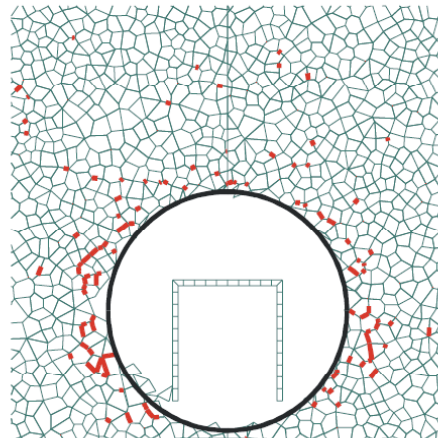
(c) Overburden at 350 m

Source: *Drift Degradation Analysis* (BSC 2004 [DIRS 166107], Figure 7-27, p. 7-47)

Figure 6.7-4. Estimate of Stress-Induced Rock Mass Fracturing (seen as red block contacts) as a Function of Overburden Between 250 m and 350 m, Tptpll, Rock Mass Category 1 (Low-Strength Characteristics)

The *Drift Degradation Analysis* (BSC 2004 [DIRS 166107], Appendix S, Section S3) carries out further drift-scale modeling of lithophysal rock using homogeneous properties from the lithophysal rock mass categories together with a model of time dependent degradation of the rock (Figures 6.7-5 to 6.7-7). It was concluded that:

> It seems that category 1 underestimates the strength of the lithophysal rock mass. The tuff best-fit static-fatigue curve results in significant rockfall from the drift walls at 5 and 10 years after excavation (Figure S-37 [Figure 6.7-5 for Category 1]). The minor rockfall in Figure S-38 [Figure 6.7-6 for Category 2] predicted by the model at 5 and 10 years after excavation, would have been prevented if the ground support was taken into account in the model (note that the rockfall comes from above the springline). Based on model validation with respect to the conditions in the ESF and ECRB Cross-Drift, it seems that category 2 with a tuff best-fit static-fatigue curve is a conservative approximation of the mechanical behavior of the poorest quality lithophysal rock mass. (BSC 2004 [DIRS 166107], Appendix S, Section S3.4.1, p. S-34)

The *Drift Degradation Analysis* (BSC 2004 [DIRS 166107], Appendix S, Section S4) also considered the effect of spatially varying rock mass strength at the drift scale as summarized in this paragraph. Spatial variation of porosity (Section 6.2.1.2) was simulated inside a 50 m × 50 m × 40 m volume. The simulated porosity varies between 5 percent and 30 percent throughout the simulated region. The analysis was conducted using a two-dimensional model for three different cross sections and locations of the drift center within the simulated volume (Figure 6.7-8). Cross sections 1 and 2 are located in a region of the simulated volume with a large average porosity, while the third section is located in a region with a medium average porosity. The analysis has shown that there is no significant variability of the rockfall for different cross sections throughout the simulated volume. Using the relations between porosity and rock mass categories (Table 6.6-2) and between the rock mass categories and UDEC micro-properties (BSC 2004 [DIRS 166107], Table 6-43, p. 6-155), variable properties of the blocks (bulk and shear moduli) and the joints (normal and shear stiffness, cohesion and tensile strength) are generated. Variability of block bulk modulus for cross section 1 is shown in Figure 6.7-9. The results of the simulation for the thermal load combined with time-dependent strength degradation for cross section 1 are shown in Figure 6.7-10. The amount of minimal rockfall is very similar to the rockfall predicted for category 3, considering homogeneous rock mass properties. This is an expected result because the average properties for cross section 1 are similar to category 3 rock mass properties.

1 year

100 years

5 years

1000 years

10 years

10000 years
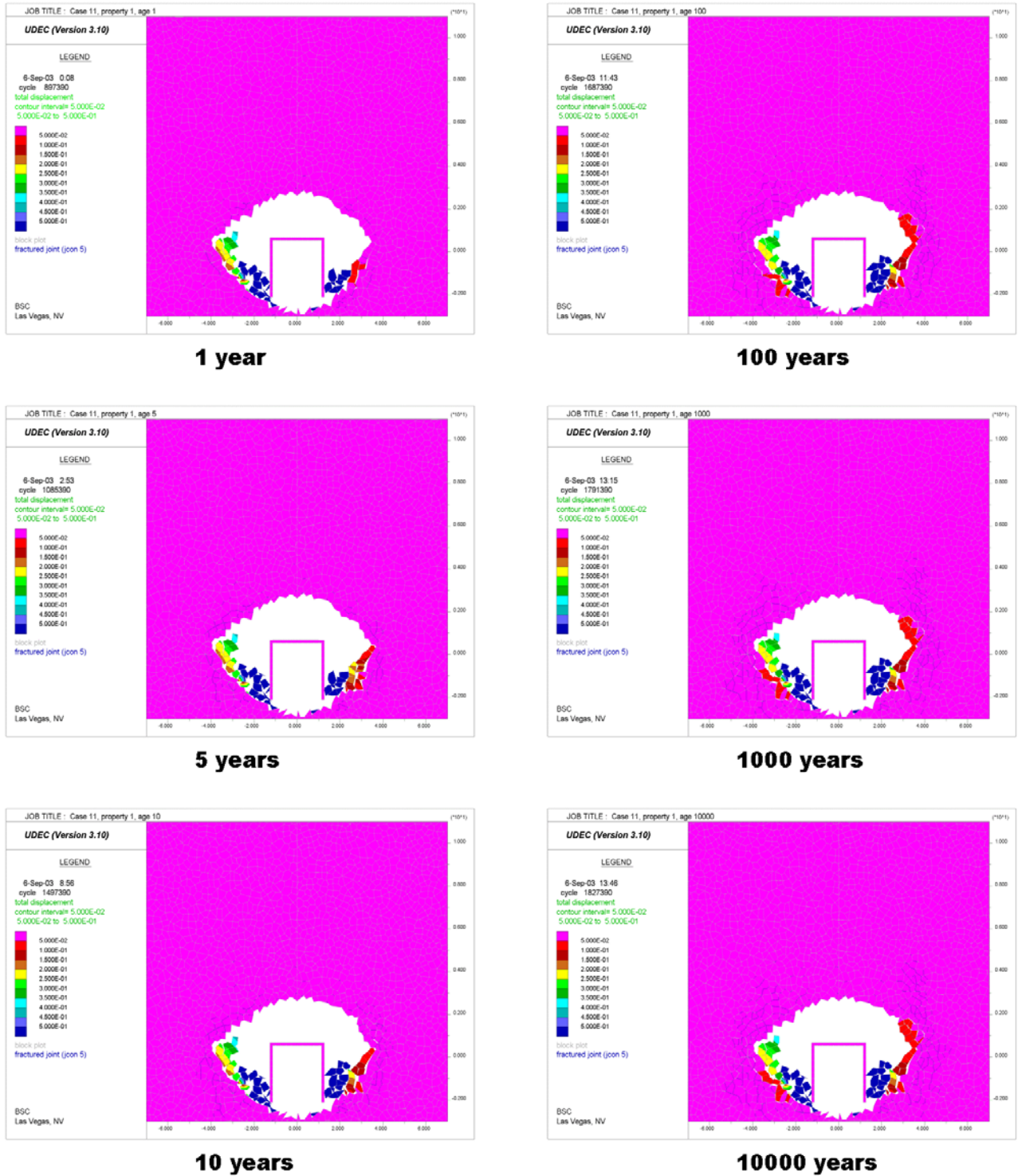
Source: *Drift Degradation Analysis* (BSC 2004 [DIRS 166107], Appendix S, Figure S-37, p. S-39)

Figure 6.7-5. Evolution of Damage Due to Strength Degradation for Category 1 – Tuff Best-Fit Static-Fatigue Curve
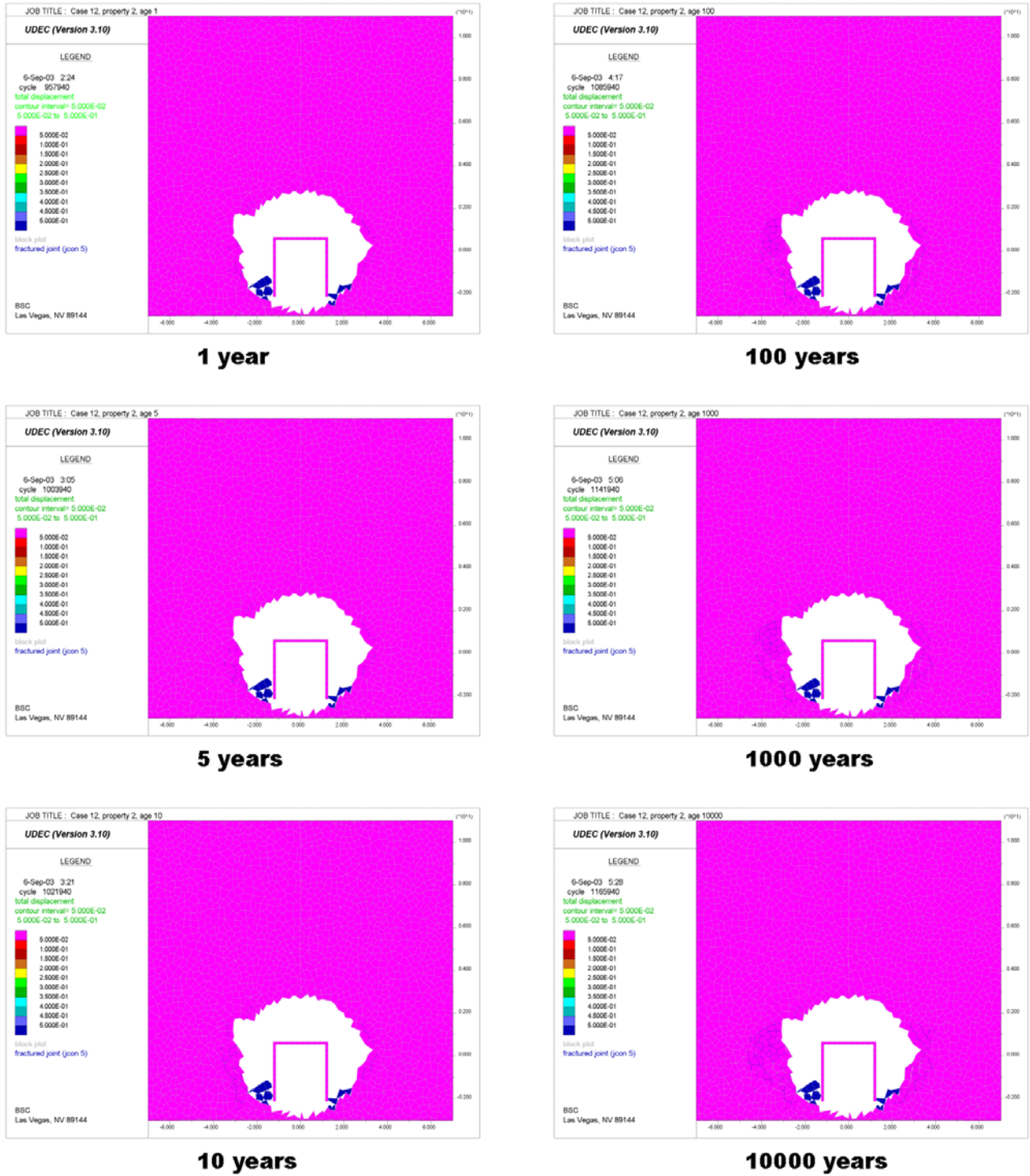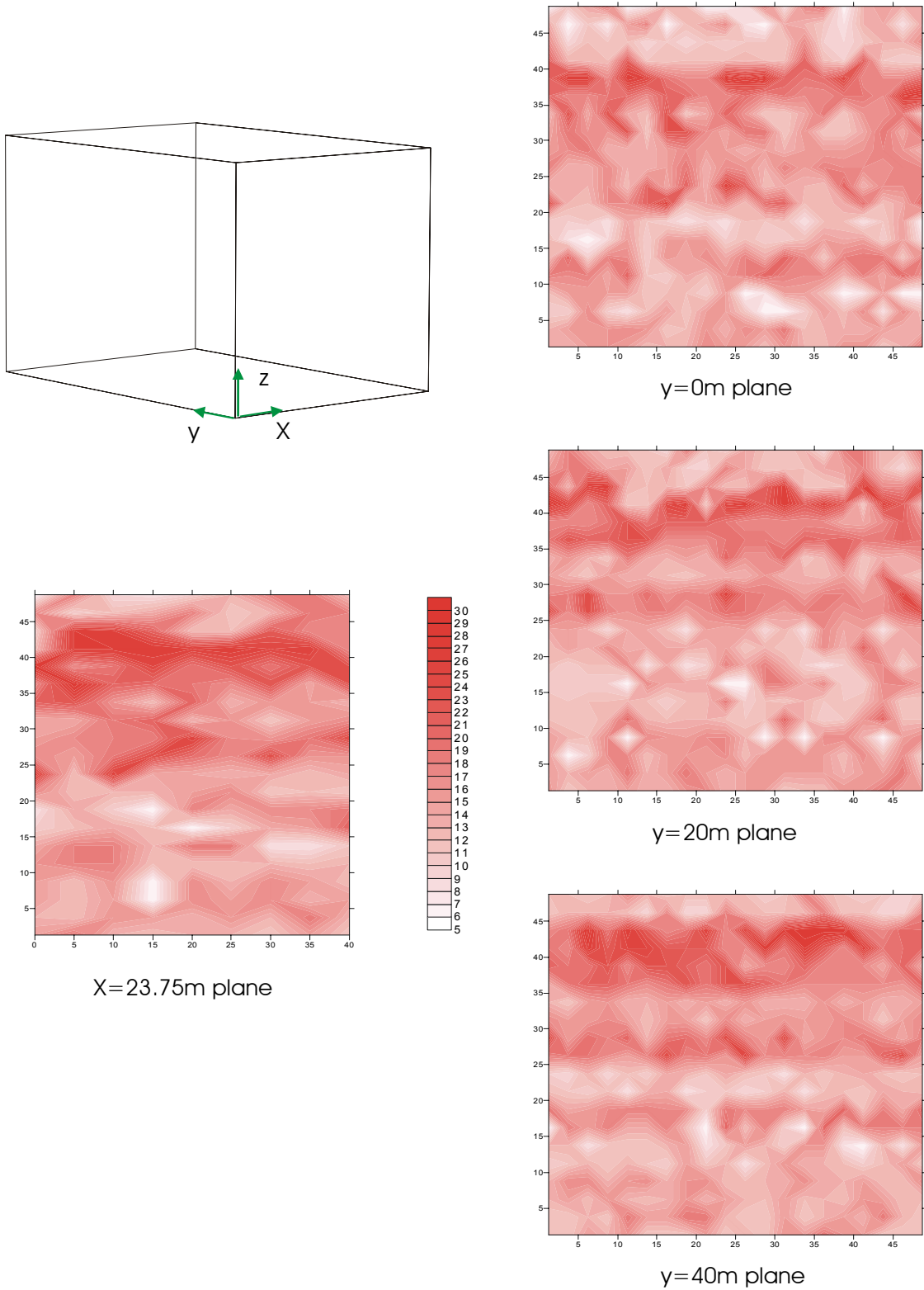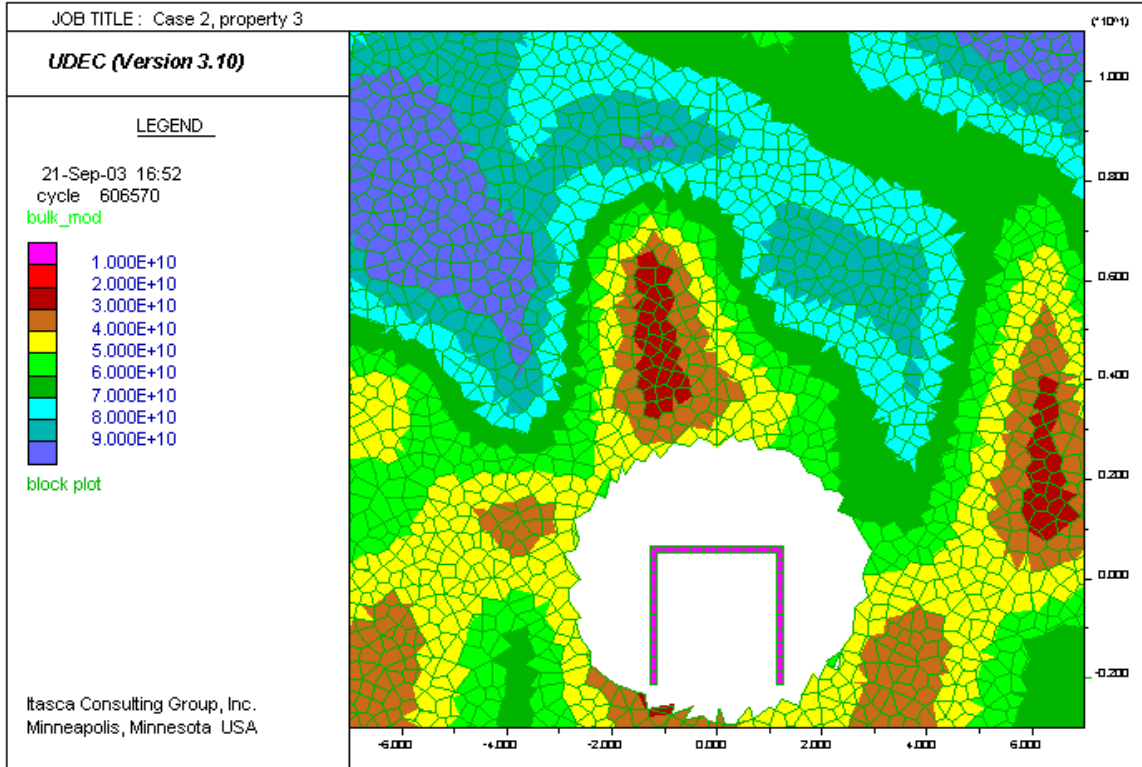
Source: *Drift Degradation Analysis* (BSC 2004 [DIRS 166107], Appendix S, Figure S-38, p. S-40)

Figure 6.7-6. Evolution of Damage Due to Strength Degradation for Category 2 − Tuff Best-Fit Static-Fatigue Curve

1 year

100 years

5 years

1000 years

10 years

10000 years
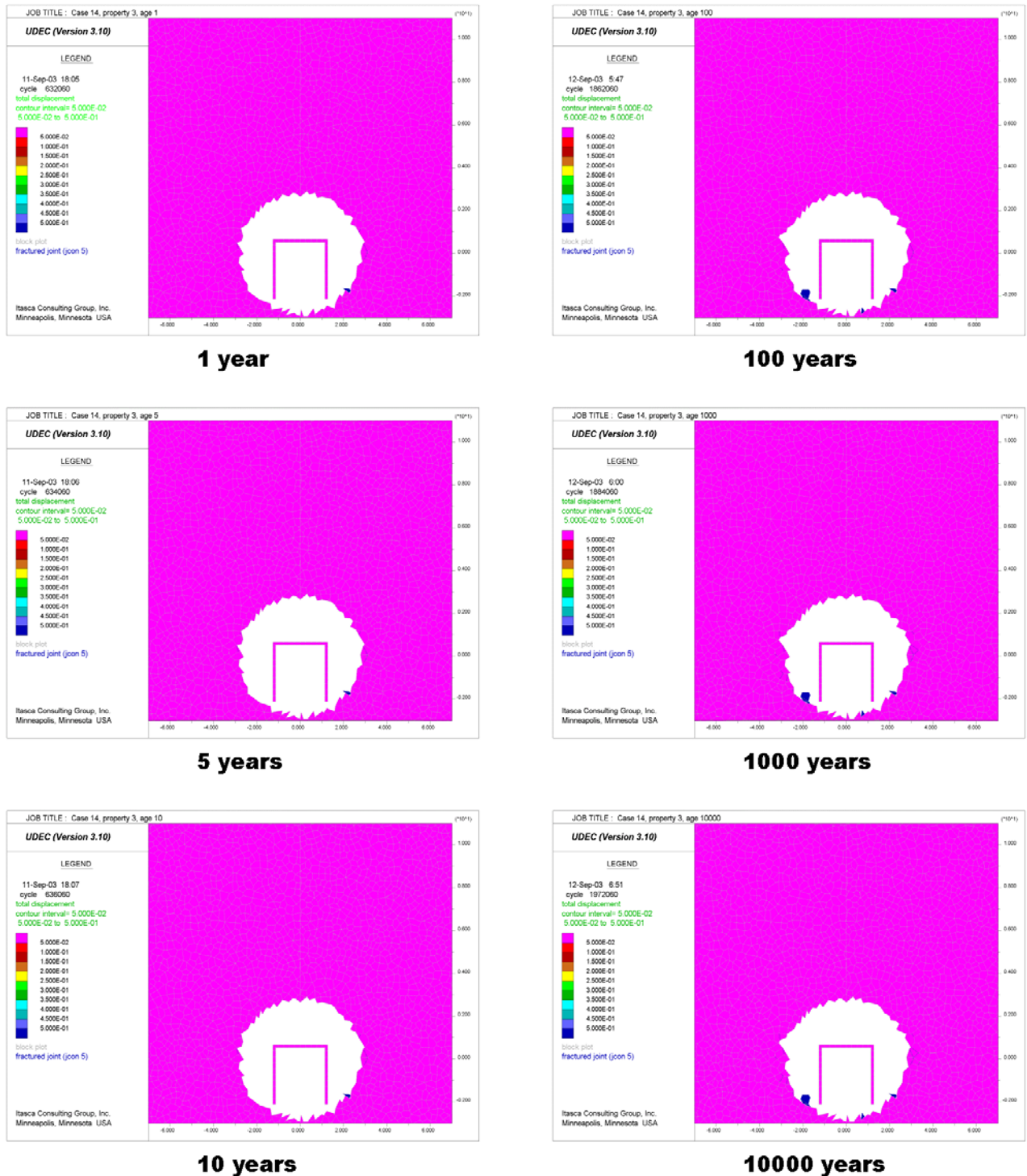
Source: *Drift Degradation Analysis* (BSC 2004 [DIRS 166107], Appendix S, Figure S-39, p. S-41)

Figure 6.7-7. Evolution of Damage Due to Strength Degradation for Category 3 – Tuff Best-Fit Static-Fatigue Curve

y=0m plane

y=20m plane

y=40m plane

X=23.75m plane

Source: *Drift Degradation Analysis* (BSC 2004 [DIRS 166107], Appendix S, Figure S-51, p. S-53)

NOTE: The y = 0 m, y = 20 m, and y = 40 m planes are cross sections 1, 2, and 3, respectively.

Figure 6.7-8. Porosity Contours in Cross Sections Through the 3D Simulated Porosity Field

Source: *Drift Degradation Analysis* (BSC 2004 [DIRS 166107], Appendix S, Figure S-52, p. S-54)

Figure 6.7-9. Distribution of Block Bulk Modulus Around Simulated Drift for Section 1
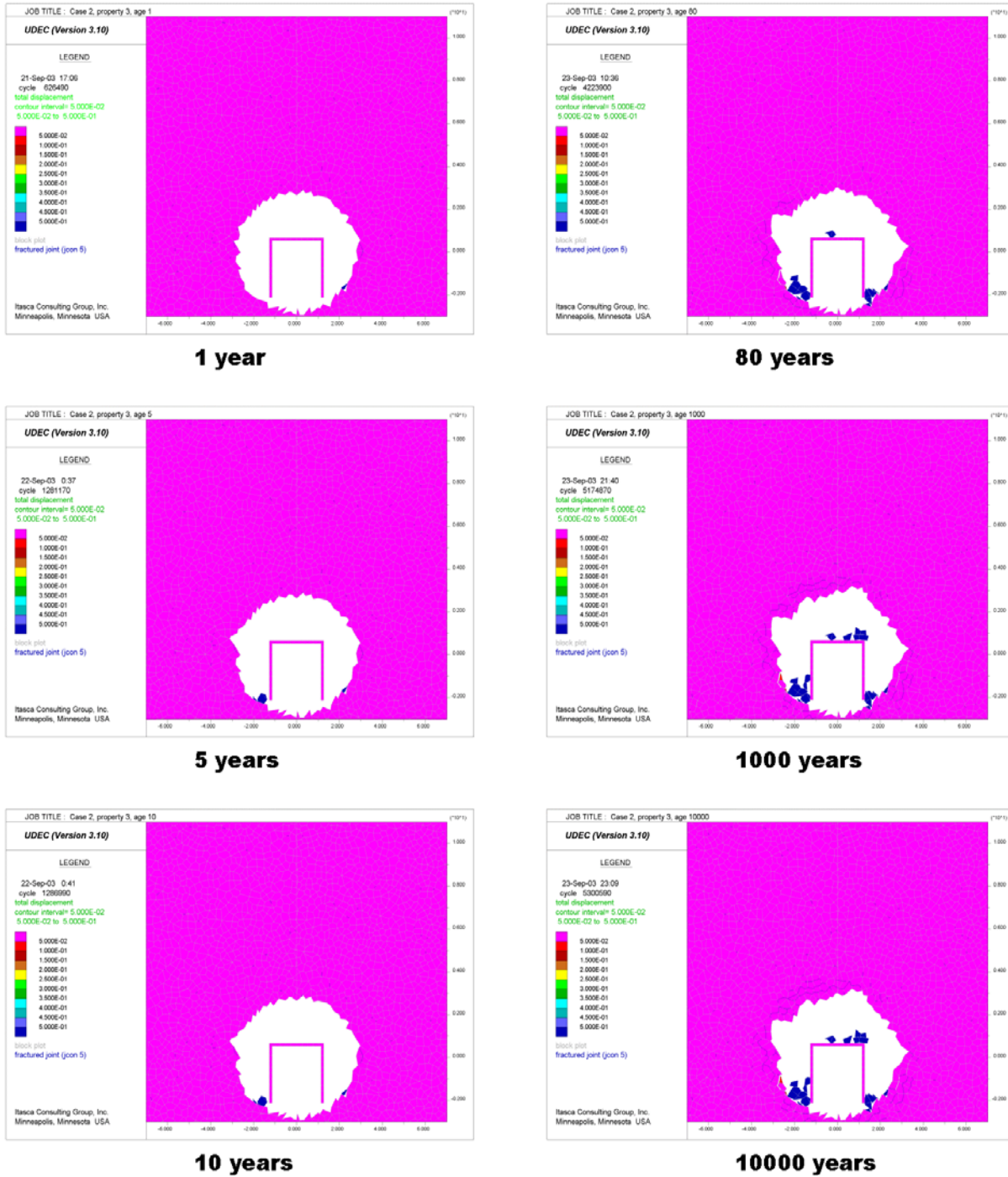
Source: *Drift Degradation Analysis* (BSC 2004 [DIRS 166107], Appendix S, Figure S-53, p. S-55)

Figure 6.7-10. Evolution of Damage Due to Strength Degradation and Thermal Load for Spatially Variable Properties, Section 1 − Tuff Best-Fit Static-Fatigue Curve

6.7.3   Rock Mass Properties from In Situ Field Tests

The mechanical field testing conducted in lithophysal rock consisted of a series of three pressurized slot tests. Details of these in situ tests are discussed in BSC 2003 [DIRS 166660], Section 8.7.4.3 and the associated DTNs are listed in Section 4.1.4. Each flatjack slot test was conducted on rock within either the Tptpll or Tptpul lithostratigraphic zones (Table 6.7-1). Slot test 1 was conducted in the ESF tunnel sidewall in poor quality Tptpll material characterized by large lithophysae and ubiquitous rock matrix fractures that is typical of the transition area between the Tptpmn and the Tptpll. Slot test 2 was conducted in the ESF tunnel sidewall of apparently good quality Tptpul. Slot test 3 was located in the floor of what was considered to be average Tptpll repository conditions in the ECRB Cross-Drift. All three tests included cycles of elastic loading and unloading at ambient rock temperature and slot test 2 included compressions at an elevated block temperature.

Table 6.7-1. Description of the In Situ Slot Tests Conducted in Lithophysal Rock

Slot Test	Location	Lithostratigraphic Unit	Temperature (°C)	Location
1	ESF 57+77	Tptpll	25	Wall
2	ESF 63+83 ESF 63+83	Tptpul Tptpul	25 heated to 90	Wall Wall
3	ECRB 21+25	Tptpll	25	Floor

Source: DTNs listed in Table 4-3

NOTE: Metric stationing is used throughout the ESF and ECRB Cross-Drift, so that Station 57+77 is located 5,777 m from the start of the tunnel.

The tests involved cutting two thin, parallel slots, separated by approximately 1.2 m, in the sidewall or floor of the tunnel (Figure 6.7-11). The lithophysal content from the face and slots of the blocks were mapped to estimate the size, shape, and percentage of block lithophysae and spots. The parallel saw cuts isolate approximately 1 to 2 m^3 of rock between them (Microsoft Excel file, *Rock Tendon Stress Calc.xls*, which can be found on the attached CD-ROM (Table B-1, Appendix B). Steel flatjack bladders were inserted into the slots and pressurized to load the sample in a state that approximates uniaxial compression (three "sides" of the rectangular sample are not free to shorten since they are part of the intact rock). The flatjack slots were excavated larger than the bearing plate area to minimize end effects due to block attachment to the surrounding solid rock. An instrumentation borehole (approximately 30.5 cm in diameter, Figures 6.7-11 and 6.7-12) was drilled in a central location between the slots to allow observation of the interior of the rock sample and to monitor deformations during the flatjack pressurization. During testing, the flatjacks' pressure was raised in a series of pressure cycles to monitor hysteresis effects and time-dependent strain at increasing levels of applied stress.
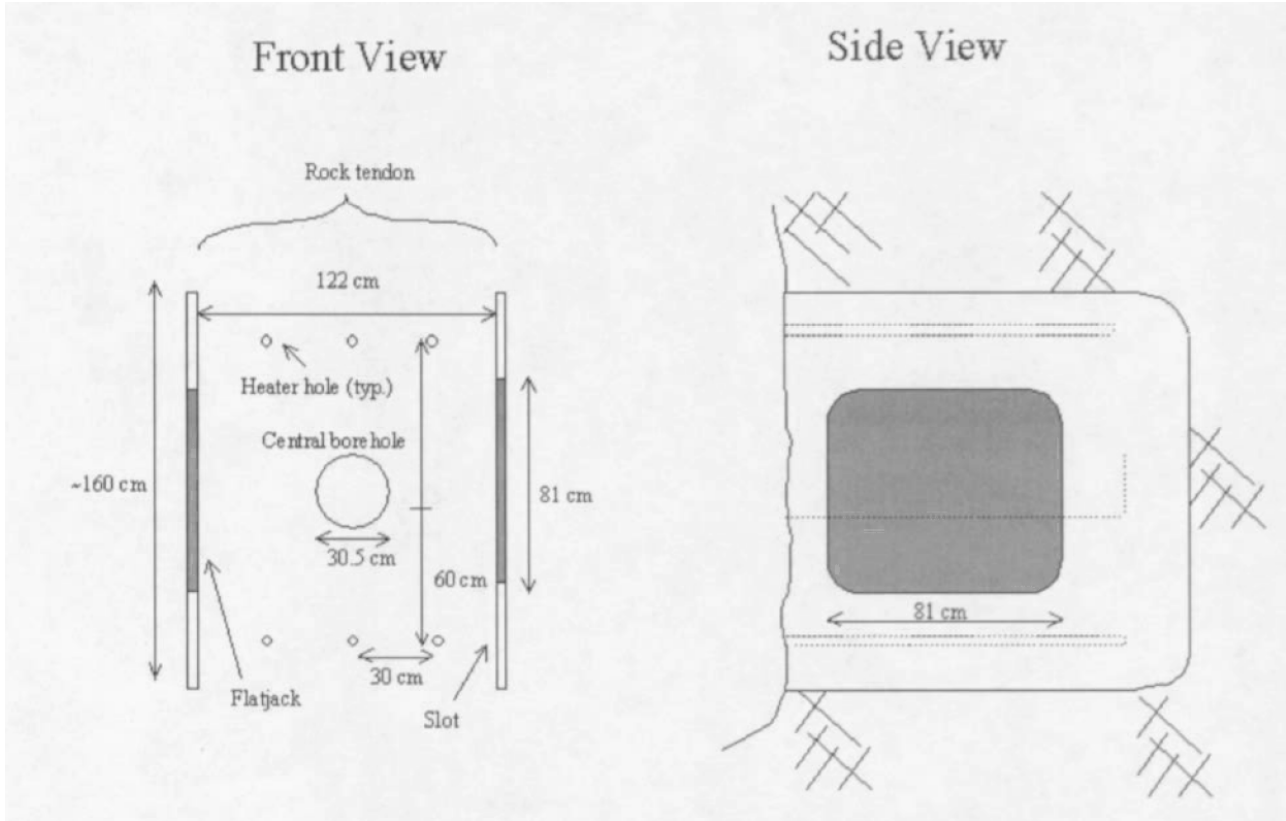
Source: DTN SN0212F4102102.004 (scientific notebook MOL.20030319.0040, Figure 1)

Figure 6.7-11. Typical Pressurized Slot Test Layout
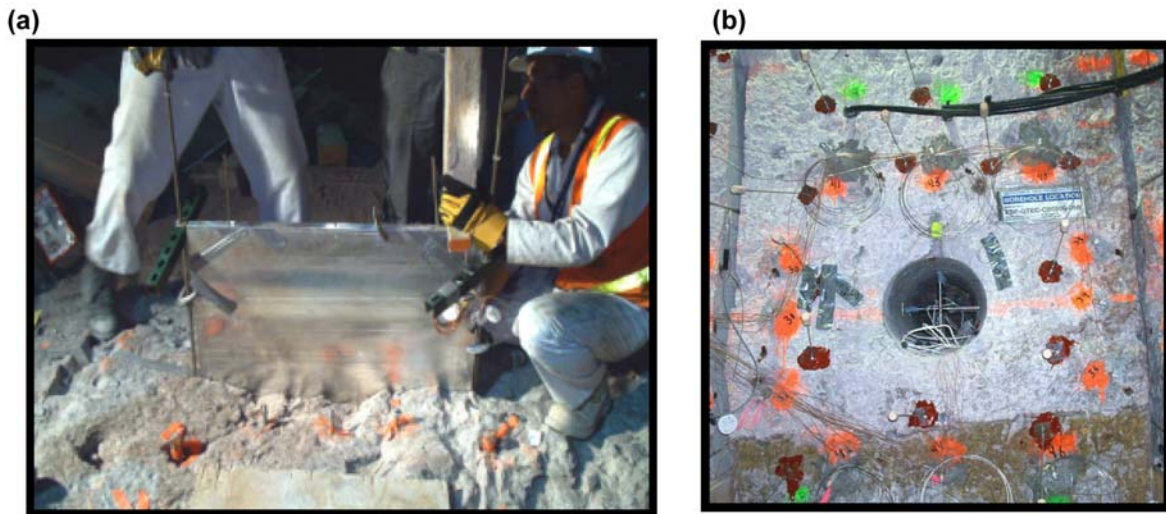
00387DC_015.ai

NOTE: Photograph (a) shows the lowering of a flatjack into place within the right sawcut slot. Photograph (b) shows the instrumentation of the central hole and the two parallel slots.

Figure 6.7-12. Photographs of (a) Preparation of Slot Test 3 in the Floor of the ECRB Cross-Drift (Tptpll) and (b) Slot Test 2 in the ESF wall (Tptpul)

Figure 6.7-13 shows flatjack pressure versus instrumentation hole diametral deformation for the three tests. The loading results show a typical elastic-plastic response in which a linear loading slope is followed by yield and plastic deformation. Yielding of the rock was typically in shear, emanating from the central borehole, and resulting in rockfall in the form of small rock particles in the central borehole during yield. The results, summarized in Table 6.7-2, show that the in situ deformation modulus is approximately 1.0 to 3.0 GPa (slot test 1, located in the poorest quality failed rock in the tunnel springline area, yielded a modulus of 0.5 GPa) and a Poisson's ratio of approximately 0.2 to 0.3. The tested lithophysal rock mass has an average deformation modulus that lies near the lower end of the design range given in Figure 6.6-5, which corresponds to rock mass category 1. The low values of modulus indicate that the skin of rock surrounding the tunnels, particularly at the sidewalls, is likely in a damaged state due to excavation effects induced by the tunnel boring machine.

No rock tendon failure stresses have been reported (only peak flatjack pressures). The failure results illustrate the difficulties with performing large in situ slot tests. Failure was induced near the top of the right platen in slot test 1, along a continuous fracture trace that developed through a series of preexisting but previously discontinuous fractures (Howard et al. 2003 [DIRS 166047], p. 377). Slot test 2 resulted in movement of a wedge block along a preexisting fracture that was located outside the rock tendon, without failing the block itself (Howard et al. 2003 [DIRS 166047], p. 379). Slot test 3 resulted in significant fracturing and vertical movement of rock in the tunnel floor possibly prior to actually failing the rock block between the flatjacks (DTN SN0301F4102102.006, MOL.20030319.0019, p. 32). It is estimated that the poor quality Tptpll rock of slot test 1 failed at approximately 5 MPa (Table B-1, Appendix B, Microsoft Excel file *Rock Tendon Stress Calc.xls*). Although the other slot tests likely did not fail the tendon blocks, the compressive stress at the end of the test in the blocks ranged from about 3 to 5 MPa (Table B-1, Appendix B, Microsoft Excel file *Rock Tendon Stress Calc.xls*).

Since the slot test results may illustrate the impact of excavation-related damage in the immediate sidewall of the tunnels, they may not necessarily be representative of the rock mass strength and elastic moduli. However, the tests do illustrate some component of the size effect present as sample size is increased from 0.3 m to approximately 1 m. It is estimated that the lithophysal porosity (including the instrumentation hole) is on the order of 20 percent for all three slot-test rock blocks (Table B-1, Appendix B, Microsoft Excel file *Rock Tendon Stress Calc.xls*). The available results are within the predicted range of Young's modulus and rock uniaxial compressive strength, but the values lie close to the lower bounds (Figures 6.6-1 and 6.6-2) and plot in the vicinity of lithophysal rock mass category 1 (Figure 6.6-5).
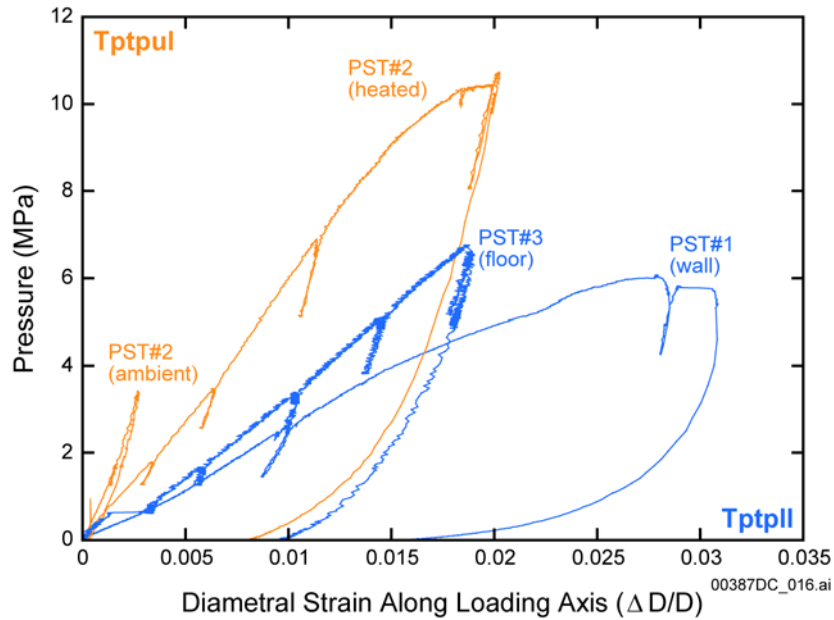
Source: DTN SN0208F4102102.002 (MOL.20021022.0151, Figure 7); DTN SN0212F4102102.004 (MOL.20030319.0040, Figures 7 and 9); DTN SN0301F4102102.006 (MOL.20030319.0019, Figure 7).

Figure 6.7-13. Composite of Flatjack Pressure versus Central Hole Diametral Strain for the Three Pressurized Slot Tests

Table 6.7-2. Summary of Mechanical Properties Results from the Pressurized Slot Tests

Slot Test	Rock Unit	Temperature (°C)	E (loading, GPa)	Poisson's Ratio	Estimated Lithophysal Porosity (%)
1	Tptpll	25	0.5 ± 0.3	0.2	12[a]
2	Tptpul	25	3.0 ± 0.5	0.2	13[a]
2	Tptpul	90	1.5 ± 0.5	0.2	13[a]
3	Tptpll	25	1.0 ± 0.3	0.33	8[a]

Source: DTNs listed in Table 4-3

NOTE: [a] Results do not account for presence of the large central hole, which may increase lithophysal porosity by 15 to 20 percent.

6.8   CONCLUSIONS FROM THE VALIDATION TESTS

The validation tests demonstrate the following:

- The mechanical model, implemented within the UDEC program has been calibrated against laboratory compression tests to reproduce the basic deformability and strength properties of the lithophysal rock.   To account for variability introduced by lithophysal porosity, lithophysal rock mass categories are used that cover the entire deformability and strength ranges.   The base model was calibrated to reproduce both the mean Young's modulus and uniaxial compressive strength for each of these categories.   The calibrated model is capable of reproducing the basic axial splitting fracturing and failure mode of lithophysal samples observed in laboratory uniaxial compression, while reproducing the proper compressive strength and elastic moduli.

- The calibrated model was applied to several boundary value problems to demonstrate reasonable ability to predict failure mode and failure extent observed in the field.   The model was applied to represent tunnel response of the ECRB Cross-Drift at various depths. Sidewall springline fracturing and yield occur in the model for the lower end of the calibrated strength range for depths of around 300 to 350 m.   The model predicts sidewall fracturing, parallel to the tunnel surface developing at the springline region and extending less than 1 m into the sidewall.   This agrees qualitatively to observations of springline fracturing in boreholes and alcoves observed in the lower lithophysal (Tptpll) exposures in the ECRB Cross-Drift and ESF main loop.   Observations show that wall-parallel fractures in the springline extend approximately 0.5 m in depth.   For the Tptpul, the UDEC models predict that minimal fracturing should be present, and underground observations confirm this prediction.   Although Tptpul rock is of the same general strength range as Tptpll rock, the shallower depth of burial results in stresses insufficient to fail the Tptpul rock mass.

- The model shows minimal fracturing for rock with lithophysal rock mass categories 2 or higher at the current time.   This is consistent with the typical condition within the ESF and ECRB Cross-Drift, which shows no observation of sidewall yield.   This observation is also consistent with the general lithophysal porosity determined from the detailed study of Tptpll rock along the ECRB Cross-Drift (Figure 6.4-8), showing that approximately 80 percent of the Tptpll rock is indicative of a rock mass category of 3 or higher, with about 94 percent of the rock classified as Category 2 and greater.   In other words, the small number of observations of sidewall spalling is consistent with the relatively infrequent occurrence of rock mass classified as category 1 or 2.

- The results of in situ field compressive tests (slot tests) of approximately 1 m size rock blocks resulted in values of Young's modulus and compressive strength that were within the predicted range of properties but near the lower bound of category 1 lithophysal rock mass. The values of Young's modulus and strength are low since the skin of rock surrounding the tunnels, particularly at the sidewalls, is likely in a damaged state due to excavation-induced stress and excavation effects induced by the tunnel boring machine.

7. SUMMARY AND CONCLUSIONS

The combined uncertainty and spatial variation of Young's modulus and uniaxial compressive strength for lithophysal rock of Topopah Spring Tuff has been estimated using laboratory and Yucca Mountain field data, and calibrated numerical models of simulated lithophysal rock. This combined uncertainty and spatial variation of lithophysal rock mass mechanical properties is high due to the limited amount of site-specific test data available. To suitably account for this large variability, the rock properties range has been subdivided into five rock mass categories that cover the entire range of expected deformability and strength. For each lithophysal rock mass category there corresponds an approximate range of lithophysal porosity, an estimated value of Young's modulus, and a bounded range of uniaxial compressive strength. These calculated rock mass properties are reasonable compared to the inputs used, and are realistically bounded. Additional numerical modeling, field observations, and in situ field-testing provide confidence in the estimated uncertainty and spatial variation of the parameters. The lithophysal rock mass properties documented in this report are suitable for their intended use in engineering design, preclosure safety analysis, and postclosure performance assessment, according to the guidelines provided below.

The mechanical behavior of lithophysal rock is found to strongly depend on rock porosity based on laboratory and numerical testing. A two-component conceptual model of lithophysal rock is adopted, consisting of rock matrix material and lithophysal cavities, and is used to determine the laboratory correlations between the mechanical parameters (Young's modulus and uniaxial compressive strength) and lithophysal porosity. Estimates of the uncertainty and spatial variability of lithophysal porosity at the repository scale are developed from field measurements and an assumption of stratiform geometry of rock zones (Tptpul and Tptpll). The expected ranges of in situ mechanical lithophysal rock properties are predicted using the characterized lithophysal porosity as a surrogate property.

For convenience five lithophysal rock mass categories are established with category 1 rock being mechanically weak (associated with high lithophysal porosity) and category 5 rock being relatively stiff and strong (associated with low lithophysal porosity). About 80 percent of repository rock is estimated to be of higher geomechanical quality (rock mass categories 3 and higher). The lower-quality rock categories 1 and 2 have a range of lithophysal porosity that are observed to occur in approximately 20 percent (6 percent for category 1 rock alone) of the measured sample of repository lithophysal rock. These areas of high porosity are observed to occur at approximately the meter scale, creating only localized pockets of mechanical weakness. In situ compressive tests of lithophysal rock mass at the meter scale resulted in properties near the predicted lower bound of rock mass category 1; the low values are considered to be a consequence of excavation-related damage in the immediate sidewall of the tunnels. Accordingly, these field test results are considered to be unrepresentative of the rock mass in the confined state away from the tunnel excavation disturbed zone. Numerical simulations of lithophysal tuff at the drift scale coupled with underground observations were used to establish and confirm a lower bound strength cutoff for category 1 to 3 rock mass.

The PFC and UDEC computer programs were calibrated to reproduce the basic compressive strength and elastic moduli as functions of lithophysal porosity as well as to provide a basic understanding of the mechanisms of deformation and yielding in this material. The introduction of voids within rock produces a distinctly different mechanical failure mechanism from that found in nonlithophysal rock. It was found that the primary strength-decreasing effect of the lithophysae is due to the formation of tensile splitting between neighboring lithophysae under uniaxial compressive load. Numerical modeling of tuff with no voids exhibits brittle behavior, but increasing lithophysal porosity results in an increasingly ductile post–peak response. This predicted failure mechanism and deformation response is consistent with observations of lithophysal rock fracturing observed in laboratory testing and underground. The transition from using circles to more realistic lithophysal shapes and void distributions result in greater variability in test results (particularly at low porosities) and a lower estimate of mean uniaxial compressive strength and Young's modulus. The variability is largely a function of the distribution of solid matrix length between lithophysae. The numerical models of laboratory uniaxial compressive strength tests were used to extrapolate the mechanical properties for lithophysal rock masses over the range of in situ conditions determined from the detailed field study of lithophysae in Tptpll rock. These generated data provide a more detailed estimate of the range of variability of the properties. Constitutive models of yielding for rock – Mohr-Coulomb and Hoek-Brown – were fit to the laboratory and model extrapolation data, and their strength parameters were determined. The PFC and UDEC modeling approach provides a viable methodology for simulating the mechanical response of welded lithophysal tuff to stressing and this tool is useful in studying the variability of material response in addition to laboratory and field testing.

Proper use of the rock mass category data from this calculation depends on a suitable choice of representative range of lithophysal porosity for the rock under consideration. The highly variable measurement of lithophysal porosity in lithophysal rock (especially vertically, Figure 1-2) contributes to highly variable mechanical behavior of the rock. An assumption of homogeneous rock properties at the drift scale requires that an appropriate value or range of lithophysal porosity be selected, the corresponding rock mass category be identified (from Table 6.6-2), and the entire range of mechanical properties associated with that rock mass category be considered. Use of only the baseline mean values of rock category mechanical properties will not reflect the spatial heterogeneity or range of parameters estimated in this calculation. Adopting a more realistic variation of lithophysal porosity at the meter to 5 m scale (e.g., the simulation in Appendix A) may require employing the bounding range data from multiple rock mass rock categories (as depicted in Figure 6.7-9) without using the limiting 10 MPa strength cutoff value for category 1 to 3 rock (Table 6.6-1). The confirmation activities of Section 6.7 further illustrate the proper use of rock mass category data of this calculation.

These estimates of mechanical rock parameters are not applicable to nonlithophysal rock mass, except for lithophysal subzones (Figure 1-2), since nonlithophysal rock typically has higher stiffness and compressive strength than those of category 5 lithophysal rock mass. The reported mechanical parameters and rock behavior described assume no effects of geochemical alterations to the rock that might significantly alter geomechanical rock mass properties. The property estimates of this calculation reflect the best current understanding of lithophysal rock behavior based on laboratory, field and numerical modeling.

Since the mechanical parameters estimated in this calculation are inputs to subsurface design, preclosure safety analysis, and postclosure performance assessment, these geotechnical parameters are candidates for performance confirmation. In this regard it is important to confirm the assumptions of Section 5 on which the parameter estimates depend. Furthermore, the relationship between porosity and mechanical behavior could be better understood by further numerical modeling of lithophysal rock to address the limitations stated in Section 6.5.8.

8. REFERENCES

8.1 DOCUMENTS CITED

165036 Board, M. 2003. *Resolution Strategy for Geomechanically-Related Repository Design and Thermal-Mechanical Effects (RDTME)*. REV 00. Las Vegas, Nevada: Bechtel SAIC Company. ACC: MOL.20030708.0153.

100653 Brodsky, N.S.; Riggins, M.; Connolly, J.; and Ricci, P. 1997. *Thermal Expansion, Thermal Conductivity, and Heat Capacity Measurements for Boreholes UE25 NRG-4, UE25 NRG-5, USW NRG-6, and USW NRG-7/7A*. SAND95-1955. Albuquerque, New Mexico: Sandia National Laboratories. ACC: MOL.19980311.0316.

102003 Brown, E.T., ed. 1981. *Rock Characterization Testing & Monitoring, ISRM Suggested Methods*. New York, New York: Pergamon Press. TIC: 209865.

159530 BSC (Bechtel SAIC Company) 2002. *Rock Properties Model Analysis Model Report*. MDL-NBS-GS-000004 REV 00 ICN 03. Las Vegas, Nevada: Bechtel SAIC Company. ACC: MOL.20020429.0086.

164670 BSC (Bechtel SAIC Company) 2003. *Heat Capacity and Thermal Expansion Coefficients Analysis Report*. ANL-NBS-GS-000013 REV 00. Las Vegas, Nevada: Bechtel SAIC Company. ACC: DOC.20030820.0002.

166660 BSC (Bechtel SAIC Company) 2003. *Subsurface Geotechnical Parameters Report*. 800-K0C-WIS0-00400-000-00A. Las Vegas, Nevada: Bechtel SAIC Company. ACC: ENG.20040108.0001.

165572 BSC (Bechtel SAIC Company) 2003. *Underground Layout Configuration*. 800-P0C-MGR0-00100-000-00E. Las Vegas, Nevada: Bechtel SAIC Company. ACC: ENG.20031002.0007.

164519 BSC (Bechtel SAIC Company) 2004. *D&E / PA/C IED Subsurface Facilities*. 800-IED-WIS0-00101-000-00A. Las Vegas, Nevada: Bechtel SAIC Company. ACC: ENG.20040309.0026.

168370 BSC (Bechtel SAIC Company) 2004. *D&E / PA/C IED Subsurface Facilities*. 800-IED-WIS0-00103-000-00A. Las Vegas, Nevada: Bechtel SAIC Company. ACC: ENG.20040309.0028.

166107 BSC (Bechtel SAIC Company) 2004. *Drift Degradation Analysis*. ANL-EBS-MD-000027 Rev. 03. Las Vegas, Nevada: Bechtel SAIC Company. ACC: DOC.20040915.0010.

170029 BSC (Bechtel SAIC Company) 2004. *Geologic Framework Model (GFM2000)*. MDL-NBS-GS-000002 REV 02. Las Vegas, Nevada: Bechtel SAIC Company. ACC: DOC.20040827.0008.

170137   BSC (Bechtel SAIC Company) 2004. *Peak Ground Velocities for Seismic Events at Yucca Mountain, Nevada.* ANL-MGR-GS-000004, Rev. 00. Las Vegas, Nevada: Bechtel SAIC Company. ACC: N/A

168361   BSC (Bechtel SAIC Company) 2004. *Q-List.* 000-30R-MGR0-00500-000-000 REV 00. Las Vegas, Nevada: Bechtel SAIC Company. ACC: ENG.20040721.0007.

169854   BSC (Bechtel SAIC Company) 2004. *Thermal Conductivity of the Potential Repository Horizon.* MDL-NBS-GS-000005 REV 01. Las Vegas, NV: Bechtel SAIC Company. ACC: DOC.20040928.0006.

169862   BSC (Bechtel SAIC Company) 2004. *Ventilation Model and Analysis Report.* ANL-EBS-MD-000030 , Rev. 04. Las Vegas, Nevada: Bechtel SAIC Company. ACC: DOC.20041025.0002.

169734   BSC (Bechtel SAIC Company) 2004. *Yucca Mountain Site Description.* TDR-CRW-GS-000001 REV 02 ICN 01. Two volumes. Las Vegas, Nevada: Bechtel SAIC Company. ACC: DOC.20040504.0008; Replacement for 168845.

101433   Buesch, D.C. and Spengler, R.W. 1998. "Character of the Middle Nonlithophysal Zone of the Topopah Spring Tuff at Yucca Mountain." *High-Level Radioactive Waste Management, Proceedings of the Eighth International Conference, Las Vegas, Nevada, May 11-14, 1998.* Pages 16-23. La Grange Park, Illinois: American Nuclear Society. TIC: 237082.

107236   Buesch, D.C. and Spengler, R.W. 1999. "Stratigraphic Framework of the North Ramp Area of the Exploratory Studies Facility, Yucca Mountain." *Hydrogeology of the Unsaturated Zone, North Ramp Area of the Exploratory Studies Facility, Yucca Mountain, Nevada.* Rousseau, J.P.; Kwicklis, E.M.; and Gillies, D.C., eds. Water-Resources Investigations Report 98-4050. Denver, Colorado: U.S. Geological Survey. ACC: MOL.19990419.0335.

165483   Buesch, D.C.; Beason, S.C.; and Spengler, R.W. 1999. "Relations Among Welding, Vapor-Phase Activity, Crystallization, and Fractures in the Tiva Canyon and Topopah Spring Tuffs, at Yucca Mountain, Nevada." *Abstracts with Programs - Geological Society of America, 31,* (7), A-476 - A-477. Boulder, Colorado: Geological Society of America. TIC: 254857.

101202   Buesch, D.C.; Nelson, J.E.; Dickerson, R.P.; Drake, R.M., II; Spengler, R.W.; Geslin, J.K.; Moyer, T.C.; and San Juan, C.A. 1996. *Distribution of Lithostratigraphic Units Within the Central Block of Yucca Mountain, Nevada: A Three-Dimensional Computer-Based Model, Version YMP.R2.0.* Open-File Report 95-124. Denver, Colorado: U.S. Geological Survey. ACC: MOL.19970618.0573.

100106   Buesch, D.C.; Spengler, R.W.; Moyer, T.C.; and Geslin, J.K. 1996. *Proposed Stratigraphic Nomenclature and Macroscopic Identification of Lithostratigraphic Units of the Paintbrush Group Exposed at Yucca Mountain, Nevada.* Open-File Report 94-469. Denver, Colorado: U.S. Geological Survey. ACC: MOL.19970205.0061.

104639   Byers, F.M., Jr.; Carr, W.J.; Orkild, P.P.; Quinlivan, W.D.; and Sargent, K.A. 1976. *Volcanic Suites and Related Cauldrons of Timber Mountain-Oasis Valley Caldera Complex,*

Southern Nevada. Professional Paper 919. Washington, D.C.: U.S. Geological Survey. TIC: 201146.

160705   Hoek, E. 2000. *[Practical] Rock Engineering, [2000 Edition].* Toronto, Ontario, Canada: RocScience. TIC: 253544.

162204   Hoek, E.; Carranza-Torres, C.; and Corkum, B. 2002. "Hoek-Brown Failure Criterion – 2002 Edition." [5th North American Rock Mechanics Symposium and 17th Tunnelling Association of Canada Conference: NARMS-TAC 2002, July 7-10, University of Toronto]. Toronto, Ontario, Canada: Rocscience. Accessed March 17, 2003. TIC: 253954. http://www.rocscience.com/Anon/ResearchPapers/NARMS.pdf

166047   Howard, C.L.; Schuhen, M.D.; George, J.T.; Lee, M.Y.; Taylor, R.S.; and Bronowski, D.R. 2003. "Rock-Mass Deformation Modulus Testing of Lithophysal Stratigraphic Units at the Yucca Mountain Project." *Soil and Rock America 2003, 12th Panamerican Conference on Soil Mechanics and Geotechnical Engineering, 39th U.S. Rock Mechanics Symposium, June 22-26, 2003, Cambridge, Massachusetts, USA.* Culligan, P.J.; Einstein, H.H.; and Whittle, A.J., eds. *1,* 375-380. Essen, Germany: Verlag Glückauf GmbH. TIC: 255152.

100773   Lipman, P.W.; Christiansen, R.L.; and O'Connor, J.T. 1966. *A Compositionally Zoned Ash-Flow Sheet in Southern Nevada.* Professional Paper 524-F. Washington, D.C.: U.S. Geological Survey. TIC: 219972.

149850   Mongano, G.S.; Singleton, W.L.; Moyer, T.C.; Beason, S.C.; Eatman, G.L.W.; Albin, A.L.; and Lung, R.C. 1999. *Geology of the ECRB Cross Drift - Exploratory Studies Facility, Yucca Mountain Project, Yucca Mountain, Nevada.* [Deliverable SPG42GM3]. Denver, Colorado: U.S. Geological Survey. ACC: MOL.20000324.0614.

102941   Price, R.H. 1983. *Analysis of the Rock Mechanics Properties of Volcanic Tuff Units from Yucca Mountain, Nevada Test Site.* SAND82-1315. Albuquerque, New Mexico: Sandia National Laboratories. ACC: NNA.19870406.0181.

106589   Price, R.H. 1986. *Effects of Sample Size on the Mechanical Behavior of Topopah Spring Tuff.* SAND85-0709. Albuquerque, New Mexico: Sandia National Laboratories. ACC: NNA.19891106.0125.

170894   Price, R.H. 2004. *The Mechanical Properties of Lithophysal Tuff: Laboratory Experiments.* TDR-EBS-MD-000027 REV 00. Las Vegas, Nevada: Bechtel SAIC Company. ACC: DOC.20040506.0001.

106590   Price, R.H. and Bauer, S.J. 1985. "Analysis of the Elastic and Strength Properties of Yucca Mountain Tuff, Nevada." *Research & Engineering Applications in Rock Masses, Proceedings of the 26th U.S. Symposium on Rock Mechanics, Rapid City, South Dakota, June 26-28, 1985.* Ashworth, E., ed. Pages 89-96. Boston, [Massachusetts]: A.A. Balkema. TIC: 218790.

100173   Price, R.H.; Connolly, J.R.; and Keil, K. 1987. *Petrologic and Mechanical Properties of Outcrop Samples of the Welded, Devitrified Topopah Spring Member of the Paintbrush Tuff.*

SAND86-1131. Albuquerque, New Mexico: Sandia National Laboratories. ACC: NNA.19870601.0013.

161290   Price, R.H.; Martin, R.J., III; Boyd, P.J.; and Noel, J.S. 1994. "Mechanical and Bulk Properties in Support of ESF Design Issues." *High Level Radioactive Waste Management, Proceedings of the Fifth Annual International Conference, Las Vegas, Nevada, May 22-26, 1994. 4,* 1987-1992. La Grange Park, Illinois: American Nuclear Society. TIC: 210984.

106602   Price, R.H.; Nimick, F.B.; Connolly, J.R.; Keil, K.; Schwartz, B.M.; and Spence, S.J. 1985. *Preliminary Characterization of the Petrologic, Bulk, and Mechanical Properties of a Lithophysal Zone Within the Topopah Spring Member of the Paintbrush Tuff.* SAND84-0860. Albuquerque, New Mexico: Sandia National Laboratories. ACC: NNA.19870406.0156.

100075   Sawyer, D.A.; Fleck, R.J.; Lanphere, M.A.; Warren, R.G.; Broxton, D.E.; and Hudson, M.R. 1994. "Episodic Caldera Volcanism in the Miocene Southwestern Nevada Volcanic Field: Revised Stratigraphic Framework, {superscript 40}Ar/{superscript 39}Ar Geochronology, and Implications for Magmatism and Extension." *Geological Society of America Bulletin, 106,* (10), 1304-1318. Boulder, Colorado: Geological Society of America. TIC: 222523.

104580   Sawyer, D.A.; Wahl, R.R.; Cole, J.C.; Minor, S.A.; Laczniak, R.J.; Warren, R.G.; Engle, C.M.; and Vega, R.G. 1995. *Preliminary Digital Geological Map Database of the Nevada Test Site Area, Nevada.* Open-File Report 95-0567. Denver, Colorado: U.S. Geological Survey. TIC: 232986.

107248   Schuraytz, B.C.; Vogel, T.A.; and Younker, L.W. 1989. "Evidence for Dynamic Withdrawal from a Layered Magma Body: The Topopah Spring Tuff, Southwestern Nevada." *Journal of Geophysical Research, 94,* (B5), 5925-5942. Washington, D.C.: American Geophysical Union. TIC: 225936.

144352   Sparks, R.S.J.; Bursik, M.I.; Carey, S.N.; Gilbert, J.S.; Glaze, L.S.; Sigurdsson, H.; and Woods, A.W. 1997. *Volcanic Plumes.* 574. New York, New York: John Wiley & Sons. TIC: 247134.

8.2   CODES, STANDARDS, REGULATIONS, AND PROCEDURES

156605   10 CFR 63. Energy: Disposal of High-Level Radioactive Wastes in a Geologic Repository at Yucca Mountain, Nevada. Readily available.

169575   AP-17.1Q, Rev. 3, ICN 2. *Records Management.* Washington, D.C.: U.S. Department of Energy, Office of Civilian Radioactive Waste Management. ACC: DOC.20040407.0004.

165065   AP-2.14Q, Rev. 3, ICN 0. *Document Review.* Washington, D.C.: U.S. Department of Energy, Office of Civilian Radioactive Waste Management. ACC: DOC.20030827.0018.

170665   AP-2.22Q, Rev. 1, ICN 1. *Classification Analyses and Maintenance of the Q-List.* Washington, D.C.: U.S. Department of Energy, Office of Civilian Radioactive Waste Management. ACC: DOC.20040714.0002.

168413   AP-3.12Q, Rev. 2, ICN 2. *Design Calculations and Analyses.* Washington, D.C.: U.S. Department of Energy, Office of Civilian Radioactive Waste Management. ACC: DOC.20040318.0002.

169267   AP-3.15Q, Rev. 4, ICN 4. *Managing Technical Product Inputs.* Washington, D.C.: U.S. Department of Energy, Office of Civilian Radioactive Waste Management. ACC: DOC.20040510.0004.

168062   AP-SIII.3Q, Rev. 2, ICN 1. *Submittal and Incorporation of Data to the Technical Data Management System.* Washington, D.C.: U.S. Department of Energy, Office of Civilian Radioactive Waste Management. ACC: DOC.20040226.0001.

168938   AP-SV.1Q, Rev. 1, ICN 1. *Control of the Electronic Management of Information.* Washington, D.C.: U.S. Department of Energy, Office of Civilian Radioactive Waste Management. ACC: DOC.20040308.0001.

166275   Canori, G.F. and Leitner, M.M. 2003. *Project Requirements Document.* TER-MGR-MD-000001 REV 02. Las Vegas, Nevada: Bechtel SAIC Company. ACC: DOC.20031222.0006.

171539   DOE (U.S. Department of Energy) 2004. *Quality Assurance Requirements and Description.* DOE/RW-0333P, Rev. 16. Washington, D.C.: U.S. Department of Energy, Office of Civilian Radioactive Waste Management. ACC: DOC.20040907.0002. Replacement for 171386

168412   LP-SI.11Q-BSC, Rev. 0, ICN 0. *Software Management.* Washington, D.C.: U.S. Department of Energy, Office of Civilian Radioactive Waste Management. ACC: DOC.20040225.0007

163274   NRC (U.S. Nuclear Regulatory Commission) 2003. *Yucca Mountain Review Plan, Final Report.* NUREG-1804, Rev. 2. Washington, D.C.: U.S. Nuclear Regulatory Commission, Office of Nuclear Material Safety and Safeguards. TIC: 254568.

8.3   SOURCE DATA, LISTED BY DATA TRACKING NUMBER

161910   GS021008314224.002. Lithophysal Data Study from the Tptpll in the ECRB from Stations 14+44 to 23+26. Submittal date: 01/28/2003.

163440   GS030483351030.001. Bulk Density, Rock-Particle Density, Porosity Properties of Core Samples of Spot, Rim & Matrix-Groundmass from 17 Boreholes in the Upper & Lower Lithophysal Zones of the Topopah Spring Tuff from the ESF & ECRB Cross Drift. Submittal date: 04/24/2003.

171367   GS040608314224.001. Large-Lithophysal Inventory Data from the Tptpll and Tptpln in the ECRB from Stations 14+44 to 25+35. Submittal date: 08/19/2004.

153777   MO0012MWDGFM02.002. Geologic Framework Model (GFM2000). Submittal date: 12/18/2000.

155271 MO0103COV01031.000. Coverage: BORES3Q. Submittal date: 03/22/2001.

166073 MO0311RCKPRPCS.003. Intact Rock Properties Data on Uniaxial and Triaxial Compressive Strength. Submittal date: 11/04/2003.

168901 MO0402DQRIRPPR.003. Intact Rock Properties Data on Poisson's Ratio and Young's Modulus. Submittal date: 02/19/2004.

171483 MO0408MWDDDMIO.002. Drift Degradation Model Inputs and Outputs. Submittal date: 08/31/2004.

165429 SN0207F4102102.001. Rock Modulus Slot Test #1, Location 57+70 in the ESF. Submittal date: 07/22/2002.

161874 SN0208F4102102.002. Rock Mass Mechanical Properties, Slot Test #1, Location 57+77 in the ESF. Submittal date: 08/27/2002.

161871 SN0208L0207502.001. Mechanical Properties of Lithophysal Tuff, Batch #1 (Test Dates: July 31, 2002 through August 16, 2002). Submittal date: 08/20/2002.

161872 SN0211L0207502.002. Mechanical Properties of Lithophysal Tuff, Batch #2 (Test Dates: October 22, 2002 through October 25, 2002). Submittal date: 11/13/2002.

165432 SN0212F4102102.003. Rock Modulus Slot Test #2, Location 63+83 in the ESF. Submittal date: 12/04/2002.

161875 SN0212F4102102.004. Rock Mass Mechanical Properties, Slot Test #2, Location 63+83 in the ESF. Submittal date: 12/17/2002.

165437 SN0301F4102102.005. Rock Modulus Slot Test #3, Location 21+25 in the ECRB. Submittal date: 01/08/2003.

161876 SN0301F4102102.006. Rock Mass Mechanical Properties, Slot Test #3, Location 21+25 in the ECRB. Submittal date: 01/14/2003.

165430 SN0301F4102102.007. Abundance of Lithophysal Features at Slot Test #1, Location 57+77 in the ESF. Submittal date: 01/23/2003.

165431 SN0301F4102102.008. Lithophysal Porosity Summary Report for Slot Test #1, Location 57+77 in the ESF. Submittal date: 01/23/2003.

165433 SN0302F4102102.009. Abundance of Lithophysal Features at Slot Test #2, Location 63+83 in the ESF. Submittal date: 02/14/2003.

165436 SN0302F4102102.010. Lithophysal Porosity Summary Report for Slot Test #2, Location 63+83 in the ESF. Submittal date: 02/14/2003.

165014 SN0302L0207502.003. Mechanical Properties of Lithophysal Tuff, Room Temperature Batch #4, Set 1 (Test Dates: 01/21/03 through 01/23/03). Submittal date: 02/25/2003.

165439 SN0303F4102102.011. Abundance of Lithophysal Features at Slot Test #3, Location 21+25 in the ECRB. Submittal date: 03/12/2003.

165440 SN0303F4102102.012. Lithophysal Porosity Summary Report for Slot Test #3, Location 21+25 in the ECRB. Submittal date: 03/12/2003.

165013 SN0305L0207502.004. Mechanical Properties of Lithophysal Tuff, Batch #4, Set 2 (Test Dates: March 5, 2003 through March 13, 2003). Submittal date: 05/01/2003.

163373 SN0305L0207502.005. Material Abundances from Point Counts on Laboratory Mechanical Property Specimens for Batch #1 and Batch #2. Submittal date: 05/20/2003.

165747 SN0305L0207502.006. Porosity of Laboratory Mechanical Properties Test Specimens for Batch #1 and Batch #2. Submittal date: 05/20/2003.

165015 SN0306L0207502.008. Revised Mechanical Properties of Welded Tuff from the Lower Lithophysal Zone of the Topopah Spring Tuff, Batch #3 (Test Dates: March 6, 2003 through April 18, 2003). Submittal date: 06/20/2003.

120572 SNL02030193001.001. Mechanical Properties Data for Drillhole USW NRG-6 Samples from Depth 22.2 ft. to 328.7 ft. Submittal date: 05/17/1993.

120575 SNL02030193001.002. Mechanical Properties Data for Drillhole USW NRG-6 Samples from Depth 22.2 ft. to 427.0 ft. Submittal date: 06/25/1993.

108415 SNL02030193001.004. Mechanical Properties Data for Drillhole USW NRG-6 Samples from Depth 462.3 ft. to 1085.0 ft. Submittal date: 08/05/1993.

108416 SNL02030193001.012. Mechanical Properties Data for Drillhole UE25 NRG-5 Samples from Depth 847.2 ft. to 896.5 ft. Submittal date: 12/02/1993.

109609 SNL02030193001.014. Mechanical Properties Data for Drillhole UE25 NRG-4 Samples from Depth 378.1 ft. to 695.8 ft. Submittal date: 01/31/1994.

120619 SNL02030193001.016. Mechanical Properties Data for Drillhole USW NRG-7/7A Samples from Depth 18.0 ft. to 472.9 ft. Submittal date: 03/16/1994.

109611 SNL02030193001.018. Mechanical Properties Data for Drillhole USW NRG-7/7A Samples from Depth 344.4 ft. Submittal date: 04/11/1994.

108431 SNL02030193001.019. Mechanical Properties Data for Drillhole USW NRG-7/7A Samples from Depth 507.4 ft. to 881.0 ft. Submittal date: 06/29/1994.

108432 SNL02030193001.020. Mechanical Properties Data for Drillhole USW NRG-7/7A Samples from Depth 554.7 ft. to 1450.1 ft. Submittal date: 07/25/1994.

159978 SNL02040687003.001. Mechanical Property Data to Analyze the Response of Samples of Unit TSW2 to High Temperature and/or Low Strain Rates. Submittal date: 09/30/1992.

159592 SNSAND80145300.000. Rock Mechanics Properties of Volcanic Tuffs from the Nevada Test Site. Submittal date: 01/04/1985.

160009 SNSAND83164600.000. Experimental Data of Fully Saturated and Wet Samples; Static Mechanical Properties of GU-3 760.9 Samples; Ultrasonic Velocity Data; and Dynamic Elastic Model of GU-3 760.9 Samples Compression Test. Submittal date: 04/24/1992.

160011 SNSAND84086000.000. Petrological, Mineralogical, Mechanical and Bulk Properties of Lithophysal Tuff. Submittal date: 04/24/1992.

160016 SNSAND84110100.000. Uniaxial and Triaxial Compression Test Series on Topopah Spring Tuff from USW G-4, Yucca Mountain, Nevada. Submittal date: 02/01/1986.

160020 SNSAND85070300.000. Uniaxial and Triaxial Compression Test Series on the Topopah Spring Member from USW G-2, Yucca Mountain, Nevada. Submittal date: 09/24/1987.

8.4   SOFTWARE

161950 BSC (Bechtel SAIC Company) 2002. *Software Code: PFC2D.* V2.0. PC WINDOWS 2000/NT 4.0. 10828-2.0-00.

160612 BSC (Bechtel SAIC Company) 2002. *Software Code: PFC3D.* V.2.0. PC. 10830-2.0-00.

161949 BSC (Bechtel SAIC Company) 2002. *Software Code: UDEC.* V3.1. PC WINDOWS 2000/NT 4.0. 10173-3.1-00.

172041 BSC (Bechtel SAIC Company) 2002. *Software Implementation Report for UDEC V3.1.* 10173-SIR-3.1-00. Las Vegas, Nevada: Bechtel SAIC Company. ACC: MOL.20021105.0245.

169930 BSC (Bechtel SAIC Company) 2004. *Software Code: PFC2D.* V 2.0. PC, Windows 2000. 10828-2.0-01.

169931 BSC (Bechtel SAIC Company) 2004. *Software Code: PFC3D.* V 2.0. PC, Windows 2000. 10830-2.0-01.

153526 CRWMS M&O 2000. *EARTHVISION V5.1, Validation Test Report Rev 00.* STN: 10174-5.1-00. Las Vegas, Nevada: CRWMS M&O. ACC: MOL.20000927.0145.

171619 DOE (U.S. Department of Energy) 2004. *Validation Test Process for: PFC2D V.2.0.* 10828-VTP-2.0-00. Las Vegas, Nevada: U.S. Department of Energy, Office of Repository Development. ACC: MOL.20040227.0057.

171620   DOE (U.S. Department of Energy) 2004. *Validation Test Process for: PFC3D V.2.0.* 10830-VTP-2.0-00. Las Vegas, Nevada: U.S. Department of Energy, Office of Repository Development. ACC: MOL.20040210.0639.

167994   Dynamic Graphics 2000. *Software Code: EARTHVISION.* V5.1. SGI/IRIX 6.5. 10174-5.1-00.

160331   Itasca Consulting Group. [2002]. *Itasca Software–Cutting Edge Tools for Computational Mechanics.* Minneapolis, Minnesota: Itasca Consulting Group. TIC: 252592.

9. APPENDICES

A list of Appendices is provided in Table 9-1, including the number, title, and total pages for each Appendix.

Table 9-1. List of Appendices

Appendix Letter	Appendix Title	Number of Pages
A	Simulation of Lithophysal Porosity Spatial Variation	18
B	Computer Files Supporting Calculation	4
C	Derivation of Data Reduction Formulae	4

APPENDIX A

SIMULATION OF LITHOPHYSAL POROSITY SPATIAL VARIATION

A.1   INTRODUCTION

More than 80 percent of the planned repository excavated openings are planned to be excavated within the lower lithophysal zone of the Topopah Spring Formation (BSC 2003 [DIRS 166660], Section 5.4, p. 5-20). To assist in modeling the spatial variability of mechanical properties, a simple method of projecting the measured two-dimensional distribution of lithophysal cavity porosity to a three-dimensional distribution surrounding the tunnels has been developed. This modeling calculation is limited to rock in the lower lithophysal zone of the Topopah Spring Tuff (Tptpll), and it is based on the data from the ECRB Cross-Drift (BSC 2003 [DIRS 166660], Attachment VII). Since the ECRB Cross-Drift is inclined and dips down through the repository host lithostratigraphic zones, the ECRB Cross-Drift study data represent one of the best and most detailed descriptions of lithophysal cavity porosity available for the Tptpll. This calculation involves the projection of the measured Tptpll lithophysae data to a vertical simulated cross section of the Tptpll extending laterally from the ECRB Cross-Drift. The vertical simulated cross section characterizes the observed structural vertical variability of lithophysae by using statistical "windows," and then calculates horizontal variation of lithophysae away from the ECRB Cross-Drift based on descriptive statistics of each "window."

Four steps are used for projecting lithophysal cavity porosity data from the ECRB Cross-Drift into a cross section that is perpendicular to the tunnel. A simplified summary of these four steps is described below and is in Figure A-1, with a detailed explanation (including specific examples) provided in Section A.6.

- Step 1. Lithophysal cavity porosity values are projected along the apparent dip of the lithostratigraphic unit to a vertical line representing a simulated stratigraphic column (Figure A-1a), and this vertical line forms the center of the cross section. This assumes lateral continuity of variations in lithophysal cavity porosity (the vertical variations of porosity are statistically identifiable and traceable across the repository area (assumption described in Section 5.1). Because the slope of the ECRB Cross-Drift is very gentle (about 5 degrees, Section A.5), it can be considered to be horizontal so the vertical line is in effect perpendicular to the tunnel. For simplicity, only the two points projecting to the top and bottom of the vertical line (VL) are depicted in Figure A-1a, but any point along the tunnel can be projected in a similar manner along the same apparent dip to the vertical line.

- Step 2. The simulated stratigraphic column (vertical line) is divided into a series of successive 5 m tall sections or horizons, and these sections are projected along the apparent dip to form stratigraphically equivalent "windows" along the tunnel (Figure A-1b). Each 5 m section along the vertical line is assumed to contain the potential variability in porosity in their respective "window" along the tunnel.

- Step 3. The distribution of measured lithophysal abundances and corresponding descriptive statistics are determined for each "window" and these statistics are imparted to the correlative section on the simulated stratigraphic column or vertical line (Figure A-1c).

- Step 4. The descriptive statistics for each section on the simulated stratigraphic column (vertical line) are then propagated along a horizon across the cross section (Figure A-1d). The two-dimensional horizon of lithophysal cavity porosity values is populated by randomly

selecting single porosity values from the respective window of measured data and assigning them to individual contiguous blocks that collectively constitute the simulated horizon.
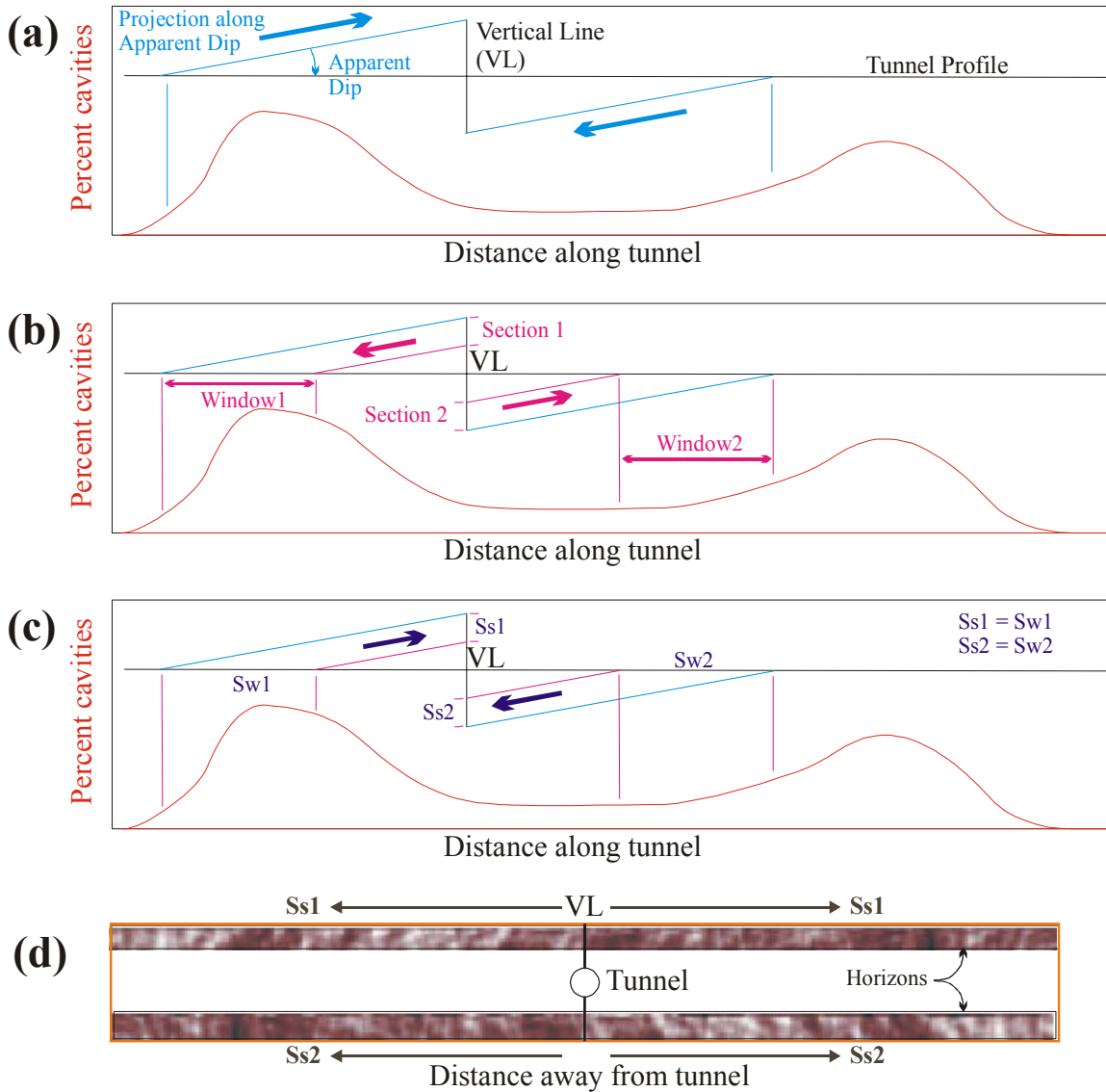
Figure A-1. Simplified Steps for Projecting and Distributing Lithophysal Cavity Porosity Values in a Tunnel into a Two-Dimensional Cross Section

A.2   INPUT DATA

The data required for the projection of lithophysal cavity porosity in a vertical cross section include (1) the distribution of the lithophysal cavity porosity along the ECRB Cross-Drift (BSC 2003 [DIRS 166660] Attachment VII) and (2) the approximate strike and dip of the top of the Tptpll in the ECRB Cross-Drift (Mongano et al. 1999 [DIRS 149850], Table 1, p. 12).

The particular distribution of the lithophysal cavity porosity used in this section comes from the "fitted" abundance curve for lithophysal cavities along the ECRB Cross-Drift, which is assumed to be representative of the actual rock conditions (Section 5.2). However, these data are preliminary since the large-lithophysae inventory has not been included as part of the "fitted" data.

A.3   SOFTWARE USED IN THE CALCULATIONS

The input data, intermediate calculations, and results of the assessment of the distribution of lithophysal cavity porosity are stored and implemented in the Microsoft Excel file "*Lithophysal projection to vertical plane.xls*" (Appendix B, Table B-1). All transfers of values, calculations, logic functions, and descriptive statistics are done with standard functions in Excel. There are three small macros embedded in the Excel file, named "Prop_Distribute," "Contour_Text," and "Contour_Fill." These macros are exempt from the qualification requirements of LP-SI.11Q-BSC [DIRS 168412], Software Management, since they are used solely for visual display of data:

1. The "Prop_Distribute" macro is an automated "copy and paste" function that takes the distributed values in a large (10×184 cell) "5 m window" table and makes a smaller (10×29 cell) "compacted" table of the values. The small table is effectively the large table, but with the "null" values removed.

2. The "Contour_Text" and "Contour_Fill" macros are basically the same and they simply change the format of the values or cells (but not the values themselves) in the 50×200 and 20×80 cell tables. The difference between these two macros is that one ("Contour_Text") colors the text (i.e., values), and the other ("Contour_Fill") changes the fill color of the cell and the color of the text (i.e., values).

3. Confirmation that the macros are operating correctly can be made with simple visual comparisons of the large and small tables for the "Prop_Distribute" macro, and the input data table with the 50×200 and 20×80 cell tables for the "Contour_Text" and "Contour_Fill" macros.

A.4 GEOMETRIC RELATIONS AND CONDITIONS IN THE CALCULATION

The simplifying assumptions used in this calculation relate to the inherent geometry of the problem and other initial conditions that need to be defined prior to carrying out the calculation. In particular, calculations of the distributed lithophysal cavity porosity in a vertical plane are based on six fundamental lithostratigraphic and geometric relations and conditions:

1. Lithostratigraphic zones and subzones (Figure 1-2) of the Topopah Spring Tuff are stratiform and are traceable across the repository area. However, some subzones might not occur across the entire repository area. In particular, this calculation assumes a stratiform distribution of Tptpll lithostratigraphic features, such as lithophysal cavity data (see assumption in Section 5.1).

2. The ECRB Cross-Drift transects the Tptpll as a shallowly inclined tunnel; therefore, the detailed study lithophysal cavity data represent vertical (and to some extent horizontal) variations in the lithostratigraphic features. The tunnel is assumed to be horizontal (Section A.1, Step 1).

3. Lateral continuity of variations in lithophysal-cavity porosity in the tunnel is projected along the apparent dip of the Tptpll to a vertical line that is perpendicular to the tunnel. The vertical line represents a simulated stratigraphic column for the sampled volume, and depending on the apparent dip, this along-the-tunnel projection distance can be as much as 311 m (for a 4.6º apparent dip).

4. The vertical line is divided into 5 m tall sections or "horizons," and these horizons are projected along the apparent dip to the tunnel to form a series of "windows" along the tunnel. The 5 m tall choice of the horizon is arbitrary.

5. Each 5 m horizon along the vertical line contains the potential variability in porosity of the respective "window" along the tunnel. Each "window" contains a unique sampling of lithophysal cavity porosity based on the population of tunnel measurements. The statistical variation of porosity in each horizon is obtained by sampling from the population of tunnel measurements (a realization of porosity).

6. The statistical variation in porosity in each 5 m tall horizon (portion of the simulated stratigraphic column) is projected away from the tunnel along a vertical cross section that is perpendicular to the tunnel. It is assumed that each perpendicular projection of porosity (realization) is translation invariant (the assumption of data stationarity).

A.5 DETERMINATION OF THE APPARENT DIPS FOR INPUT

The three-dimensional orientation of an inclined plane can be defined by a strike and dip, but an apparent dip is formed where the inclined plane intersects vertical planes along a section that is not at a right angle to the strike of the vertical plane. The strike is the angle from north of a horizontal line in the inclined plane, and the dip is the angle from horizontal measured in a vertical plane that is 90° to the strike of the inclined plane. An apparent dip is the angle from the horizontal in a vertical plane of a line formed by the intersection of an inclined plane with the vertical plane.

An example of these geometric relations is illustrated in Figure A-2 with three planes. The inclined plane is the top contact of the Tptpll in the ECRB Cross-Drift and has a strike of 270° (Mongano et al. 1999 [DIRS 149850], Table 1). The true dip is measured in a plane perpendicular to the strike of the inclined plane, and is illustrated with the 7° dip. The ECRB Cross-Drift is contained in a vertical plane that has a strike of 229°. This strike is used because it is in the direction of the heading of the tunnel and the lithostratigraphic contact is in the direction of the inclination or plunge of the tunnel. A cross section perpendicular to the ECRB Cross-Drift forms a second vertical plane with a strike of 319°. The apparent dip of the lithophysal zone contact is 4.6° to the northeast in the plane of the Cross Drift and 5.3° to the northwest in the cross section perpendicular to the ECRB Cross-Drift. If another strike and dip were used, then the apparent dips will differ. For example, accessing the Geologic Framework Model (BSC 2004 [DIRS 170029], Section 1) by using EarthVision Ver 5.1 [DIRS 167994] and the Geologic Framework Model data (DTN: MO0012MWDGFM02.002 [DIRS 153777]), the top of the Tptpll in the ECRB Cross-Drift has a strike and dip of 345° and 5.8°, respectively. The corresponding apparent dips are 5.2° northeast in the plane of the ECRB Cross-Drift and 2.5° northwest in the plane perpendicular to the ECRB Cross-Drift. For the purposes of this calculation, an apparent dip of 5° was used for projecting the data.
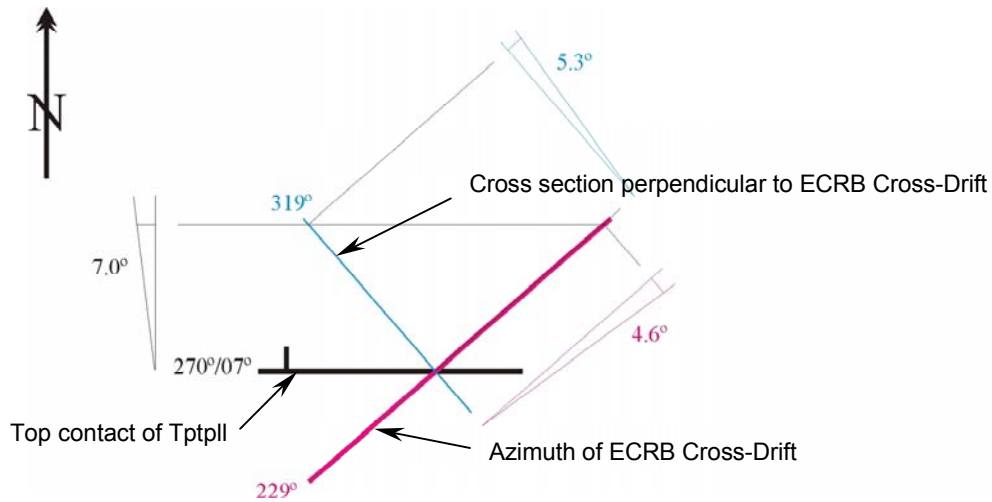
NOTES: The orientation of the Tptpll contact and the ECRB Cross-Drift is based on Mongano et al. (1999 [DIRS 149850], Table 1). The ECRB Cross-Drift is considered to be horizontal.

Figure A-2. Geometric Relations of Strike and Dip and the Apparent Dips in Cross Sections Parallel and Perpendicular to the ECRB Cross-Drift

A.6 DISTRIBUTION OF LITHOPHYSAL CAVITY POROSITY IN THE ECRB CROSS-DRIFT AND SIMULATED VERTICAL CROSS SECTION

The stratiform geometry of the zones and many subzones in the Topopah Spring Tuff occur throughout the repository area (see discussion in Section 5.1). The lower lithophysal zone has not been formally divided into subzones (Figure 1-2), but the variations in features including the lithophysal cavity porosity are consistent with identification of 5 to 12 subzones (Figure A-3).

The lateral continuity of lithostratigraphic features, and the projection of these features along the apparent dip in the ECRB Cross-Drift, forms the principal component of creating a geologically informed calculation of the distribution of lithophysal cavity porosity in a vertical plane. Identification of a 50 m tall, vertical line (section) perpendicular to the tunnel is the first step in creation of the 50×200 m cross section (Figure A-3). Based on the apparent dip, the top and bottom of the vertical section can represent rocks located several hundred meters or more away from the centerline of the section. For example, with a 5° apparent dip, the equivalent rocks at the top and bottom of the vertical section extend 286 m from either side of the vertical section (Figure A-3). With an apparent dip of 4.6° (Figure A-2), the projection from the vertical section for the top and bottom of vertical section is 311 m. This projection distance is consistent with the overall stratiform characteristics of the lithostratigraphic section.

The second step in creation of a cross section is to divide the vertical section into a series of 5 m tall sections or horizons. The projection along the apparent dip of the 5 m horizons result in a series of "windows" along the tunnel, and the position and length of each window results from the apparent dip. For example, with a 5° apparent dip, the equivalent window for the top 5 m horizon is 57 m long (Figure A-3). Each window contains unique variations in the number of measurements and the distribution of lithophysal cavity porosity values (Table A-1 and Figure A-4).

The third step in creation of a simulated cross section is to distribute the descriptive statistics of the lithophysal cavity porosity in each window in the associated 5 m tall horizon. The statistical variation in porosity in each horizon is represented by sampling the actual porosity values in the respective "window." Two methods using standard Excel functions have been used for this distribution; one function is "Choose" where the values in each window are randomly selected, and the other approach uses the random number generator in the analysis tool. For example, the first three 5 m horizons (0-5, 5-10, and 10-15 windows) in Table A-1 are depicted as Horizons 0, 5, and 10 and Y positions 1 to 15, respectively, in Tables A-2 and A-3. Comparison of values in Table A-1 and parts of Tables A-2 and A-3 indicate the same values occur in all tables.
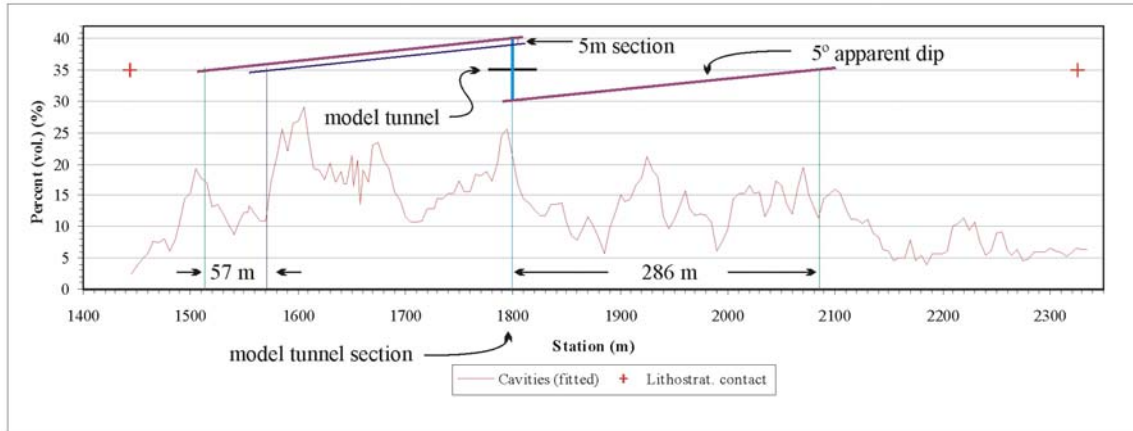
NOTE: The simulated cross section is at station 18+00 with an apparent dip of 5° for the stratiform features.

Figure A-3. Variation in Lithophysal Cavity Porosity along the ECRB Cross-Drift and the Geometric Relations of Calculation Components
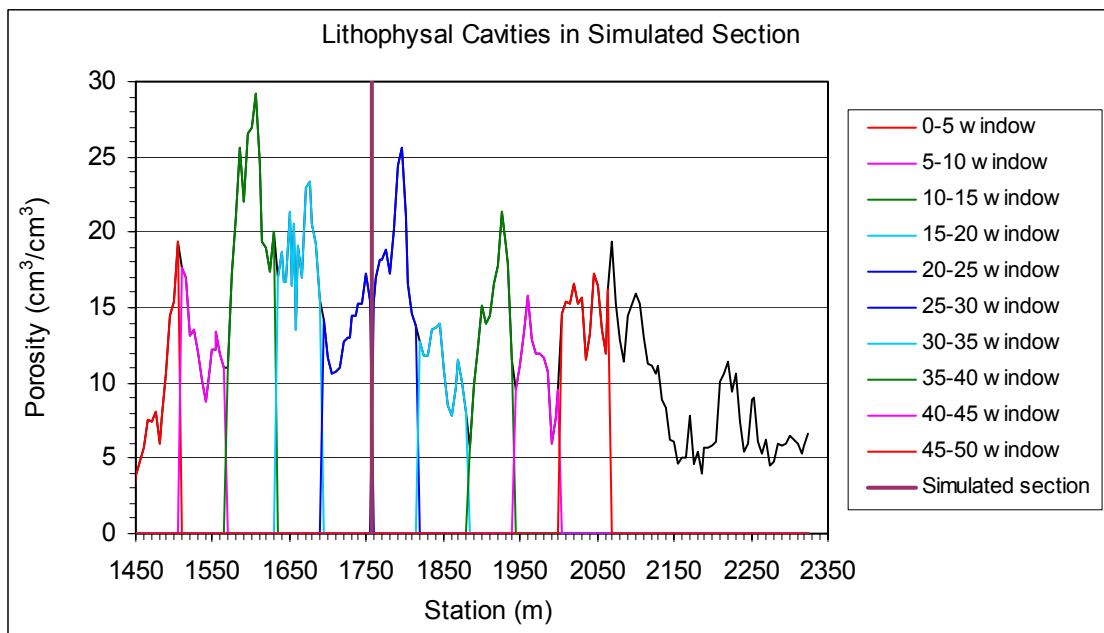
Source: Appendix B, Table B-1, Microsoft Excel file "*Lithophysal projection to vertical plane.xls*," worksheet "Window calculations."

Figure A-4. Lithophysal Cavity Porosity in the Lower Lithophysal Zone of the ECRB Cross-Drift with the Centerline of the Simulated Cross Section at Station 17+56 (Apparent Dip of 4.6°, and 10 "Windows")

Table A-1. Windows of Unique Variations of Lithophysal Cavity Porosity Values

Station (m)	Cavity "fitted"	0-5 Window	5-10 Window	10-15 Window	15-20 Window
1445	2.5	null	null	null	null
1450	3.8	3.8	null	null	null
1455	4.7	4.7	null	null	null
1460	5.7	5.7	null	null	null
1465	7.6	7.6	null	null	null
1470	7.4	7.4	null	null	null
1475	8.2	8.2	null	null	null
1480	6.0	6.0	null	null	null
1485	7.9	7.9	null	null	null
1490	10.6	10.6	null	null	null
1495	14.4	14.4	null	null	null
1500	15.3	15.3	null	null	null
1505	19.4	19.4	null	null	null
1510	17.7	null	17.7	null	null
1515	17.0	null	17.0	null	null
1520	13.2	null	13.2	null	null
1525	13.6	null	13.6	null	null
1530	12.1	null	12.1	null	null
1535	10.2	null	10.2	null	null
1540	8.8	null	8.8	null	null
1545	11.0	null	11.0	null	null
1550	12.2	null	12.2	null	null
1552.8	12.2	null	12.2	null	null
1555	13.4	null	13.4	null	null
1560	12.0	null	12.0	null	null
1565	11.0	null	11.0	null	null
1570	11.0	null	null	11.0	null
1575	17.2	null	null	17.2	null
1580	21.0	null	null	21.0	null
1585	25.6	null	null	25.6	null
1590	22.1	null	null	22.1	null
1595	26.5	null	null	26.5	null
1600	26.9	null	null	26.9	null
1605	29.2	null	null	29.2	null
1610	24.6	null	null	24.6	null
1615	19.3	null	null	19.3	null
1620	19.0	null	null	19.0	null
1625	17.4	null	null	17.4	null
1630	20.1	null	null	20.1	null
1635	17.0	null	null	null	17.0
1640	18.8	null	null	null	18.8

NOTES: This table shows a portion of the lithophysal cavity porosity input data that are divided into windows representing 5 m tall horizons in the simulated cross section. The "Cavity (fitted)" column provides adjusted measured lithophysal porosity values as described in BSC 2003 [DIRS 166660], Attachment VII (Section VII.5). Porosity values for each window are depicted in BSC 2003 [DIRS 166660], Figure 9-45. Data in the "Station (m)" and "Cavity (fitted)" columns are from BSC 2003 [DIRS 166660], Attachment VII (Section VII.6.6; see Attachment VIII, Microsoft Excel file, *Drift Deg AMR AF T-A-P Fit V1.xls*, worksheet "Volume Percent - Stats" or which can also be accessed using DTN: \MO0408MWDDDMIO.002). These data are for a calculation with a centerline of the simulated cross section at station 17+56 and an apparent dip of 4.6°.

The fourth step in creation of a simulated vertical cross section is to project the 5 m horizons in the vertical section away from the vertical section to create the cross section. For a 200 m wide cross section, the projection away from the central vertical section is 100 m to either side. In this construct, the maximum "straight line" projection distance for an apparent dip of 4.6° and an along-the-tunnel projection of 311 m is only 327 m. This projection distance is consistent with the overall stratiform characteristics of the lithostratigraphic section. Figure A-5 displays two simulations of a 50×200 m cross section using a 4.6° apparent dip, one for a center of the section at 1756 m and a second for a center at 2014 m. In these simulations, there is an overlap of 364 m along the tunnel and when projected to the vertical plane it represents an overlap of about 30 m of section (Figure A-5). Each simulation is depicted with a 50×200 cell table representing a 1×1 m grid (sections A and C) and a 20×80 cell table representing a 2.2×2.5 m grid (sections B and D). All four sections in Figure A-5 display similar stratiform relations.

Descriptive statistics (from standard Excel functions) for the input data in the various windows (Table A-4) with the selected statistics from 5 m tall horizons in the 50×200 and 20×80 cell tables indicate very good correlations. The descriptive statistics (from standard Excel functions) of the total Tptpll zone in the ECRB Cross-Drift is provided in Table A-4 (first column of values). Descriptive statistics for the total windows in the ECRB Cross-Drift (input) data and the total 50×200 and 20×80 cell tables indicate very high correlations (Table A-5). These correlations reinforce the technical soundness of this approach to project the distribution of lithophysal cavity porosity from the cross section data to a vertical plane.

Table A-2. Display of Part of the 50×200 Cell Table with Descriptive Statistics for Calculation of Lithophysal Cavity Porosity in a 50×200 m Simulated Cross Section with the Centerline Station 17+56

Table of porosity values (1×1 m grid)											
Horizon	Cell $_Y$\$^X$	1	2	3	4	5	6	7	8	9	10
0	1	7.6	4.7	19.4	7.6	8.2	8.2	10.6	7.6	7.9	3.8
0	2	6.0	7.4	8.2	19.4	7.9	10.6	14.4	7.9	15.3	7.9
0	3	6.0	15.3	15.3	7.9	7.4	6.0	4.7	3.8	15.3	7.6
0	4	10.6	10.6	10.6	7.9	3.8	3.8	19.4	7.9	7.6	7.6
0	5	8.2	15.3	7.9	10.6	5.7	8.2	7.4	6.0	7.9	7.6
5	6	13.2	11.0	17.7	11.0	17.7	10.2	12.2	12.1	12.2	12.2
5	7	11.0	12.1	12.2	10.2	12.2	8.8	12.2	11.0	12.2	12.0
5	8	12.2	13.6	12.0	12.2	11.0	8.8	12.1	12.2	11.0	12.0
5	9	17.7	13.6	10.2	17.0	10.2	17.0	8.8	11.0	12.2	10.2
5	10	12.2	12.2	12.1	11.0	12.2	10.2	13.4	12.2	13.2	17.7
10	11	26.5	26.9	22.1	25.6	19.0	21.0	17.2	26.9	17.2	26.9
10	12	11.0	26.5	24.6	26.9	19.0	29.2	19.0	21.0	17.2	19.0
10	13	24.6	17.4	26.9	19.0	19.0	19.0	19.3	29.2	25.6	17.4
10	14	17.4	26.5	17.2	17.2	24.6	21.0	26.9	26.5	20.1	26.9
10	15	22.1	17.2	19.0	17.4	26.9	26.9	21.0	11.0	17.2	21.0
15	16	18.8	16.5	13.6	20.5	20.5	22.9	21.4	20.6	16.5	20.6
15	17	16.8	15.5	22.9	20.5	16.5	17.0	13.6	19.1	13.6	17.0
15	18	20.6	19.3	15.5	17.0	17.0	19.3	20.6	19.1	16.8	17.0
15	19	20.5	13.6	23.4	16.8	23.4	16.8	20.6	22.9	15.5	20.5
15	20	23.4	21.4	19.3	15.5	16.8	21.4	20.5	17.0	21.4	17.0
20	21	10.7	15.5	13.0	15.5	11.0	15.3	15.3	15.3	12.8	15.3
20	22	13.0	14.5	17.3	11.0	11.7	13.0	17.3	14.5	10.6	10.6
20	23	15.5	15.3	11.7	15.3	14.2	14.5	10.6	14.5	10.6	11.0
20	24	15.3	14.5	15.5	13.0	15.5	15.3	11.7	14.5	13.0	10.7
20	25	10.7	10.6	11.0	15.5	11.0	14.5	15.3	11.0	15.3	14.5
25	26	16.9	24.5	17.3	20.1	18.1	15.5	20.1	18.1	13.8	13.8
25	27	18.1	25.6	14.5	17.3	18.1	20.1	21.1	17.3	14.5	14.5
25	28	17.3	15.5	18.8	18.1	17.3	21.1	17.3	18.8	17.3	18.1
25	29	20.1	20.1	18.1	24.5	18.8	21.1	18.1	13.8	18.1	21.1
25	30	18.1	18.1	15.5	18.1	13.8	18.1	14.5	24.5	18.1	21.1
30	31	12.7	13.5	8.5	12.7	13.5	8.5	8.5	12.7	11.6	10.0
30	32	8.1	11.8	10.8	13.9	13.9	13.5	13.9	7.8	8.1	8.5
30	33	9.7	12.7	9.7	9.7	10.8	10.0	11.8	13.9	9.7	11.6
30	34	13.5	10.0	11.8	13.6	13.6	7.8	13.6	13.9	11.6	11.8
30	35	7.8	10.0	10.8	13.6	10.0	8.5	13.6	7.8	10.8	8.5
35	36	12.3	19.1	21.3	12.3	17.8	12.3	13.9	15.2	5.7	21.3
35	37	15.2	5.7	12.3	16.6	13.9	12.3	14.4	5.7	16.6	17.8
35	38	19.1	5.7	5.7	19.1	11.6	15.2	14.4	18.0	18.0	18.0
35	39	21.3	13.9	12.3	19.1	12.3	13.9	17.8	16.6	18.0	15.2
35	40	15.2	13.9	9.8	19.1	15.2	17.8	16.6	9.8	16.6	16.6

(NOTE: Table continued on next page)

Table A-2. Display of Part of the 50×200 Cell Table with Descriptive Statistics for Calculation of Lithophysal Cavity Porosity in a 50×200 m Simulated Cross Section with the Centerline Station 17+56 (Continued)

Table of porosity values (1×1 m grid)

Horizon	Cell $_Y$\$^X$	1	2	3	4	5	6	7	8	9	10
40	41	10.7	10.7	12.9	11.1	13.3	7.7	15.8	9.6	7.7	11.7
40	42	7.7	13.3	10.7	13.3	10.7	10.7	11.9	15.8	6.0	11.1
40	43	7.7	11.9	11.7	9.6	6.0	12.9	15.8	11.7	13.3	12.9
40	44	11.9	6.0	7.7	10.7	11.1	11.9	12.9	12.9	12.9	11.1
40	45	15.8	9.6	12.9	9.6	6.0	12.9	11.1	11.9	7.7	7.7
45	46	12.0	16.5	17.3	17.3	16.3	16.3	13.2	15.3	16.3	11.6
45	47	13.5	12.0	11.6	13.2	16.6	11.6	15.6	15.3	15.3	13.5
45	48	15.6	12.0	15.3	15.6	16.6	15.2	16.6	13.5	15.3	15.6
45	49	12.0	15.3	17.3	15.3	16.3	16.3	13.2	17.3	11.6	14.5
45	50	16.3	16.3	13.5	13.2	17.3	13.2	16.6	15.2	16.6	13.5

Descriptive Statistics

Simulated "X" position	1	2	3	4	5	6	7	8	9	10
Mean	14.4	14.6	14.5	15.2	14.2	14.5	15.2	14.5	13.8	14.3
Standard Error	0.7	0.7	0.7	0.6	0.7	0.8	0.6	0.8	0.6	0.7
Median	13.5	13.9	13.2	15.4	13.9	14.2	14.5	14.2	13.7	13.6
Mode	6.0	15.3	15.5	19.1	11.0	8.2	12.2	14.5	12.2	7.6
Standard Deviation	5.0	5.3	4.8	4.5	4.9	5.3	4.2	5.5	4.1	5.0
Sample Variance	24.6	28.1	22.6	20.0	23.8	28.6	17.2	30.7	17.1	25.2
Kurtosis	-0.4	0.4	-0.1	0.1	0.2	0.2	0.5	0.4	0.2	0.1
Skewness	0.4	0.6	0.6	0.5	0.2	0.5	0.2	0.6	0.1	0.5
Range	20.5	22.2	21.2	19.3	23.1	25.4	22.2	25.4	19.9	23.1
Minimum	6.0	4.7	5.7	7.6	3.8	3.8	4.7	3.8	5.7	3.8
Maximum	26.5	26.9	26.9	26.9	26.9	29.2	26.9	29.2	25.6	26.9
Sum	720.3	731.0	726.9	758.6	711.3	723.6	758.2	727.1	689.7	715.6
Count	50	50	50	50	50	50	50	50	50	50
Confidence Level (95.0%)	1.4	1.5	1.3	1.2	1.4	1.5	1.2	1.5	1.1	1.4

Explanation of symbols (percent lithophysal cavity porosity)

	<=5		<=10		<=15		<=20		<=25		>25

Source: Appendix B, Table B-1, Microsoft Excel file "*Lithophysal projection to vertical plane.xls*," worksheet "Window calculations," starting at cell AB13 ("50×200 model cross section" table).

NOTE: Every time a "command" or "action" is implemented on the "Window calculation" worksheet (for example typing something in a cell and using the return key, or running the macros) the values in the "model cross section" cells change due to use of the random number function. However, it can be noted that the descriptive statistics for the total 50x200 and 20x80 cell tables (listed in the worksheet) will compare very closely with each subsequent version of the table and also compare closely with the actual rock statistics from the "windows" descriptive statistics located in cells O201 to P214.

Table A-3. Display of Part of the 20×80 Cell Table with Descriptive Statistics for Calculation of Lithophysal Cavity Porosity in a 50×200 m Simulated Cross Section with the Centerline at Station 17+56

Table of porosity values (2.5×2.5 m grid)											
Horizon	Cell $_Y$\$^X$	2.5	5.0	7.5	10.0	12.5	15.0	17.5	20.0	22.5	25.0
0	2.5	15.3	7.4	7.9	5.7	8.2	6.0	5.7	7.4	5.7	15.3
0	5.0	7.4	8.2	8.2	10.6	8.2	8.2	3.8	6.0	14.4	10.6
5	7.5	12.0	12.2	11.0	17.0	12.2	10.2	10.2	12.1	8.8	12.2
5	10.0	13.4	10.2	13.6	12.0	11.0	17.0	10.2	12.2	11.0	17.7
10	12.5	29.2	21.0	19.0	26.9	17.4	17.2	29.2	19.0	17.4	19.0
10	15.0	24.6	29.2	25.6	25.6	11.0	19.0	19.0	17.4	21.0	17.4
15	17.5	18.8	17.0	13.6	18.8	20.5	21.4	19.3	17.0	23.4	15.5
15	20.0	19.1	20.6	20.5	16.8	15.5	16.8	16.8	15.5	19.1	22.9
20	22.5	13.0	15.3	13.0	14.5	10.7	14.5	11.0	13.0	11.0	14.5
20	25.0	15.3	14.5	15.3	17.3	11.7	11.7	10.7	10.6	15.5	17.3
25	27.5	15.5	13.8	18.1	16.9	25.6	16.9	18.1	25.6	18.8	20.1
25	30.0	14.5	16.9	25.6	18.1	18.1	21.1	17.3	18.1	25.6	16.9
30	32.5	7.8	10.8	9.7	7.8	11.8	12.7	11.8	10.8	11.8	11.6
30	35.0	9.7	11.8	12.7	13.6	8.5	9.7	9.7	10.8	12.7	7.8
35	37.5	9.8	9.8	11.6	19.1	5.7	21.3	16.6	17.8	17.8	5.7
35	40.0	21.3	15.2	9.8	19.1	9.8	12.3	14.4	15.2	21.3	17.8
40	42.5	9.6	12.9	9.6	11.9	9.6	11.9	6.0	12.9	11.7	13.3
40	45.0	9.6	11.1	11.9	10.7	9.6	9.6	10.7	6.0	11.1	11.9
45	47.5	14.5	17.3	15.2	17.3	15.3	13.5	16.6	15.6	16.6	15.2
45	50.0	15.3	16.6	14.5	16.5	12.0	16.5	15.6	13.2	16.5	16.6

Descriptive Statistics

Simulated "X" position	2.5	5.0	7.5	10.0	12.5	15.0	17.5	20.0	22.5	25.0
Mean	14.8	14.6	14.3	15.8	12.6	14.4	13.6	13.8	15.6	15.0
Standard Error	1.3	1.1	1.2	1.2	1.1	1.0	1.3	1.1	1.1	0.9
Median	14.5	14.1	13.3	16.9	11.4	14.0	13.1	13.1	16.0	15.4
Mode	14.5	#N/A	#N/A	19.1	8.2	#N/A	10.2	10.8	#N/A	#N/A
Standard Deviation	5.6	5.1	5.2	5.2	4.8	4.5	5.9	4.8	5.1	4.2
Sample Variance	31.8	25.9	26.6	27.3	23.3	20.5	34.3	22.7	26.4	17.3
Kurtosis	1.0	2.3	0.5	0.4	1.5	-0.9	1.3	0.7	-0.5	0.3
Skewness	1.0	1.2	1.0	0.2	1.2	0.0	0.6	0.4	0.1	-0.5
Range	21.8	21.8	17.8	21.2	19.9	15.4	25.4	19.6	20.0	17.2
Minimum	7.4	7.4	7.9	5.7	5.7	6.0	3.8	6.0	5.7	5.7
Maximum	29.2	29.2	25.6	26.9	25.6	21.4	29.2	25.6	25.6	22.9
Sum	295.8	291.7	286.4	316.3	252.4	287.7	272.6	276.5	311.4	299.5
Count	20	20	20	20	20	20	20	20	20	20
Confidence Level (95.0%)	2.5	2.2	2.3	2.3	2.1	2.0	2.6	2.1	2.3	1.8

Explanation of symbols (percent lithophysal cavity porosity)

	<=5		<=10		<=15		<=20		<=25		>25

Source: Appendix B, Table B-1, Microsoft Excel file "*Lithophysal projection to vertical plane.xls,*" worksheet "Window calculations," starting at cell AB91 ("20×80 model cross section" table)
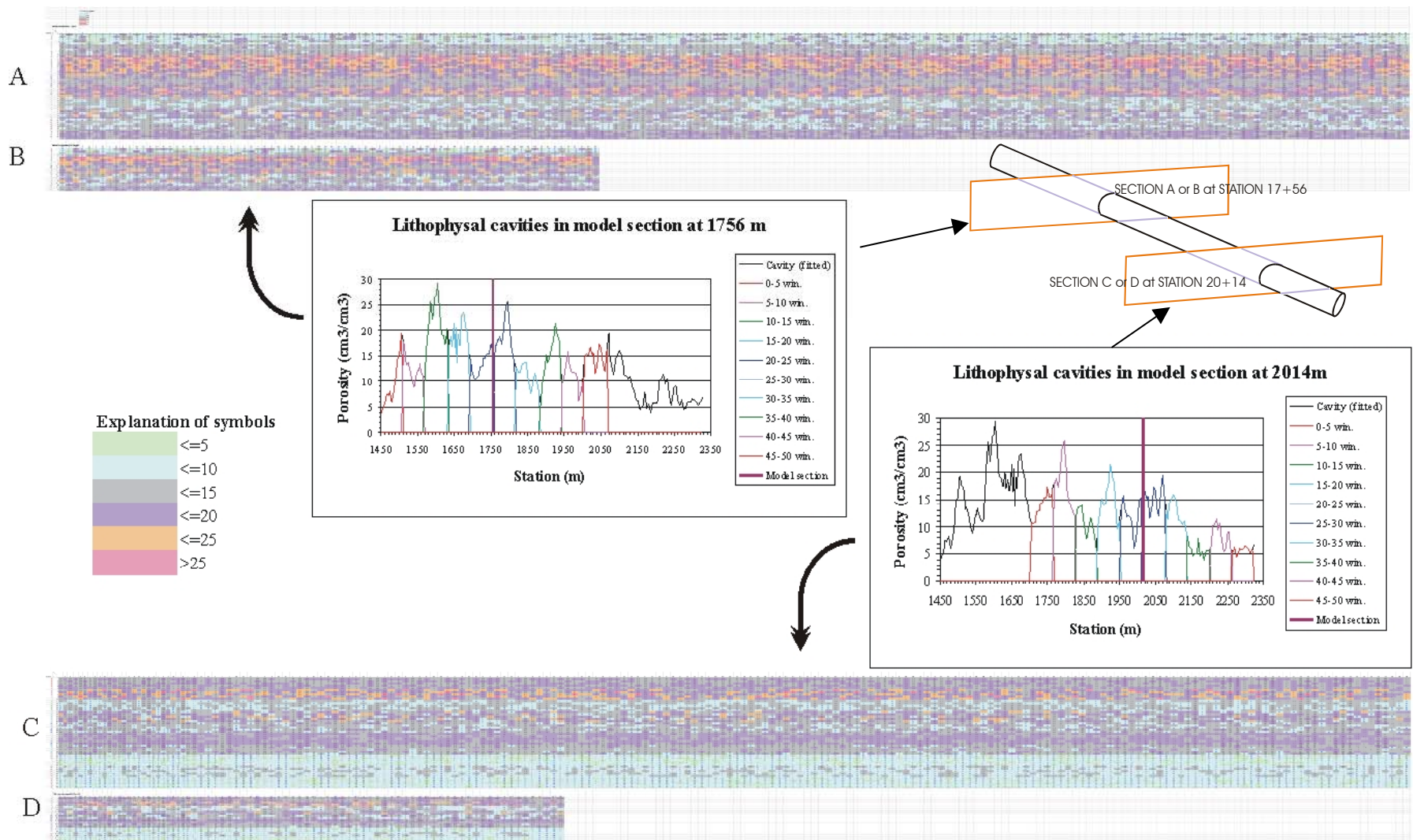
NOTES: Cross section A is a 50×200 cell table representing a 1×1 m grid, and cross section B is a 20×80 cell table representing a 2.5×2.5 m grid for the simulated section at 17+56. Cross section C is a 50×200 cell table representing a 1×1 m grid, and cross section D is a 20×80 cell table representing a 2.5×2.5 m grid for the simulated section at Station 20+14.

Figure A-5. Two 50×200 m Simulated Cross Sections of Lithophysal Cavity Porosity at Stations 17+56 and 20+14 (Apparent dip of 4.6°)

Table A-4. Comparison of Descriptive Statistics for the Total Tptpll Zone in the ECRB Cross-Drift, Individual Windows from the Input Data, and Selective Statistics for 5 m Tall Horizons in a 50×200 m Simulated Cross Section with 1×1 m and 2.5×2.5 m Grids

Descriptive Statistics (for Total Input and Windows)																
Statistic	Total ECRB Cross-Drift Data	0-5 Window	0-5 1×1 Grid	0-5 2.5×2.5 Grid	5-10 Window	5-10 1×1 Grid	5-10 2.5×2.5 Grid	10-15 Window	10-15 1×1 Grid	10-15 2.5×2.5 Grid	15-20 Window	15-20 1×1 Grid	15-20 2.5×2.5 Grid	20-25 Window	20-25 1×1 Grid	20-25 2.5×2.5 Grid
Mean	12.9	9.2	9.1	9.3	12.6	12.6	12.3	21.5	21.2	22.4	18.6	18.6	18.3	13.5	13.6	13.6
Standard Error	0.4	1.4	0.1	0.4	0.7	0.1	0.2	1.4	0.1	0.4	0.7	0.1	0.2	0.5	0.1	0.2
Median	12.7	7.7	—	—	12.2	—	—	21.0	—	—	18.8	—	—	13.6	—	—
Mode	17.0	#N/A	—	—	12.2	—	—	#N/A	—	—	17.0	—	—	13.0	—	—
Standard Deviation	5.4	4.8	4.6	4.7	2.5	2.3	2.4	5.0	4.7	4.6	2.8	2.7	2.6	2.0	2.0	2.0
Sample Variance	29.6	22.7	21.1	21.9	6.2	5.5	5.9	24.8	22.2	20.8	7.7	7.0	7.0	4.2	3.9	3.8
Kurtosis	-0.2	0.3			0.8			0.1			-0.6			-0.8		
Skewness	0.4	1.1	1.0	1.0	0.9	0.8	0.9	-0.4	-0.2	-0.5	0.2	0.2	0.1	0.0	0.0	0.0
Range	26.7	15.5	—	—	8.9	—	—	18.2	—	—	9.8	—	—	6.7	—	—
Minimum	2.5	3.8	—	—	8.8	—	—	11.0	—	—	13.6	—	—	10.6	—	—
Maximum	29.2	19.4	—	—	17.7	—	—	29.2	—	—	23.4	—	—	17.3	—	—
Sum	2352.1	110.9	—	—	164.4	—	—	279.9	—	—	279.2	—	—	189.5	—	—
Count	183	12	—	—	13	—	—	13	—	—	15	—	—	14	—	—
Confidence Level (95.0%)	0.8	2.7	—	—	1.3	—	—	2.7	—	—	1.4	—	—	1.1	—	—

Table A-4   Comparison of Descriptive Statistics for the Total Tptpll Zone in the ECRB Cross-Drift, Individual Windows from the Input Data, and Selective Statistics for 5 m Tall Horizons in a 50×200 m Simulated Cross Section with 1×1 m and 2.5×2.5 m Grids (continued)

Descriptive Statistics (for Total Input and Windows)																
Statistic	Total ECRB Cross-Drift Data	25-30 Window	25-30 1×1 Grid	25-30 2.5×2.5 Grid	30-35 Window	30-35 1×1 Grid	30-35 2.5×2.5 Grid	35-40 Window	35-40 1×1 Grid	35-40 2.5×2.5 Grid	40-45 Window	40-45 1×1 Grid	40-45 2.5×2.5 Grid	45-50 Window	45-50 1×1 Grid	45-50 2.5×2.5 Grid
Mean	12.9	18.5	18.6	18.2	11.1	11.0	11.0	14.6	14.6	14.6	11.0	11.0	10.8	14.8	14.9	14.6
Standard Error	0.4	0.9	0.1	0.3	0.6	0.1	0.2	1.3	0.1	0.4	0.7	0.1	0.2	0.5	0.1	0.1
Median	12.7	18.1	—	—	11.6	—	—	14.8	—	—	11.4	—	—	15.3	—	—
Mode	17.0	18.1	—	—	11.8	—	—	#N/A	—	—	#N/A	—	—	#N/A	—	—
Standard Deviation	5.4	3.4	3.3	3.3	2.1	2.0	2.0	4.4	4.1	4.6	2.6	2.4	2.7	1.8	1.7	1.8
Sample Variance	29.6	11.6	10.8	10.6	4.4	4.1	4.1	19.0	17.2	20.8	6.7	5.9	7.5	3.2	2.9	3.3
Kurtosis	-0.2	0.5	—	—	-1.2	—	—	0.2	—	—	0.6	—	—	-0.6	—	—
Skewness	0.4	0.9	0.8	0.8	-0.2	-0.2	-0.1	-0.5	-0.5	-0.6	-0.2	-0.2	-0.3	-0.6	-0.6	-0.3
Range	26.7	11.9	—	—	6.1	—	—	15.6	—	—	9.8	—	—	5.7	—	—
Minimum	2.5	13.8	—	—	7.8	—	—	5.7	—	—	6.0	—	—	11.6	—	—
Maximum	29.2	25.6	—	—	13.9	—	—	21.3	—	—	15.8	—	—	17.3	—	—
Sum	2352.1	259.4	—	—	143.8	—	—	175.8	—	—	132.3	—	—	192.9	—	—
Count	183	14	—	—	13	—	—	12	—	—	12	—	—	13	—	—
Confidence Level (95.0%)	0.8	1.8	—	—	1.1	—	—	2.5	—	—	1.5	—	—	1.0	—	—

Source: Appendix B, Table B-1, Microsoft Excel file "*Lithophysal projection to vertical plane.xls*," worksheet "Window calculations." Total and windows descriptive statistics comes from cells B201 to L214. The descriptive statistics for the 1×1 m simulated cross section grids (200 realizations) come from cells HU13 to HU62.   The descriptive statistics for the 2.5×2.5 m simulated cross section grids (80 realizations) come from cells HU91 to HY109.

NOTE: Every time a "command" or "action" is implemented on the "Window calculation" worksheet (for example typing something in a cell and using the return key, or running the macros) the values in the simulated "cross section" grids change due to use of the random number function. However, it can be noted that the descriptive statistics for the total 50x200 and 20x80 cell tables (listed in the worksheet) will compare very closely with each subsequent version of the table and also compare closely with the actual rock statistics from the "windows" descriptive statistics located in cells O201 to P214.

Table A-5. Comparison of Descriptive Statistics for the Total Windows from ECRB Cross-Drift (Input) Data and the Total 50×200 m Simulated Cross Section with 1×1 m and 2.5×2.5 m Grids

Descriptive Statistics for Total Windows							
Statistic	ECRB Cross-Drift Data	1×1 Grid	2.5×2.5 Grid	Statistic	ECRB Cross-Drift Data	1×1 Grid	2.5×2.5 Grid
Mean	14.7	14.5	14.5	Skewness	0.4	0.4	0.4
Standard Error	0.4	0.0	0.1	Range	25.4	25.4	25.4
Median	14.4	13.9	13.9	Minimum	3.8	3.8	3.8
Mode	17.0	11.6	11.6	Maximum	29.2	29.2	29.2
Standard Deviation	4.9	4.9	5.1	Sum	1928.1	145404.3	23193.6
Sample Variance	24.0	24.0	25.5	Count	131.0	10000	1600
Kurtosis	0.2	0.2	0.2	Confidence Level (95.0%)	0.8	0.10	0.25

Source: Appendix B, Table B-1, Microsoft Excel file "*Lithophysal projection to vertical plane.xls*," worksheet "Window calculations," from descriptive statistics located in cells O201 to O214 and descriptive statistics associated with the 1×1 m and 2.5×2.5 m simulated cross section grids (located in cells IA13 to IA26 and IA91 to IA104).

A.7   LIMITATIONS OF THE CALCULATION

The calculations of the distribution of lithophysal cavity porosity from the ECRB Cross-Drift to a vertical plane that is perpendicular to the tunnel is based on sound geologic and geometric relations; however, there are a few limitations to the results:

1. The calculations exemplified in this simulation are based on the consideration that the ECRB Cross-Drift is horizontal. The gradient of the tunnel is 1.5 percent (0.86°) from 07+73 to 16+02 and is 0.9 percent (0.52°) from 16+02 to 24+67 (Mongano et al. 1999 [DIRS 149850], pp. 3 and 6). So, although these inclinations are small, they can be factored into the apparent dip of the lithostratigraphic units and features to enhance the geologic and construction conditions.

2. Using a constant apparent dip of 4.6° from the strike and dip of 270/07 for the top contact of the lower lithophysal zone in the ECRB Cross-Drift (Mongano et al. 1999 [DIRS 149850], Table 1) and the total intercept of the lower lithophysal zone in the ECRB Cross-Drift (from 14+44 to 23+26), the calculated thickness of the lower lithophysal zone is only 71 m. This calculated thickness is less than what is calculated and depicted by a variety of other methods, so the apparent dip of 4.6° is probably too shallow; therefore, the number and the distribution of values in each window along the tunnel might be over represented.

3. The simulated cross section is constructed perpendicular to the tunnel; however, it does not include the apparent dip in the plane of the cross section. For example, using the features and data depicted in Figure A-2, the apparent dip in the cross section is 5.3° to the northwest.

Because the values in each cell in the 50×200 and 20×80 cell tables are independently and randomly allocated, locally there are a few geologically inconsistent results. While this allocation technique results in very high correlations of the descriptive statistics between the

input data and resulting cross section horizons, it is possible that locally, the minimum and maximum values in a window or in adjacent windows can be in adjacent cells. This extreme change in lithophysal cavity porosity has not been observed in the ECRB Cross-Drift as shown by the gradual increase or decrease in values (although sharp changes can occur across distances of 5 to 10 m; Figure A-3). One result of this random allocation of values and the potential juxtaposition of large and small (or mostly values of one end of the distribution or another) is the variation in descriptive statistics in vertical sections (X positions; Tables A-2 and A-3). The effect of this juxtaposition of minimum and maximum values is probably greater in the 20×80 cell table that represents a 2.5×2.5 m grid than in the 50×200 cell table that represents a 1×1 m grid. One way to minimize this effect is to filter the values in the tables and remove (or change) one or both of the juxtaposed values. Development of such a filter needs to focus on diminishing the anomalies, but maintaining the statistical integrity of the resultant calculated values.

APPENDIX B

COMPUTER FILES SUPPORTING CALCULATION

COMPUTER FILES SUPPORTING CALCULATION

The standard functions of commercial off-the-shelf software, including Microsoft Excel 2000 SP-3, JMP Version 5.1, and CorelDRAW Version 8.369, were used. Calculation files were developed in this calculation to perform support calculation activities and visual representation as described in Section 6, and associated Appendices. Appendix B provides a listing of all calculation files (Table B-1), including the location in this report where specific details of the calculation can be found. Microsoft Excel 2000 SP-3, JMP Version 5.1, and CorelDRAW Version 8.369 are exempted software applications in accordance with LP-SI.11Q-BSC, Section 2.1. All software in this category was performed on personal computers with a Pentium microprocessor and Microsoft Windows 2000 operating system. All supporting files are archived on a CD-ROM as part of this calculation and submitted to the records processing center as part of the records package for this calculation.

Table B-1. List of Supporting Calculation Files

File Name	File Type	Brief Description	References
Drift Deg AMR AF T-A-P Fit_V1_DBR.xls	Microsoft Excel 2000 SP-3	Calculation file for descriptive statistics and histograms for lithophysal abundance and lithophysal characteristics in the ECRB Cross-Drift. Used and described in Section 6 and Appendix A.	GS021008314224.002 and GS040608314224.001. Updated with information from Table 4-1 (DTN: GS021008314224.002). Modified from BSC 2003 [DIRS 166660], Attachment VIII, file *Drift Deg AMR AF T-A-P Fit.xls*.
LithophysalRockRanges_Calc.xls	Microsoft Excel 2000 SP-3	Calculation file listing the following inputs: large-core mechanical properties and PFC2D, PFC3D, and UDEC program output results. Inputs are plotted, descriptive statistics are given with histograms, curve fits are made, and bounds on data are determined. Used in Section 6.	Compressive and Porosity Data REV00B_PorosityOnly_Tpt.xls; shapestudy.xls; Summary2_newest.xls; and BSC 2004 [DIRS 166107], Appendix A, PFC and UDEC Inputs & Outputs archived under DTN MO0408MWDDDMIO.002).
Compressive and Porosity Data REV00B.xls	Microsoft Excel 2000 SP-3	File of intact laboratory testing database of samples with porosity. Used by the Excel file "Compressive and Porosity Data REV00B_PorosityOnly_Tpt.xls."	BSC 2003 [DIRS 166660], Attachment VIII, Table VIII-1, Microsoft Excel File "Compressive and Porosity Data.xls"
Compressive and Porosity Data REV00B_PorosityOnly_Tpt.xls	Microsoft Excel 2000 SP-3	File of intact laboratory testing database of samples with porosity from the Topopah Spring Tuff lithostratigraphic units. Used and described in Section 6.3.	Source DTNs SNSAND84086000.000, SN0208L0207502.001, SN0211L0207502.002, SN0305L0207502.006, MO0311RCKPRPCS.003, and MO0402DQRIRPPR.003. See file "Compressive and Porosity Data REV00B.xls"
shapestudy.xls	Microsoft Excel 2000 SP-3	Summary file of PFC2D and PFC3D shape study modeling results of lithophysal rock. Used by the Excel file "LithophysalRockRanges_Calc.xls."	BSC 2003 [DIRS 166660], Attachment VIII, CD#2 "PFC_runs\ShapeStudy\

Table B-1.   List of Supporting Calculation Files (Continued)

File Name	File Type	Brief Description	References
Summary2_newest.xls	Microsoft Excel 2000 SP-3	Summary file of UDEC shape study modeling results of lithophysal rock. Used by the Excel file "LithophysalRockRanges_Calc.xls."	BSC 2003 [DIRS 166660], Attachment VIII, CD#20 "UDEC_CD1\"
PFC&UDEC_Plots.xls	Microsoft Excel 2000 SP-3	Calculation file with plots of combined PFC2D and UDEC lithophysal shape study results. Used in Section 6.5.	Compressive and Porosity Data REV00B_PorosityOnly_Tpt.xls; ShapeStudy_bf2-bf4.xls; and Summary2_newest.xls.
ShapeStudy_bf2-bf4.xls	Microsoft Excel 2000 SP-3	Summary file of PFC2D shape study modeling results of lithophysal rock. Used by the Excel file "PFC&UDEC_Plots.xls."	BSC 2003 [DIRS 166660], Attachment VIII, CD#2 "PFC_runs\ShapeStudy\
Lithophysal projection to vertical plane.xls	Microsoft Excel 2000 SP-3	Calculation file for projecting mapped lithophysal porosity outward in three dimensions. Used and described in Appendix A.	Buesch and Spengler 1998 [DIRS 101433], Buesch et al. 1996 [DIRS 100106], Mongano et al. 1999 [DIRS 149850]
LargeCoreLithophysalData.JMP	JMP Ver5.1	Calculation file for determining 95% confidence intervals around the linear fit line of large-core mechanical test data. Used in Figure 6.4-5 and Microsoft Excel file "LithophysalRockRanges_Calc.xls," Worksheet "LC E-por (Range)" In Appendix B.	N/A
Rock Tendon Stress Calc.xls	Microsoft Excel 2000 SP-3	Calculations of slot test geometry, loaded area, approximate rock failure stresses, and lithophysal porosity.	Slot Test 1: SN0207F4102102.001, SN0208F4102102.002, SN0301F4102102.007, SN0301F4102102.008. Slot Test 2: SN0212F4102102.003, SN0212F4102102.004, SN0302F4102102.009, SN0302F4102102.010. Slot Test 3: SN0301F4102102.005, SN0301F4102102.006, SN0303F4102102.011, SN0303F4102102.012.

INTENTIONALLY LEFT BLANK

APPENDIX C

DERIVATION OF DATA REDUCTION FORMULAE

DERIVATION OF DATA REDUCTION FORMULAE

C.1   DERIVATION OF POISSON'S RATIO FORMULA

The UDEC model uses the two-dimensional plane strain assumption in which loading is uniform in the z-axis direction, and because of the loading and geometry, the strain in the z-direction is assumed to be unchanging. In the theory of elasticity the equations of stress and strain for the assumption of plane strain are well known:

$$\sigma_z = \nu(\sigma_x + \sigma_y)$$
$$\varepsilon_z = 0$$
$$\varepsilon_x = \frac{1}{E}\left[(1-\nu^2)\sigma_x - \nu(1+\nu)\sigma_y\right] \tag{C-1}$$
$$\varepsilon_y = \frac{1}{E}\left[(1-\nu^2)\sigma_y - \nu(1+\nu)\sigma_x\right]$$

For simulation of the uniaxial test, the stress along the x-axis direction is zero ($\sigma_x = 0$), so Eqs. C-1 simplify to

$$\sigma_z = \nu\sigma_y$$
$$\varepsilon_z = 0$$
$$\varepsilon_x = -\frac{\nu(1+\nu)\sigma_y}{E} \tag{C-2}$$
$$\varepsilon_y = \frac{(1-\nu^2)\sigma_y}{E}$$

Now the slope of the elastic volumetric strain to axial strain plots (S_e) for the plane strain, uniaxial stress case is

$$S_e = \frac{elastic \;\; volumetric \;\; strain}{elastic \;\; axial \;\; strain} = \frac{\varepsilon_x + \varepsilon_y + \varepsilon_z}{\varepsilon_y} = \frac{\varepsilon_x + \varepsilon_y}{\varepsilon_y} \tag{C-3}$$

Substitute Eqs C-2 into Eq C-3,

$$S_e = \frac{1-\nu-2\nu^2}{1-\nu^2} = \frac{(1-2\nu)\,(1+\nu)}{(1-\nu)\,(1+\nu)} = \frac{1-2\nu}{1-\nu} \tag{C-4}$$

Solving for Poisson's ratio in Eq. C-4 gives

$$\upsilon = \frac{1-S_e}{2-S_e} \tag{C-5}$$

C.2   DERIVATION OF DILATION ANGLE FORMULA

The dilation angle (ψ) is calculated from the slope of the expansive (plastic) portion of volumetric strain versus axial strain curve. A flow rule, used in plasticity theory and associated with the yield criterion g^s, has the form (Itasca Consulting Group 2002 [DIRS 160331], Manuals/UDEC/Theory and Background/Section 2.4.2: Mohr-Coulomb Model, Eq. 2.47)

$$\Delta\varepsilon_i^p = \lambda^s \frac{\partial g^s}{\partial \sigma_i} \qquad i = 1 \text{ to } 3 \tag{C-6}$$

where $\Delta\varepsilon^p$ is a small principal strain increment , λ^s is a positive scalar factor of proportionality that is initially unknown, and g^s is the shear potential function defined as (Itasca Consulting Group 2002 [DIRS 160331], Manuals/UDEC/Theory and Background/Section 2.4.2, Eq. 2.41)

$$g^s = \sigma_1 - \sigma_3 N_\psi \tag{C-7}$$

where ψ is the dilation angle and N_ψ has the form (Itasca Consulting Group 2002 [DIRS 160331], Manuals/UDEC/Theory and Background/Section 2.4.2, Eq. 2.42)

$$N_\psi = \frac{1 + \sin\psi}{1 - \sin\psi} \tag{C-8}$$

Using Eqs. C-6 with Eqs. C-7 and C-8, after partial differentiation these equations become (Itasca Consulting Group 2002 [DIRS 160331], Manuals/UDEC/Theory and Background/Section 2.4.2, Eq. 2.48):

$$\begin{aligned}
\Delta\varepsilon_1^p &= \lambda^s \\
\Delta\varepsilon_2^p &= 0 \\
\Delta\varepsilon_3^p &= -\lambda^s N_\psi
\end{aligned} \tag{C-9}$$

Summing Eqs. C-9 over A constant increments of principal strain, where A is an arbitrary constant results in Eqs. C-10:

$$\begin{aligned}
\varepsilon_1^p &= A\lambda^s \\
\varepsilon_2^p &= 0 \\
\varepsilon_3^p &= -A\lambda^s N_\psi
\end{aligned} \tag{C-10}$$

Now the slope of the plastic volumetric strain versus axial strain curve, S_p, is defined as

$$S_p = \frac{\varepsilon_1^p + \varepsilon_2^p + \varepsilon_3^p}{\varepsilon_1^p} \tag{C-11}$$

Substituting the plastic strains from Eqs. C-10 into Eq. C-11 and simplifying gives

$$S_p = 1 - N_\psi = -\frac{2\sin\psi}{1 - \sin\psi} \tag{C-12}$$

Algebraic manipulation gives

$$\sin\psi = \frac{S_p}{S_p - 2} \qquad\qquad (C\text{-}13)$$

Due to the sign convention in rock mechanics wherein compression is positive, the S_p terms are replaced with $(-S_p)$ in Eq. C-12 to obtain

$$\sin\psi = \frac{-S_p}{-S_p - 2} = \frac{S_p}{S_p + 2} \qquad\qquad (C\text{-}14)$$

Finally, solving for the dilation angle (in radians) gives

$$\psi(\text{rad}) = \arcsin\left(\frac{S_p}{S_p + 2}\right) \qquad\qquad (C\text{-}15)$$